frontiers | Research Topics

Environmental contamination solutions for complex heterogeneous systems

Edited by
Ravi Naidu, Balaji Seshadri and Aravind Surapaneni

Published in
Frontiers in Environmental Science
Frontiers in Environmental Chemistry

ISSN 1664-8714
ISBN 978-2-83251-678-2
DOI 10.3389/978-2-83251-678-2

About Frontiers

Frontiers is more than just an open access publisher of scholarly articles: it is a pioneering approach to the world of academia, radically improving the way scholarly research is managed. The grand vision of Frontiers is a world where all people have an equal opportunity to seek, share and generate knowledge. Frontiers provides immediate and permanent online open access to all its publications, but this alone is not enough to realize our grand goals.

Frontiers journal series

The Frontiers journal series is a multi-tier and interdisciplinary set of open-access, online journals, promising a paradigm shift from the current review, selection and dissemination processes in academic publishing. All Frontiers journals are driven by researchers for researchers; therefore, they constitute a service to the scholarly community. At the same time, the *Frontiers journal series* operates on a revolutionary invention, the tiered publishing system, initially addressing specific communities of scholars, and gradually climbing up to broader public understanding, thus serving the interests of the lay society, too.

Dedication to quality

Each Frontiers article is a landmark of the highest quality, thanks to genuinely collaborative interactions between authors and review editors, who include some of the world's best academicians. Research must be certified by peers before entering a stream of knowledge that may eventually reach the public - and shape society; therefore, Frontiers only applies the most rigorous and unbiased reviews. Frontiers revolutionizes research publishing by freely delivering the most outstanding research, evaluated with no bias from both the academic and social point of view. By applying the most advanced information technologies, Frontiers is catapulting scholarly publishing into a new generation.

What are Frontiers Research Topics?

Frontiers Research Topics are very popular trademarks of the *Frontiers journals series*: they are collections of at least ten articles, all centered on a particular subject. With their unique mix of varied contributions from Original Research to Review Articles, Frontiers Research Topics unify the most influential researchers, the latest key findings and historical advances in a hot research area.

Find out more on how to host your own Frontiers Research Topic or contribute to one as an author by contacting the Frontiers editorial office: frontiersin.org/about/contact

Environmental contamination solutions for complex heterogeneous systems

Topic editors

Ravi Naidu — The University of Newcastle, Australia

Balaji Seshadri — The University of Newcastle, Australia

Aravind Surapaneni — Independent researcher, Australia

Citation

Naidu, R., Seshadri, B., Surapaneni, A., eds. (2023). *Environmental contamination solutions for complex heterogeneous systems*. Lausanne: Frontiers Media SA.

doi: 10.3389/978-2-83251-678-2

Table of contents

frontiers in Environmental Science

ORIGINAL RESEARCH
published: 20 July 2021
doi: 10.3389/fenvs.2021.633165

Desulfurization of Vulcanized Rubber Particles Using Biological and Couple Microwave-Chemical Methods

*C. Valdés[1], C. Hernández[2], R. Morales-Vera[2,3] and R. Andler[2]**

[1]Centro de Investigación de Estudios Avanzados Del Maule (CIEAM), Vicerrectoría de Investigación y Postgrado, Universidad Católica Del Maule, Talca, Chile, [2]Centro de Biotecnología de Los Recursos Naturales (CENBIO), Escuela de Ingeniería en Biotecnología, Universidad Católica Del Maule, Talca, Chile, [3]Facultad de Ingeniería, Ciencias y Tecnología, Universidad Bernardo O'Higgins, Santiago, Chile

Currently, recycling or degradation treatments for tires are an enormous challenge. Despite efforts to dispose of or recycle it, rubber waste is increasing year by year worldwide. To create a rubber-recycling system, several researchers have proposed tire desulfurization. In this study, we compare two methods: one biological, using *Acidobacillus ferroxidans* in shake 250 ml flask experiments, and one chemical using, for the first time, microwaves and an aqueous solution. The results of these methods were analyzed through sulfate quantification, cross-linking differences, Fourier transform infrared spectroscopy (FTIR) and scanning electron microscopy with energy disperse spectroscopy (SEM-EDS). We observed that the amount of sulfates generated by the chemical system was 22.40 (mg/L)/g of rubber, which was 22-times higher than the biological system, which generated 1.06 (mg/L)/g of rubber. Similarly, after cross-linking studies, a 36% higher decrease after the chemical treatment was observed. When using FTIR analysis, the disappearance of characteristic bands corresponding to functional groups containing sulfur bonds and metal oxides were observed by treating the sample with both desulfurization methods. Morphological changes on the rubber surface structure was also demonstrated by SEM-EDS analysis with the appearance of holes, cracks and changes in the porosity of the material. This work analyzed two different non-aggressive desulfurization approaches that might be used as methods for rubber recycling processes.

Keywords: ***Acidithiobacillus ferrooxidans*, desulfurization, devulcanization, microwave treatment, rubber degradation, rubber recycling**

OPEN ACCESS

Edited by:
Ravi Naidu,
University of Newcastle, Australia

Reviewed by:
Fabiula De Sousa,
Federal University of Pelotas, Brazil
Gonzalo Martinez-Barrera,
Universidad Autónoma del Estado de México, Mexico
Mohd Mustafa Al Bakri Abdullah,
Universiti Malaysia Perlis, Malaysia

****Correspondence:***
R. Andler
randler@ucm.cl

Specialty section:
This article was submitted to Toxicology, Pollution and the Environment, a section of the journal Frontiers in Environmental Science

Received: *24 November 2020*
Accepted: *02 July 2021*
Published: *20 July 2021*

Citation:
Valdés C, Hernández C, Morales-Vera R and Andler R (2021) Desulfurization of Vulcanized Rubber Particles Using Biological and Couple Microwave-Chemical Methods. Front. Environ. Sci. 9:633165. doi: 10.3389/fenvs.2021.633165

INTRODUCTION

Millions of tires are discarded every year, representing up to 12% of the total accumulated solid waste. This type of waste increases annually by around 17 million tons. Recent studies project that, by 2030, about 1,200 million tons of tires will be discarded every year (Formela et al., 2019). Discarded tires generate problems as accumulation of mosquitos, and cause of unwanted fires generating toxic vapors (Stevenson et al., 2008). The main constituent of tires is rubber, which can be obtained from fossil sources (synthetic rubber) or from the tree *Hevea brasiliensis* (natural rubber) (Subramaniam, 1987). When analyzing the dry weight of natural rubber, it consists of 90% poly (*cis*-1,4-isoprene) and less than 10% of other constituents such as proteins, carbohydrates, lipids, resins, and inorganic salts (Nawong et al., 2018). For commercial purposes, rubber is subjected to a vulcanization process

where the poly (*cis*-1,4-isoprene) chains are cross-linked between them by heat in the presence of sulphur (Berekaa et al., 2000). The process is based on adding a percentage of elemental sulfide to rubber, which is subsequently subjected to heat at 140°C and 4 atm of pressure. As a result, the original material, which is sticky and non-elastic, becomes a non-sticky and elastic material. Due to cross-linking, it is not possible to deform the material using heat, as it is done with thermoplastics such as polyolefins (polyethylene or polypropylene) (Holst et al., 1998). In addition, to improve abrasion resistance, carbon black is added to the rubber during vulcanization (Larsen et al., 2006). Carbon black together with silica are the second major components of a tire, after the polymer of rubber (Bockstal et al., 2019).

Since procedures such as tire burning, tire burying, and depositing tires on landfills are harmful, several methods and mechanisms for rubber degradation have been studied (Sienkiewicz et al., 2017; Mok and Eng, 2018). Rubber waste can be treated by chemical, mechanical and biological processes. However, as a result of the high degradation resistance of rubber materials, no clean and efficient processes have been established to date. One of the reasons that vulcanized rubber is difficult to degrade is due to the presence of disulfide bridges, which link the rubber molecules together in a strong bond (Bredberg et al., 2002). Consequently, a first desulfurization step is essential for improving the overall degradation process (Andler, 2020).

Biological desulfurization methods as rubber degradation of ground tires has been reported. (Li et al., 2011). The Fourier Transform Infrarred Spectroscopy (FTIR) and X-ray photoelectron spectroscopy (XPS) analysis has been demonstrated how *Thiobacillus ferrooxidans* was able to breakdown sulfur crosslinks. In another work using the same bacteria, the bioconversion from sulfide to sulfate was studied. After a 20 days cultivation, an 8% conversion was reached with changes in the physical properties of the material (Chritiansson et al., 1998).

Acidithiobacillus is a gram-negative bacterium of the chemolithotrophic type. It was initially cataloged in the genus *Thiobacillus* (Vishniac and Santer, 1957); however, due to its high acidity tolerance, it was reclassified in the genus *Acidithiobacillus* (Kelly and Wood, 2000). This genus is divided into two groups: sulfur-oxidizing species and sulfur- and iron-oxidizing species. *Acidithiobacillus ferrooxidans* corresponds to the latter group (Wang et al., 2019). This bacterium stands out for being used in mining to promote the oxidation of iron and sulfur compounds. A group of genes involved in the oxidation of reduced inorganic sulfur compounds (RISCs) has been described in *A. ferrooxidans*. Two genes homologous to *doxDA* encode a protein with thiosulfate/quinone oxidoreductase activity (AFE0044; AFE0048), and another five genes encode sulfur thiosulfate transferase proteins (AFE2558, AFE2364, AFE1502, AFE0529, and AFE0151). To date, the role they play in sulfur oxidation is not yet clear (Valdes et al., 2008).

Chemical treatments are another alternative for rubber recycling purposes (Sun et al., 2017), after treating waste silicone rubber composite insulator with H_2O_2 combine with graphite in an acid medium, obtained a material with better mechanical and thermal properties (Sun et al., 2017). Sulfuric acid has been used to treat crumb rubber in combination with ultraviolet light, as a result, the rubber's stiffness increased (Alawais and West, 2019). Surface modification of halloysite nanotubes have been reported to interact with rubber nanocomposites, using the vulcanization accelerant N-cyclohexyl-2-benzothiazole sulfenamide, improving the mechanical properties of the material (Zhong et al., 2016). Chemical methods supplemented with mechanical treatments have shown positive changes of the rubber properties, 2,2′-dibenzothiazoledisulfde (DM), in combination with mechanical treatment, increases the content of oxygenated groups on the surface, increasing the swelling degree of the material 1.5 times (Liu et al., 2020).

Green chemistry approaches as ultrasound and microwaves treatments have been reported for rubber treatment. Ultrasound treatments for rubber particles of 100–150 μm were obtained with a devulcanized surface (Dobrotă and Dobrotă, 2018). The energy consumption was around 2.5 times lower than a conventional mill (Formela et al., 2019). The use of microwaves at low temperatures is also described as a devulcanization treatment. Microwave treatment allows oxidation and degradation of rubber as an environmentally friendly alternative. Even with conventional microwaves, appreciable structural rubber changes can be detected by a thermo-oxidation process (Scuracchio et al., 2007). Although there are methods to digest complex compounds such as rubber using microwaves, it requires a high amount of acids. Alternative methods using moderate amounts of acids are needed to fulfill the green chemistry requirements (Pinheiro et al., 2019).

Devulcanization of rubber using microwaves is one of the most promising procedures due to its efficiency and low environmental consequences. An important advantage when compared against to conventional methods is that the application of heat is homogeneous and does not depend on conduction and/or convection of heat. Studies have reported the importance of the exposure time of the samples to microwaves, affecting the cross-linking of rubber. The polymer itself, such as copolymers of isoprene-butadiene, natural rubber, and butylated rubber, are important during the desulfurization process (de Sousa et al., 2017). It has been reported that the use of microwaves can decrease the toxic volatiles released in the pyrolysis of the waste crumb rubber used to generate asphalt, being a pretreatment option for this material (Yang et al., 2020).

Consequently, an efficient and environmentally friendly method is needed for the devulcanization of rubber in order to provide alternatives for recycling or degrading rubber waste. In this study, we compared two processes for the desulfurization of rubber particles. A chemical method based on microwaves at low acid concentrations, and a biological method using the bacterium *A. ferrooxidans* in shake flask experiments.

MATERIALS AND METHODS

Rubber Material

Rubber particles were purchased from Trelleborg AB, Germany. For all the experiments performed, a particle size between 1–2 mm was used.

Microwave Treatment

An Ethos Easy microwave with an SK-15 rotor was used for the chemical desulfurization treatment. A total of 250 mg of rubber

particles were added to 10 ml of 1% HNO_3. The temperature program was set at 180°C for 5 min and 200°C for 30 min.

Bacterial Strains and Cultivation Conditions

The bacterial strain used in this study was *A. ferrooxidans* ATCC 23270. For culture maintenance, the strain was grown using the medium DSMZ 70, adjusting the initial pH to 2.0. For the desulfurization cultures, a modified 9K medium was used supplemented with 1% of vulcanized rubber particles. The particles were previously washed using ethanol 70% v/v for 24 h. The medium composition was: $(NH_4)_2SO_4$, 3.00 g; K_2HPO_4, 0.50 g; $MgSO_4{\cdot}7H_2O$, 0.50 g; KCl, 0.10 g; Ca $(NO_3)_2$, 0.01 g; and $FeSO_4{\cdot}7H_2O$, 3.30 g. Two cultivation conditions were evaluated: 1) with 1% w/w rubber particles and 2) without rubber particles. The pH was initially adjusted to two using 4M HCl and monitored during the cultivations. Cultures were performed in 250 ml shake flasks at 30°C, 150 rpm for 4 weeks. Cell growth was measured by total cell count using a Neubauer chamber. Samples were analyzed every 7 days.

Sulfate Ion Quantification

The sulfate ion content was measured at the beginning and at the end of the cultivation e for all the biological assays and the microwave treatment. Consequently, 5 ml of supernatant (for the biological treatment) and 5 ml of the 1% HNO_3 solution (for the chemical treatment) were mixed with 100 µL of a barium chloride solution (Ba_2Cl, 20 g; acetic acid 10 N, 75 ml; glycerol 25% v/v, 25 ml). The mixture was mixed vigorously, and the absorbance was measured using a spectrophotometer at 420 nm. Sodium sulfate was used as standard in a range of 0.02–1.00 mg/µL^{-1}. Sulfate quantification data was analyzed by ANOVA using the software SPSS10. The multiple comparison test Tukey was performed for significant differences of the treatments. Sulfate analysis was performed in duplicates.

Cross-Link Density Determination

To determine the cross-link density, the method described by Mok and Eng (2018) was performed using toluene as the organic solvent. Rubber particles (0.5 g) were mixed with 1 ml of toluene and incubated for 5 days in the dark using a fume hood. After this period, the solvent was discarded, and the mass was determined (m_3). The mass of the dry polymer (m_1) was obtained by heating the particles at 70°C for 72 h. The mass of the solvent in the swollen sample (m_2) was calculated as follows:

$$m_2 = m_3 - m_1 \tag{1}$$

The volume fraction of the rubber in its swollen state (Vr) was calculated as follows:

$$V_r = \frac{(m_1/\rho_1)}{(m_1/\rho_1) + (m_2/\rho_2)} \tag{2}$$

where V_r is the volume fraction of the rubber in its swollen state, and ρ_1 and ρ_2 are the density of the dry polymer sample and the density of the solvent (mol/cm^3), respectively.

The cross-link density (ν) was calculated as follows (Liu et al., 2020):

$$\nu = \frac{-1}{2v_s} \frac{\ln(1 - V_r) + V_r + \chi V_r^2}{V_r^{1/3} - V_r/2} \tag{3}$$

where ν is the cross-link density mole per unit of volume (mol/cm^3) and χ is the Flory–Huggins polymer-solvent interaction parameter (0.35 for the rubber-toluene mixture; (Dzulkifli et al., 2016).

Fourier Transform Infrared Spectroscopy Analysis

The rubber particles were separated from the reaction medium by filtration using a glass filter with a porosity of 3 (nominal pore size: 16–40 mm). A 10 mg of dried rubber particles were analyzed by attenuated total reflectance (ATR)-FTIR. The infrared spectra were obtained using a FTIR spectrometer (Agilent, Cary 630) with the ATR technique. Absorbance was measured in the wavelength range of 400–4,000 cm^{-1}, whereas the resolution was 4 cm^{-1}. For each sample, 64 scans were performed, and the background was subtracted using Agilent MicroLab PC software.

Scanning Electron Microscopy/Elemental Analysis by Energy Dispersive

The method was based on ASTM E1508 standard " Standard Guide for Quantitative Analysis by Energy-Dispersive Spectroscopy". The microscope used was TESCAN VEGA 3 with probe EDS BRUKER QUANTAX, samples were covered by a cathodic spray system with Palladium Gold in Hummer 6.2 equipment.

RESULTS

Growth of *Acidithiobacillus ferrooxidans* in Shake Flasks

The *A. ferrooxidans* cultures were kept under constant agitation with a controlled temperature for 4 weeks, while cell growth and pH was monitored every 7 days. **Figure 1** shows the bacterial growth of *A. ferrooxidans* and the pH evolution over time. It was possible to observe that cell growth was enhanced with the presence of rubber particles, showing maximum growth over 3 weeks, while culture without rubber in the medium showed lower growth, reaching 3.4×10^6 cells/mL. Rubber treatment with *T. ferrooxidans* has been reported for the desulfurization of tire rubber, where a similar culture medium (modified Silverman medium) was used for a 30 days incubation period (Li et al., 2011). In that experiment, cell growth was negatively affected when rubber was added to the medium (after 24 h). This difference could be attributed to the fact that rubber was not treated with ethanol for partial elimination of residues present in the rubber that might prevent the growth of the bacteria. However, a similar cell density was reached in both studies (Li et al., 2011). Rubber treatments using 9K culture medium have been previously reported under similar conditions, where the oxidative capacity of iron *T. ferrooxidans* was also measured.

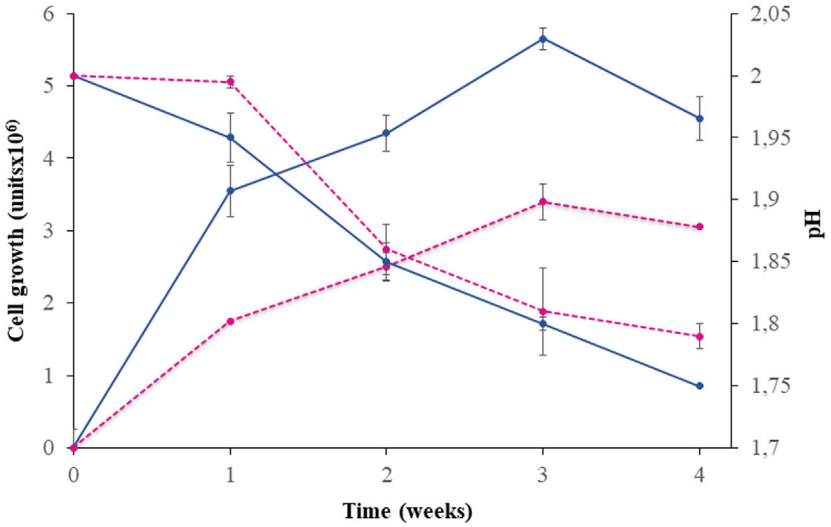

FIGURE 1 | Growth of *A. ferrooxidans* **(A)** and pH variation **(B)** in shake flasks over 4 weeks. The cultivation medium was the modified 9K medium supplemented with 1% w/w rubber particles **(solid line)**, and without rubber particles **(dashed line)**. Measurements were done in duplicates and the standard error is presented in the figure.

TABLE 1 | Quantification of sulfate ion and determination of cross-link densities after biological and chemical treatments for Gram of rubber. For the biological negative control, the cultivation medium did not include rubber particles. For the chemical negative control, rubber particles were suspended in 1% HNO_3 without the microwave treatment. ND: not detected. Statistical analysis showed significant differences between all the different treatments. Standard error is showed for sulfate quantification.

Treatment	Sulfate (mg/L)/g of rubber	Cross-link densities (mol/cm^3)/g of rubber
Biological	1.06 ± 0.16	13 × 10^3
Biological control	0.20 ± 0.06	20.4 × 10^3
Chemical	22.40 ± 0.19	8.0 × 10^3
Chemical control	ND	20.4 × 10^3

(Jiang et al., 2010). In the present study, it was possible to detect a decrease in the pH in all treatments after the first week, reaching a final pH between 1.7 and 1.8. which do not interfere with *T. ferrooxidans* growth, as it is mentioned in previous studies (Valdes et al., 2008).

The culture was then subjected to analysis as sulfate quantification and rubber surface analysis by FTIR and SEM-EDS.

Sulfate Ion Quantification

Sulfates were quantified in order to evaluate the desulfurizing capacity of *A. ferrooxindans* and the microwave treatment. As shown in **Table 1**, cultures containing rubber particles and iron reached a sulfur concentration of 1.06 ± 0.16 (mg/L)/g of rubber after 30 days of cultivation. An increment of sulfate was observed when rubber was present in the cultivation medium over sulfate concentration reached in the absence of rubber (0.10 ± 0.03 g/L). A sulfate concentration of 0.17 g/L was reported by Li et al. (Li et al., 2011) in cultures of *A. ferrooxidans* after 14 days. In another report using the same microorganism, 0.18 g/L of sulfate ion was obtained after 20 days of cultivation (Jiang et al., 2010). Desulfurization in latex gloves has been reported with *A. ferroxidans* with a release of sulphate up to 8% w/w over 20 days; this result is more efficient when comparing with *Thiobacillus thioparus* and *Acidianus brierleyi*, under the same treatment conditions (Chritiansson et al., 1998). It is known that *A. ferrooxidans* can couple sulfur oxidation with electron transfer with a high redox potential for CO_2 fixation, releasing sulfate ions at the end of the oxidation process (Zhan et al., 2019).

For a proper comparison, the same initial concentration of rubber particles was tested in both processes. When analyzing the sulfate concentration after the chemical desulfurization with a microwave, 5.6 g/L was obtained; this is about 10 times higher than the biological treatment. No investigations were found regarding sulfate quantification by microwaves with the present technique. It is relevant to mention that the use of acids is reported as a medium of desulfurization; for example, sulfuric acid has been used for the desulfurization of fuels such as diesel and kerosene in the absence of catalysts (Shakirullah et al., 2010). Sulfur carbon desulfurization has also been reported in the presence of acids, and can also remove minerals (Mukherjee and Borthakur, 2001). Our results show the feasibility of optimizing

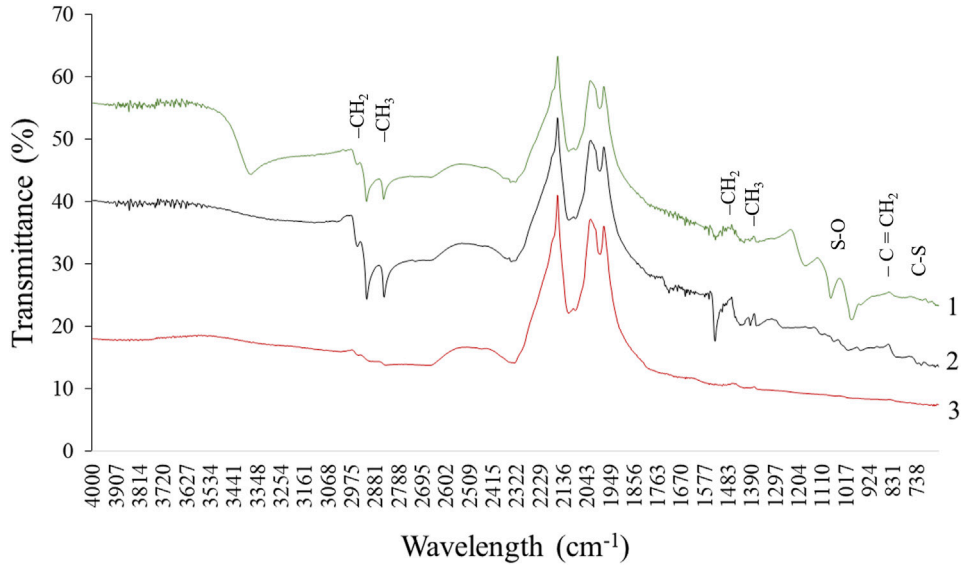

FIGURE 2 | FTIR spectra of rubber particles after biological treatment **(A)**, after chemical treatment **(C)**, and without treatment as a negative control **(B)**.

the best balance between desulfurization and the concentration of acid to be used.

Cross-Link Density

The Flory–Rehner equation was employed to determine the cross-link density for the rubber particles after both the biological and the microwave treatment (**Table 1**). It was possible to observe differences in the cross-linking between the treated and untreated rubber particles as well as differences between the biological and chemical methods. Using the microwave method, a greater decrease in cross-linking was observed. From the untreated rubber (control), the cross-link density of the samples after the biological treatment decreased 36%, reaching a value of 13 (mol/cm^3)/g of rubber, while a decrease of 60% was obtained after the chemical treatment with the microwave, reaching a value of 8.0×10^{-3} (mol/cm^3)/g of rubber. In previous biological treatments of rubber where the cross-link density was studied, values of 5.8×10^{-5} mol/cm^3 were reported (Jiang et al., 2010). Depending on the rubber content filling (phr), different cross-link densities can be obtained between 8.0×10^{-4} and 1.3×10^{-3} mol/cm^3 (Li et al., 2011).

Rubber Particle Analysis by Fourier Transform Infrared Spectroscopy

In order to evaluate structural variations at the surface of the particles after the desulfurization treatments. Rubber particles were recovered, dried, and analyzed using FTIR (**Figure 2**). It was possible to detect a variation in the polymer structure after the biological and chemical treatments corresponding to groups (– C = CH_2) at a wavelength of 874 cm^{-1} (Colom et al., 2016). This chemical structure is characteristic of the isoprene repetitive unit in tire rubber. The band at 1,360 cm^{-1} was also modified in both desulfurization approaches, which is related to (–CH_3) groups of the rubber structure (de Sousa et al., 2017). When analyzing peaks at 750 and 1,083 cm^{-1}, relating to C-S and S-O bonds respectively (de Sousa et al., 2017), strong variations were found. A clear modification of the group was shown after the biological treatment due to superficial exposure of the functional groups. On the other hand, those groups were lost after the microwave treatment, showing stronger variations and a release of the C-S and S-O groups from the rubber particle surface. A band close to 1,452 cm^{-1} corresponding to methylene, part of the isoprene structure (Colom et al., 2016), was observed in the control sample, and no visible in the spectra corresponding to the microwave treatment. The band close to 1,021 cm^{-1} was associated with rubber carbon black (Colom et al., 2016). This band was altered after the biological treatment and was not observe after the microwave treatment. The peaks 2,924 cm^{-1} and 2,854 cm^{-1} are attributable to CH_2 and CH_3 streching respectively, detected in artificial and natural rubber (Gorassini et al., 2016).

Rubber Particle Analysis by Scanning Electron Microscopy/Elemental Analysis by Energy Dispersive

SEM photographs show that the surface suffered small fractures after treating the rubber with both biological and chemical desulfurization methods (**Figure 3**). However, at 500x an increase in surface pores by the chemical treatment was observed, accounting for the greater wear of the surface product of the severity of the treatment. EDS analysis shows a decrease in O and S content at the rubber surface after treatments, increasing the observable C versus the control. The chemical

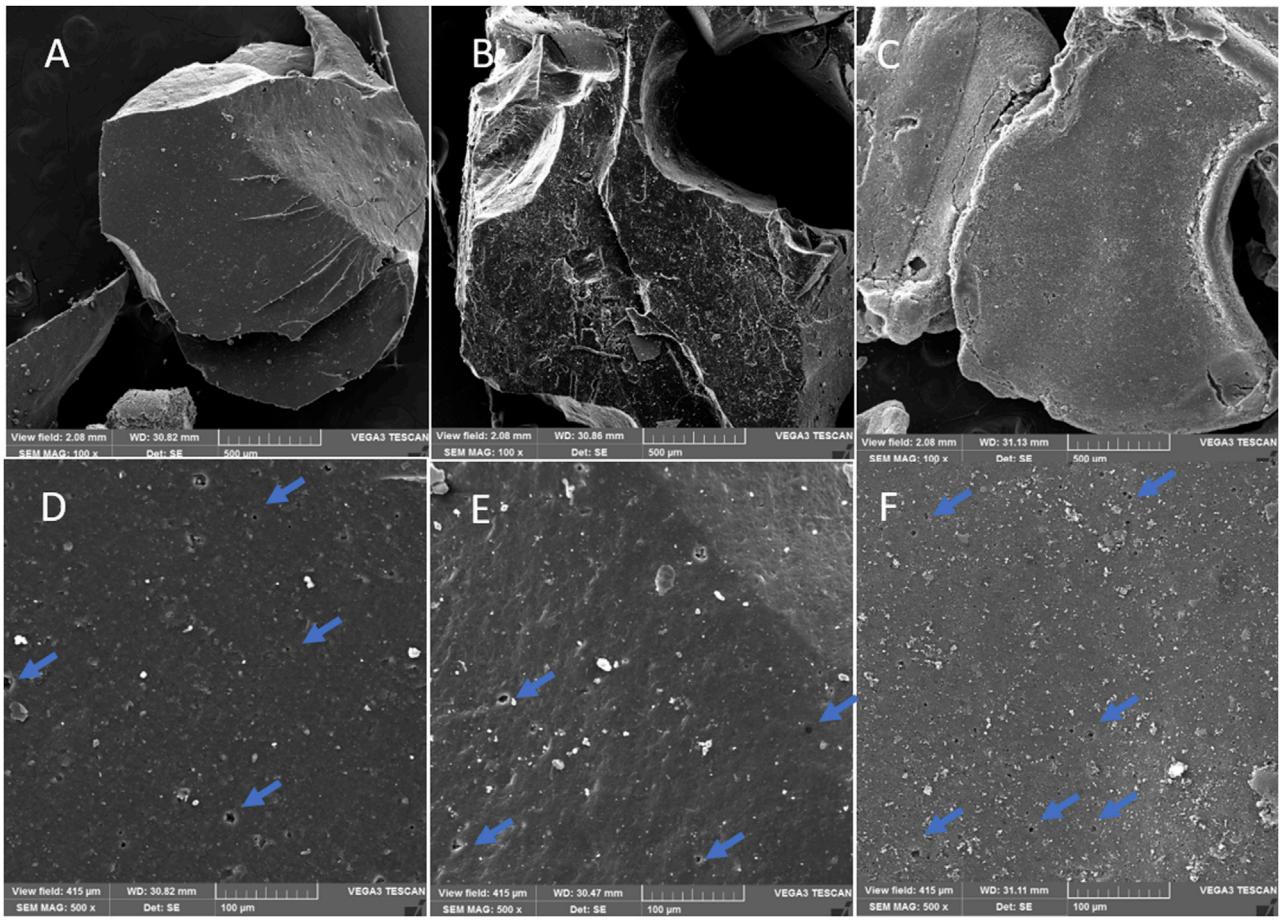

FIGURE 3 | Particle morphology and observable porosity in the analyzed samples, corresponding to control at 100x **(A)** and 500x **(D)**, biological treatment at 100x **(B)** and 500x **(E)**, and chemical treatment at 100x **(C)** and 500x **(F)**. Blue arrows show pores on the surface.

treatment shows a Si content 10-times higher than the control, indicating the oxidation of the rubber surface, exposing the Si of the innermost layers. No relevant modification is appreciated by the biological treatment. Other elements such as Al, K, and Mg were detected with less than 0.01%.

DISCUSSION

Biochemistry of Biological and Chemical Desulfurization Processes

The sulfur-uptake mechanism in *A. ferrooxidans* is not completely clear and some key enzymes have still not been identified. A sulfur dioxygenase (SDO) has been reported in *Acidithiobacillus*, the first enzyme reported for elemental oxidation of extracellular sulfur. SDO activity has also been detected in mitochondria, animals, and heterotrophic bacteria, where persulfide dioxygenase (ETHE1) and persulfide dioxygenase (PDO) are proposed as homologs of SDO in mitochondria and heterotrophic bacteria, respectively (Kabil and Banerjee, 2012; Sattler et al., 2015). Sulfur oxygenase reductase (SOR) is also found in *Acidithiobacillus*, which can generate molecules such as thiosulfate, sulfite, and sulfide (Ghosh and Dam, 2009). The tetrathionate hydrolase (ThetH) protein has been reported in *A. ferroxidans* (Sugio et al., 2009). This enzyme can also generate thiosulfate, sulphite, and sulfur from reduced sulfur species; however, ThetH's mechanism is still unclear (Tano et al., 1996; Beard et al., 2011). Knockout studies of this gene have been done in *A. Ferroxidans*, demonstrating the need for the ThetH to oxidize sulfur compounds present in selective media (Yu et al., 2014). However, it has been reported that this protein could be present extracellularly (Beard et al., 2011), which suggests that this is one of the enzymes that degrades the solid rubber present outside the bacterium when treatment systems in bioreactors by heterogeneous catalysis are used.

From a biochemical point of view, treatment using microorganisms allows the action of enzymes which causes the desulfurization of the material. The ability of microorganisms to desulfurize dibenzothiophene (a sulfur compound from petroleum) through the sulfoxide-sulfone-sulfinate-sulfate (4S)

pathway has been proposed, where sulfate can also be consumed as an assimilation pathway by microorganisms (Soleimani et al., 2007). It has been reported in other genera of bacteria that the desulfurization performance of the dszA and dszC enzymes during the desulfurization of dibenzothiophene does not increase in the presence of metals such as Fe^{+2}, Fe^{+3}, and Cu^{+}, and no decrease in activity was detected in the presence of Ethylenediaminetetraacetic acid (EDTA), suggesting that they do not depend on metallic cofactors (Ohshiro et al., 1997). Therefore, it is proposed that the presence of such enzymes would have a similar effect on the cross-linking of vulcanized rubber.

Regarding the microwave treatment, when rubber is subjected to temperatures of 200°C or more, devulcanization and shortening of the polymers is generated by rearrangement of the disulfide cross-links and the breakage of carbon–carbon bonds. The cross-links can be lost in volatile compounds in the shape of hydrogen sulfide (H_2S), carbon disulfide (CS_2), and sulfur dioxide (SO_2) (Asaro et al., 2018). This also shows that, in our microwave desulfurization tests, not all sulfur residues removed from the rubber structure would be present in the solution in forms such as sulfones, sulfates, or mercaptans.

During the microwave treatment, microwave energy is converted into thermal energy after being absorbed by the material. The polar molecules of a medium with dielectric characteristics move in the electric's direction field where thermal movement interferes with other molecules and the obstruction of intermolecular interactions generates internal friction. This converts the energy absorbed from the electrical field into thermal energy, increasing the temperature of the system (Tao et al., 2014). The thermal effects of microwaves can be associated with the ability to convert electromagnetic energy into thermal energy at a particular temperature and frequency; this capacity can be measured with the tangent of loss of the material (tan δ) (Didier et al., 2006), where ε" is the dielectric of material loss (which indicates the efficiency of the conversion of electrical energy into thermal energy) and ε' is the dielectric constant that indicates the polarization capacity (Ma et al., 2011).

Regarding the use of microwaves for treating rubber, temperature is a key factor, since it has been shown that oxidation can be generated by heat treatment of rubber and additives such as carbon black. Carbon black is an excellent microwave absorber (Ganchev et al., 1994; Formela et al., 2019) inducing the heat of non-polar compounds such as isoprene. Despite, the effect of conventional microwaves on the devulcanization of rubber, in the absence of solvents, has been reported, an advantage of using acids in the treatment of rubber is the possibility of releasing toxic compounds such as metals (Shakya et al., 2006). *A. ferrooxidans* decreases its catalytic activity as an iron oxidant in the presence of metals such as zinc (Cho et al., 2008), which is a common component in rubber, used as an activator of the vulcanization process (Adachi and Tainosho, 2004). The amount of nitric acid used in this study is low, so the contaminating effect of this solvent is not significant compared to conventional rubber digestion (for elemental analysis) where pure acid is used (Monadjemi et al., 2016). Therefore, dilute nitric acid for microwave usage, it seems promising treatment for rubber desulfurization. The desulfurization capacity of materials such as coal in an acidic medium and in the presence of microwaves has also been reported. Up to 97% of inorganic sulfur can be removed by acid washing in combination with microwaves. In the presence of microwaves, the binding energy of C-S is weakened, facilitating its breakdown in the presence of acids; this result has been verified by FTIR analysis (Tao et al., 2014). It is noteworthy to mention that a low acid concentration (1%) is used in the proposed chemical method, versus other described methods for treating rubber, which use high acid concentrations such as H_2SO_4 (95%). In addition, treatment with concentrated acid may require subsequent neutralization with base, which must also be in high concentrations (Cepeda-Jiménez et al., 2000; Alawais and West, 2019).

TABLE 2 | Elemental distribution of C, O and S on rubber particles after biological and chemical desulfurization treatments.

Treatment	C (%)	O (%)	S (%)	Si (%)
Biological	85.6	13.1	0.4	0.05
Chemical	91.1	6.9	0.1	0.38
Control	80.6	16.1	1.5	0.03

Analysis of Rubber Particles After Biological and Microwave Treatments

For the first time, the use of an aqueous phase during a microwave treatment is reported. Previously, authors have studied the effect on cross-linking using dried rubber and the microwave technique. Their results pointed out that cross-link densities after treatments were between 6.0×10^{-5} and 12.0×10^{-5} mol/cm^3, using temperatures of 72, 115, 146, 160, 200, and 220°C (de Sousa et al., 2017). Considering that the dissociation energy of the monosulfidic, disulfidic, and polysulfidic cross-links is between 268 and 285 kJ/mol; is less than the dissociation energy of a C-C bond with 351 kJ/mol (Formela et al., 2019). Rubber desulfurization by microwave advantages adjusting parameters such as power, temperature, and incubation time, is the energy consumption, since is less energy intense than other reported treatments (Moseley and Woodman, 2009; Grewal et al., 2013).

The presence of new bands in FTIR analysis after the biological treatment indicate surface transformations possibly associated with rubber-decomposition processes. It can be seen that the chemical treatment with the microwave was more effective since the low concentration of nitric acid that was used increased the porosity of the material, facilitating the diffusion of thermal energy to break down sulfur bonds and other components that are part of the rubber surface. Tao et al. (2014) using FTIR method, observed the loss of sulfur bonds after a desulfurization treatment in an acidic and microwave medium. In the present study, the treatment of rubber using microwaves, bands corresponding to the CH_2 groups (1,475–1,450 cm^{-1}) and

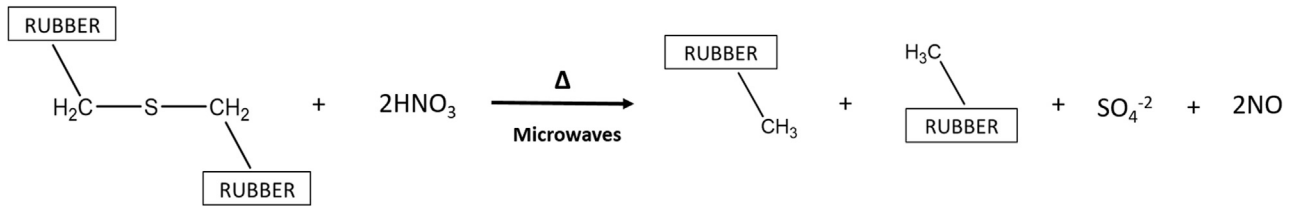

FIGURE 4 | Proposed mechanism for rubber desulfurization using HNO_3 and microwaves.

bands corresponding to the CH_3 group (1,390–1,372 cm^{-1}) are lost. This is a reliable indicator of the effectiveness of the microwave in combination with acid since, in the absence of acid, the persistence of these functional groups has been reported for microwave treatments (de Sousa et al., 2017). Moreover, losing bands near 1,096 cm^{-1} and 1,540 cm^{-1}, corresponding to ZnO and SiO_2 (Colom et al., 2016), respectively, demonstrates the capacity of this system to remove the metal oxide in the structure of the treated rubber. Analysis of the desulfurization processes by FTIR is not only useful for analyzing materials such as rubber: this technique has also been reported for monitoring different desulfurization processes as acid treatments in fuels such as kerosene, where the loss of functional groups of molecules such as mercaptans has been observed (Tao et al., 2014; Colom et al., 2016).

The SEM analysis has been used to demonstrate the changes in the rubber surface against mechanical, chemical or biological treatments (Li et al., 2012; Aboelkheir et al., 2019). In this study, SEM analysis reveal morphological changes of the analyzed rubber surface after biological and chemical treatments in comparison with the control. Both treatments methods used, show a particle size of approximately 500–1,000 μm, so the particle size is not influenced by the treatments carried out compared to a reported work (Li et al., 2012). The size reported in this work is compatible for the treatments of our study, facilitating its implementation in systems with lower-performance grinding. Samples observed at 500x show an increase in porosity after the chemical treatment of rubber, which is not observed in the rubber particle after the biological treatment. This result is also related to EDS analysis of C, O, S, and Si in the surface (**Table 2**), where the carbon and silicium content increases in the rubber particles subjected to the treatments, especially after the application of the chemical treatment. The opposite occurs with O and S, due to the fact of the increase of sulfates detected in the reaction mediums, probably as a result of a detachment from the rubber surface in addition to assimilation processes of these elements in the case of the biological treatment. Sulfur oxidation in *A. ferrooxidans* is a complex process that includes several enzymatic reactions, and some are still unknown (Zhan et al., 2019). It is proposed that there are oxidative mechanisms that allow the release of sulfur, transforming it to SO_2. When sulfur is used as a substrate in aerobic cultures of *A. ferrooxidans*, the oxidation of reducing inorganic sulfur is carried out by a sulfur dioxygenase (Zhang et al., 2016) and sulfite is formed. Sulfites is a necessary intermediate during the oxidation of reduced sulfur, which can be further oxidized by two different mechanisms (Hirose et al., 1991). One is the direct oxidation by the action of sulfite cytochrome c oxidoreductase and the other is an indirect oxidation to sulfate considering three sequential steps as indicated in the following equations (Zhan et al., 2019):

$$2\,SO_2^{-3} + 2AMP \rightarrow 2APS + 4e^-$$
$$(\text{APS reductase})\ (\text{Adenylyl-sulfate reductase})$$
$$2\,APS + 2Pi\ (2) \rightarrow 2ADP + 2SO2 - 4\,(\text{ADP sulfurylase})$$
$$2\,ADP \rightarrow AMP + ATP\ (\text{adenylate kinase})$$

The mechanism of desulfurization by microwaves in the presence of HNO_3 has not been reported, it is proposed that HNO_3 oxidize and remove S from rubber, obtaining SO_4 and NO as a product (**Figure 4**).

CONCLUSION

Rubber desulfurization was achieved through a biological process by the bacteria *A. ferrooxidans*, and a chemical process using microwaves with low nitric acid concentration. From the performed experiments it can be established that the chemical/microwave treatment was more effective than the biological treatment. This was corroborated when comparing the results regarding sulfate measurement (22.40 vs 1.06 (mg/L)/g of rubber), cross-link density (4.0×10^3 vs 6.5×10^3 (mol/cm^3)/g of rubber) for biological and chemical/microwave treatments respectively. Additionally, FTIR analysis showed clear rubber surface modification in terms of the available functional groups when both of the treatments were performed. Regarding the use of microwaves, it is worth noting the low amount of nitric acid (1%) used to promote strong structural changes in the rubber's surface, this is complemented by the SEM/EDS analysis that shows an increase in surface porosity and modification of the distribution of the C, O, S, and Si elements of the rubber. Finally, both biological and chemical methods could be used as industrial desulfurization processes. Combining these methods might potentially increase the rubber devulcanization result, which is needed for rubber recycling.

DATA AVAILABILITY STATEMENT

The original contributions presented in the study are included in the article/**Supplementary Material**, further inquiries can be directed to the corresponding author.

AUTHOR CONTRIBUTIONS

CV conducted the experiments, analyzed the data and drafted the manuscript. CH conducted the experiments helped in providing information and preparation of tables and figures. RM-V revised, corrected and commented on the manuscript. RA conceptualised, analyzed the data and edited the manuscript. All authors read and approved the final manuscript.

FUNDING

This research was financially supported by FONDECYT Grant 11190220 from ANID (Chile).

SUPPLEMENTARY MATERIAL

The Supplementary Material for this article can be found online at: https://www.frontiersin.org/articles/10.3389/fenvs.2021.633165/full#supplementary-material

REFERENCES

Aboelkheir, M. G., Bedor, P. B., Leite, S. G., Pal, K., Toledo Filho, R. D., and Gomes De Souza, F., Jr. (2019). Biodegradation of Vulcanized SBR: A Comparison between *Bacillus Subtilis, Pseudomonas aeruginosa* and *Streptomyces* Sp. *Scientific Rep.* 9, 19304. doi:10.1038/s41598-019-55530-y

Adachi, K., and Tainosho, Y. (2004). Characterization of Heavy Metal Particles Embedded in Tire Dust. *Environ. Int.* 30, 1009–1017. doi:10.1016/j.envint.2004.04.004

Alawais, A., and West, R. P. (2019). Ultra-violet and Chemical Treatment of Crumb Rubber Aggregate in a Sustainable concrete Mix. *J. Struct. Integrity Maintenance* 4, 144–152. doi:10.1080/24705314.2019.1594603

Andler, R. (2020). Bacterial and Enzymatic Degradation of Poly(cis-1,4-Isoprene) Rubber: Novel Biotechnological Applications. *Biotechnol. Adv.* 44, 107606. doi:10.1016/j.biotechadv.2020.107606

Asaro, L., Gratton, M., Seghar, S., and Aït Hocine, N. (2018). Recycling of Rubber Wastes by Devulcanization. *Resour. Conservation Recycling* 133, 250–262. doi:10.1016/j.resconrec.2018.02.016

Beard, S., Paradela, A., Albar, J., and Jerez, C. (2011). Growth of *Acidithiobacillus Ferrooxidans* ATCC 23270 in Thiosulfate under Oxygen-Limiting Conditions Generates Extracellular Sulfur Globules by Means of a Secreted Tetrathionate Hydrolase. *Front. Microbiol.* 2, 79. doi:10.3389/fmicb.2011.00079

Berekaa, M. M., Linos, A., Reichelt, R., Keller, U., and SteinbÃ¼chel, A. (2000). Effect of Pretreatment of Rubber Material on its Biodegradability by Various Rubber Degrading Bacteria. *FEMS Microbiol. Lett.* 184, 199–206. doi:10.1111/j.1574-6968.2000.tb09014.x

Bockstal, L., Berchem, T., Schmetz, Q., and Richel, A. (2019). Devulcanisation and Reclaiming of Tires and Rubber by Physical and Chemical Processes: A Review. *J. Clean. Prod.* 236, 117574. doi:10.1016/j.jclepro.2019.07.049

Bredberg, K., Andersson, B. E., Landfors, E., and Holst, O. (2002). Microbial Detoxification of Waste Rubber Material by wood-rotting Fungi. *Bioresour. Technol.* 83, 221–224. doi:10.1016/s0960-8524(01)00218-8

Cepeda-Jiménez, C. M., Pastor-Blas, M. M., Ferrándiz-Gómez, T. P., and Martín-Martínez, J. M. (2000). Surface Characterization of Vulcanized Rubber Treated with Sulfuric Acid and its Adhesion to Polyurethane Adhesive. *J. Adhes.* 73, 135–160. doi:10.1080/00218460008029303

Cho, K. S., Ryu, H. W., and Choi, H. M. (2008). Toxicity Evaluation of Complex Metal Mixtures Using Reduced Metal Concentrations: Application to Iron Oxidation by *Acidithiobacillus Ferrooxidans*. *J. Microbiol. Biotechnol.* 18, 1298–1307.

Chritiansson, M., Stenberg, B., Wallenberg, L. R., and Holst, O. (1998). Reduction of Surface sulphur upon Microbial Devulcanization of Rubber Materials. *Biotechnol. Lett.* 20, 637–642. doi:10.1023/a:1005306220566

Colom, X., Faliq, A., Formela, K., and Cañavate, J. (2016). FTIR Spectroscopic and Thermogravimetric Characterization of Ground Tyre Rubber Devulcanized by Microwave Treatment. *Polym. Test.* 52, 200–208. doi:10.1016/j.polymertesting.2016.04.020

de Sousa, F. D. B., Scuracchio, C. H., Hu, G.-H., and Hoppe, S. (2017). Devulcanization of Waste Tire Rubber by Microwaves. *Polym. Degrad. Stab.* 138, 169–181. doi:10.1016/j.polymdegradstab.2017.03.008

Didier, S., Michel, D., and Christopher, R. (2006). *Microwaves in Organic Synthesis*. Weinheim: Wiley VCH.

Dobrotă, D., and Dobrotă, G. (2018). An Innovative Method in the Regeneration of Waste Rubber and the Sustainable Development. *J. Clean. Prod.* 172, 3591–3599. doi:10.1016/j.jclepro.2017.03.022

Dzulkifli, A. I., Said, C. M. S., Han, C. C., and Mohd, A. F. (2016). "Rubber-Solvent Interaction Parameter (χ1, 2) of NR/SBR Rubber Blend Solution in Determination of Crosslink Concentration for Vulcanized Rubber Blend," in *Advanced Materials Research: Trans Tech Publ*, 75–81.

Formela, K., Hejna, A., Zedler, L., Colom, X., and Canavate, J. (2019). Microwave Treatment in Waste Rubber Recycling - Recent Advances and Limitations. *Express Polym. Lett.* 13, 565–588. doi:10.3144/expresspolymlett.2019.48

Ganchev, S. I., Bhattacharyya, J., Bakhtiari, S., Qaddoumi, N., Brandenburg, D., and Zoughi, R. (1994). Microwave Diagnosis of Rubber Compounds. *IEEE Trans. Microwave Theor. Techn.* 42, 18–24. doi:10.1109/22.265523

Ghosh, W., and Dam, B. (2009). Biochemistry and Molecular Biology of Lithotrophic Sulfur Oxidation by Taxonomically and Ecologically Diverse Bacteria and Archaea. *FEMS Microbiol. Rev.* 33, 999–1043. doi:10.1111/j.1574-6976.2009.00187.x

Gorassini, A., Adami, G., Calvini, P., and Giacomello, A. (2016). ATR-FTIR Characterization of Old Pressure Sensitive Adhesive tapes in Historic Papers. *J. Cult. Heritage* 21, 775–785. doi:10.1016/j.culher.2016.03.005

Grewal, A., Kumar, K., Redhu, S., and Bhardwaj, S. (2013). Microwave Assisted Synthesis: a green Chemistry Approach. *Int. Res. J. Pharm. Appl. Sci.* 3, 278–285.

Hirose, T., Suzuki, H., Inagaki, K., Tanaka, H., Tano, T., and Sugio, T. (1991). Inhibition of Sulfur Use by Sulfite Ion in Thiobacillus Ferrooxidans. *Agric. Biol. Chem.* 55, 2479–2484. doi:10.1271/bbb1961.55.2479

Holst, O., Stenberg, B., and Christiansson, M. (1998). Biotechnological Possibilities for Waste Tyre-Rubber Treatment. *Biodegradation* 9, 301–310. doi:10.1023/a:1008337708006

Jiang, G., Zhao, S., Luo, J., Wang, Y., Yu, W., and Zhang, C. (2010). Microbial Desulfurization for NR Ground Rubber by *Thiobacillus Ferrooxidans*. *J. Appl. Polym. Sci.* 116, 2768–2774. doi:10.1002/app.31904

Kabil, O., and Banerjee, R. (2012). Characterization of Patient Mutations in Human Persulfide Dioxygenase (ETHE1) Involved in H2S Catabolism. *J. Biol. Chem.* 287, 44561–44567. doi:10.1074/jbc.m112.407411

Kelly, D. P., and Wood, A. P. (2000). Reclassification of Some Species of Thiobacillus to the Newly Designated Genera Acidithiobacillus Gen. nov., Halothiobacillus Gen. Nov. And Thermithiobacillus Gen. Nov. *Int. J. Syst. Evol. Microbiol.* 50, 511–516. doi:10.1099/00207713-50-2-511

Larsen, M., Schultz, L., Glarborg, P., Skaarupjensen, L., Damjohansen, K., Frandsen, F., et al. (2006). Devolatilization Characteristics of Large Particles of Tyre Rubber under Combustion Conditions. *Fuel* 85, 1335–1345. doi:10.1016/j.fuel.2005.12.014

Li, Y., Zhao, S., and Wang, Y. (2012). Microbial Desulfurization of Ground Tire Rubber by Sphingomonas sp.: A Novel Technology for Crumb Rubber Composites. *J. Polym. Environ.* 20, 372–380. doi:10.1007/s10924-011-0386-1

Li, Y., Zhao, S., and Wang, Y. (2011). Microbial Desulfurization of Ground Tire Rubber by Thiobacillus Ferrooxidans. *Polym. Degrad. Stab.* 96, 1662–1668. doi:10.1016/j.polymdegradstab.2011.06.011

Liu, H., Wang, X., and Jia, D. (2020). Recycling of Waste Rubber Powder by Mechano-Chemical Modification. *J. Clean. Prod.* 245, 118716. doi:10.1016/j.jclepro.2019.118716

Ma, S., Yao, J., Jin, X., Cui, J., and Ma, J. (2011). Progress for thermal and Non-thermal Effects of Microwave Chemistry. *Chem. Bull./Huaxue Tongbao* 74, 41–46.

Mok, K., and Eng, A. (2018). Characterisation of Crosslinks in Vulcanised Rubbers: From Simple to Advanced Techniques. *Malaysian J. Chem.* 20, 118–127.

Monadjemi, S., Mcmahan, C. M., McMahan, C., and Cornish, K. (2016). Effect of Non-rubber Constituents on Guayule and Hevea Rubber Intrinsic Properties. *J. Res. Updates Polym. Sci.* 5, 87–96. doi:10.6000/1929-5995.2016.05.03.1

Moseley, J. D., and Woodman, E. K. (2009). Energy Efficiency of Microwave- and Conventionally Heated Reactors Compared at Meso Scale for Organic Reactions. *Energy Fuels* 23, 5438–5447. doi:10.1021/ef900598m

Mukherjee, S., and Borthakur, P. C. (2001). Chemical Demineralization/desulphurization of High sulphur Coal Using Sodium Hydroxide and Acid Solutions. *Fuel* 80, 2037–2040. doi:10.1016/s0016-2361(01)00094-1

Nawong, C., Umsakul, K., and Sermwittayawong, N. (2018). Rubber Gloves Biodegradation by a Consortium, Mixed Culture and Pure Culture Isolated from Soil Samples. *Braz. J. Microbiol.* 49, 481–488. doi:10.1016/j.bjm.2017.07.006

Ohshiro, T., Suzuki, K., and Izumi, Y. (1997). Dibenzothiophene (DBT) Degrading Enzyme Responsible for the First Step of DBT Desulfurization by Rhodococcus Erythropolis D-1: Purification and Characterization. *J. Ferment. Bioeng.* 83, 233–237. doi:10.1016/s0922-338x(97)80985-3

Pinheiro, F. C., Babos, D. V., Barros, A. I., Pereira-Filho, E. R., and Nóbrega, J. A. (2019). Microwave-assisted Digestion Using Dilute Nitric Acid Solution and Investigation of Calibration Strategies for Determination of as, Cd, Hg and Pb in Dietary Supplements Using ICP-MS. *J. Pharm. Biomed. Anal.* 174, 471–478. doi:10.1016/j.jpba.2019.06.018

Sattler, S. A., Wang, X., Lewis, K. M., Dehan, P. J., Park, C.-M., Xin, Y., et al. (2015). Characterizations of Two Bacterial Persulfide Dioxygenases of the Metallo-β-Lactamase Superfamily. *J. Biol. Chem.* 290, 18914–18923. doi:10.1074/jbc.m115.652537

Scuracchio, C. H., Waki, D. A., and Da Silva, M. L. C. P. (2007). Thermal Analysis of Ground Tire Rubber Devulcanized by Microwaves. *J. Therm. Anal. Calorim.* 87, 893–897. doi:10.1007/s10973-005-7419-8

Shakirullah, M., Ahmad, I., Ahmad, W., and Ishaq, M. (2010). Desulphurization Study of Petroleum Products through Extraction with Aqueous Ionic Liquids. *J. Chilean Chem. Soc.* 55, 179–183. doi:10.4067/s0717-97072010000200007

Shakya, P. R., Shrestha, P., Tamrakar, C. S., and Bhattarai, P. (2006). Studies and Determination of Heavy Metals in Waste Tyres and Their Impacts on the Environment. *Pakistan J. Anal. Chem.* 7, 70–76.

Sienkiewicz, M., Janik, H., Borzędowska-Labuda, K., and Kucińska-Lipka, J. (2017). Environmentally Friendly Polymer-Rubber Composites Obtained from Waste Tyres: A Review. *J. Clean. Prod.* 147, 560–571. doi:10.1016/j.jclepro.2017.01.121

Soleimani, M., Bassi, A., and Margaritis, A. (2007). Biodesulfurization of Refractory Organic Sulfur Compounds in Fossil Fuels. *Biotechnol. Adv.* 25, 570–596. doi:10.1016/j.biotechadv.2007.07.003

Stevenson, K., Stallwood, B., and Hart, A. G. (2008). Tire Rubber Recycling and Bioremediation: A Review. *Bioremediation J.* 12, 1–11. doi:10.1080/10889860701866263

Subramaniam, A. (1987). "Natural Rubber," in *Rubber Technology*. Editor M. Morton (Boston, MA: Springer US), 179–208. doi:10.1007/978-1-4615-7823-9_6

Sugio, T., Taha, T. M., and Takeuchi, F. (2009). Ferrous Iron Production Mediated by Tetrathionate Hydrolase in Tetrathionate-, Sulfur-, and Iron-GrownAcidithiobacillus ferrooxidansATCC 23270 Cells. *Biosci. Biotechnol. Biochem.* 73, 1381–1386. doi:10.1271/bbb.90036

Sun, B., Du, Z., Cao, H., Du, L., and Yu, W. (2017). Oxidation-grafting Surface Modification of Waste Silicone Rubber Composite Insulator Powder: Characterizations and Properties of EPDM/modified Waste Powder Composites. *J. Appl. Polym. Sci.* 134, 45438. doi:10.1002/app.45438

Tano, T., Kitaguchi, H., Harada, M., Nagasawa, T., and Sugio, T. (1996). Purification and Some Properties of a Tetrathionate Decomposing Enzyme fromThiobacillus Thiooxidans. *Biosci. Biotechnol. Biochem.* 60, 224–227. doi:10.1271/bbb.60.224

Tao, X., Xu, N., Xie, M., and Tang, L. (2014). Progress of the Technique of Coal Microwave Desulfurization. *Int. J. Coal Sci. Technol.* 1, 113–128. doi:10.1007/s40789-014-0006-5

Valdes, J., Pedroso, I., Quatrini, R., Dodson, R. J., Tettelin, H., Blake, R., 2nd, et al. (2008). Acidithiobacillus Ferrooxidans Metabolism: from Genome Sequence to Industrial Applications. *BMC Genomics* 9, 597. doi:10.1186/1471-2164-9-597

Vishniac, W., and Santer, M. (1957). The Thiobacilli,. *Bacteriol. Rev.* 21, 195–213. doi:10.1128/br.21.3.195-213.1957

Wang, R., Lin, J.-Q., Liu, X.-M., Pang, X., Zhang, C.-J., Yang, C.-L., et al. (2019). Sulfur Oxidation in the Acidophilic Autotrophic Acidithiobacillus Spp. *Front. Microbiol.* 9, 3290. doi:10.3389/fmicb.2018.03290

Yang, X., Shen, A., Li, B., Wu, H., Lyu, Z., Wang, H., et al. (2020). Effect of Microwave-Activated Crumb Rubber on Reaction Mechanism, Rheological Properties, thermal Stability, and Released Volatiles of Asphalt Binder. *J. Clean. Prod.* 248, 119230. doi:10.1016/j.jclepro.2019.119230

Yu, Y., Liu, X., Wang, H., Li, X., and Lin, J. (2014). Construction and Characterization of tetH Overexpression and Knockout Strains of *Acidithiobacillus Ferrooxidans*. *J. Bacteriol.* 196, 2255–2264. doi:10.1128/jb.01472-13

Zhan, Y., Yang, M., Zhang, S., Zhao, D., Duan, J., Wang, W., et al. (2019). Iron and Sulfur Oxidation Pathways of *Acidithiobacillus Ferrooxidans*. *World J. Microbiol. Biotechnol.* 35, 60. doi:10.1007/s11274-019-2632-y

Zhang, R., Wei, D., Shen, Y., Liu, W., Lu, T., and Han, C. (2016). Catalytic Effect of Polyethylene Glycol on Sulfur Oxidation in Chalcopyrite Bioleaching by *Acidithiobacillus Ferrooxidans*. *Minerals Eng.* 95, 74–78. doi:10.1016/j.mineng.2016.06.021

Zhong, B., Jia, Z., Hu, D., Luo, Y., Guo, B., and Jia, D. (2016). Surface Modification of Halloysite Nanotubes by Vulcanization Accelerator and Properties of Styrene-Butadiene Rubber Nanocomposites with Modified Halloysite Nanotubes. *Appl. Surf. Sci.* 366, 193–201. doi:10.1016/j.apsusc.2016.01.084

Conflict of Interest: The authors declare that the research was conducted in the absence of any commercial or financial relationships that could be construed as a potential conflict of interest.

frontiers in Environmental Chemistry

ORIGINAL RESEARCH
published: 20 September 2021
doi: 10.3389/fenvc.2021.729779

The Effect of Heterogeneity on the Distribution and Treatment of PFAS in a Complex Geologic Environment

Rick McGregor[1]* *and Leticia Benevenuto*[2]

[1]InSitu Remediation Services Ltd., St George, ON, Canada, [2]InSitu Remediation Services Ltd., Campina, Brazil

Per-and polyfluoroalkyl substances (PFAS) have been identified as emerging contaminants of concern in the environment in a wide variety of media including groundwater. Typically, PFAS-impacted groundwater is extracted by pump and treat systems and treated using sorptive media such as activated carbon and ion exchange resin. Pump and treat systems are generally considered ineffective for the remediation of dissolved phase contaminants including PFAS but instead are considered applicable for plume containment. An alternative to pump and treat is *in-situ* treatment. The demonstrated use of *in-situ* treatment for PFAS-impacted groundwater is limited with only colloidal activated carbon (CAC) being shown to effectively attenuate PFAS over short and moderate time periods. Active research topics for the *in-situ* treatment of PFAS include the effect of heterogeneity on the distribution of the CAC, the lifespan of the CAC itself, the effect of competitive adsorption/absorption, and the effect of other geochemical conditions on the removal process. This study looked at the effect of heterogeneity on the distribution of CAC and subsequent treatment of PFAS at a site with a multiple aquifer system. The site's geology varied from a silty sand to sand to fractured bedrock with all three units being impacted by PFAS and benzene (B), toluene (T), ethylbenzene (E), and xylene (X). Parameters evaluated included the distribution of the CAC as well as the subsequent treatment of the PFAS and BTEX. Results of groundwater sampling indicated that the PFAS detected within the groundwater were treated effectively to below their respective reporting limits for the duration of the 1-year test in both the silty sand and sand aquifers. The PFAS in the fractured rock aquifer showed a different treatment profile with longer carbon chained PFAS being attenuated preferentially compared to the shorter carbon chained PFAS. These results suggest that competitive sorptive reactions were occurring on the CAC within the fractured rock. Analysis of the unconsolidated aquifer materials determined that direct push injection of the CAC was effective at delivering the CAC to the target injection zones with post-injection total organic carbon (TOC) concentrations increasing by up to three orders of magnitude compared to pre-injection TOC concentrations. Heterogeneity did have an impact on the CAC distribution with higher hydraulic conductivity zones receiving more CAC mass than lower hydraulic conductivity zones.

Keywords: PFAS, BTEX, colloidal, activated carbon, in-situ, groundwater, remediation

Edited by:
Balaji Seshadri,
The University of Newcastle, Australia

Reviewed by:
Chin Wei Lai,
University of Malaya, Malaysia
Xianqiang Yin,
Northwest A and F University, China

***Correspondence:**
Rick McGregor
rickm@irsl.ca

Specialty section:
This article was submitted to Sorption Technologies, a section of the journal Frontiers in Environmental Chemistry

Received: *23 June 2021*
Accepted: *07 September 2021*
Published: *20 September 2021*

Citation:
McGregor R and Benevenuto L (2021) The Effect of Heterogeneity on the Distribution and Treatment of PFAS in a Complex Geologic Environment. Front. Environ. Chem. 2:729779. doi: 10.3389/fenvc.2021.729779

INTRODUCTION

The *in-situ* treatment of groundwater impacted by petroleum hydrocarbons and chlorinated solvents is well established (Interstate Technology and Regulatory Council ITRC, 2005; Huling and Pivetz, 2006; Petri et al., 2011; Usman et al., 2012; Sra et al., 2013; Kashir and McGregor, 2015; Saeed et al., 2021) with *in-situ* chemical oxidation (ISCO), *in-situ* chemical reduction (ISCR), and enhanced bioremediation (EBR) being the most applied.

The *in-situ* treatment of emerging compounds of concern such as per and polyfluoroalkyl substances (PFAS), synthetic dyes and synthetic musks have become a topic of interest over the past few years as stakeholders look for more economical and technically feasible options for treating groundwater impacted by these compounds (McGregor, 2018; McGregor and Maziarz, 2021; McGregor and Zhao, 2021; McGregor and Carey, 2019). The emerging compounds of concern that have garnered the most attention is the PFAS with most studies focused on the above-ground treatment. Simon (2020) estimated that there may be greater than 42,000 PFAS-impacted sites around the world which could cost over $80 billion to address. The *in-situ* treatment of PFAS is limited to a few field studies (Darlington et al., 2018; Interstate Technology and Regulatory Council ITRC, 2018; McGregor, 2018; Ross et al., 2018; McGregor, 2020a; McGregor and Zhao, 2021). The treatment of PFAS-impacted groundwater is complex due to numerous physical and chemical factors. These include PFAS' resistance to biological and chemical degradation due to the strong carbon-fluoride bonding (National Ground Water Association National Ground Water Association Press, 2017); the low regulatory guidelines for treatment; poorly understood environmental fate and transport processes; and limited proven remedial approaches (Simon et al., 2019). These factors combined with other technical challenges including distribution, required contact between the PFAS and the remedial reagent, and back/matrix diffusion can all influence the outcome of *in-situ* treatment.

Laboratory and field studies for the *in-situ* treatment of dissolved PFAS have focused on using sorptive media for the removal of the PFAS with chemical oxidation also being evaluated. (Higgins and Luthy, 2006; Park et al., 2016; Bruton and Sedlak., 2017; Eberle et al., 2017; Dombrowski et al., 2018; McGregor, 2018; Aly et al., 2019; Barajas, 2019; Carey and McGregor, 2019; McGregor, 2020a; Interstate Technology and Regulatory Council ITRC, 2020; Liu et al., 2020; McGregor and Zhao, 2021). Sorptive media for the *in-situ* treatment of dissolved PFAS is limited by the amount of sorptive capacity of the media itself (Higgins and Luthy, 2006; Yu et al., 2009; Carter and Farrell, 2010). In the case of activated carbon, the mass of PFAS removed is a function of the activated carbon's surface area. Xiao et al. (2017) determined that while granular and powdered activated carbon were effective over the short and moderate term at removing various PFAS. Particle size had a significant influence on breakthrough with powdered activated carbon having a longer breakthrough time than granular activated carbon (Xiao et al., 2017). Other factors affecting the effectiveness of activated carbon include the type of carbon being used (i.e., coal vs. plant based); the ratio of macro, meso, and micropores of the activated carbon; and the hydrophobicity of the individual PFAS. Other limitations include the delivery method and resulting distribution of the remedial reagents. To overcome some of these limitations, a colloidal form of activated carbon was developed for the injection into the subsurface. Colloidal activated carbon offers advantages over powdered and granular due to its smaller particle size making it easier to inject while having a larger surface area and sorptive capacity on a unit weight basis compared to granular and powdered activated carbon.

Colloidal transport within unconsolidated and fractured geologic media has shown that various colloids can be present within groundwater including inorganic and organic colloids. The transport of colloids within groundwater is controlled by advection and diffusion (De Jong et al., 2004; Frimmel et al., 2007). The advantages of using colloidal reagents for *in-situ* remediation include the ease of injection compared to powdered/granular reagent forms (i.e., less pressure required) and potentially larger areas of influence.

McGregor (2020a, 2020b) demonstrated that CAC could be effectively delivered to the target injection areas using direct push technology (DPT) with greater than 90 percent of the targeted aquifers having CAC being measured within the solids. Coarse-grained materials such as powdered activated carbon (PAC), ion exchange resin and biochar were significantly affected by heterogeneities within the aquifer which subsequently impacted the performance of the media. Specifically, the remedial reagents preferentially accumulated in higher hydraulic conductivity zones when compared to zones of lower hydraulic conductivity. The heterogenetic distribution of the various reagents was determined to be a result of the particle size of the reagents with reagents greater than 10 microns being heavily influenced by heterogeneities within the aquifers. Other concerns with using sorptive media for PFAS removal include competition between the PFAS and other organic and inorganic compounds within the groundwater. In addition to matrix-diffusion and desorption issues in heterogeneous geologic materials over the long term (Carey et al., 2015; Carey and McGregor, 2019).

Limited *in-situ* field studies using colloidal sorptive media for the removal of PFAS suggests that over short and moderate time, PFAS can be removed from solution to below regulatory requirements. McGregor (2020a, 2018) showed that CAC is effective at removing both PFAS and other organic compounds of concern including benzene (B), toluene (T), ethylbenzene (E), xylene (X), gasoline, and diesel range petroleum hydrocarbons (GRO and DRO). McGregor and Zhao (2021) demonstrated at a site with trichloroethene (TCE) and its dichlorination by-products; 1.2 cis dichloroethene (1,2 DCE), and vinyl chloride could be treated to regulatory requirements within a moderately heterogenetic aquifer system. Numerical modeling of field data by Carey and McGregor (2019) estimated that CAC would be effective at controlling back/matrix diffusion reactions over several decades.

The use of CAC in complex geologic settings for treatment of PFAS is not well demonstrated in the literature. McGregor (2018)

demonstrated that CAC could be injected into an unconsolidated silty sand aquifer containing a seam of higher hydraulic conductivity sand. The unconfined aquifer was impacted by petroleum hydrocarbons and PFAS. Testing of the aquifer solids, post injection, indicated that the CAC was effectively distributed within the target injection zone. Monitoring of the groundwater over a 5-year period showed that the various PFAS detected within the groundwater prior to the injection of the CAC remain below their respective reporting limits. Numerical modeling of the results of the study by Carey and McGregor (2019) predicted that the CAC would continue to remove the PFAS from the groundwater for decades indicating that processes such as back and matrix diffusion could be effectively controlled at this site.

McGregor (2020a) completed a field study within a sand aquifer using a series of six reactive zones with each zone testing a unique reagent including CAC, PAC, ion exchange resin, biochar, hydrogen peroxide, and sodium persulphate. The results of the 18-months study indicated that the CAC removed the relevant PFAS to below their respective reporting limits whereas the oxidants were not effective at attenuating the PFAS. The PAC, ion exchange resin, and biochar were partially effective at removing the relevant PFAS, however lower carbon chained PFAS (i.e., C4 and C5) was measured downgradient of the reactive zones. The PFAS within the groundwater broke though downgradient due to poor reagent distribution, related to grain size. McGregor and Zhao (2021) implemented a field study involving the injection of CAC in an unconfined silty sand aquifer containing a higher hydraulic conductivity sand lens. The groundwater was impacted by PFAS, TCE, and its dichlorination by-products; 1,2 DCE, and vinyl chloride. The study showed that the CAC could be effectively injected and distributed into the target injection zone. Subsequent monitoring of the groundwater determined that the relevant PFAS and chlorinated ethenes were removed to below their reporting limits over the 24-months monitoring period.

While the aquifers at these sites were mildly heterogenetic, the PFAS were contained within a single aquifer and thus represented a relatively simplistic hydrogeologic/geologic system. The use of CAC to treat PFAS within complex multiple aquifer systems remains unstudied with no peer-reviewed literature available to date. This study evaluated the effectiveness of treating PFAS in a three-aquifer system that had a complex geologic environment consisting of a silty sand till, alluvial sand unit and a fractured dolostone bedrock. The objectives of the study were to determine if CAC could be effectively distributed within a three-aquifer system and effectively treat various PFAS within the groundwater over a short and moderate period.

SITE DESCRIPTION

The study site is in Central Canada at a small industrial location that was the scene of a fire in which fire-fighting foam was used to suppress the fire. The foam contained various PFAS which were released to the shallow groundwater during and following fire suppression operations. The site is underlain by an approximately 6-m (m) thick layer of glacial till dominated by silty sand. A thin (~0.05 m) sandy layer occurs within the silty sand at a depth of approximately 4 m below ground surface (mbgs). Underlying the silty sand till is a medium grained sand unit that is up to 3 m thick. The sand unit overlies a fractured dolostone bedrock. The site acts as a groundwater recharge area with the water table situated within the silty sand till unit at a depth of approximately 2.5 mbgs.

METHODOLOGY

The characterization and monitoring of the site was completed with the aid of a series of multilevel wells and continuous cores. The groundwater was monitored using three CMT Multilevel Systems (Solinst, Canada) including one 3-channel system and two 7-channel systems (**Figure 1**). In addition to the CMT systems, three 0.07-m diameter boreholes were advanced into the shallow bedrock to a depth of 15 mbgs to allow for determination of fracture locations, hydraulic conductivity testing, and subsequent groundwater sampling. The bedrock boreholes were cased and cemented into the shallow bedrock with the bedrock annulus being left open to allow for the installation of inflatable packers (RST Instruments, Canada) (**Figure 1**). The boreholes for the CMT systems were drilled using 0.2 m-diameter hollow-stem augers with the 0.15-m long CMT screens being surrounded by coarse silica sand and sealed above and below each screen with hydrated bentonite.

To characterize the groundwater prior to and post-injection, groundwater samples were collected for analyses of various chemical parameters including PFAS, BTEX, major cations [calcium (Ca), magnesium (Mg]) potassium (K), sodium (Na), iron (Fe)], manganese [Mn], and anions [chloride (Cl), nitrate (NO_3), and sulfate (SO_4)] using low-flow sampling methods (Puls and Barcelona, 1996). The major cations were analyzed following United States Environmental Protection Agency (US EPA) Method 3010D which employs inductively coupled plasma optical emission spectroscopy (ICP/OES). Iron and Mn were analyzed using modified EPA 200.8 methodology employing inductively coupled plasma mass spectrometry (ICP/MS). The anions were analyzed following method SM 4100B using ion chromatography (IC). The PFAS concentrations were determined using solid phase extraction/liquid chromatography mass spectrometric detection (SPE/LCMS). The BTEX concentrations were measured using gas chromatography with mass spectrometric detection (GC/MS).

Select chemical parameters, including pH, oxidation-reduction potential (ORP), temperature, specific conductivity, turbidity, and dissolved oxygen (DO), were measured at the wellhead using a flow-through cell connected to a YSI Professional Plus hand-held multi-parameter meter (YSI; Yellow Springs, Ohio). The pH meter was calibrated to solutions of 4.0, 7.0, and 10.0 standard units prior to each sampling event, whereas the ORP was checked with Zobell's solution (Nordstrom, 1977) prior to each sample measurement. Specific conductivity was calibrated to a National Institute of Standards and Technology (NIST) traceable standard solution. The samples for anions, PFAS and BTEX analyses were not filtered, whereas samples for alkalinity and dissolved cations were filtered with a 0.45-micron cellulose acetate membrane.

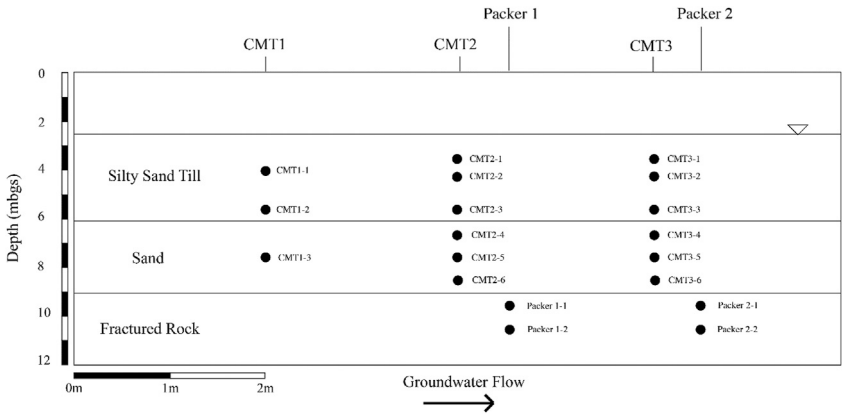

FIGURE 1 | Cross sectional view of test area showing monitoring locations.

The cation samples were acidified to pH below 2 with nitric acid (HNO_3). Groundwater samples for PFAS and BTEX analysis were collected on seven occasions: 7 days prior to (Day -7) and on 182-, 273-, and 366-days post injection (Day 182, Day 273, and Day 366). Samples for the inorganic and general chemistry were collected on the Day-7 and Day 366 sampling events.

Horizontal hydraulic conductivity (K_H) estimates within the overburden aquifers were completed using a flexible wall permeameter (ASTM International Inc. ASTM, 2016). Aquifer samples were collected using continuous cores, subdivided into 0.15 to 0.20 m-long samples. Estimates of the K_H for the shallow bedrock were completed using straddle packers. Half-metre-long intervals of the bedrock boreholes were tested using constant head methods to determine K_H with depth within each borehole. The K_H tests for the three aquifers were completed under constant-head conditions using site groundwater.

Prior to testing for K_H, samples of each core were collected for analysis of total organic carbon (TOC) to determine the organic matter content of the silty sand and sand aquifers prior to the injection. Additional cores were collected from the injection area 3 days post-injection to determine the distribution of the CAC. The samples were submitted to a commercial laboratory for TOC analysis following the combustion methods outlined by ASTM (ASTM International Inc. ASTM, 2011 and 2013). Cores of the fractured bedrock aquifer were collected pre- and post-injection of the CAC, however, due to the introduction of water during drilling operations, the CAC within the fracture zones was flushed away, thus making analysis for TOC inaccurate.

The CAC used in this study is sold under the brand name PlumeStop™ (Regenesis, San Clemente, CA). PlumeStop™ is a mixture of CAC and an organic carbon substrate that biodegrades over a short period of time. Once the substrate biodegrades, the CAC drops out of solution and coats the aquifer solids. The injection event was conducted over a 1-week period and involved the injection of 30,000 L (L) of CAC solution at 20 locations within the silty sand and sand aquifers. The number of injection locations was based on a 2.5 m grid spacing. At each location, the solution was injected over five vertical intervals to ensure vertical coverage of the two aquifers. The CAC was injected into the unconsolidated aquifers using DPT which delivered the CAC solution to the targeted injection areas via advective transport over the short term (i.e., minutes). Monitoring of the groundwater post injection indicated that the organic substrate degraded within 4 weeks of injection suggesting that the CAC was dispersed within the aquifer by advection processes during the injection event. The volume of solution was estimated based on an estimated pore volume of approximately 60,000 L with a replacement volume of 50 percent being targeted (i.e., 30,000 L). The ten-weight percent CAC solution was injected at flow rates ranging from 9.8 to 14.6 L/min (LPM) at pressures of up to 45 pounds per square inch (psi). The flow rate and pressure used during the injection program was minimized to reduce the possibility of hydraulic fracturing within the unconsolidated geologic media. Fracturing of the media can result in heterogenetic distribution of the reagents resulting in incomplete treatment of the PFAS (McGregor, 2020b). Within the bedrock, approximately 500 kg of CAC solution was injected at each of the six interval/packer during the week-long injection (**Figure 1**). Advection under injection and groundwater flow conditions are considered the dominant delivery mechanisms for the CAC solution within the fractured bedrock.

RESULTS

Hydrogeology

The water table at the site was measured over the 1-year monitoring period to be at a mean depth of approximately 2.5 mbgs. The water table varied up to a 0.11 m during the observation period. The aquifers are unconfined and the area acts as a groundwater recharge area with vertical hydraulic gradients averaging 0.018 downwards during the testing period.

Three continuous cores of the silty sand till and sand units were collected and subdivided for K_H analysis using a flexible wall permeameter. A total of 42 samples were tested with 18 being measured from the sand aquifer and the 24 being tested from the silty sand aquifer. Within the silty sand aquifer, a thin (~0.05 m) seam of sand was present within all three cores at a depth of

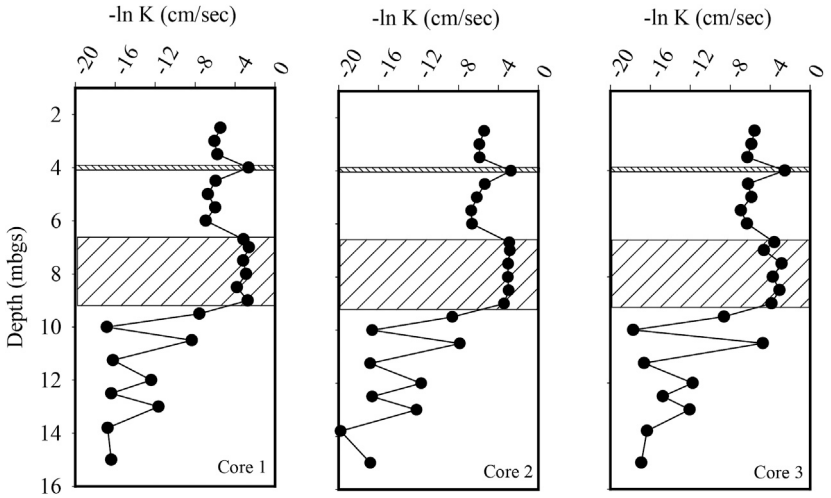

FIGURE 2 | Horizontal hydraulic conductivity (K_H) profiles within the three-aquifer system. The hatched area represents sand aquifer which is overlain by a silty sand till and underlain by a fractured dolostone.

approximately 4.0 mbgs. The geometric mean K_H of the silty sand aquifer was 3.5 x 10^{-3} cm per second (cm/sec). The K_H ranged from 9.7 x 10^{-4} cm/s to 8.0 x 10^{-2} cm/s with the highest K_H values being associated with the sand seam (**Figure 2**). The K_H geometric mean for the sand aquifer was 3.9 x 10^{-2} cm/s, ranging from 9.8 x 10^{-3} cm/s to 7.3x10^{-2} cm/s (**Figure 2**). The mean horizontal hydraulic gradient across the injected area was 0.003 during the test period. Based on these measured K_H values and an assumed effective porosity of 0.2, the mean horizontal groundwater flow velocity was calculated to range from 12 m/year in the silty sand unit to 220 m/year in the sand unit.

To characterize the hydrogeology of the underlying fractured dolostone bedrock, three boreholes were advanced to a depth of 15 mbgs. The boreholes were cased through the overburden and then left open to allow for testing by a two-packer system that allowed for the isolation of 0.5 m long sections of the borehole. A total of 27 tests were conducted with the results shown in **Figure 2**. The tests identified three fracture zones located at 9.5, 10.5, and 12 mbgs, with the K_H ranging from 4.1 x 10^{-6} to 8.9 x 10^{-3} cm/s within the fracture zones. In the bedrock with no interpreted fractures the K_H geometric mean was 1.1 x 10^{-7} cm/s (**Figure 2**).

Distribution of Colloidal Activated Carbon

For successful *in-situ* treatment of PFAS to occur, the CAC must be distributed effectively within the aquifer to maximize contact between the CAC and the PFAS. At this site, the CAC was injected into the silty sand and sand aquifers using direct push technology. Within the bedrock, the CAC solution was injected into the fractured rock aquifer using pneumatic packers within the wells. Distribution of CAC is dominated by advection during the injection process. While diffusive-based transport of the CAC can occur, it is considered insignificant compared to advection at this site. Based on visual observations during the monitoring period, the CAC remained in solution for less than 4 weeks in the unconsolidated aquifers and less than 90 days within the fractured rock aquifer.

Prior to the injection of the CAC, three cores of the silty sand and sand aquifers were collected to determine the TOC concentration of the aquifer solids. The TOC concentration within the 24 samples collected from the silty sand aquifer ranged from the detection limit of 0.5–0.6 g per kilogram (g/kg), averaging 0.53 g/kg (SD = 0.04 g/kg) (**Figure 3**). Following the injection of the CAC solution, three additional cores of the aquifer were collected with the mean TOC concentration of the 24 samples being calculated to be 8.1 g/kg (SD = 2.50 g/kg) within the silty sand aquifer (**Figure 3**). Overall, the mean concentration of TOC within the silty sand aquifer increased by approximately 1,300 percent following the injection of the CAC solution. Post-injection, the highest TOC concentrations were measured in the three sand seam samples at a depth of approximately four mbgs with an average TOC concentration of 13.0 g/kg being calculated. The mean TOC concentration of the remaining 21 silty sand samples averaged 7.4 g/kg indicating that the CAC preferentially accumulated within the sand seam during the injection process by 74 percent on average.

Total organic carbon concentrations determined from the 18 sand aquifer samples averaged 0.52 g/kg (SD = 0.04 g/kg) prior to the injection of the CAC (**Figure 3**). Following the injection of the CAC solution, the mean TOC concentration increased to 7.99 g/kg (SD = 1.03 g/kg) for the 18 samples collected from the aquifer (**Figure 3**). This represents an increase of 1,430 percent in TOC concentration, similar to what was calculated for the overlying silty sand aquifer.

Due to sampling and analytical challenges, no analysis of TOC was completed on the bedrock samples.

General Chemistry

To establish if the injection of CAC altered the overall groundwater geochemical conditions within the three aquifers, pre and post-injection groundwater samples were collected from

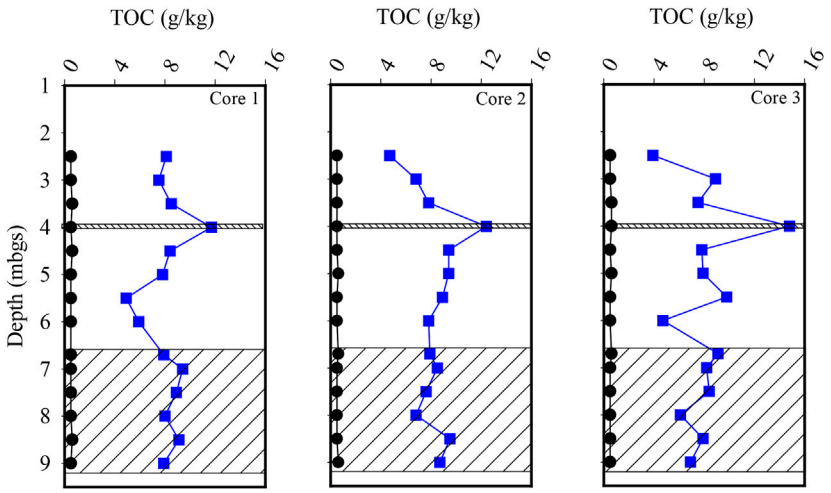

FIGURE 3 | Vertical profiles of total organic carbon within the silty sand and sand (hatched) aquifers. The black circles represent pre-injection results, and the blue squares represent post-injection results.

the three aquifers. Groundwater sampling was conducted on two occasions, on Day -7 (pre injection) and on Day 366 (post injection) and analyzed for various inorganic and general chemical parameters including pH, ORP, dissolved oxygen, chloride, nitrate, sulphate, dissolved iron, dissolved manganese, and alkalinity.

Prior to the injection of the CAC solution, the mean pH of the groundwater collected from the 20 monitoring points within the silty sand and sand aquifers were 6.98 and 6.58, respectively. The pH of the groundwater sampled from the four bedrock monitoring points averaged 7.12.

One year after the injection of the CAC, the mean pH of the groundwater sampled from the eight sampling locations within the silty sand aquifer was 6.99 vs. a mean pH of 6.61 for groundwater collected from the six sampling locations within the sand aquifer where the CAC was injected. The mean pH of the four monitoring points within the fractured rock aquifer was 7.18 following the injection of the CAC solution.

Corresponding to the increase in the mean pH of the three aquifers following the CAC injection were increases in the groundwater alkalinity. Prior to the injection of the CAC within the silty sand and sand aquifers, the mean alkalinity of the groundwater was 420 and 357 mg/L (as $CaCO_3$), respectively. Following the injection of the CAC solution, the mean alkalinity of the groundwater sampled from the silty sand and sand aquifers was 435 and 411 mg/L (as $CaCO_3$), respectively. The mean alkalinity of the groundwater sampled from the four sampling locations within the shallow bedrock was 187 mg/L (as $CaCO_3$) prior to the injection of the CAC. Following injection of the CAC, the mean alkalinity increased to 214 mg/L (as $CaCO_3$) on Day 366. The increased alkalinity within the three aquifers is attributed to buffering reactions associated with increased biological activity due to the addition of the organic carbon-based CAC substrate and the subsequent reactions between the organic matter and nitrate within the groundwater in a biological-mediated denitrification reaction such as:

$$5CH_2O + 4NO_{3^-} \rightarrow 2N_2 + 4HCO_{3^-} + CO_2 + 3H_2O \quad (1)$$

Concentrations of dissolved iron and manganese decreased following the injection of the CAC within all three aquifers. Prior to the injection of the CAC, the mean dissolved iron and manganese concentrations in groundwater sampled from the silty sand aquifer were 1.9 and 0.5 mg/L, respectively. The mean dissolved iron and manganese concentrations within the sand aquifer were 1.51 and 0.48 mg/L, respectively. Mean dissolved iron concentrations measured on Day 366 within the silty sand and sand aquifers were 0.5 and 1.2 mg/L, respectively. The dissolved manganese concentrations on Day 366 were determined to be less than the reporting limit of 0.005 mg/L for both aquifers. The decrease in dissolved iron and manganese within the groundwater is thought to be the results of sulphide mineral precipitation due to sulphate reduction reactions. Sulphate was detected within the silty sand, sand, and bedrock aquifers at mean concentrations of 2.9, 5.8, and 15.8 mg/L, respectively, on sampling event Day -7. On sampling event Day 366, sulphate mean concentrations were determined to be less than the reporting limit of 0.5 mg/L in all three aquifers, suggesting that sulphate reducing reactions were occurring post injection of CAC. This decrease in sulphate within the groundwater which corresponded to decreases in dissolved iron and manganese, is attributed to sulphate reduction reactions and the subsequent precipitation of sulphide minerals. The reduction of sulphate by organic matter is illustrated through the following reactions:

$$\text{Organic Matter} + SO_4^{2-} \rightarrow S^{2-} + H_2O + CO_2 \quad (2)$$

$$Fe^{2+} + HS^- \rightarrow FeS_{(S)} + H^+ \quad (3)$$

The acidity produced in these reactions is buffered by the carbonate minerals present within the aquifer including dolomite ($MgCa(CO_3)_2$) and calcite ($CaCO_3$) as measured by the increase in alkalinity post injection. Corresponding to the detection of dissolved iron and manganese within the three aquifers was the

presence of reducing geochemical conditions as reflected by the ORP. Prior to the injection of the CAC, the mean ORP measured for the silty sand, sand, and bedrock aquifers was −126, −147, and 45 mV, respectively, Following the injection of the CAC, the mean ORP for the silty sand, sand, and bedrock aquifers decreased to −155, −186, and −125, respectively. The decrease in ORP is likely the result of the addition of organic carbon associated with CAC. Nitrate was not detected within any monitoring wells prior to or post injection of the CAC.

TABLE 1 | Summary of maximum concentrations of detected PFAS within the three aquifers prior to the injection of the CAC. All units ng/L.

PFAS	Silty sand	Sand	Fractured rock
PFBA	6,405	840	175
PFPeA	24,000	12,450	850
PFHxA	15,740	3,125	250
PFHxS	<2	<2	4.2
PFHpA	7,250	<2	85
PFOA	520	910	24
PFOS	<2	2,105	75
PFNA	165	<2	3.4
PFBS	<2	<2	6.5

The results of the general chemistry groundwater sampling suggests that prior to the injection of the CAC the groundwater within the three aquifers was buffered by carbonate minerals at a near neutral pH. The aquifers were reducing in nature, most likely the result of the presence of petroleum hydrocarbons, which have depleted most electron acceptors such as oxygen, nitrate, and sulphate. The addition of the CAC and its associated organic-carbon carrier fluid, appears to have enhanced the reducing conditions of the three aquifers and further promoted the reduction of sulphate in the groundwater. Resulting in the presumed precipitation of iron and manganese sulphide

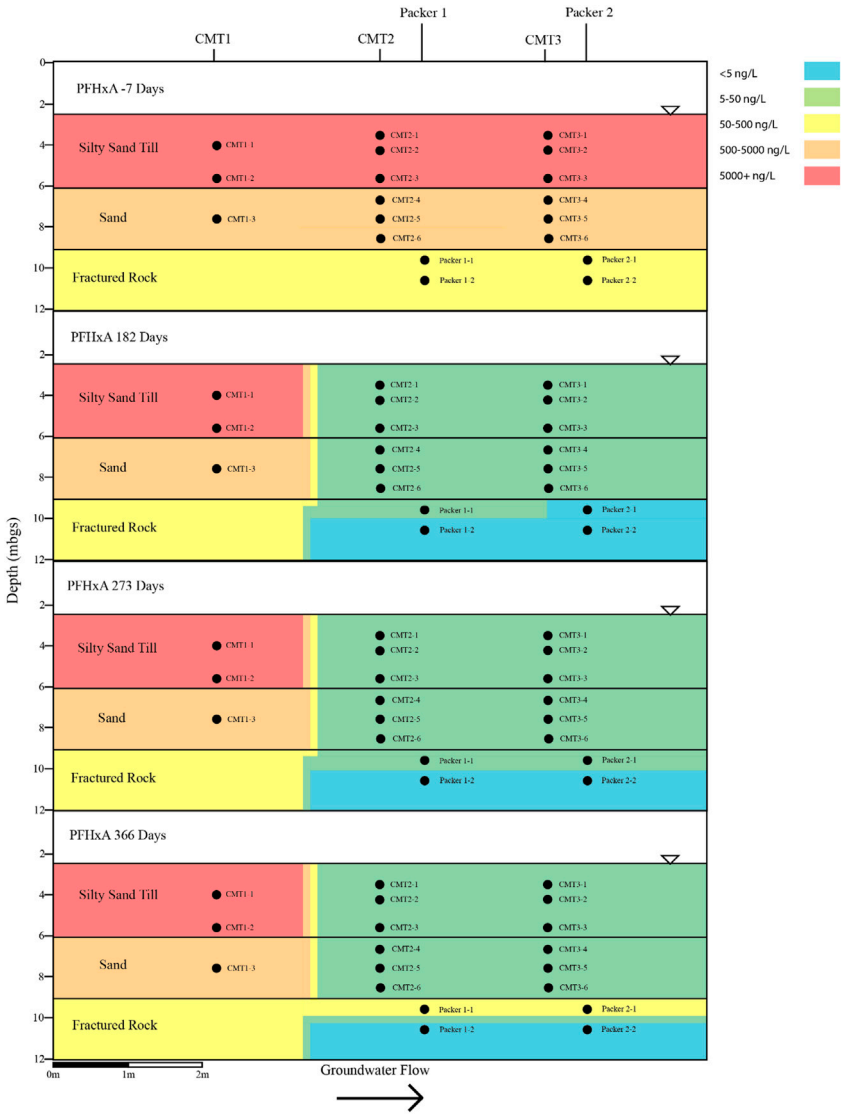

FIGURE 4 | Cross sectional view of PFHxA within groundwater determined pre- and post-injection of the CAC within the three aquifers.

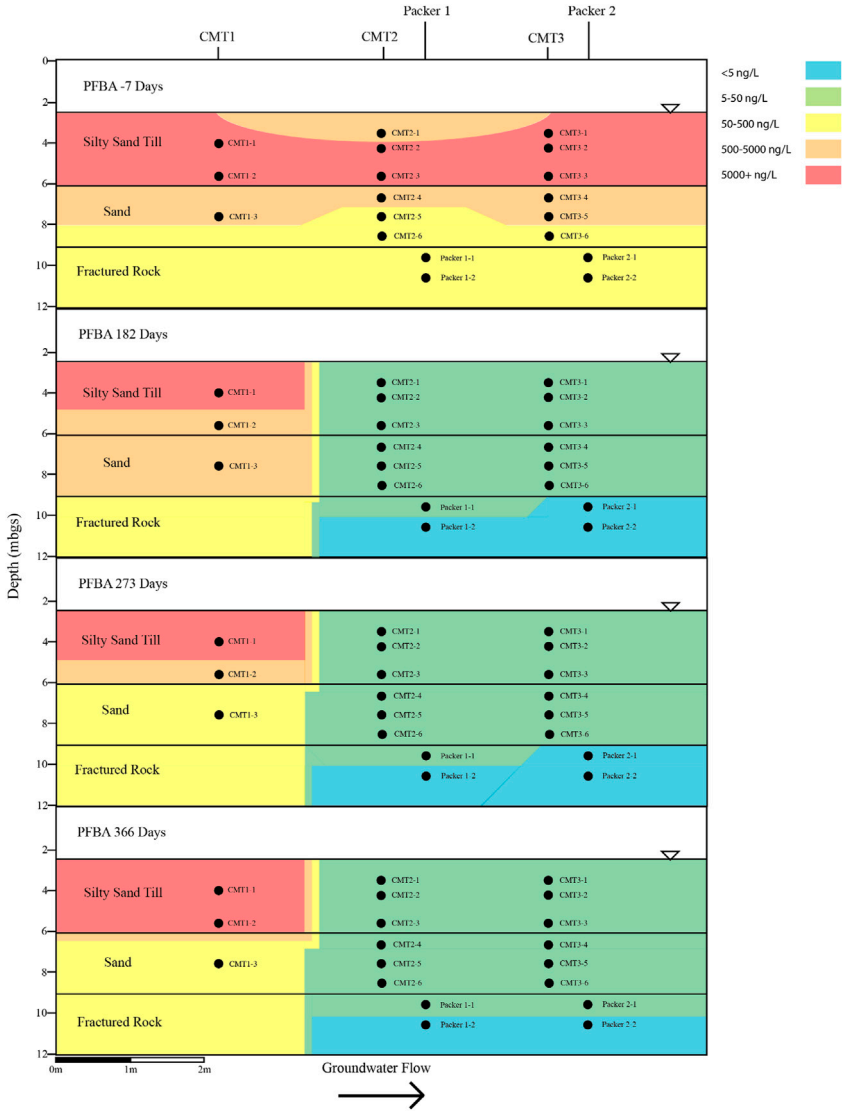

FIGURE 5 | Cross sectional view of PFBA within groundwater determined pre- and post-injection of the CAC within the three aquifers.

minerals which decreased the dissolved iron and manganese concentrations within the groundwater.

PFAS Behaviour

Prior to the injection of the CAC solution within the three aquifers, a total of nine PFAS were detected above the method reporting limit within the groundwater including PFBA, PFBS, PFPeA, PFHxA, PFHxS, PFHpA, PFOA, PFOS, and PFNA. **Table 1** and **Figures 4–7** provide summaries of the detected PFAS within the three aquifers including the six PFAS detected prior to the injection of the CAC in the silty sand aquifer, the five PFAS were detected prior to the injection of the CAC solution in the sand aquifer and the nine PFAS detected within the fractured bedrock prior to the injection of the CAC.

Following the injection of the CAC solution, the concentration of the PFAS detected within the silty sand and sand aquifers decreased to below their respective reporting limits within 182 days of injection (**Figures 4–7**). Concentrations of PFAS within the groundwater sampled from both the silty sand and sand aquifers remained below their respective reporting limits for the duration of the sampling period (i.e., 366 days).

Within the fractured bedrock, groundwater PFAS concentrations decreased following the injection of the CAC with PFAS concentrations within Packer two borehole being measured below their respective reporting limits on Day 182 (**Figures 4–7**). Groundwater collected from Packer one borehole had concentrations of 24 ng/L for PFHxA and 5.2 ng/L for PFOA for groundwater sampled from the fracture zone situated at approximately 9.5 mbgs during the Day 182 sampling event. During the Day 273 sampling event the number and concentration of PFAS detected within the shallow fracture zone (i.e., 9.5 mbgs) increased in both Packer one and Packer

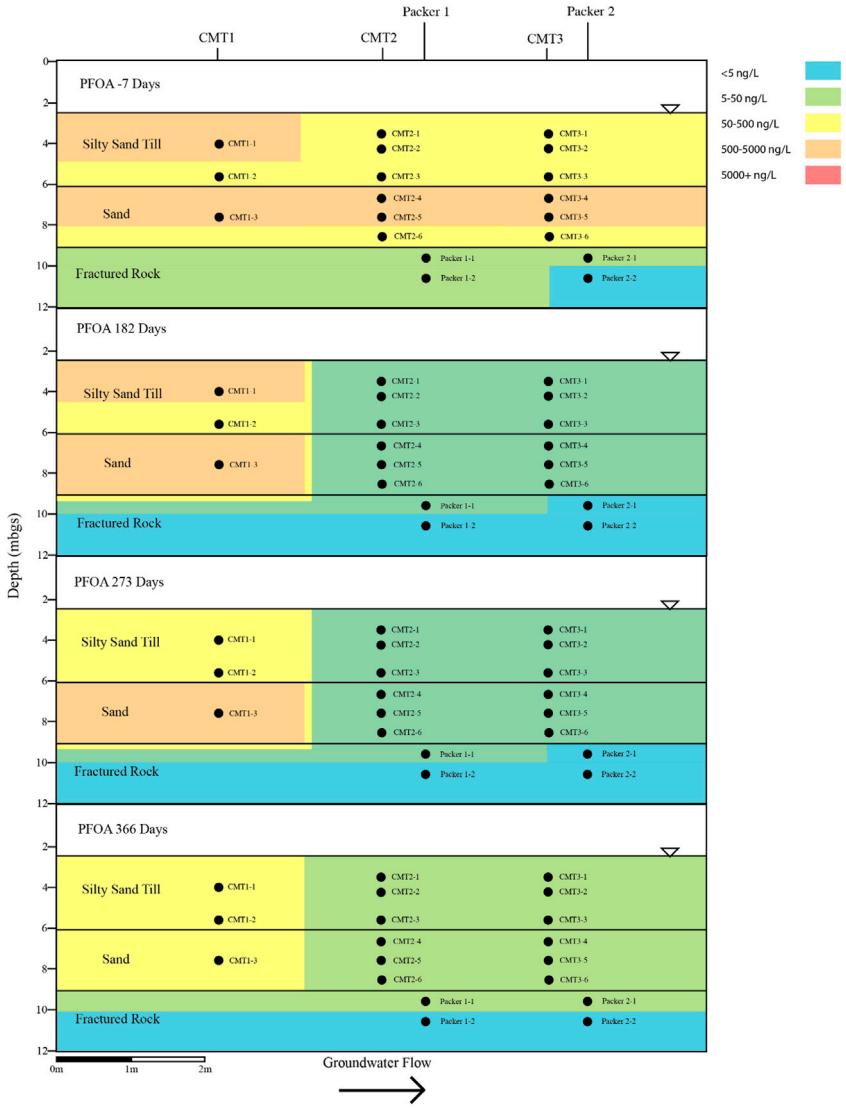

FIGURE 6 | Cross sectional view of PFOA within groundwater determined pre and post-injection of the CAC within the three aquifers.

two boreholes with six PFAS being detected within the groundwater collected from Packer one and Packer two boreholes. These included PFBA, PFHpA, PFHxA, PFOA, PFOS, and PFPeA. Groundwater sampling of the shallow fracture zone in Packer one and Packer two boreholes on Day 366 indicated that PFAS concentrations continued to increase with time in addition to the number of different PFAS being detected within the groundwater. During the Day 366 sampling event, seven PFAS were detected above the reporting limit including the six PFAS detected during the Day 273 event plus PFHxS which was measured at 2.8 ng/L (**Figure 7**). Concentrations of PFAS within the fracture zone located at a depth of 10.5 mbgs remained below their respective reporting limits during the 366-days testing period (**Figures 4–7**).

Based on the observed breakthrough of the PFAS within the bedrock aquifer, it appears that the carboxylic acids breakthrough prior to the sulfonic acids with the short carbon chained carboxylic acids being more mobile in the presence of CAC than the longer carbon chained carboxylic acids.

BTEX Behaviour

The PFAS plume is comingled, with a BTEX plume within the three aquifers underlying the site. The bulk of the BTEX mass within the groundwater is associated with the silty sand aquifer with BTEX concentrations generally decreasing with depth. The maximum concentration of BTEX within silty sand aquifer was 6,160 µg per litre (µg/L) which was measured in CMT1-2 on the Day -7 sampling event (**Figure 8**). The majority of mass within the BTEX plume is associated with the xylene and ethylbenzene fractions which make up 93 percent of the total BTEX within the sample collected from CMT1-2 on the Day -7 sampling event.

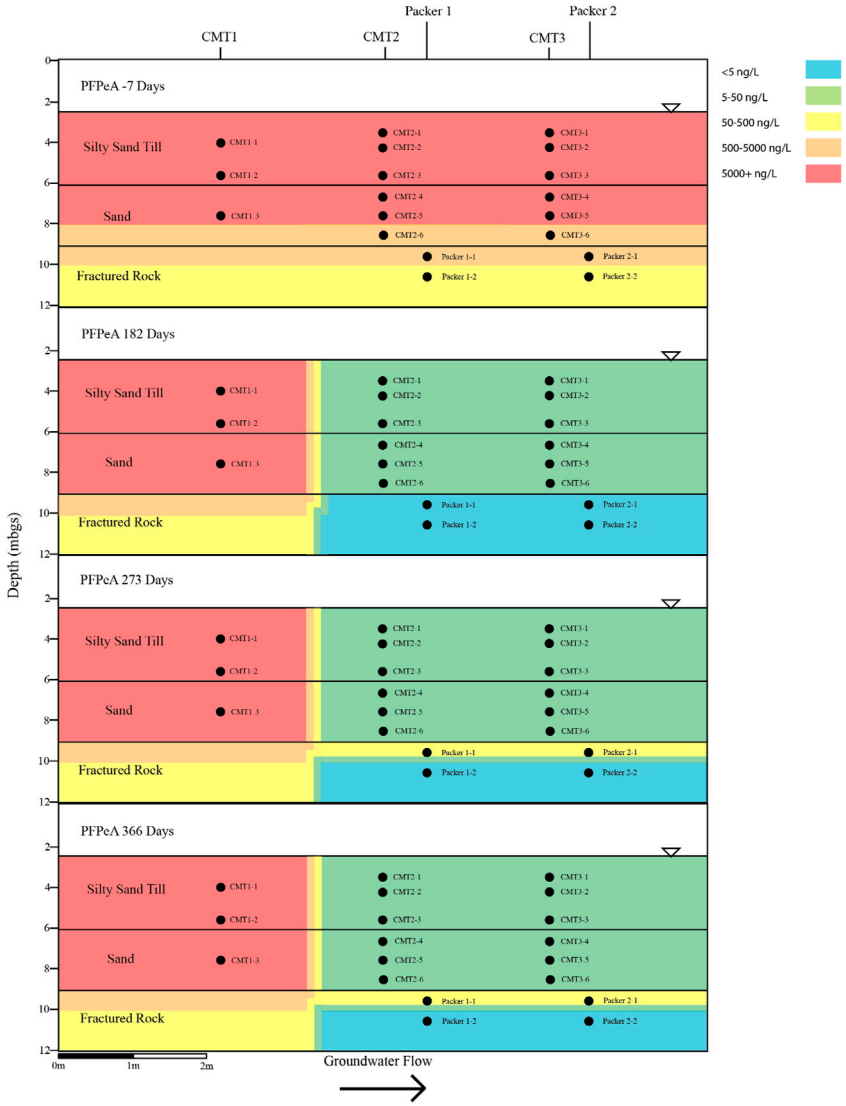

FIGURE 7 | Cross sectional view of PFPeA within groundwater determined pre and post-injection of the CAC within the three aquifers.

Following the injection of the CAC, BTEX concentrations within the silty sand aquifer decreased to below their respective reporting limits for all three sampling events except for the Day 182 event where benzene was detected in samples collected from CMT2-1 and CMT3-1 (**Figure 8**). Benzene adsorption onto activated carbon has been shown to have less affinity for activated carbon than TEX, thus it would be expected to be the last to be removed via sorptive processes from the groundwater when present with other BTEX compounds.

The BTEX within the sand aquifer showed a similar behaviour, as with the BTEX within the silty sand aquifer. Concentrations of BTEX decreased following the injection of the CAC to below their respective reporting limits for all three sampling events apart from benzene being detected in groundwater sampled from CMT2-4 on the Day 182 sampling event (**Figure 8**). The maximum total concentration of BTEX within the sand aquifer prior to the injection of the CAC was 703 µg/L (CMT1-3, **Figure 8**).

The maximum concentration of BTEX within the fractured dolostone prior to the injection of the CAC solution was 9.6 µg/L (Packer 2-1, Day -7, **Figure 8**) with benzene and total xylene both being detected at 4.8 µg/L. Following the injection of CAC, the BTEX concentrations decreased to below their respective reporting limits for all three sampling events (i.e., Day 182, Day 273, and Day 366). Overall, the CAC was effective at removing the BTEX from the groundwater within the three aquifers with greater than 99.99 percent removal being calculated within the groundwater after 273 days of treatment.

SUMMARY

The presence of PFAS within groundwater has been identified by many regulatory agencies as being a threat to human health and

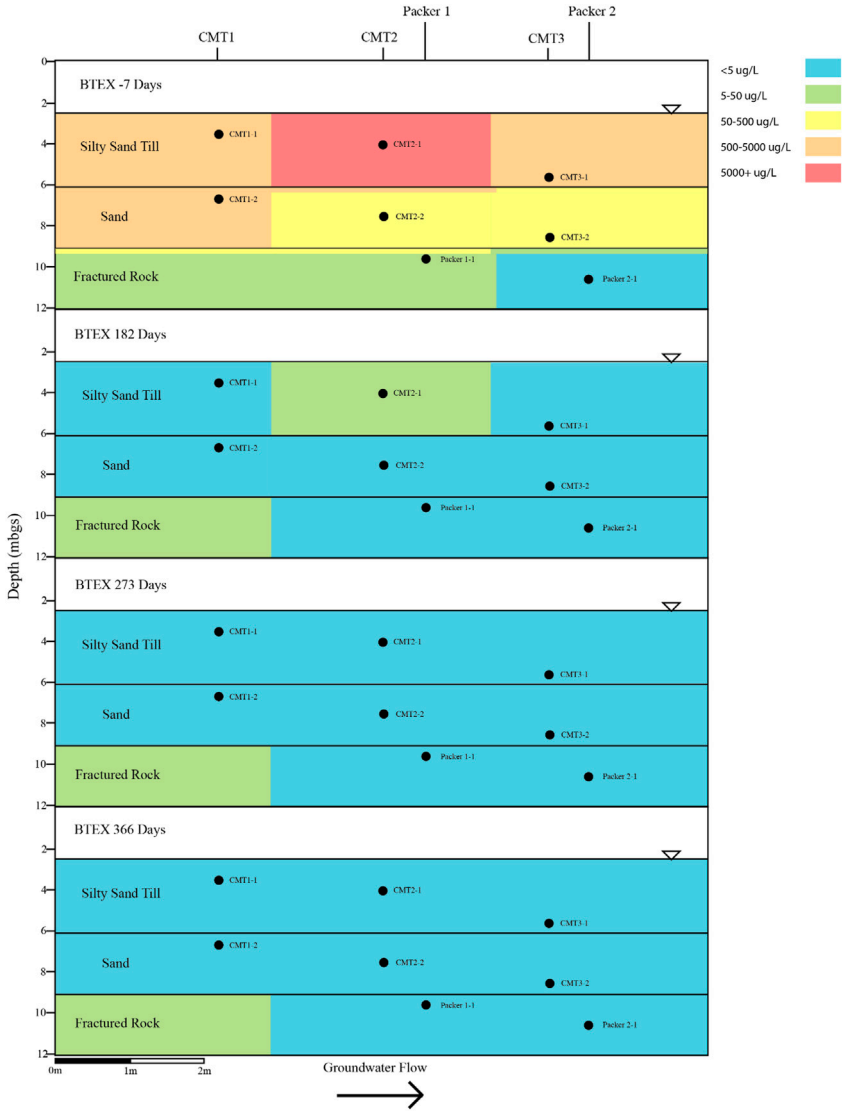

FIGURE 8 | Cross sectional view of BTEX groundwater concentrations determined on pre- and post-injection of the CAC within the three aquifers.

the ecology as some of PFAS have been confirmed or suspected of being cariogenic. The treatment of PFAS-impacted groundwater is currently dominated by pump and treat methods that employ activated carbon and/or ion exchange resins to remove the PFAS from solution. Limited laboratory and field studies have been conducted to evaluate the effectiveness of using *in-situ* methods to address PFAS in groundwater as an alternative to pump and treat. These studies have been conducted in relatively simple geologic and hydrogeologic environments and thus the effect of complex geology on the distribution and subsequent treatment of PFAS is not well understood.

This field study evaluated the *in-situ* treatment of a mixed BTEX-PFAS plume at a site in Central Canada. The site, underlain by three aquifers including a silty sand till aquifer, a sand aquifer, and a fractured dolostone aquifer, was impacted by BTEX and PFAS during a fire suppression event. The groundwater within the silty sand, sand and dolostone aquifers was impacted with BTEX concentrations up to 6,160, 703, and 9.6 ug/L, respectively. Concentrations of nine PFAS ranged up to 24,000 ng/L for PFPeA, up to 15,740 ng/L for PFHxA, up to 7,250 for PFHpA, up to 6,405 ng/L for PFBA, up to 2,105 ng/L for PFOS, up to 910 ng/L for PFOA, up to 165 ng/L for PFNA, up to 6.5 ng/L for PFBS, and up to 4.2 ng/L for PFHxS were detected within the three aquifers.

To mitigate the BTEX and PFAS within the three aquifers, a CAC solution was injected using a combination of direct push technology for the overburden aquifers and a series of injection wells within the fractured dolostone. Sampling of the groundwater for a variety of inorganic and general chemical parameters prior to and post CAC injection indicated that the groundwater within the three aquifers was reducing, with most electron acceptors being depleted because of reactions with the

petroleum hydrocarbons within the groundwater. These reactions appear to have been buffered to near neutral pH conditions by reactions with carbonate minerals within the three aquifers. The addition of CAC and its associated organic carbon-based substrate enhanced the reducing reactions occurring within the aquifers with further depletion of sulphate and assumed precipitation of iron- and manganese-based sulphide minerals.

Total organic carbon concentrations within the silty sand and sand aquifer solids increased from pre-injection concentrations of 0.53 and 0.52 g/kg, respectively, to 8.10 and 7.99 g/kg, respectively, following the injection of the CAC. Analysis of the silty sand aquifer solids pre- and post-injection indicated that the distribution of the CAC was influenced by small scale heterogeneities within the silty sand aquifer with a thin higher K_H sand seam being enriched with TOC relative to the surrounding aquifer material. The high K_H seam had a mean TOC concentration of 13.0 g/kg compared to a mean of 7.40 g/kg for the surrounding silty sand aquifer material.

Sampling of the groundwater over a 12-month period post CAC injection indicated that the nine PFAS detected within the groundwater prior to treatment were treated to below their analytical reporting limits within the silty sand and sand aquifers. Similar results were also observed for the BTEX within the silty sand and sand aquifers over the 12-months monitoring period. The BTEX concentrations decreased to below their analytical reporting limits following the injection of the CAC solution and remained there over the duration of the monitoring period. The exception was benzene, which was measured near its analytical reporting limit in two shallow wells during the Day 182 event. After the Day 182 event, benzene was not detected within the groundwater at concentrations greater than its reporting limit.

The BTEX concentrations within the fractured dolostone aquifer decreased to below their respective reporting limits following the injection of the CAC solution and remained below their reporting limits for the duration of the 1-year test. Total concentrations of detectable PFAS within the fractured dolostone decreased from a maximum of 1,332 to 37 ng/L within 182 days of injection, with only three of the original nine PFAS being detected within the groundwater on the Day 182 sampling event. The PFAS detected during the Day 182 sampling event were short carbon chained carboxylic acids. Groundwater collected during the Day 366 sampling event detected seven of the nine PFAS originally found with concentrations increasing with time following the CAC injection suggesting that the CAC within the fracture zone was at or near capacity for short and moderate carbon chain carbon carboxylic acid PFAS.

The results of the field study suggested that CAC could be effectively injected using direct push technology into the two unconsolidated aquifers with effective treatment of BTEX and PFAS being obtained within 6 months of application. The concentrations of BTEX and PFAS within the groundwater remained below their respective reporting limits for the 1-year monitoring period. The results gathered from the fractured dolostone aquifer indicated that BTEX could be effectively removed to below their respective reporting limits over the 1-year monitoring period, whereas PFAS was only partially attenuated with short carbon chain carboxylic acid PFAS breaking through within 6 months of CAC application. The partial attenuation of the PFAS is attributed to competitive adsorption between the BTEX and various PFAS as well as the limited sorptive sites due to the limited mass of CAC within the fractures themselves.

DATA AVAILABILITY STATEMENT

The datasets presented in this article are not readily available because Confidential site and data, site location can not be shared. Requests to access the datasets should be directed to rickm@irsl.ca.

AUTHOR CONTRIBUTIONS

RC and LB contributed to interpretation and writing the article.

REFERENCES

Aly, Y. H., McInnis, D. P., Lombardo, S. M., Arnold, W. A., Pennell, K. D., Hatton, J., et al. (2019). Enhanced Adsorption of Perfluoro Alkyl Substances for *In Situ* Remediation. *Environ. Sci. Water Res. Technol.* 5, 1867–1875. doi:10.1039/c9ew00426b

ASTM International Inc.ASTM (2016). *ASTM D5084-16a. Standard Test Methods for Measurement of Hydraulic Conductivity of Saturated Porous Materials Using a Flexible wall Permeameter*. West Conshohocken, PA: Author. doi:10.1520/d5084-16a

ASTM International Inc. ASTM (2011). *ASTM E1019-11. Standard Test Methods for Determination of Carbon, Sulfur, Nitrogen, and Oxygen in Steel, Iron, Nickel, and Cobalt Alloys by Various Combustion Fusion Techniques*. West Conshohocken, PA: Author. doi:10.1520/e1019-11

ASTM International Inc. ASTM (2013). *ASTM E1409-13. Standard Test Methods for Determination of Oxygen and Nitrogen in Titanium and Titanium Alloys by Inert Gas Fusion*. West Conshohocken, PA: Author. doi:10.1520/e1409-05

Barajas, F. (2019). *Bench-scale Treatability Studies on Emerging Contaminants: PFAS and 1,4 Dioxane Presented at Air and Waste Management Association*. June 13. Austin, Texas.

Bruton, T. A., and Sedlak, D. L. (2017). Treatment of Aqueous Film-Forming Foam by Heat-Activated Persulfate under Conditions Representative of *In Situ* Chemical Oxidation. *Environ. Sci. Technol.* 51, 13878–13885. doi:10.1021/acs.est.7b03969

Carey, G. R., Chapman, S. W., Parker, B. L., and McGregor, R. (2015). Application of an Adapted Version of MT3DMS for Modeling Back-Diffusion Remediation Timeframes. *Remediation* 25 (4), 55–79. doi:10.1002/rem.21440

Carey, G. R., McGregor, R., Pham, A. L.-T., Sleep, B., and Hakimabadi, S. G. (2019). Evaluating the Longevity of a PFAS *In Situ* Colloidal Activated Carbon Remedy. *Remediation* 29, 17–31. doi:10.1002/rem.21593

Carter, K. E., and Farrell, J. (2010). Removal of Perfluorooctane and Perfluorobutane Sulfonate from Water via Carbon Adsorption and Ion Exchange. *Separat. Sci. Tech.* 45 (6), 762–767. doi:10.1080/01496391003608421

Darlington, R., Barth, E., and McKernan, J. (2018). The Challenges of PFAS Remediation. *Mil. Eng.* 110 (712), 58–60.

De Jonge, L. W., Kjaergaard, C., and Moldrup, P. (2004). Colloids and Colloid-Facilitated Transport of Contaminants in Soils: An Introduction. *Vadose Zone J.* 3 (2), 321–325. doi:10.2113/3.2.321

Dombrowski, P. M., Kakarla, P., Caldicott, W., Chin, Y., Sadeghi, V., Bogdan, D., et al. (2018). Technology Review and Evaluation of Different Chemical Oxidation Conditions on Treatability of PFAS. *Remediation* 28 (2), 135–150. doi:10.1002/rem.21555

Eberle, D., Ball, R., and Boving, T. B. (2017). Impact of ISCO Treatment on PFAA Co-contaminants at a Former Fire Training Area. *Environ. Sci. Technol.* 51 (9), 5127–5136. doi:10.1021/acs.est.6b06591

Frimmel, F. H., von der Kammer, F., and Flemming, H-C. (2007). *Colloidal Transport in Porous media*. Spring, 292.

Higgins, C. P., and Luthy, R. G. (2006). Sorption of Perfluorinated Surfactants on Sediments. *Environ. Sci. Technol.* 40 (23), 7251–7256. doi:10.1021/es061000n

Huling, S. G., and Pivetz, B. E. (2006). *Engineering Issue:* In-Situ *Chemical Oxidation.* Cincinnati, OH: EPA/600/R-06/072U.S. Environmental Protection Agency Office of Research and Development, National Risk Management Research Laboratory.

Interstate Technology and Regulatory Council ITRC (2005). "*In Situ* Chemical Oxidation Team," in *Technical and Regulatory Guideline for* in Situ *Chemical Oxidation of Contaminated Soil and Groundwater*. (Washington, D.C.: ISCO-2Interstate Technology and Regulatory Council).

Interstate Technology and Regulatory Council ITRC (2018). "*In Situ* Chemical Oxidation Team," in *Remediation Technologies and Methods for Per- and Polyfluoroalkyl Substances (PFAS)* (Washington, DCWashington, D.C.: ISCO-1Interstate Technology and Regulatory Council).

Interstate Technology and Regulatory Council ITRC (2020). *PFAS – Per- and Polyfluoroalkyl Substances TeamRemediation Technologies and Methods for Per- and Polyfluoroalkyl Substances (PFAS).* Washington, DCWashington, D.C.: ISCO-1Interstate Technology and Regulatory Council. https://pfas-1.itrcweb.org/12-treatment-technologies/.

Kashir, M., and McGregor, R. (2015). Chemical Oxidation Performance in High Temperature, saline Groundwater Impacted with Hydrocarbons. *Remediation* 25 (2), 55–70. doi:10.1002/rem.21424

Liu, C., Hatton, J., Arnold, W. A., Simcik, M. F., and Pennell, K. D. (2020). *In Situ* sequestration of Perfluoroalkyl Substances Using Polymer-Stabilized Powdered Activated Carbon. *Environ. Sci. Technol.* 54 (11), 6929–6936. doi:10.1021/acs.est.0c00155

McGregor, R. (2020b). Distribution of Colloidal and Powdered Activated Carbon for the *In Situ* Treatment of Groundwater. *J. Water Resource Prot.* 12, 1001–1018. in press. doi:10.4236/jwarp.2020.1212060

McGregor, R. (2018). *In Situ* treatment of PFAS-Impacted Groundwater Using Colloidal Activated Carbon. *Remediation* 28, 33–41. doi:10.1002/rem.21558

McGregor, R., and Maziarz, A. (2021). The *In Situ* Treatment of Basic Violet 16 Synthetic Dye in Groundwater. *Remediation* 31, 27–34. doi:10.1002/rem.21689

McGregor, R. (2020a). Six Pilot-scale Studies Evaluating the *In Situ* Treatment of PFAS in Groundwater. *Remediation* 30, 39–50. doi:10.1002/rem.21653

McGregor, R., and Zhao, Y. (2021). The *In Situ* Treatment of TCE and PFAS in Groundwater within a Silty Sand Aquifer. *Remediation* 31, 7–17. doi:10.1002/rem.21675

National Ground Water Association Press (2017). *Groundwater and PFAS: State of Knowledge and Practice*. Westerville, OH: Author.

Nordstrom, D. K. (1977). Thermochemical Redox Equilibria of ZoBell's Solution. *Geochimica et Cosmochimica Acta* 41 (12), 1835–1841. doi:10.1016/0016-7037(77)90215-0

Park, S., Lee, L. S., Medina, V. F., Zull, A., and Waisner, S. (2016). Heat-activated Persulfate Oxidation of PFOA, 6:2 Fluorotelomer Sulfonate, and PFOS under Conditions Suitable for *In-Situ* Groundwater Remediation. *Chemosphere* 145, 376–383. doi:10.1016/j.chemosphere.2015.11.097

Petri, B. G., Watts, R. J., Tsitonaki, A., Crimi, M., Thomson, N. R., and Teel, A. L. (2011). Fundamentals of ISCO Using Persulfate. in: Editors. R. L. Siegrist, M. Crimi, and T. J. Simpkin, In Situ *Chemical Oxidation for Groundwater Remediation* (pp. 147–191). New York, NY: Springer. doi:10.1007/978-1-4419-7826-4_4

Puls, R. W., and Barcelona, M. J. (1996). *Low-flow (Minimal Drawdown) Groundwater Sampling Procedures*. EPA groundwater issue, EPA/540/S-95/504. Washington, DC: US Environmental Protection Agency, Office of Solid Waste and Emergency Response.

Ross, I., McDonough, J., Miles, J., Storch, P., Thelakkat Kochunarayanan, P., Kalve, E., et al. (2018). A Review of Emerging Technologies for Remediation of PFASs. *Remediation* 28, 101–126. doi:10.1002/rem.21553

Saeed, W., Shouakar-Stash, O., Barker, J., Thomson, N., and McGregor, R. (2021). Laboratory Experiments to Evaluate the Effectiveness of Persulfate to Oxidize BTEX in Saline Environment and at Elevated Temperature Using Stable Isotopes. *Hydrology* 8 (139). doi:10.3390/hydrology8030139

Simon, J. A., Abrams, S., Bradburne, T., Bryant, D., Burns, M., Cassidy, D., et al. (2019). PFAS Experts Symposium: Statements on Regulatory Policy, Chemistry and Analytics, Toxicology, Transport/fate, and Remediation for Per- and Polyfluoroalkyl Substances (PFAS) Contamination Issues. *Remediation* 29 (4), 31–48. doi:10.1002/rem.21624

Simon, J. A. (2020). Editor's Perspective-Just How Large Is the PFAS Problem? *Remediation* 30, 3–4. doi:10.1002/rem.21643

Sra, K. S., Thomson, N. R., and Barker, J. F. (2013). Persulfate Treatment of Dissolved Gasoline Compounds. *J. Hazard. Tox. Radioact. Waste* 17 (1), 9–15. doi:10.1061/(asce)hz.2153-5515.0000143

Usman, M., Faure, P., Ruby, C., and Hanna, K. (2012). Remediation of PAH-Contaminated Soils by Magnetite Catalyzed Fenton-like Oxidation. *Appl. Catal. B: Environ.* 117-118, 10–17. doi:10.1016/j.apcatb.2012.01.007

Xiao, X., Ulrich, B. A., Chen, C. P., and Higgins, C. P. (2017). Sorption of Poly- and Perfluoroalkyl Substances (PFASs) Relevant to Aqueous Film-Forming Foam (AFFF)-impacted Groundwater by Biochars and Activated Carbon. *Environ. Sci. Technol.* 51 (11), 6342–6351. doi:10.1021/acs.est.7b00970

Yu, Q., Zhang, R., Deng, S., Huang, J., and Yu, G. (2009). Sorption of Perfluorooctane Sulfonate and Perfluorooctanoate on Activated Carbons and Resin: Kinetic and Isotherm Study. *Water Res.* 43 (4), 1150–1158. doi:10.1016/j.watres.2008.12.001

Conflict of Interest: RM and LB are employed by InSitu Remediation Services Ltd.

The authors declare that the research was conducted in the absence of any commercial or financial relationships that could be construed as a potential conflict of interest.

Publisher's Note: All claims expressed in this article are solely those of the authors and do not necessarily represent those of their affiliated organizations, or those of the publisher, the editors and the reviewers. Any product that may be evaluated in this article, or claim that may be made by its manufacturer, is not guaranteed or endorsed by the publisher.

frontiers in Environmental Science

ORIGINAL RESEARCH
published: 01 October 2021
doi: 10.3389/fenvs.2021.739775

Collecting Microplastics in Gardens: Case Study (i) of Soil

*Zahra Sobhani[1], Yunlong Luo[1,2], Christopher T. Gibson[3,4], Youhong Tang[3], Ravi Naidu[1,2], Mallavarapu Megharaj[1,2] and Cheng Fang[1,2]**

[1]*Global Centre for Environmental Remediation (GCER), College of Engineering, Science and Environment, University of Newcastle, Callaghan, NSW, Australia,* [2]*Cooperative Research Centre for Contamination Assessment and Remediation of the Environment (CRC CARE), University of Newcastle, Callaghan, NSW, Australia,* [3]*Flinders Institute for NanoScale Science and Technology, College of Science and Engineering, Flinders University, Adelaide, SA, Australia,* [4]*Flinders Microscopy and Microanalysis, College of Science and Engineering, Flinders University, Adelaide, SA, Australia*

As an emerging contaminant, microplastic is receiving increasing attention. However, the contamination source is not fully known, and new sources are still being identified. Herewith, we report that microplastics can be found in our gardens, either due to the wrongdoing of leaving plastic bubble wraps to be mixed with mulches or due to the use of plastic landscape fabrics in the mulch bed. In the beginning, they were of large sizes, such as > 5 mm. However, after 7 years in the garden, owing to natural degradation, weathering, or abrasion, microplastics are released. We categorize the plastic fragments into different groups, 5 mm–0.75 mm, 0.75 mm–100 μm, and 100–0.8 μm, using filters such as kitchenware, meaning we can collect microplastics in our gardens by ourselves. We then characterized the plastics using Raman image mapping and a logic-based algorithm to increase the signal-to-noise ratio and the image certainty. This is because the signal-to-noise ratio from a single Raman spectrum, or even from an individual peak, is significantly less than that from a spectrum matrix of Raman mapping (such as 1 vs. 50 × 50) that contains 2,500 spectra, from the statistical point of view. From the 10 g soil we sampled, we could detect the microplastics, including large (5 mm–100 μm) fragments and small (<100 μm) ones, suggesting the degradation fate of plastics in the gardens. Overall, these results warn us that we must be careful when we do gardening, including selection of plastic items for gardens.

Keywords: microplastics, garden soil, Raman mapping, released microplastics, algorithm

OPEN ACCESS

Edited by:
Andrew Hursthouse, University of the West of Scotland, United Kingdom

Reviewed by:
Nicholas Kiprotich Cheruiyot, National Kaohsiung University of Science and Technology, Taiwan
Jheng-Jie Jiang, Chung Yuan Christian University, Taiwan

****Correspondence:***
Cheng Fang
cheng.fang@newcastle.edu.au
0000-0002-3526-6613

Specialty section:
This article was submitted to Toxicology, Pollution and the Environment, a section of the journal Frontiers in Environmental Science

Received: *11 July 2021*
Accepted: *18 August 2021*
Published: *01 October 2021*

Citation:
Sobhani Z, Luo Y, Gibson CT, Tang Y, Naidu R, Megharaj M and Fang C (2021) Collecting Microplastics in Gardens: Case Study (i) of Soil. Front. Environ. Sci. 9:739775. doi: 10.3389/fenvs.2021.739775

INTRODUCTION

Accumulation of plastic wastes is increasing in marine and terrestrial ecosystems. Plastics are released into the environment in different sizes, ranging from macroscale to nanoscale. While macroplastics (>5 mm) can be collected and recycled, the severe environmental issue is related to microplastics (5 mm–1 μm) (Hartmann et al., 2016) and nanoplastics (<1,000 nm) (Gigault et al., 2018), both of which are seemingly difficult to be recycled. The primary source of the microplastics and nanoplastics is the direct plastic items from domestic and industrial usage, while the secondary source is their generation as a result of plastic degradation by abiotic or biotic processes (Arthur et al., 2009; Browne 2015). In the latter case, the fragmentation of the large plastics over the long term results in the continuous increase in the small-sized ones, including microplastics and nanoplastics (Andrady 2017). Unfortunately, microplastics and nanoplastics not only release potentially toxic chemicals (e.g., residual monomers and additives) but also exhibit high specific surface areas to

adsorb/accumulate other environmental contaminants (Wright and Kelly 2017). Furthermore, microplastics and nanoplastics are highly durable and potentially susceptible to bioaccumulation, and their presence in the food chain has been documented (Liebezeit and Liebezeit 2014; Cox et al., 2019; Koelmans et al., 2019). Accumulation of plastic particles in living organisms may result in adverse effects, such as internal abrasions and blockages (Mattsson et al., 2017). Understanding the environmental fate and risk of microplastics requires their physicochemical characterization in terms of concentration, size, shape, ageing, and plastic types.

However, due to the limitations in their characterization, the source of microplastics and nanoplastics is still not fully understood. While the microplastics are found in the gardening mulch, where they come from is still an open question (Steinmetz et al., 2016; Zhang et al., 2018). For example, if they are not directly originating from the mulch itself during fabrication, plastic packaging (for transportation and market) might be another source of microplastics, similar to the opening of a plastic bag as previously reported (Sobhani et al., 2020a). Once the mulch is used in the gardens, some items might also release microplastics as extra sources, such as from the wrongdoing of leaving plastic bubble wraps to be mixed with the mulch or use of plastic landscape fabrics as mulch beds, which will be identified here.

Proper characterization of microplastics/nanoplastics is necessary to identify their source. Raman spectroscopy is among the most common techniques for chemical identification of plastics. Using the intensity of their unique characteristic peaks, an image can be generated to directly visualize the microplastics and nanoplastics *via* mapping, once the position information is available. For the Raman image, although confocal Raman spectroscopy can achieve the lateral resolution to less than 1 μm, its signal-to-noise ratio is sometimes low, especially for environmental samples (Sobhani et al., 2019; Sobhani et al., 2020a). The possible reasons for the low signal-to-noise ratio include the background noise, the fluorescence emission of organic matter, and the spectrum interference from other inorganic contamination and plastic additives (Ivleva et al., 2017). Our previous studies reported different approaches in order to increase the signal-to-noise ratio and the mapping certainty (Sobhani et al., 2020b; Fang et al., 2020; Fang et al., 2021c). By doing so, we intend to avoid false-positive and false-negative results, which is important for analyzing an environmental sample.

Finally, we tried to collect more Raman signals from multipeaks for images and merge them *via* logic-based algorithms. In this case, the image, in particular, the merged image by mapping multipeaks of the Raman scanning spectrum matrix, yields a signal-to-noise ratio significantly different from that of a single Raman spectrum or even an individual peak (Fang et al., 2021a; Fang et al., 2021b). We wonder if this approach can be applied to analyze the actual environmental sample when the signal-to-noise ratio is low.

As mentioned, analysis of the environmental microplastics/nanoplastics is still challenging, due to the complexity of the background of environmental samples. Once they are exposed to the environment, weathering, ageing, and fragmentation may change the particle surface properties. The formation of biofilms further complexes the analysis (Vroom et al., 2017). Usually, sample preparation is a time-consuming process requiring pretreatment. Chemical digestion and enzymatic degradation are available options for removing interference to enhance the signal-to-noise ratio (Ivleva et al., 2017).

In this report, we validate the multipeak mapping imaging and logic-based algorithm approach to directly collect microplastics that are released in our garden. Using this approach, due to the enhanced signal-to-noise ratio, we can simplify the sample preparation process. Thus, our sampling involves only using kitchenware to collect and categorize microplastics in the ranges of 5 mm–0.75 and 0.75 mm −100 μm and is carried out in our backyard garden. To collect small ones, such as those in the size range of 100–0.8 μm, we need sample pretreatment to further increase the signal-to-noise ratio, which should be conducted in the lab. We also recommend Raman spectroscopy to collect images of microplastics from the environmental samples.

MATERIALS AND METHODS

Chemicals, Filters, and Other Materials

All chemicals, including ethanol, zinc chloride, sulphuric acid (H_2SO_4), and hydrogen peroxide (H_2O_2), were purchased from Sigma–Aldrich (Australia) and used as received.

Kitchenware was purchased from the local stores in Australia, including Woolworths and Harris Scarf. Two stainless filters were used, 1) a net with a grid pore size of 0.75 mm (diagonal size of ~ 1.06 mm) and 2) a coffee filter with a grid pore size of 50 μm × 100 μm (diagonal size of ~112 μm), as shown in **Supplementary Figures S1, S2** (Supporting Information). The second filter was assigned to collect microplastics >100 μm in this report. The third filter made of a porous silver membrane with a pore diameter of ~0.8 μm was purchased from Sterlitech (United States).

Using these filters, we can categorize the collected microplastics into three subgroups, 5–0.75 mm, 0.75 mm–100 μm, and 100–0.8 μm, respectively. There might be some overlaps in these size category boundaries, but they have a limited effect on our test. For example, the diagonal size of the square pore is slightly larger than its length and width. The pore size of the silver membrane is also an average one from the statistical point of view, as shown in **Supplementary Figure S1** (Supporting Information).

All containers of glass, stainless steel, chinaware, or earthenware were used, including bowls and dishes. For stirring and sample transportation, a wood stick was used, as listed in **Supplementary Figure S2** (Supporting Information). Table salt was used to help the microplastics float if the collection is conducted in the backyard garden, as discussed in the following sections. During the sampling process and test, cotton clothes were recommended, such as blue jeans and jackets, gloves, and metal shovels. All the processes were carried out on wooden tables and benches, if conducted in the backyard garden. All glass containers and stainless filters were washed with Milli Q (MQ) water and acetone before sample preparation in the lab.

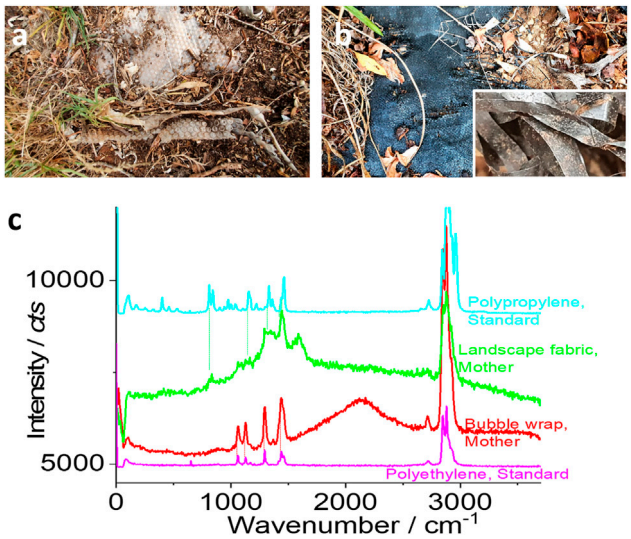

FIGURE 1 | Two sampling sites **(A, B)** and the typical Raman spectra **(C)**. Microplastics might be released from the buried "mother matrix," including the white bubble wrap **(A)** and the black landscape fabrics **(B)**. **(C)** The typical Raman spectrum collected from the "mother matrix." For comparison, the standard Raman spectra of polyethylene and polypropylene are also presented.

Sample Preparation and Pretreatment

Sample Collection

Soil samples from a typical Australian garden were collected in summer (December 2020) from South Australia, Bellevue Heights, 5050. They are sandy as shown in **Figure 1**. For the sampling process, an area of 10 cm × 10 cm size with a depth of ~2 cm (~1 cm above and another ~1 cm below, if the plastic layer is still identifiable) was sampled with a weight of ~1,000 g, after removing large stones, plant roots, mulches, etc. The samples were air-dried.

In this study, two types of soil samples around the plastic items were collected, including 1) a white bubble wrap of polyethylene that has been buried under wood mulches for 7 years, due to inappropriate discarding and 2) a black landscape fabric of polypropylene (to control weeds) that has been used as a mulch bed for 7 years. The garden history suggested that the mulch was paved in the summer of 2013.

Sample Preparation On-Site in the Backyard Garden

Soil samples of ~10 g were mixed with ~100 ml of tap water. After removing the large items using stainless tweezers, a spoon of table salt (5–10 g) was added to increase the density of water and to help floating of the microplastics. After stirring with a wood stick to reach salt saturation, some salt precipitated at the bottom and was mixed with the soil, which is acceptable.

The floating items were collected with a filter of 0.75 mm first and then with another filter of 100 μm. These filtration processes can be conducted in the backyard garden directly.

The samples collected in the filters were washed with tap water at least 3 times. They were air-dried and transported to a glass slide for the Raman test, and the amount was calculated using microscopy, in duplicates.

Note that this sample preparation approach might not yield a 100% recovery of the microplastics, because 1) some microplastics and nanoplastics were still embedded in the soils and sediments and so they could not float on the water surface for collection and 2) during the sample preparation process, some microplastics were found to be released from large fragments (>5 mm), as shown in **Supplementary Figure S3** (Supporting Information).

Sample Preparation Off-Site in the Lab

To increase the signal-to-noise ratio and to collect small microplastics, another sample preparation was carried out in the laboratory. In this case, the tap water was replaced with MQ water and table salt was replaced with zinc chloride. In the meantime, chemical washing was introduced using ethanol.

In brief, soil samples of ~10 g were mixed with MQ water of ~50 ml and saturated with zinc chloride. The floating items were collected with a filter of 0.75 mm first, followed by 100 μm and 0.8 μm filters. The collected samples were washed with MQ water three times and then with ethanol three times. They were air-dried and transported to the glass slide for the Raman test. For the sample filtered with a 0.8 μm porous silver membrane, this transport was found unnecessary, as indicated later.

For the Raman test, use of glass slides is a good choice owing to their clean background. Before the distribution of microplastics on its surface, the glass slide had been cleaned by dipping in a piranha solution (2:1 H_2SO_4: H_2O_2, *v/v*) (warning: this solution reacts vigorously with organic compounds).

Sample Pretreatment in the Lab

To further increase the signal-to-noise ratio, chemical digestion was introduced, particularly for the analysis of microplastics in the size range of 0.8–100 μm. In this case, the liquid obtained after filtering with a 100 μm filter was digested using H_2O_2 at 3% for 24 h at 50°C. Then, a similar protocol was followed, intended to enhance the Raman signal by decreasing the spectrum background by cleaning the surface.

Blank Samples

For the QA/QC control, blank samples were prepared, including the backyard garden and the laboratory. In the backyard garden, a blank sample was prepared in parallel without the soil sample to check the possible contamination from the table salt and tap water. In the laboratory, similarly, the blank sample was prepared using only MQ water. We did collect a tiny amount of microplastics (<10) in the blanks, which is not comparable with the amount of microplastics obtained from the garden, as reported herein. This blank sample was also validated in a commercial laboratory (Eurofins, Australia).

Raman Spectra

The Raman spectra were recorded in the air using a WITec confocal Raman microscope (Alpha 300RS, Germany) equipped with a 532 nm laser diode (<30 mW), as reported before (Sobhani et al., 2019; Sobhani et al., 2020b; Fang et al., 2020). In general, a charge-coupled device detector was used to collect Stokes–Raman signals under a 20×, 40×, or 100× objective lens at room temperature (~24°C).

To map the image, a piezo-driven scanning stage was employed for each Raman signal collection at each pixel, which was varied by adjusting the moving speed and integration time, from 1 μm × 1 μm to 500 nm × 500 nm, 100 nm × 100 nm, or 40 nm × 40 nm, as indicated in the following. Note that the scanning duration was increased accordingly. For example, to image an area of 10 μm × 10 μm, the scanning duration is increased from 100 s (with a pixel size of 1 μm × 1 μm, to collect 100 spectra as a matrix) to 10,000 s (with a pixel size of 100 nm × 100 nm, to collect 10,000 spectra as a matrix) and to 62,500 s (with a pixel size of 40 nm × 40 nm, to collect 62,500 spectra as a matrix) if each pixel takes 1 s of integration to collect the Raman signal as a Raman spectrum.

For Raman image mapping, the different plastics exhibit different Raman activities and emit different intensities of Raman spectra, as suggested before (Sobhani et al., 2019). For example, the Raman signal at 2,890 cm^{-1} was collected to image polyethylene, along with other characteristic peaks of fingerprint at 1,060, 1,120, 1,300, and 1,440 cm^{-1}. The intensities at different peaks were mapped as different images.

The collected Raman signal was analyzed using WITec Project software. By just collecting the net intensity of the unique/characteristic peaks for image mapping, the interference which might originate from the spectrum background noise (such as fluorescence), or organic matter, can be effectively avoided by subtracting the baseline of the collected Raman spectra (the peak area or sum, after automatic integration *via* software) at the selected peaks. The background has been generally subtracted using the collected signal at both sides of the selected Raman peak at the pixels as the spectrum background. To further avoid the "bias and false" imaging, an imaging-algorithm analysis is recommended.

Image Analysis: Logic-Based Algorithm

From the Raman spectra matrix, several images were simultaneously mapped from the same spectrum at different peaks, such as for polyethylene at 1,060, 1,120, 1,300, 1,440, and 2,890 cm^{-1}. At these peak positions, the intensity signal can be mapped as different colors of images. Two or more images as parent images, which correspond to two or more different characteristic peaks, can be merged as a daughter image, either by logic-OR or logic-AND.

For the algorithm analysis, we employed ImageJ software. In general, the parent Raman images are opened by the software and processed and merged with a calculator of logic-OR or logic-AND.

In the case of "logic-OR," any mapped signal (or dot or pixel) from any image (parent images) will be fetched and merged into a new image (daughter image). Obviously, any "bias and false" noise from the parent images (mapped at two different Raman peaks) might be collected. However, the advantage is that it can significantly reduce signal loss.

In the case of "logic-AND," the parent Raman images are opened by the software and converted from red-green-blue (RGB) to an 8-bit format. Then, the images are processed and merged with a calculator of logic-AND. After merging, the new image is painted to the selected color in the displaying value range of 0–100, which can be converted back to the RGB format as the daughter image. The image certainty is increased statistically.

RESULTS AND DISCUSSION

Sampling and the Mother Matrix

In this study, we tested two soil samples and their sampling sites are shown in **Figures 1A,B**. The primary material is made of either polyethylene or polypropylene, as suggested by its Raman spectra from the "mother matrix" (brand new from the market) in **Figure 1C**. During the fabrication process of the "mother matrix," some pigments or dyes might be formulated to control the color of the products and some additives might be introduced as well to enhance the properties. Consequently, from **Figure 1C**, it can be seen that it is difficult to get the exactly matched spectrum with the standard ones including polypropylene and polyethylene.

In the meantime, the broad peaks for black carbon, which appear at ~1,360 and ~1,580 cm^{-1} (Dychalska et al., 2015), were observed from the black landscape fabrics. Fortunately, the prominent characteristic peaks for polypropylene (green) and polyethylene (red), along with the broad peak at 2,890 cm^{-1} (that is assigned to the C-H bond), can be observed for the landscape fabrics and bubble wrap, as marked in **Figure 1C**. These peaks are marked with dashed lines and selected to identify microplastics as given in the following.

From the spectra shown in **Figure 1C**, we confirm that the items in **Figures 1A,B** and their mother matrices are mainly made of plastics, including polypropylene and polyethylene. We then tried to collect their degradation products, the released small fragments or microplastics, formed after 7 years in the garden. Note that these samples might not be representative and vary from gardens to gardens, depending on the ageing, weathering, soil properties, planting, etc. In this case study, however, we intend to collect the released microplastics from the mother matrices to monitor their breakdown fate in one garden.

Bubble Wraps

Microplastics in the Range of 5–0.75 mm, Without Pretreatment

Figure 2 shows the characterization of microplastics released from the bubble wrap in the size range from 0.75 to 5 mm, which is visible to our naked eyes and through a smartphone camera as well. As shown in **Figure 2A**, from the photo image taken with a smartphone, we can assign the floating items on the water surface to microplastics, which are transparent slight-white fragments. A general estimation is that there are ~150 pieces of microplastics in a ~10 g sample. This number is significant, and the potential contamination should be avoided. That is, the bubble wrap should be collected and should not be mixed with the mulch, as the wrongdoing shown here.

As shown in **Figures 2B,C**, the photo images were recorded during the Raman test process. The typical spectra are shown in **Figure 2D**. When compared with the spectra of the "mother matrix," only the main peak at 2,890 cm^{-1} can be identified clearly. Consequently, the mapped patterns in **Figure 2E** are

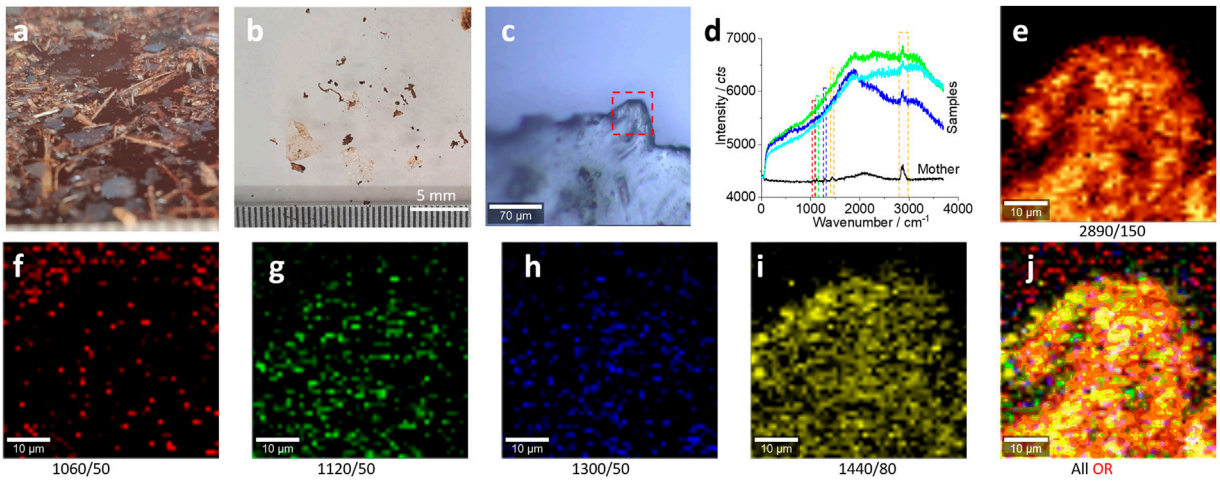

FIGURE 2 | Microplastics **(without pretreatment)** in the range of 5–0.75 mm released from the bubble wrap and their characterizations. **(A)** The floating microplastics on the water surface, as transparent **(slight white)** films/fragments. After drying, the sample was distributed on a glass surface for the Raman test **(B, C)**. **(D)** The typical Raman spectra collected from the squared area in **(C)** for images **(E–J)**. All Raman spectra were collected with an objective lens of 20×, for a scanning area of 50 μm × 50 μm, with a pixel of 1 μm × 1 μm and integration time of 1 s. The intensity images **(E–I)** are mapped at the characterized peaks, as marked (and the peak width), with 10% color off-setting. **(J)** An image after merging all the intensity images **(E–I)** using logic-OR.

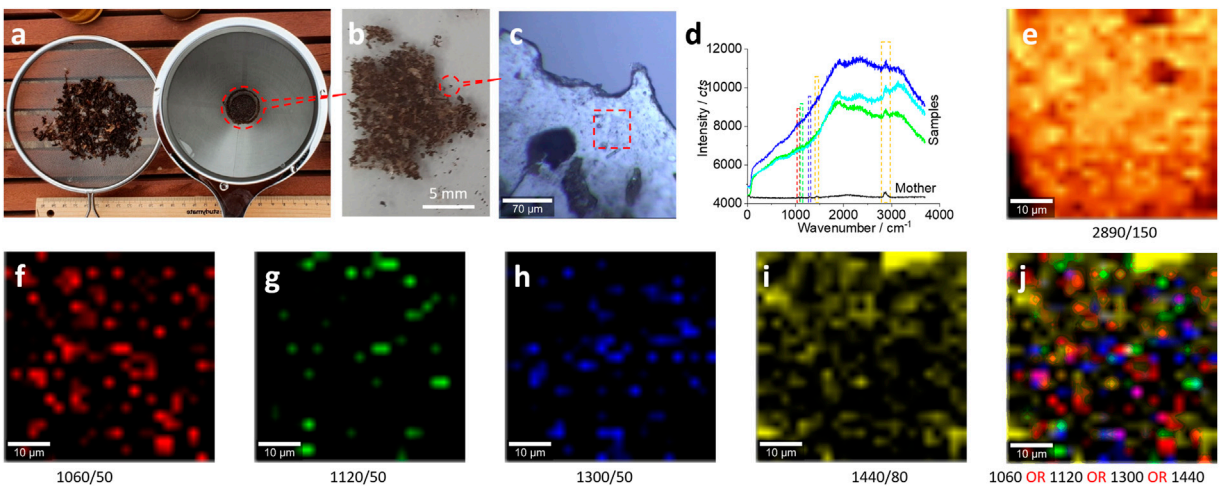

FIGURE 3 | Microplastics **(without pretreatment)** in the size range of 0.75 mm–100 μm released from the bubble wrap and their characterizations. **(A)** The collected microplastics after drying using a net **(left)** to collect samples in the range of 5–0.75 mm and a coffee filter **(right)** to collect samples in the range of 0.75 mm–100 μm, respectively. The latter were distributed on a glass surface for the Raman test **(B, C)**. **(D)** The typical Raman spectra collected from the squared area in **(C)** for images **(E–J)**. All Raman spectra were collected with an objective lens of 20×, for an area of 50 μm × 50 μm, with a pixel of 1 μm × 1 μm and integration time of 1 s. The intensity images **(E–I)** are mapped at the characterized peaks, as marked [and the peak width as well, also squared in **(D)**], with 10% color off-setting. **(J)** A merged image of **(F–I)** using logic-OR.

well matched with the photo image squared in **Figure 2C**, suggesting the existence of the microplastics.

As can be seen from **Figure 2D**, the other characteristic peaks (squared) of polyethylene from the collected microplastics are weak. However, we can still map their intensities as images. **Figures 2F–I** show the generated intensity images at the selected peaks for polyethylene. We can see the matched patterns of images with those in **Figure 2C**, including the characteristic peaks at 1,060 cm^{-1} (f), 1,120 cm^{-1} (g), 1,300 cm^{-1} (h), and 1,440 cm^{-1} (i) (Sobhani et al., 2019). The reason for this successful image is that these images are generated from the Raman scanning spectrum matrix, which contains 50 × 50 spectra. When the peak intensity is obtained by integration, accumulation, and averaging of the peak area, the signal-to-noise ratio can be enhanced significantly. After mapping as an image, the signal-to-noise ratio of the image is different from that of a single spectrum (50 × 50 vs. 1), from the statistical point of view.

Using logic-OR, we can merge all these images into one (Fang et al., 2021c). The imaged pattern is much clear, as shown in **Figure 2J**. In effect, all the images in **Figure 2E,G–J** show the

well-matched pattern with those in **Figure 2C**, except the image in **Figure 2F**. This is because the peak at 1,060 cm^{-1} is intrinsically weaker than other peaks, as observed in **Figure 1D**.

From the results in **Figure 2**, we can see the success of the capture of microplastics, in the range of 0.75–5 mm, even without special pretreatment. When the size shrinks, the test results are different as reported in the following.

Microplastics in the Range of 0.75 mm–100 μm, Without Pretreatment

Figure 3A shows a photo image of the collected samples in the range of 5–0.75 mm (left) and 0.75 mm–100 μm (right). In this part, we focus our test on the microplastics in the range of 0.75 mm–100 μm. The sample was transported to a glass surface, as shown in **Figure 3B**. The photo image under the microscope is shown in **Figure 3C** for the Raman test.

Under the microscope, it is estimated that there are ~136 pieces of microplastics in ~10 g soil in the range of 100 μm–0.75 mm. This estimated amount is comparable with ~150 pieces of microplastics in 10 g soil in the range of 5–0.75 mm, which can witness the degradation fate of the bubble wrap, from larger ones to smaller ones. In other words, we can collect microplastics (5 mm–100 μm) from our garden using kitchenware, that is, ~28.6 pieces of microplastics per gram soil.

Similarly, the Raman spectra in **Figure 3D** can confirm the existence of plastics, particularly in **Figure 3E**, to map the peak at 2,890 cm^{-1}. The images in **Figures 3F–J**, which map other characteristic peaks of polyethylene in **Figure 3D**, further confirm the presence of plastics in the scanning area.

There might be some organic matter on the plastic surface, given the simple sample preparation was conducted on-site in our backyard garden. This might be the reason why there is a strong spectrum background in the Raman spectrum shown in **Figure 3D** and the reason why the images in **Figures 3F–I** just show a few bright dots. However, even though the signal of microplastics is weak and might be shielded by the background, as shown in **Figures 3E–I**, we can assume that the scanning area is mainly made of microplastics. This assumption can be observed clearly in **Figure 3J**, when the images (f–i) have been merged together to enhance the mapping certainty *via* enhancing the signal-to-noise ratio.

Therefore, Raman mapping is recommended for microplastic characterization. From the statistical point of view, the intensity image contains the signal from the Raman spectrum matrix, which includes 2,500 spectra here. Consequently, the signal-to-noise ratio for an image is different from that for an individual spectrum, even for a single peak from this individual spectrum. This is why the images in **Figures 3E–J** can analyze the microplastics, while the spectrum in **Figure 3D** is difficult to analyze.

Microplastics in the Range of 100–0.8 μm, With Pretreatment

The signal-to-noise ratio is weak in **Figures 2D, 3D**. When the size of microplastics shrinks, it becomes difficult to identify them. In order to increase the signal-to-noise ratio, we employed the sample pretreatment. To this end, we intend to decrease the noise by cleaning the surface of the microplastics, *via* digestion using H_2O_2 and washing using organic solvents such as ethanol. The results are presented in **Figure 4**. This pretreatment should be carried out in a laboratory rather than in the backyard. Without this kind of sample pretreatment, although we can still analyze the microplastics, as shown in **Supplementary Figure S4** (Supporting Information), it is difficult to identify them due to the low signal-to-noise ratio.

Figure 4A shows a photo image by microscopy. The samples were not transported to the glass surface but localized on the silver membrane/filter surface. **Figure 4B** shows the enhanced spectrum after the sample pretreatment (green curve), particularly for the peak at 2,890 cm^{-1}. Compared to the spectrum collected before the sample pretreatment (black curve), the background fluorescence after the pretreatment is significantly decreased. In the meantime, the peak at 1,560 cm^{-1} becomes apparent, which is assigned to black carbon (Dychalska et al., 2015). Consequently, the mapped images in **Figures 4C–I** are presented with a higher certainty, suggesting the success of the sample pretreatment.

When the Raman signal is weak, we should be careful in selecting the peak width to integrate the peak intensity with image generation. The reason is that the weak Raman signal can experience a gentle shift on the peak position. Consequently, by comparing the image in **Figure 4C** with that in Figure 4D, we can see the slightly changed pattern when the peak width is narrowed from 150 cm^{-1} to 80 cm^{-1}. Similarly, an improvement from the image in **Figure 4F** to the image in Figure 4G is achieved by broadening the peak width from 50 to 80 cm^{-1}. Therefore, we require caution in the selection of the peak position and width to avoid signal loss.

Even so, the signal-to-noise ratio is still low. While we need to enhance the ratio further, we might also keep in mind that this issue is difficult to be avoided for the environmental sample. Ageing and weathering make the surface of microplastics covered with organic matter. From **Figure 4A**, we can even know the scanning area is occupied by the bubble wrap fragment, and the mapped images in **Figures 4C–J** only generate the blurred profile of the fragment. Due to the low signal-to-noise ratio, logic-OR, rather than logic-AND, is recommended to merge the images, as presented in **Figure 4J**. Logic-AND might lead to significant signal loss.

For confocal Raman spectroscopy, on the contrary, the Raman signal is mainly collected from the focusing plane, as discussed before (Sobhani et al., 2019). When the plastic fragment is thick and the surface is rough, under the confocal Raman spectroscopy, the top and the bottom parts of the same plastic fragments are not localized on the same focus plane (along the z-axle). If we focus on the top of the microplastic, the bottom part cannot be effectively mapped and thus will be omitted in the mapping image and vice versa; when focus is on the bottom part, the top cannot be mapped effectively. That is, the possible reason for the blurred mapping profile in **Figure 4** is that the scanning area is not flat to be localized on the same plane.

We recommend mapping the image for microplastic analysis. The reason has been discussed above and summarized as follows: 1) The signal-to-noise ratio averaged from a matrix of the Raman spectrum is significantly higher than that from an individual Raman spectrum and a single peak. 2) The multipeak mapping

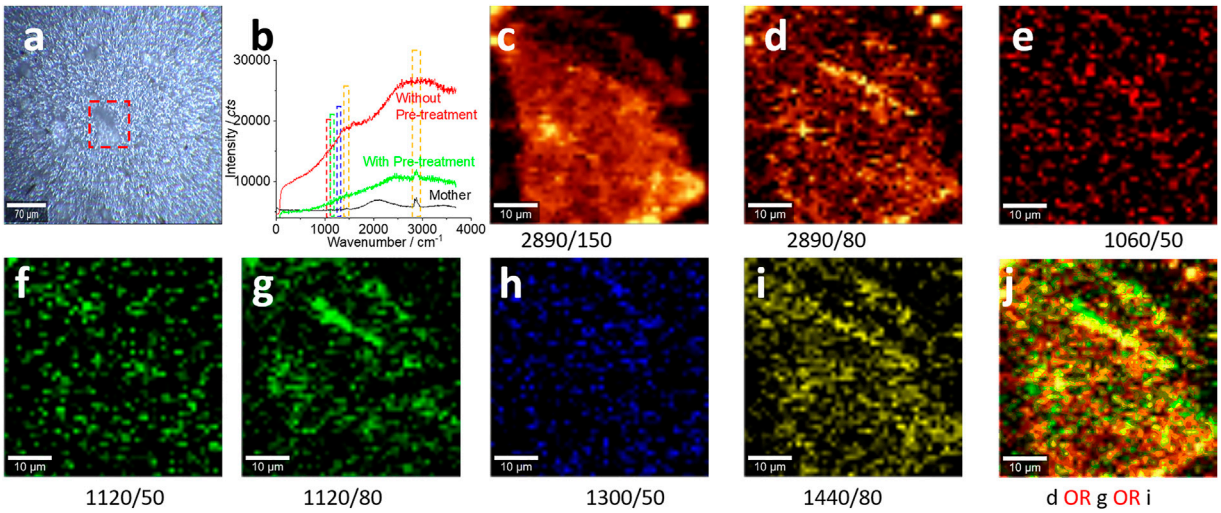

FIGURE 4 | Microplastics **(with pre-treatment)** in the size range of 100–0.8 μm and their characterizations. **(A)** A photo image of the collected microplastics on the silver membrane surface for the Raman test in **(B–J)**. All Raman spectra were collected with an objective lens of 20×, for an area of 50 μm × 50 μm, with a pixel of 1 μm × 1 μm and integration time of 1 s. The intensity images **(C–I)** are mapped at the characterized peaks, as marked (and the peak width as well), with 10% color off-setting. **(J)** A merged image using logic-OR.

can generate multi-images. While the individual image can be used to justify the microplastic, multi-images can be merged for cross-checking, such as by the logic-based algorithm, to increase the analysis certainty. 3) As obtained from the image, if the scanning area is uniformly made of the same material, position identification of one area can be expanded to the whole area, as shown in**Figures 3J** and **4J**. That is, the blurred pattern with bright dots can be considered to represent a whole unique item within the available profile or boundary. Further research is needed here.

In **Figure 4A**, a window view is of 0.35 mm × 0.3 mm in size, containing ~15 pieces of microplastics (per 0.105 mm^2). The silver membrane is of a diameter of 13 mm (~133 mm^2), which has been employed to collect the microplastics in this range of 0.8–100 μm. Therefore, there are around 1.9×10^4 pieces of microplastics in this range if they are uniformly collected and distributed on the silver filer surface. This number is much higher than that of the large pieces (~286), suggesting the breakdown pathway from the "mother" item, a large bubble wrap at the very beginning. That is, after the large wrap has been subject to 7 year's breakdown, which deteriorate the wrap, akin ant-chewing from the peripheral to form a sawtooth boundary, small pieces can be easily released as microplastics, as shown in **Supplementary Figure S3** (Supporting Information).

This kind of test needs much research because of the difficulty to find nanoplastics, mainly due to the low signal-to-noise ratio. Therefore, the test for nanoplastics needs more research, particularly for the environmental samples.

Landscape Fabrics

Microplastics in the Range of 5–0.75 mm, Without Pretreatment

Similarly, we tried to collect microplastics released from landscape fabrics. In **Figure 1B**, we can see the original width of the fabric is ~2 mm. The spectrum in **Figure 1C** suggests that the fabric is made of polypropylene mainly, with a background either from the black carbon (Dychalska et al., 2015) or from the fluorescence. After serving as the mulch bed to cover the soil ground for 7 years, fragments were released as microplastics, as shown in **Figure 5**.

Figure 5A shows the typical Raman spectra recorded from the samples, which are positioned in **Figure 5B**. **Figure 5B** shows the typical fragments collected by us, where one is longer than 5 mm, considered as macroplastics, and the rest are generally categorized as microplastics, from fibers to irregular fragments, as shown in **Figures 5C,D**. The fractured parts in **Figure 5C** suggest the breakdown process of the fabric. This fracture can also be confirmed from the structure shown in **Figure 5D**, where another fiber (with a diameter or width of ~12 μm) has been fractured from the fabric trunk. All these microplastics might be released and fractured from the original fabric with a width of ~2 mm.

To further confirm the released microplastics, we scan the squared area in **Figure 5D** and map the Raman intensity images again. The selected peaks have the characteristics of polypropylene. In **Figures 5E–H**, the mapped pattern is well matched with that in **Figure 5D**, confirming the presence of microplastics of polypropylene. Because the surface of the microplastics had not been effectively cleaned, some organic matter or derived groups might interfere with the Raman test. This is the reason why the mapping images just yield the boundary or the profile. Another reason for the blurred image is that the confocal Raman spectra just collects the signal from the focus plane, which is localized at the boundary, as mentioned above.

Using logic-OR, we can merge all the obtained images and generate an image as shown in **Figure 5I**, further confirming the

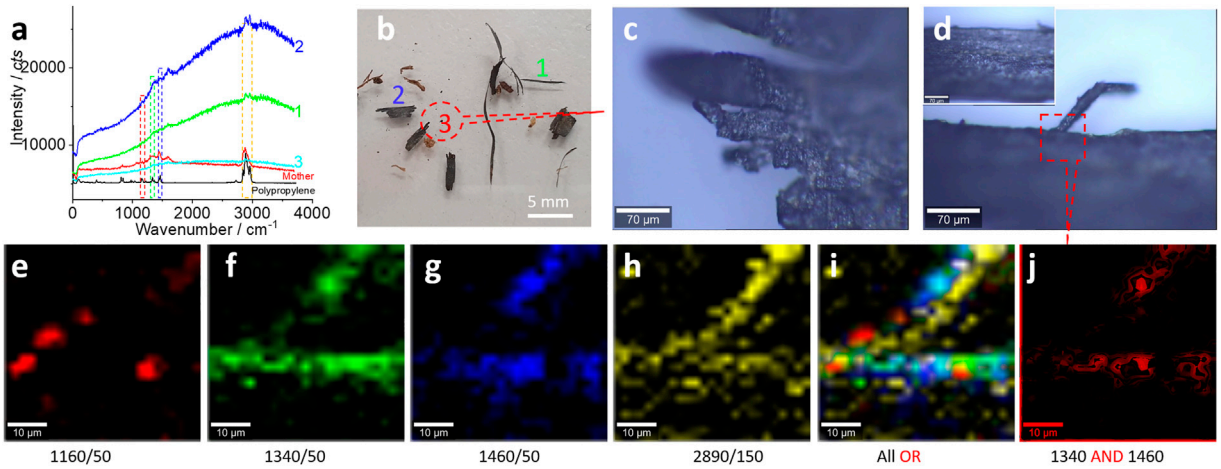

FIGURE 5 | Microplastics **(without pretreatment)** in the range of 5–0.75 mm released from the landscape fabric and their characterizations. **(A)** The typical Raman spectra and the comparison with the spectra of standard polypropylene and the mother matrix. **(B)** The positions to collect the Raman spectra in **(A)**. Among them, item #1 is zoomed in **(D)**, #2 is a mulch, and #3 is zoomed in **(C)**. In **(D)**, the square area is scanned for the Raman mapping images **(E–H)** at the characteristic peaks, as marked (and the peak width), with 10% color off-setting. **(I, J)** The merged images of the selected Raman images using logic-OR or logic-AND, as indicated. The Raman spectra were collected with an objective lens of 20×, for an area of 50 µm × 50 µm, with a pixel of 2 µm × 2 µm and integration time of 2 s.

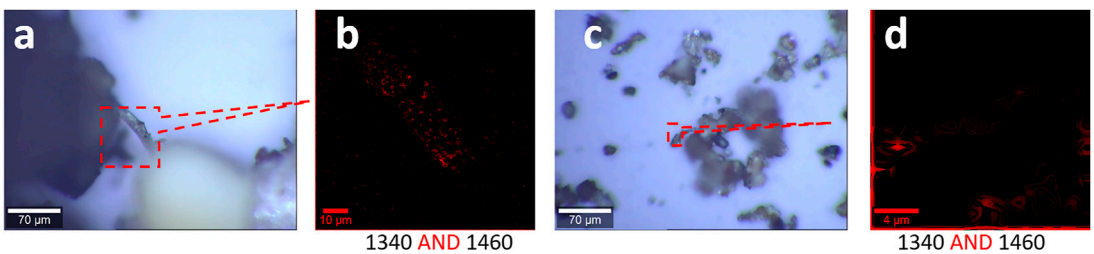

FIGURE 6 | Microplastics **(without pretreatment)** in the range of 0.75 mm–0.8 µm released from the landscape fabric and their characterizations, including photo images **(A, C)** and Raman images **(B, D)**. **(A, B)** Results in the size range of 0.75 mm–100 µm. **(C, D)** Results in the size range of 100–0.8 µm. The Raman spectra were collected with an objective lens of 40×, with a pixel of 1 µm × 1 µm and integration time of 1 s, with 10% color off-setting. Both Raman images are the merged image of the two images mapped at the marked peaks using logic-AND.

presence of microplastics of polypropylene. To increase the image certainty, we generated an image shown in **Figure 5J**, using logic-AND by merging two images (Figures 5f, g) with strong signals. By doing so, we can cross-check the existence of microplastics. In other words, the image certainty has been increased, from the statistical point of view again.

Microplastics in the Range of 0.75 mm–0.8 µm, Without Pretreatment

When the released polypropylene microplastics shrink in size, the Raman identification gets more complicated. Unlike the bubble wrap that is transparent/white which is easy to be identified and localized under the optical microscope for characterization, the black landscape fabric's microplastics are mixed with soil, black matter, plant roots, etc. The signal-to-noise ratio is decreased, too. Overall, when the size shrinks, it becomes difficult to characterize the microplastics.

To simplify the analysis process, we fix the Raman mapping parameters, which have been employed in **Figure 5**, to generate two images individually and merge them together *via* logic-AND. The different sizes of microplastics are mapped in **Figure 6**, including the size range of 0.75 mm–100 µm (a, b) and 100–0.8 µm (c, d). The pattern of images in **Figures 6B,D** are well matched with the pattern in **Figures 6A,C** , suggesting the success of the capture of the microplastics.

In general, we can collect the microplastics, although the image certainty varies. This mapping and merging approach *via* the logic algorithm is reckoned for microplastic analysis, in particular, when the signal is weak.

Microplastics in the Range of 100–0.8 µm, With Pretreatment

In order to increase the signal-to-noise ratio, again, we performed the pretreatment of the microplastics in the range of 100–0.8 µm, and the results are presented in **Figure 7**. **Figures 7A,B** show the effect of the focus plane, where (a) is focused on the top of the large fragments, while (b) is focused on the bottom of them and also the surface of the silver membrane that has been employed as

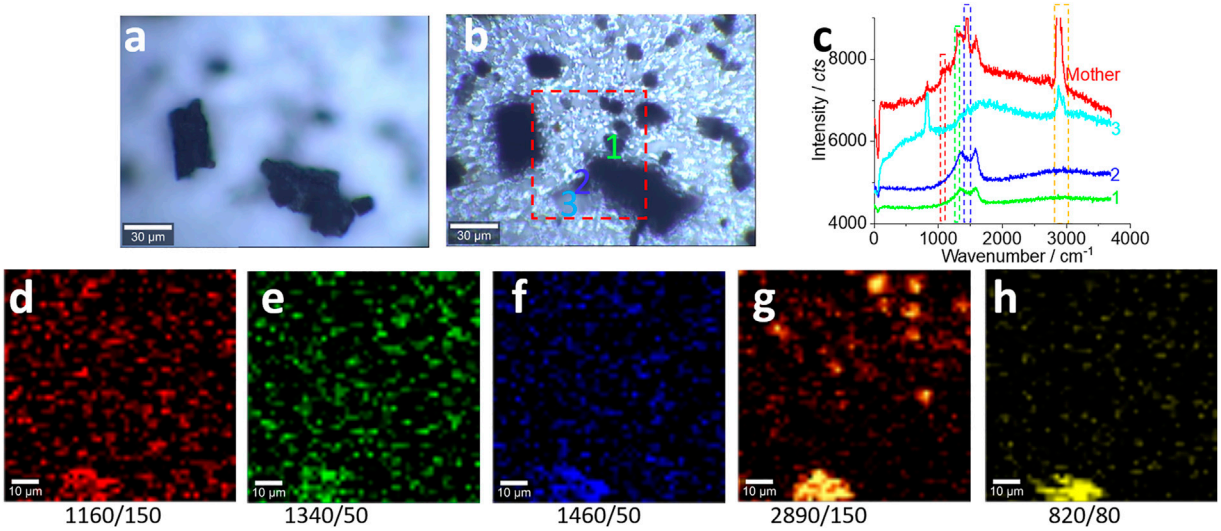

FIGURE 7 | Microplastics **(with pretreatment)** in the range of 100–0.8 μm released from the landscape fabric and their characterizations. **(A, B)** The effect of the focusing position at the top **(A)** or at the bottom **(B)**, where **(B)** is selected to collect the Raman signal by confocal Raman spectroscopy. **(C)** The typical Raman spectra collected from the marked positions in **(B)**. All Raman spectra were collected with an objective lens of 40×, for an area of 85 μm × 85 μm, with a pixel of 1.75 μm × 1.75 μm and integration time of 1 s. The intensity images **(D–G)** are mapped at the characterized peaks, as marked **(and the peak width)**, with 10% color off-setting. **(H)** The background that might be assigned to other items.

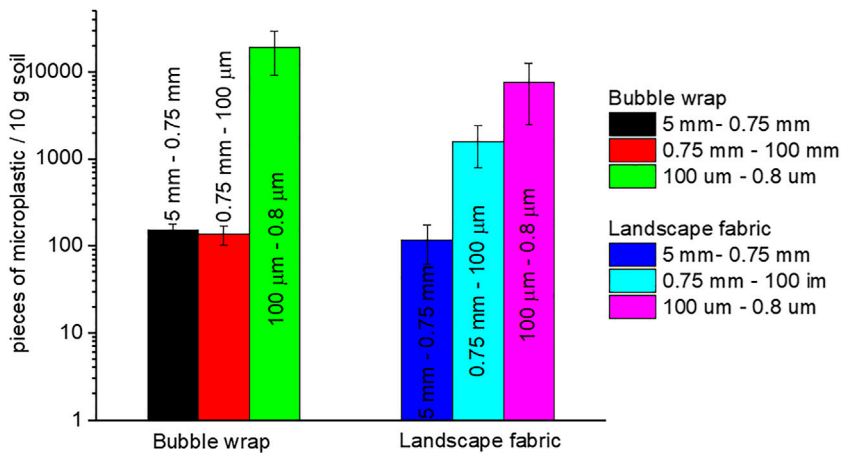

FIGURE 8 | Amount of the released microplastics.

the filter to collect the microplastics. The different focusing planes are the main reason why the confocal Raman spectroscopy cannot map all the fragments, as shown in **Figures 7D–G**.

Compared with the sample without pretreatment shown in **Figures 6C,D**, for the analysis in the same size range, the samples in **Figure 7** were not transported to the glass surface. Also, after the pretreatment, the microplastics have been concentrated to some degree and the identification of the microplastics becomes easier than that shown in **Figure 6**. As can be seen from **Figure 6C**, most of the items are usually soil and organic matter. However, in **Figures 7A,B**, most items are identified as microplastics. **Figure 7C** shows the Raman spectra that have been collected on the indicated positions in (b). Basically, the signal-to-noise ratio has been improved, compared with that before the pretreatment.

Even so, the mapping images in **Figures 7D–G** just show the profile of the fragments. Among these images, **Figure 7G** yielded a higher (more bright) signal-to-noise ratio, which is due to the strong signal at the peak of C-H. This pattern is matched with that in **Figure 7B**. Some extra-mapped "fragments" might be the false positives and false negatives produced due to the low signal-to-noise ratio. On the contrary, the resolution of the photo image in **Figure 7B** is not high enough to visualize all small microplastics and nanoplastics, while the Raman image can,

which is the advantage of the Raman mapping (Fang et al., 2020; Fang et al., 2021c). Again, we recommend mapping, rather than of an individual Raman spectrum, to analyze microplastics particularly, when the signal-to-noise ratio is low, such as for the environmental samples, as shown here. As mentioned above, within the scanning area, identification of one position and assignment of the microplastic can be expanded to a whole fragment, such as the bright position mapped on the middle-bottom part of the images. The cross-check in **Figures 7D–G** can assume that the microplastics are presented at the middle-bottom part, which can be expanded to the whole fragment in **Figure 7B** to assume that the large fragment is made of plastic as well.

However, the image in **Figure 7H** might be assigned to other items, such as slat or other interference sources (Sobhani et al., 2019; Sobhani et al., 2020b), which needs more research.

We can also estimate the amount of the released microplastics, and the results are shown in **Figure 8**. Admittedly, the estimation suffers from significant variations, particularly for the small ones in the range of 100–0.8 μm, and the test for the nanoplastics (<0.8 μm) is not available here. Generally, small fragments (100–0.8 μm) attain a higher number than large ones. The reason has been discussed earlier and shown in **Supplementary Figure S3** (Supporting Information). Furthermore, unlike the wrongly discarded bubble wrap that is just a small piece at the beginning as the "mother," the landscape fabric can cover the whole garden. In this case, for a covered area of 1 m^2 in our garden, the released amount of microplastics can reach hundreds of millions, according to our estimation.

CONCLUSION

We demonstrate here that we can collect microplastics from our gardens, *via* a simplified sample preparation process of Raman imaging, as a case study. We consider the Raman imaging and logic-based algorithm to increase the signal-to-noise ratio and the image certainty. This approach is helpful in analyzing the weak signal of the environmental samples, particularly when the signal is almost shielded by the background.

We also show that the release of microplastics in our garden is profound, either due to the wrongly discarded plastic items such as bubble wrap or due to the use of plastic items such as landscape fabrics as the mulch bed. Although the nanoplastic characterization is not available in this study, the released amount is expected to be significant. For example, a piece of plastic at a size of 5 mm × 5 mm × 5 mm is equivalent, in mass or weight, to 1×10^9 pieces of microplastics at a size of 5 μm × 5 μm × 5 μm or equivalent to 1×10^{18} pieces of nanoplastics at a size of 5 nm × 5 nm × 5 nm. Therefore, if we care about the contamination from microplastics and nanoplastics, we must be very cautious about the use of plastic items in our garden.

DATA AVAILABILITY STATEMENT

The original contributions presented in the study are included in the article/**Supplementary Material**; further inquiries can be directed to the corresponding author.

AUTHOR CONTRIBUTIONS

CF, MM, and RN were involved in experiment design and management. ZS and CG participated in data collection and sample preparation. YT and YL supported the manuscript preparation and reviewing process.

FUNDING

The authors appreciate the funding support from the CRC CARE and the University of Newcastle, Australia.

ACKNOWLEDGMENTS

For the Raman measurements, the authors acknowledge the use and support of the South Australian node of Microscopy Australia (formerly known as AMMRF) at Flinders University, South Australia.

SUPPLEMENTARY MATERIAL

The Supplementary Material for this article can be found online at https://www.frontiersin.org/articles/10.3389/fenvs.2021.739775/full#supplementary-material

REFERENCES

Andrady, A. L. (2017). The Plastic in Microplastics: A Review. *Mar. Pollut. Bull.* 119 (1), 12–22. doi:10.1016/j.marpolbul.2017.01.082

Arthur, C., Baker, J. E., and Bamford, H. A. (2009). in Proceedings of the International Research Workshop on the Occurrence, Effects, and Fate of Microplastic Marine Debris, September 9-11, 2008 (Tacoma, WA, USA: University of Washington Tacoma).

Browne, M. A. (2015). "Sources and Pathways of Microplastics to Habitats," in *Marine Anthropogenic Litter* (Springer), 229–244. doi:10.1007/978-3-319-16510-3_9

Cox, K. D., Covernton, G. A., Davies, H. L., Dower, J. F., Juanes, F., and Dudas, S. E. (2019). Human Consumption of Microplastics. *Environ. Sci. Technol.* 53 (12), 7068–7074. doi:10.1021/acs.est.9b01517

Dychalska, A., Popielarski, P., Franków, W., Fabisiak, K., Paprocki, K., and Szybowicz, M. (2015). Study of CVD diamond Layers with Amorphous Carbon Admixture by Raman Scattering Spectroscopy. *Mater. Science-Poland.* 33, 799–805. doi:10.1515/msp-2015-0067

Fang, C., Luo, Y., Zhang, X., Zhang, H., Nolan, A., and Naidu, R. (2021a). Identification and Visualisation of Microplastics via PCA to Decode Raman Spectrum Matrix towards Imaging. *Chemosphere* 286, 131736. doi:10.1016/j.chemosphere.2021.131736

Fang, C., Sobhani, Z., Zhang, D., Zhang, X., Gibson, C. T., Tang, Y., et al. (2021b). Capture and Characterisation of Microplastics Printed on Paper via Laser

Printer's Toners. *Chemosphere* 281, 130864. doi:10.1016/j.chemosphere.2021.130864

Fang, C., Sobhani, Z., Zhang, X., Gibson, C. T., Tang, Y., and Naidu, R. (2020). Identification and Visualisation of Microplastics/Nanoplastics by Raman Imaging (Ii): Smaller Than the Diffraction Limit of Laser? *Water Res.* 183, 116046. doi:10.1016/j.watres.2020.116046

Fang, C., Sobhani, Z., Zhang, X., McCourt, L., Routley, B., Gibson, C. T., et al. (2021c). Identification and Visualisation of Microplastics/Nanoplastics by Raman Imaging (Iii): Algorithm to Cross-Check Multi-Images. *Water Res.* 194, 116913. doi:10.1016/j.watres.2021.116913

Gigault, J., Halle, A. t., Baudrimont, M., Pascal, P.-Y., Gauffre, F., Phi, T.-L., et al. (2018). Current Opinion: What Is a Nanoplastic? *Environ. Pollut.* 235, 1030–1034. doi:10.1016/j.envpol.2018.01.024

Hartmann, N. B., Skjolding, L. M., Nolte, T., and Baun, A. (2016). *Aquatic Ecotoxicity Testing of Nanoplastics-Lessons Learned from Nanoecotoxicology*. SETAC Europe, 43–44.

Ivleva, N. P., Wiesheu, A. C., and Niessner, R. (2017). Microplastic in Aquatic Ecosystems. *Angew. Chem. Int. Ed.* 56 (7), 1720–1739. doi:10.1002/anie.201606957

Koelmans, A. A., Mohamed Nor, N. H., Hermsen, E., Kooi, M., Mintenig, S. M., and De France, J. (2019). Microplastics in Freshwaters and Drinking Water: Critical Review and Assessment of Data Quality. *Water Res.* 155, 410–422. doi:10.1016/j.watres.2019.02.054

Liebezeit, G., and Liebezeit, E. (2014). Synthetic Particles as Contaminants in German Beers. *Food Additives & Contaminants: A* 31 (9), 1574–1578. doi:10.1080/19440049.2014.945099

Mattsson, K., Johnson, E. V., Malmendal, A., Linse, S., Hansson, L.-A., and Cedervall, T. (2017). Brain Damage and Behavioural Disorders in Fish Induced by Plastic Nanoparticles Delivered through the Food Chain. *Sci. Rep.* 7 (1), 11452. doi:10.1038/s41598-017-10813-0

Sobhani, Z., Al Amin, M., Naidu, R., Megharaj, M., and Fang, C. (2019). Identification and Visualisation of Microplastics by Raman Mapping. *Analytica Chim. Acta* 1077, 191–199. doi:10.1016/j.aca.2019.05.021

Sobhani, Z., Lei, Y., Tang, Y., Wu, L., Zhang, X., Naidu, R., et al. (2020a). Microplastics Generated when Opening Plastic Packaging. *Sci. Rep.* 10 (1), 4841. doi:10.1038/s41598-020-61146-4

Sobhani, Z., Zhang, X., Gibson, C., Naidu, R., Megharaj, M., and Fang, C. (2020b). Identification and Visualisation of Microplastics/nanoplastics by Raman Imaging (I): Down to 100 Nm. *Water Res.* 174, 115658. doi:10.1016/j.watres.2020.115658

Steinmetz, Z., Wollmann, C., Schaefer, M., Buchmann, C., David, J., Tröger, J., et al. (2016). Plastic Mulching in Agriculture. Trading Short-Term Agronomic Benefits for Long-Term Soil Degradation? *Sci. Total Environ.* 550, 690–705. doi:10.1016/j.scitotenv.2016.01.153

Vroom, R. J. E., Koelmans, A. A., Besseling, E., and Halsband, C. (2017). Aging of Microplastics Promotes Their Ingestion by marine Zooplankton. *Environ. Pollut.* 231, 987–996. doi:10.1016/j.envpol.2017.08.088

Wright, S. L., and Kelly, F. J. (2017). Plastic and Human Health: a Micro Issue? *Environ. Sci. Technol.* 51 (12), 6634–6647. doi:10.1021/acs.est.7b00423

Zhang, L., Sintim, H. Y., Bary, A. I., Hayes, D. G., Wadsworth, L. C., Anunciado, M. B., et al. (2018). Interaction of Lumbricus Terrestris with Macroscopic Polyethylene and Biodegradable Plastic Mulch. *Sci. Total Environ.* 635, 1600–1608. doi:10.1016/j.scitotenv.2018.04.054

Conflict of Interest: The authors YL, RN, MM, and CF are employed at CRC CARE Pty Ltd.

The remaining authors declare that the research was conducted in the absence of any commercial or financial relationships that could be construed as a potential conflict of interest.

Publisher's Note: All claims expressed in this article are solely those of the authors and do not necessarily represent those of their affiliated organizations, or those of the publisher, the editors, and the reviewers. Any product that may be evaluated in this article, or claim that may be made by its manufacturer, is not guaranteed or endorsed by the publisher.

frontiers in Environmental Science

ORIGINAL RESEARCH
published: 18 October 2021
doi: 10.3389/fenvs.2021.746195

Rapid In-Field Approaches for Delineating VOC in Both Soil Vapour and Groundwater for Vapour Intrusion Assessment

Liang Wang[1,2]*, *Ying Cheng*[1,2], *Ravi Naidu*[1,2], *Peter Gell*[2] and *Mark Bowman*[3]

[1]Global Centre for Environmental Remediation, Faculty of Science, University of Newcastle, Callaghan, NSW, Australia, [2]CRC for Contamination Assessment and Remediation of the Environment, University of Newcastle, Callaghan, NSW, Australia, [3]The Department of Defence, Canberra BC ACT, Canberra, NSW, Australia

Traditional contaminated site characterisation approaches are time-consuming, labour-intensive, and demand a high level of expertise. This case study provides a rapid field-based solution to investigating a VOC contaminated site and its vapour incursion by combining soil vapour and groundwater survey. To fully assess the volatile organic compound (VOC) distribution in a contaminated site, a number of self-developed soil vapour sampling probes (SVSPs) were placed vertically at different locations in a grid with different depths. Hence, 3D subsurface contour maps for VOC concentrations in soil vapour can be obtained and used to help identify hot spots and the migration patterns of VOCs. This SVSP is "easy-to-install" in the field and a cost-effective solution for rapid assessment of soil vapour samples. The SVSPs can be installed both vertically and horizontally. If there is a requirement to take soil vapour samples beneath an existing building from a potential contamination source zone, SVSPs can be horizontally installed beneath the building without compromising its structural integrity. In addition, to ascertain the correct groundwater channels that are likely to carry contaminants from a potential source zone, an electrical resistivity tomography technique was employed to provide the preliminary information for groundwater delineation in a complex groundwater channel network.

Keywords: vapour intrusion assessment, horizontal soil vapour probes, volatile organic compound, portable gas chromatography - mass spectrometer, earth resistivity tomography, subsurface imaging

OPEN ACCESS

Edited by:
Jane A. Entwistle, Northumbria University, United Kingdom

Reviewed by:
Luchun Duan, The University of Newcastle, Australia
Michael Edward Deary, Northumbria University, United Kingdom
José Carlos Rocha Gouvêa Júnior, Companhia Siderúrgica Nacional, Brazil

***Correspondence:**
Liang Wang
Liang.Wang@newcastle.edu.au

Specialty section:
This article was submitted to Toxicology, Pollution and the Environment, a section of the journal Frontiers in Environmental Science

Received: *23 July 2021*
Accepted: *30 September 2021*
Published: *18 October 2021*

Citation:
Wang L, Cheng Y, Naidu R, Gell P and Bowman M (2021) Rapid In-Field Approaches for Delineating VOC in Both Soil Vapour and Groundwater for Vapour Intrusion Assessment. Front. Environ. Sci. 9:746195. doi: 10.3389/fenvs.2021.746195

INTRODUCTION

Groundwater flows through a contaminated area can carry volatile organic compound (VOC) contaminants off-site, where VOC vapours could migrate vertically and laterally through the soil in a residential area, and subsequently through building foundations to contaminate residential indoor air, a process known as vapour intrusion. For a vapour intrusion risk assessment, the conventional method is to install a network of groundwater monitoring wells around targeted locations. Nevertheless, using this conventional method to locate and identify the correct groundwater channels that require the most treatment is costly and inefficient without firstly being able to identify the source zone.

A solution for identifying the source zone is to install a network of soil vapour monitoring bores. Traditional vapour sampling bores take time to construct and install and is technically challenging.

Furthermore, monitoring soil vapour beneath a functional building without jeopardising its structural integrity presents some difficulties. Horizontal vapour probes or wells are commonly used for soil vapour extraction and remediation because they provide good access to horizontally moving contaminants or subsurface areas without causing damage to surface structures (Spuij et al., 1995; Armstrong et al., 1996; Osborn et al., 2011). However, it appears that horizontal soil vapour probes have not been utilised for soil vapour sampling and monitoring. Most likely, this is because of the need to isolate the sampling/monitoring probes to avoid ambient air intrusion on the underground sampling point.

In our prior study (Wang et al., 2021), an easy-to-install and retractable soil vapour sampling probe (SVSP) was introduced to rapidly sample soil vapour (Ayolabi et al., 2013). After being installed in a pre-drilled borehole and sealed with bentonite, it was found to work satisfactorily for soil vapour samples collecting from a range of soil depths. In this current study, using the horizontal drilling approach, the SVSP was further designed to be able to be horizontally installed beneath a functioning building to assess a possible contamination source zone. This study also showed that sampling with the SVSP is a cost-effective way to rapidly identify a potential source zone.

Following the identification of a source zone, groundwater remediation treatments are normally applied to the groundwater channels that intersect the source zone which may appear in the subsurface as a complex network of channels. The earth resistivity topology (ERT) technique can be used to outline the groundwater channel distribution in an intricate groundwater channel network situation, making it easier to identify areas for groundwater well placement. Over the past decade, ERT is a technology that has been widely used to identify and delineate groundwater channels (Mastrocicco et al., 2010; Müller et al., 2010; Saad et al., 2012; Meyerhoff et al., 2014). ERT is a geophysical technique that produces vertical 2D (length and depth) images of the electrical resistivity distribution in the subsoil. To conduct an ERT survey, cables connected to the ERT instrument leading to several steel electrodes are placed on the ground. The electrodes are attached at a set distance according to a specific electrode configuration. Using a four-electrode measurement methodology, the ERT techniques can be applied to investigate electrical resistivity in the subsurface. By producing changes in the electrical potential a known current flow is introduced to two electrodes to another set of electrodes at a set distance away. The potential difference between the electrodes is recorded (Meyerhoff et al., 2014) and inversion algorithms, such as Res2Dinv, are applied to generate electrical resistivity tomography. Changes in soil lithology, saturation, and salinity, as well as groundwater and groundwater contamination, all contribute to geologic variations in ground resistivity values. Furthermore, ERT can be used to relate soil contaminant characteristics, such as hydrocarbon pollution (Arrubarrena Moreno and Arango-Galván, 2013; Ayolabi et al., 2013) and heavy metals (Bravo and Benavides-Erazo, 2020). In this study, ERT was used to identify and locate naturally developed groundwater channels that cross the source zone. Several groundwater monitoring wells were installed and sampled to validate the ERT findings.

In this study, instead of employing typical laboratory analytical procedures, such as USEPA Methods TO-14 and TO-15 (Compendium Method TO-15, 1997; Method-14, 1999), a portable gas chromatography-mass spectrometer (GC/MS) was used to determine VOCs in the field. The analysis of VOCs and SVOCs in indoor and outdoor air samples has been extensively used by portable GC/MS in a variety of applications (Shakoor et al., 1997; Barnes et al., 2004; Fair et al., 2010; Gorder and Dettenmaier, 2011; Hopler, 2012; Leary et al., 2016) and the instrument can approach detection limits that satisfy criteria required by environmental protection authorities (EPA). With the fast in-field sample preparation and pre-concentration processes, such as employing the solid-phase micro-extraction (SPME) approach to sample conditioning, studies have demonstrated that the portable GC/MS instrument is reliable for rapid in-field quantitative analysis of VOCs for contaminated site vapour intrusion assessment (Hook et al., 2002; Wang et al., 2021).

MATERIALS AND METHODS

SVSP Installation

In a prior paper (Wang et al., 2021), the self-developed SVSP was introduced with results that it worked faultlessly when installed in a pre-drilled borehole and back-filled with bentonite and soil to isolate the sampling point from. The SVSP comprises a 100 mm long and 80 mm diameter stainless steel cylindrical vapour chamber coupled to a non-absorbent Teflon sampling tube, 6 mm inner diameter, that connects the vapour chamber to the ground level, from which samples can be gathered. By preventing soil particles from clogging the sampling tube, the chamber permits soil vapour to be collected from the surrounding subsurface soil. The sampler tubing protrudes above the soil surface and is protected by a rigid galvanised pipe with a diameter of 20 mm that is attached to the chamber. The pipe is sealed internally with bentonite to guarantee that vapour is only sampled through the soil surrounding the chamber. The SVSP was fitted with brass fittings, and the depth of the SVSP in the subsoil was modified using different lengths of galvanised pipe to meet a specific sampling demand. At the soil surface, Tedlar bags or vapour canisters are utilised to collect the sample. In this case study, 84 SVSPs were installed vertically at 28 locations over an area of 320 m × 160 m on a seven by four grid, at depths of 1, 2, and 3 m at each location, to obtain data to prepare sub-surface contour maps showing the VOC concentrations in soil vapour at different depths. **Figure 1** shows the locations of the SVSP installation and the source zone.

To access the soil vapour samples beneath a building without compromising the building's structural integrity, three of SVSPs were installed horizontally (**Figure 2**) into pre-drilled boreholes. A Ditch Witch® fitted with a directional drill with a 95 mm wide bit was utilised to construct the boreholes. The initial plan was to drill a pilot hole and then open up with a back reamer drilling in the reverse direction, however, it was found that the pilot holes were wide enough for the installation of the SVSPs. The borehole was developed at a drilling angle (Ø) of 20° downward from horizontal, with a finished borehole length of 15 m. Using trigonometry, the

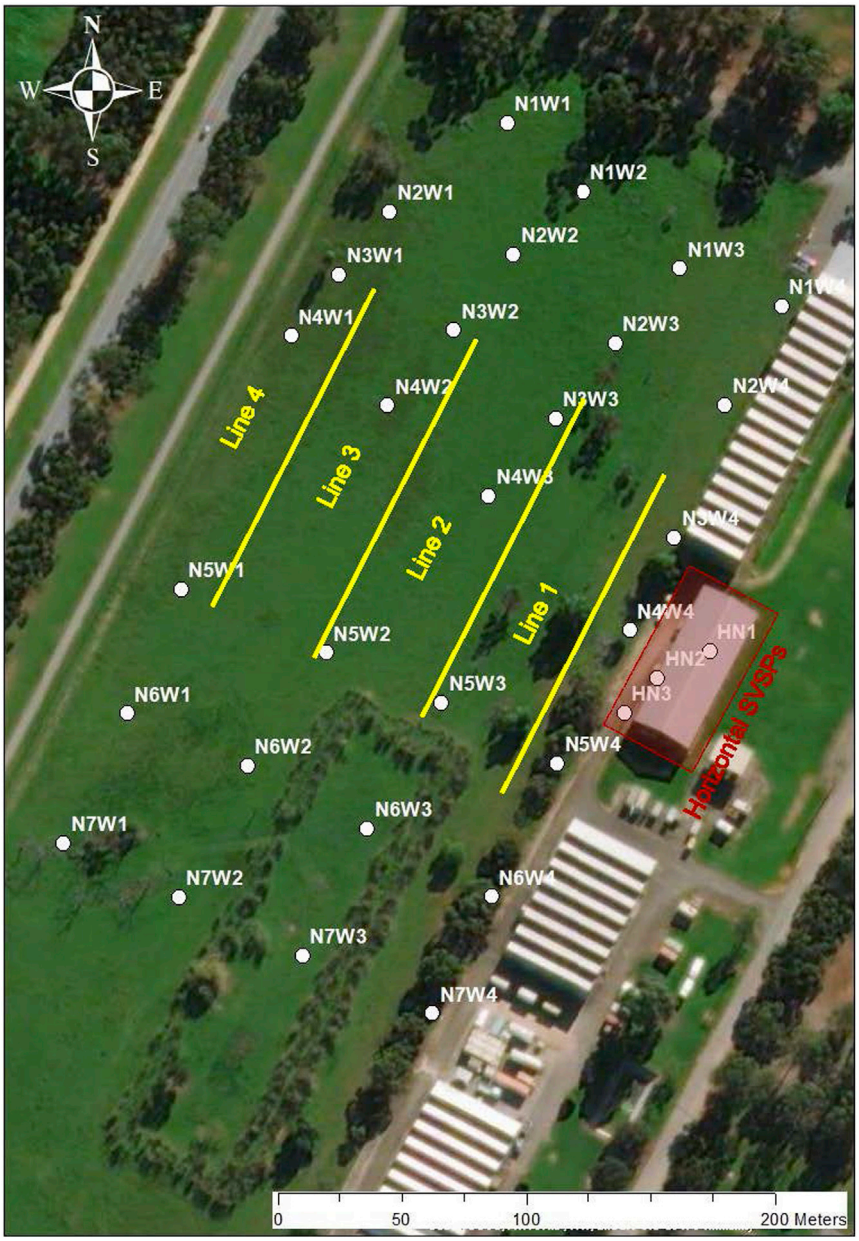

FIGURE 1 | Locations of SVSP installation and ERT measurement lines (in yellow). SVSP locations: N_xW_x are the locations of vertical SVSPs, and NH_x are the locations of horizontal SVSPs.

depth of the wells was calculated to be about 5 m below the surface. Once the borehole (95 mm diameter) had been drilled, the vapour bore chamber fitted with a suitable length Teflon sample tubing was pushed into the borehole using 50 mm diameter PVC pipes. The borehole was then backfilled with dry fine sand to cover the chamber, then dry bentonite is filled through the channel borehole to provide a seal to separate the sampling point from the ambient air, which could result in sample dilution. Finally, the borehole is backfilled with clean soil. The Teflon sample tubing connected to the sampling chamber was long enough to extend from the backfilled borehole to allow for soil vapour sampling.

Portable Gas Chromatography - Mass Spectrometer

For the in-field VOC measurements, a Torion T-9 Portable GC/MS was employed (Wang et al., 2021). A 5 m length and 0.18 mm inner diameter MXT-5 stainless steel column, inner coating with 0.4 μm thickness diphenyl dimethylpolysiloxane, is used in the portable GC/MS. With the temperature programming mode to increase the resolution of GC separation. The temperature was set initially at 50°C and held for 10 s before it was increased by 2°C per second to 200°C. Under this temperature sequence, the retention time for TCE was at 25.5 s, with the molecular

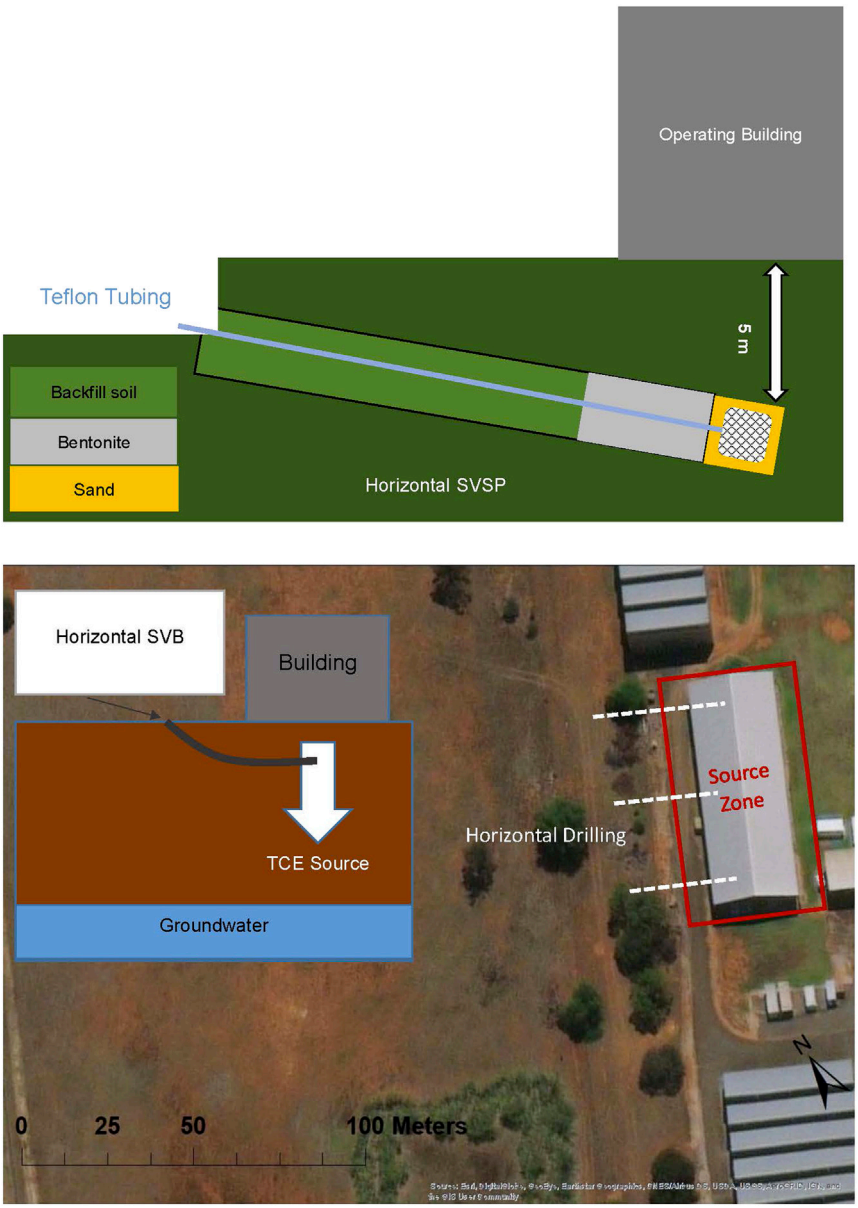

FIGURE 2 | Description of horizontal SVSP installation.

fragments from 130 to 136 m/z. The battery or external power supply can be used to power the portable GC/MS. At 170 kPa GC column head pressure, the portable instrument has a 90 ml stainless steel helium cylinder, with about 1–2 ml/min flow rate, which can support about 8 h of field measurement.

Using this sampling preparation method can optimise the SPME extraction efficiency. Extraction duration, temperature, and solvent have been investigated as causal factors that affect the extraction efficiency of SPME in laboratory benchtop experiments (Zhao et al., 2011; Zhang and Harrington, 2015; Jia et al., 2000). Based on our investigation, an infield soil gas sample preparation method was introduced in our previous study (Wang et al., 2021). Soil vapour samples were obtained using 1 L Tedlar sample bags. The sample bags were placed over ice in a cooler box during the sample extraction and after collection to keep the samples close to 4°C after 1 µl of ethanol had been injected. To collect a sample for analysis, a solid-phase micro-extraction (SPME) syringe needle pierced through the sample bag's septum and the internal SPME fibre, 65 µm polydimethylsiloxane/divinylbenzene, then exposed to the vapour sample for 8 min to extract the analytes from the vapour. By using this sample conditioning method for TCE vapour determination, the detection limit of the portable GC/MS has been improved from 1,000 to approximately 100 µg/m^{3}fn3. However, because sampling conditioning caused the SPME to become saturated more quickly than unconditioned samples,

different calibration curves for concentrations exceeding saturation were necessary. For calibration, the standard TCE solutions were prepared with ethanol, then injected into the Tedlar bags. The vapour was then collected and transferred to the portable GC/MS using the SPME with the same conditioning procedure.

To measure the concentration of VOCs in groundwater, 10 ml of groundwater was sampled into a clean container and mixed with 3 g of sodium chloride in a 40 ml vial. For extraction of the sample for analysis, the SPME fibre was exposed to the headspace above the water sample for 10 min at ambient temperature (Fabbri et al., 2007; Zhou et al., 2013; George et al., 2015). After the sample molecules were collected on the fibre, the SPME was immediately inserted into a portable GC/MS for the VOC analysis. The OpenChrom software was employed to analyse the portable GC/MS results. The contour maps of TCE concentrations for both soil vapour and groundwater samples were generated using the Krig interpolation algorithm in ArcGIS.

The correlations between the GC signal (peak area) and TCE concentrations for both soil vapour and groundwater were applied for the calibration. As demonstrated in our previous study (Wang et al., 2021), the mean of relative errors between the predicted results from the portable GC/MS and the convention air canister sampling method (TO-15), was about 9% for the measurement of the conditioned samples.

Earth Resistivity Topology

The Universal64 resistivity imaging instrument (ZZ Resistivity Imaging Pty Ltd., Australia) with FlashRES resistivity meter was applied in this application. The system which applies the electrode potential uses an external 12 V battery to supply the transmitter with the 250 W of power to provide a current of up to 3 A for the earth resistivity measurements. The sequence of measurements, including survey parameter, and electric current duration, can be set manually on the field or planned and uploaded to the system's microcontroller via laptop. Wenner configuration was used in the 2D electrical resistivity tomography survey (Perrone et al., 2014; Cheng et al., 2019). During the in-field procedure, 64-electrode arrays were laid out in a line on the ground at a separation distance of 2 m between electrodes to achieve a survey distance of 128 m. Four 128 m survey lines were completed in this study - the locations are shown in **Figure 1**. The resistivity values between every two individual electrodes were measured with a FlashRES resistivity meter, yielding a total of 62,000 data points. The instrument calculates the resistance using the ratio of voltage to current. The received voltage causes an average of 6% noise. Using the acquired data, the 2.5D inversion software (F-INV, ZZ), with Occam's inversion model was used to create resistivity inversion imaging of the area under the investigated ERT line, with the resolution value of 0.25.

RESULTS AND DISCUSSION

Soil Vapour Investigation

According to the results from the portable GC/MS, a chlorinated VOC, trichloroethylene (TCE), was found at various concentrations following the analysis of vapour in the headspace of soil samples taken in the soil profile at 1, 2, and 3 m depths. There is no other VOC detected in the soil vapour samples. The TCE concentration distribution contours were plotted using ArcGIS, as presented in **Figure 3**. The TCE concentrations in the soil vapour samples collected from SVSPs with Summa Canisters at the same locations and respective sample depths were compared. The mean of relative errors between the predicted results from the portable GC/MS and the convention air canister sampling method (TO-15), was about 9% for the measurement of the conditioned samples.

The TCE concentrations were generally higher in the soil vapour samples collected from the deeper SVSPs. For example, the TCE concentration in soil vapour samples from the three SVSPs at location N4W4, was around 5,000 $\mu g/m^3$ at 1 m depth but more than 20,000 and 30,000 $\mu g/m^3$ at 2 and 3 m, respectively. According to our hydrological report, the groundwater layer is around 10–12 m below the ground and the free-product and dissolved TCE is thought to be carried by groundwater that intersects with the source zone, which then is then released as a vapour which migrates to the ground surface as per vapour intrusion theory (Unnithan et al., 2021). The deeper the soil vapour samples obtained, the closer to the groundwater and the higher the detected concentration. Additionally, vapour in the topsoil profile has more opportunity to come into contact with the ambient air, resulting in dilution of the TCE and hence a lower detected concentration.

The TCE hotspot was detected along the south-eastern boundary of the investigation site, with the highest TCE concentrations detected in the soil vapour samples collected from the deeper vertical SVSPs at location N4W4, and from three horizontal SVSPs, NH1, NH2 and NH3, which were installed from the close vicinity of N4W4 to beneath an in-use building adjoining the initial investigation site. The TCE concentrations in the soil vapour samples collected from the three horizontal SVSPs were substantially greater than in the samples collected from the vertical SVSPs at N4W4. The results from the portable GC/MS indicated that the TCE concentrations in the soil vapour samples from the three horizontal SVSPs were all above 50,000 $\mu g/m^3$, nearly double the TCE concentrations detected in the soil vapour samples from N4W4. The horizontal SVSPs were installed at around 5 m beneath the building or below ground level. Comparatively, the vertical SVSPs were installed at only about 3 m below ground level. Based on the vapour intrusion theory, the sampling point of the horizontal SVSPs, at 5 m below ground level, was closer to the groundwater, and therefore less contact with the atmosphere. There is another assumption, as the building is located at the potential source zone, the significantly higher concentrations of TCE could be from the contaminated soil in the vadose zone, where the groundwater is at about 10–12 m below ground level.

The significant TCE concentrations detected in the soil vapour samples collected from the three horizontal SVSPs demonstrate the use of horizontally installed SVSPs are a functional device for soil vapour sampling and monitoring purposes. In previous studies, horizontal soil vapour wells were predominantly applied for remediation and vapour extractions and no horizontal soil vapour wells were identified from the literature as being employed for soil vapour sampling and monitoring. This is most likely because, for soil vapour sampling and monitoring, the installation of SVSP requires better separation between the

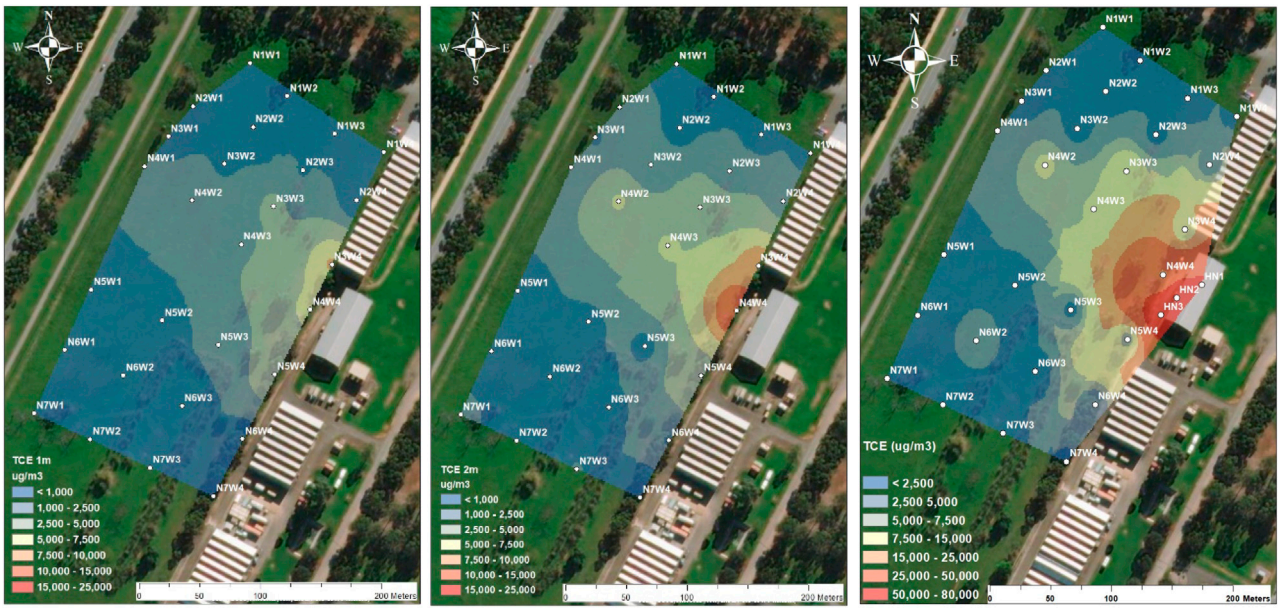

FIGURE 3 | Trichloroethylene (TCE) contours (at 1, 2 and 3 m depths) using 28 vertical SVSPs and three horizontal SVSPs. **(A)** TCE contour at 1 m depth; **(B)** TCE contour at 2 m depth; **(C)** TCE contour combing 3 m and three horizontal SVSPs (HN1, HN2 and HN3) below the functioning building. SVSP locations: N_xW_x are the locations of vertical SVSPs, and NH_x are the locations of horizontal SVSPs.

below-ground sampling point and the surface atmosphere. In horizontal SVSP installation, backfilling of the pre-drilled hole after insertion and positioning of the SVSP is difficult to achieve. Backfilling is usually done with mud concrete, made by mixing soil, cement, and water. However, when filling the pre-drilled hole with mud concrete using an air compressor could result in isolation of the sampling point from the surrounding soil and a blockage so that no sample can be collected. In our application, the borehole was backfilled with dry fine sand to cover the chamber, then dry bentonite is filled through the channel borehole to provide a seal to separate the sampling point from the ambient air, which could result in sample dilution. Finally, the borehole is backfilled with clean soil. After the backfilling, the SVSPs work satisfactorily for soil vapour samples collecting from a range of soil depths.

In the first trial, an air compressor was used to force dry sand through a slide tunnel into the end of the borehole to cover the SVSP chamber after it had been positioned. Backfilling with sand keeps the soil vapour mobile, allowing for sampling from the surface through the Teflon tubing (**Figure 2**). The evidence of high TCE from the horizontal SVSPs indicated a potential contaminant source beneath the building. According to the site history report, a demolished factory was located in the vicinity. As purported by the South Australian Environment Protection Authority (Talbot), in most instances TCE contamination is the result of historical disposal practices. Before legislative controls were applied, it was common practice for the industry to have on-site areas in which the chemical would be disposed of simply by pouring it onto the ground - assuming that it would then evaporate. Some industrial sites utilised more sophisticated methods for disposal including concrete-walled sumps and steel line bores drilled into the groundwater. According to the contour maps (**Figure 3**), except for the N4W4 hot spot area and the sampling point locations of the three horizontal SVSPs, the other relatively high TCE concentrations were observed SVSPs samples collected at the locations of N4W3, N4W2 and N4W1. This may indicate that groundwater, which may intersect with the source zone, flows toward the northwest, from N4W4 to N4W1. **Figure 4** demonstrates a 3D model of TCE in soil vapour at the contaminated site.

Groundwater Investigation

Our hydrological report has confirmed the northwest direction of groundwater flow. Groundwater may occur in the subsurface as a complex network of channels, and therefore a site investigation must delineate the groundwater channels that intersect with the contaminant source zone.

To investigate the groundwater contamination, 11 groundwater monitoring wells were installed at the site. Using a portable GC/MS in the field, the TCE concentration in the groundwater samples was analysed from which the TCE contour was generated as shown in **Figure 5**. The highest TCE concentrations were found in groundwater samples obtained from three monitoring wells located across the middle of the site, GW 2169, GW 2171, and GW 0948. GW2171 with TCE concentrations in the order of 4,500 μg/L.

TCE concentrations of less than 5 μg/L were identified in well GW 2175, which is located on the eastern extent of the potential source zone. Two wells, GW 2170 and GW 2178, in the south and

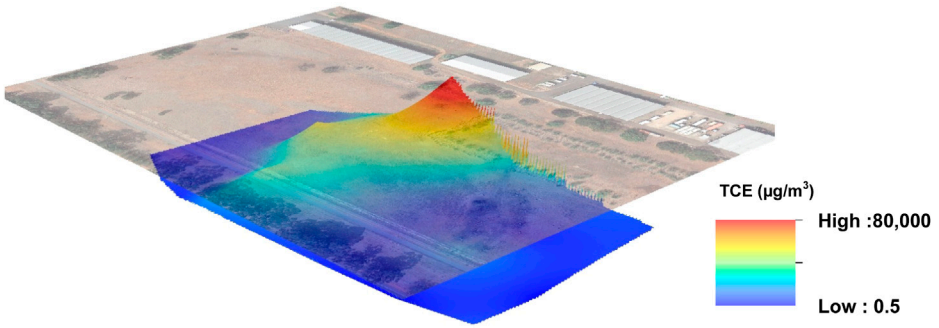

FIGURE 4 | 3D map of TCE contour in soil vapour at the contaminated site.

north of the map, respectively, also indicated low TCE concentrations of less than 10 µg/L.

The groundwater contour result can be another part of the evidence to show the interaction between the source zone and the groundwater channels. When the groundwater contour is viewed alone, it appears that the TCE hotspot was at GW 2171 then migrated to GW2169, whereas the groundwater sample from GW 2176 located to the east of GW 2171, contained only 190 g/L of TCE. Nevertheless, there is no historical documentation indicating that this groundwater sampling location was ever used for industry.

When the soil vapour and groundwater contour maps are combined, it is clear that a groundwater channel flow exists from a potential source zone beneath the building to the groundwater monitoring well GW 2171. According to the data relating to GW 2176, there may be another groundwater route that does not cross the source zone. To understand this intricate groundwater channel network, the ERT technique can be used to delineate the distribution of groundwater channels so that there can be more accurate in the selection of the locations for groundwater well installation. Taking into account both soil vapour and groundwater contours, four ERT survey lines were used to delineate the groundwater channels that cross the source zone. The locations of the four ERT survey lines are depicted in **Figure 5**. The four survey lines were selected to intersect the groundwater channels across the source zone.

The electrical conductivity (EC) measurements of all the groundwater samples were between 2,000 and 5,000 µs/cm. Groundwater with high EC values can be presented as low resistivity (<5 Ω/m) by using the ERT technique (Mastrocicco et al., 2010; Meyerhoff et al., 2014). In regards to the soil structure on the site, a layer of black loamy soil sits as a textural contrast on top of the less fertile, calcareous limey sandy soil. The resistivity of this underlying soil type is normally above 10 Ω/m, depending on soil moisture, and as the soil closer to the groundwater channels becomes saturated it has a decreased resistivity. This resistivity is detected by the ERT and with Universal64 resistivity imaging the data can be exhibited with the lowest resistivity shown in darker colours as in **Figure 6**; the assumption being that the black colour zones where the resistivity value is less than 2 Ω/m are most likely the groundwater channel intersections. The blue colour regions, where resistivity values range from 2 to 10 Ω/m, are most likely the surrounding soils that have been saturated by groundwater. The unsaturated clay soil is shown as the green areas, and soil with increased sand content likely occurs where the yellow, red, and white colour zones are indicated. According to our soil texture measurement, soil contains about 24–40% clay (Wang et al., 2021). The soil is a mixture of fertile black loamy texture contrast soils and less fertile highly calcareous sandy soils.

Figure 6 also indicates the potential groundwater pathways beneath the TCE source zone. The survey images present the measurement results in the distance (m) - the X-axis, and depth below the ground (m) - the Y-axis. For example, based on the colour along ERT survey line 1, there are likely six groundwater channels intersected by the ERT survey at about 10 m below the ground (Y-axis), and the middle three groundwater channels, from 40 to 100 m (X-axis), are likely to cross the source zone. From the ERT plots, it is apparent that the two groundwater monitoring wells, GW 2165 and GW 2176, are located beyond the source zone (**Figure 6**).

There is a considerable black colour segment in the ERT second survey area (survey line 2) from 80 to 120 m, which implies that significant TCE-contaminated groundwater is trapped or retained in this area. The TCE results from the analysis of the groundwater samples from GW 2171 and the N4W3 soil vapour samples support this assumption. On all of the four survey lines, as shown in the ERT images there are continuous black colour areas at around 60 m (X-axis). This may indicate that the groundwater channels that transport TCE away from the source zone were intercepted by the four-line ERT survey and is supported by the soil vapour contours in **Figure 4** and the groundwater flow direction.

CONCLUSION

This case study provides a novel approach to investigating a VOC-contaminated site and its vapour incursion by combining a soil vapour survey with an earth resistivity survey. The “easy to install” and retractable SVSP is demonstrated to be a useful field solution for the installation of sampling points for the rapid assessment of soil vapour samples both vertically and horizontally. The self-developed SVSP is inexpensive and therefore a large number of SVSPs can be deployed across a grid at varying depths to obtain data to generate 3D subsurface

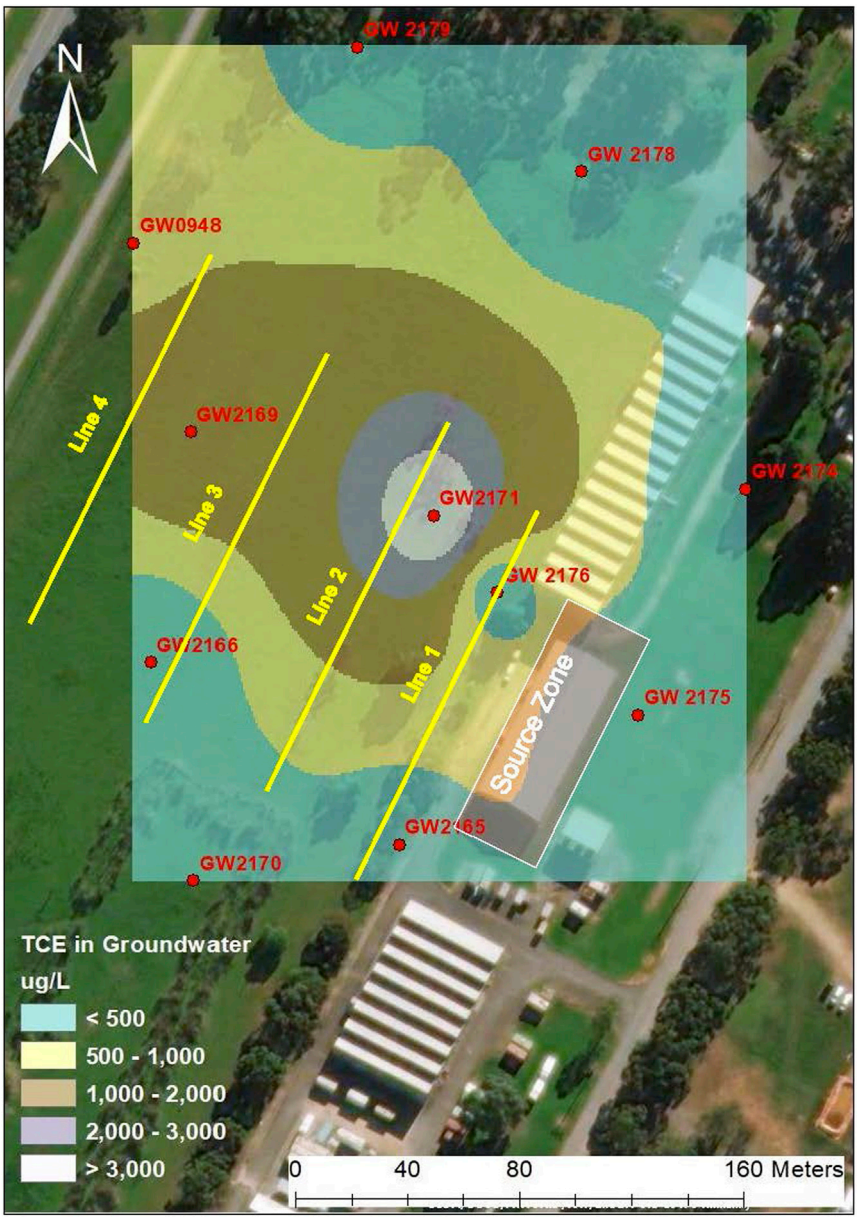

FIGURE 5 | TCE concentration in groundwater (μg/L) and four ERT survey lines (in yellow).

contour maps for VOC soil vapour concentrations. These distribution contour maps can then be used to assist in the identification of hot spots and the migration patterns of VOCs which can be carried down gradient from a source zone and result in vapour intrusion into buildings.

The ERT technique can be used to delineate the groundwater channel distribution so that there can be a more accurate selection of the locations for groundwater and soil vapour monitoring well installation. The resistivity difference between groundwater and the surrounding soil can be presented as an ERT plot with different colours showing the differing resistivity across the soil profile and hence the groundwater channel or stream. It should be noted that groundwater resistivity is determined by water quality and salt concentration, therefore groundwater with a low EC or salt content will have high resistivity, making separation of groundwater from the surrounding soil problematic. Hence other subsurface imaging techniques such as induced polarization and self-potential can be applied to provide additional information for the groundwater identification (Cygal et al., 2016; Heritiana et al., 2019). In conclusion, these non-destructive physical-geological survey methods can provide a preliminary indication of groundwater locations, which can then assist in determining the correct groundwater channels for investigation in a complex groundwater channel network.

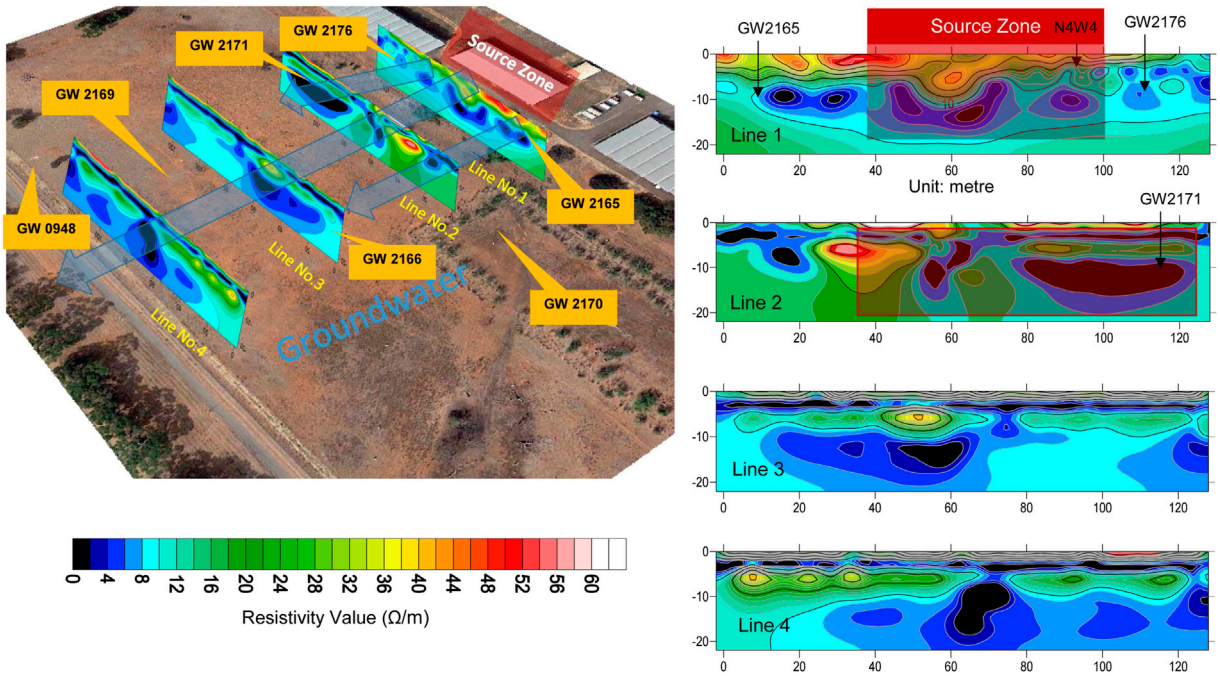

FIGURE 6 | ERT imaging (unit in meters) - The survey images present the measurement results in the distance (m) - the X-axis, and depth below the ground (m) - the Y-axis.

DATA AVAILABILITY STATEMENT

The raw data supporting the conclusions of this article will be made available by the authors, without undue reservation.

AUTHOR CONTRIBUTIONS

LW: Public responsibility for the content, including participation in the concept, design, analysis, writing, or revision of the manuscript. YC: Public responsibility for the content, including participation in the concept, design, analysis, writing, or revision of the manuscript. RN: Public responsibility for the content, including participation in the concept, design, analysis, writing, or revision of the manuscript. PG: Public responsibility for the content, including participation in the concept, design, analysis, writing, or revision of the manuscript. MB: Public responsibility for the content, including participation in the concept, design, analysis, writing, or revision of the manuscript.

FUNDING

This research was funded by CRC CARE Pty Ltd. The research was conducted in the laboratories of the Global Centre for Environmental Remediation (GCER) at the University of Newcastle.

ACKNOWLEDGMENTS

The authors would like to thank the Cooperative Research Centre for Contamination Assessment and Remediation of the Environment (CRC CARE); The Department of Defence, Australia; Perkin Elmer; and the University of Newcastle for making this research possible. The horizontal drilling service was provided by Collision Drilling, Westco Pty Ltd. The ERT survey was conducted by ZZ Resistivity Imaging Pty Ltd.

REFERENCES

Armstrong, J. E., Moore, B. J., and Dupont, R. R. 1996. Horizontal Soil Vapour Extraction: Subsurface Remedial Technology Research and Demonstration Program – Pilot Test Summary Report, .

Arrubarrena Moreno, M., and Arango-Galván, C. (2013). Use of Electrical Resistivity Tomography in the Study of Soil Pollution Caused by Hydrocarbons: Case Study in Puebla (México). *Bsgm* 65, 419–426. doi:10.18268/bsgm2013v65n2a21

Ayolabi, E. A., Folorunso, A. F., and Idem, S. S. (2013). Application of Electrical Resistivity Tomography in Mapping Subsurface Hydrocarbon Contamination. *Esr* 2. doi:10.5539/esr.v2n1p93

Barnes, A. T., Dolan, J. A., Kuk, R. J., and Siegel, J. A. (2004). Comparison of Gasolines Using Gas Chromatography-Mass Spectrometry and Target Ion Response. *J. Forensic Sci.* 49 (5), 1018–1023. doi:10.1520/jfs2004029

Bravo, D., and Benavides-Erazo, J. (2020). The Use of a Two-Dimensional Electrical Resistivity Tomography (2D-ERT) as a Technique for Cadmium Determination in Cacao Crop Soils. *Appl. Sci.* 10, 4149. doi:10.3390/app10124149

Cheng, Q., Tao, M., Chen, X., and Binley, A. (2019). Evaluation of Electrical Resistivity Tomography (ERT) for Mapping the Soil-Rock Interface in Karstic Environments. *Environ. Earth Sci.* 78, 439. doi:10.1007/s12665-019-8440-8

Compendium Method TO-15 (1997). "Determination of Volatile Organic Compounds (VOCs)," in *Air Collected in Specially Prepared Canisters and Analyzed by Gas Chromatography/mass Spectrometry (GC/MS)*, (U.S. EPA).

Cygal, A., Stefaniuk, M., Kret, A., and Kurowska, M. (2016). The Application of Electrical Resistivity Tomography (ERT), Induced Polarization (IP) and Electromagnetic Conductivity (EMC) Methods for the Evaluation of Technical Condition of Flood Embankment Corpus. *geol* 42, 279–287. doi:10.7494/geol.2016.42.3.279

Fabbri, D., Bezzi, R., Torri, C., Galletti, P., and Tagliavini, E. (2007). Determination of Tetrachloroethylene and Other Volatile Halogenated Organic Compounds in Oil Wastes by Headspace SPME GC-MS. *Chroma* 66, 377–382. doi:10.1365/s10337-007-0353-0

Fair, J. D., Bailey, W. F., Felty, R. A., Gifford, A. E., Shultes, B., and Volles, L. H. (2010). Quantitation by Portable Gas Chromatography: Mass Spectrometry of VOCs Associated with Vapor Intrusion. *Int. J. Anal. Chem.* 2010, 6. doi:10.1155/2010/278078

George, M. J., Marjanovic, L., Williams, D. B. G., and Williams, G. (2015). Solvent-Assisted Headspace Sampling Using Solid Phase Microextraction for the Analysis of Phenols in Water. *Anal. Chem.* 87, 9559–9562. doi:10.1021/acs.analchem.5b02539

Gorder, K. A., and Dettenmaier, E. M. (2011). Portable GC/MS Methods to Evaluate Sources of cVOC Contamination in Indoor Air. *Ground Water Monit. Remediation* 31 (4), 113–119. doi:10.1111/j.1745-6592.2011.01357.x

Heritiana, A, R., Riva, R., Ralay, R., and Boni, R. (2019). Evaluation of Flake Graphite Ore Using Self-Potential (SP), Electrical Resistivity Tomography (ERT) and Induced Polarization (IP) Methods in East Coast of Madagascar. *J. Appl. Geophys.* 169, 134–141. doi:10.1016/j.jappgeo.2019.07.001

Hook, G. L., Kimm, G. L., Hall, T., and Smith, P. A. (2002). Solid-phase Microextraction (SPME) for Rapid Field Sampling and Analysis by Gas Chromatography-Mass Spectrometry (GC-MS). *Trac Trends Anal. Chem.* 21 (8), 534–543. doi:10.1016/s0165-9936(02)00708-2

Hopler, R. B. (2012). "The History, Development, and Characteristics of Explosives and Propellants," in *Forensic Investigations of Explosives*. Editor A. Beveridge (U. S: Taylor & Francis Group), 1–18. doi:10.1201/b11282-2

Jia, M., Koziel, J., and Pawliszyn, J. (2000). Fast Field Sampling/sample Preparation and Quantification of Volatile Organic Compounds in Indoor Air by Solid-phase Microextraction and Portable Gas Chromatographyfication of Volatile Organic Compounds in Indoor Air by Solid-phase Microextraction and Portable Gas Chromatography. *Field Analyt. Chem. Technol.* 4, 73–84. doi:10.1002/1520-6521(2000)4:2/3<73::aid-fact2>3.0.co;2-7

Leary, P. E., Dobson, G. S., and Reffner, J. A. (2016). Development and Applications of Portable Gas Chromatography-Mass Spectrometry for Emergency Responders, the Military, and Law-Enforcement Organizations. *Appl. Spectrosc.* 70 (5), 888–896. doi:10.1177/0003702816638294

Mastrocicco, M., Vignoli, G., Colombani, N., and Zeid, N. A. (2010). Surface Electrical Resistivity Tomography and Hydrogeological Characterization to Constrain Groundwater Flow Modeling in an Agricultural Field Site Near Ferrara (Italy). *Environ. Earth Sci.* 61, 311–322. doi:10.1007/s12665-009-0344-6

Method TO-14 (1999). *Compendium of Methods for the Determination of Toxic Organic Compounds in Ambient Air*, Washington, DC, U.S. EPA.

Meyerhoff, S. B., Maxwell, R. M., Revil, A., Martin, J. B., Karaoulis, M., and Graham, W. D. (2014). Characterization of Groundwater and Surface Water Mixing in a Semiconfined Karst Aquifer Using Time-Lapse Electrical Resistivity Tomography. *Water Resour. Res.* 50, 2566–2585. doi:10.1002/2013WR013991

Müller, K., Vanderborght, J., Englert, A., Kemna, A., Huisman, J. A., Rings, J., et al. (2010). Imaging and Characterization of Solute Transport during Two Tracer Tests in a Shallow Aquifer Using Electrical Resistivity Tomography and Multilevel Groundwater Samplers. *Water Resour. Res.* 46, 1–23. doi:10.1029/2008WR007595

Osborn, S. G., Vengosh, A., Warner, N. R., and Jackson, R. B. (2011). Methane Contamination of Drinking Water Accompanying Gas-Well Drilling and Hydraulic Fracturing. *Proc. Natl. Acad. Sci.* 108, 8172–8176. doi:10.1073/pnas.1100682108

Perrone, A., Lapenna, V., and Piscitelli, S. (2014). Electrical Resistivity Tomography Technique for Landslide Investigation: A Review. *Earth-Science Rev.* 135, 65–82. doi:10.1016/j.earscirev.2014.04.002

Saad, R., Nawawi, M. N. M., and Mohamad, E. T. (2012). Groundwater Detection in Alluvium Using 2-D Electrical Resistivity Tomography (ERT). *Eletronic J. Geotechnical Eng.* 17, 369–376.

Shakoor, O., Taylor, R. B., and Behrens, R. H. (1997). Assessment of the Incidence of Substandard Drugs in Developing Countries. *Trop. Med. Int. Health* 2 (9), 839–845. doi:10.1046/j.1365-3156.1997.d01-403.x

Spuij, F., Otten, A., and Otten, A. (1995). Risk Reduction by Soil Vapour Extraction Remediation Based on Transport Mechanisms. *Contaminated Soil* 95, 1361–1362. doi:10.1007/978-94-011-0421-0_148

Talbot, M., Beverley Assessment Area – Summary of Historical Activities, Available at: http://www.epa.sa.gov.au/data_and_publications/site_contamination_monitoring/assessment_areas/beverley_woodville_west_south_findon_allenby_gdns (Accessed Jun 17, 2019).

Unnithan, A., Bekele, D. N., Chadalavada, S., and Naidu, R. (2021). Insights into Vapour Intrusion Phenomena: Current Outlook and Preferential Pathway Scenario. *Sci. Total Environ.* 796, 148885. doi:10.1016/j.scitotenv.2021.148885

Wang, L., Cheng, Y., Naidu, R., Chadalavada, S., Bekele, D., Gell, P., et al. (2021). Application of Portable Gas Chromatography-Mass Spectrometer for Rapid Field Based Determination of TCE in Soil Vapour and Groundwater. *Environ. Technology Innovation* 21, 101274. doi:10.1016/j.eti.2020.101274

Zhang, M., and Harrington, P. (2015). Determination of Trichloroethylene in Water by Liquid-Liquid Microextraction Assisted Solid Phase Microextraction. *Chromatography* 2, 66–78. doi:10.3390/chromatography2010066

Zhao, G., Song, S., Wang, C., Wu, Q., and Wang, Z. 2011. Solid-phase Microextraction with a Novel Graphene-Coated Fiber Coupled with High-Performance Liquid Chromatography for the Determination of Some Carbamates in Water Samples. *Anal. Methods* 3, 2929 2935. doi:10.1039/C1AY05358B

Zhou, Y. Y., Yu, J. F., Yan, Z. G., Zhang, C. Y., Xie, Y. B., Ma, L. Q., et al. (2013). Application of Portable Gas Chromatography-Photo Ionization Detector Combined with Headspace Sampling for Field Analysis of Benzene, Toluene, Ethylbenzene, and Xylene in Soils. *Environ. Monit. Assess.* 185, 3037–3048. doi:10.1007/s10661-012-2771-1

Conflict of Interest: The authors declare that the research was conducted in the absence of any commercial or financial relationships that could be construed as a potential conflict of interest.

The reviewer (LD) declared a past co-authorship with one of the authors (RN) and a shared affiliation with the authors (LW, YC, RN) to the handling Editor.

Publisher's Note: All claims expressed in this article are solely those of the authors and do not necessarily represent those of their affiliated organizations, or those of the publisher, the editors and the reviewers. Any product that may be evaluated in this article, or claim that may be made by its manufacturer, is not guaranteed or endorsed by the publisher.

frontiers in Environmental Science

ORIGINAL RESEARCH
published: 30 November 2021
doi: 10.3389/fenvs.2021.703851

Characterizing the Influence of Organic Polymers on the Specific Reactivity of Particulate Remedial Amendments

Katherine A. Muller[†], *Lirong Zhong and Christopher E. Bagwell* *[†]

Pacific Northwest National Laboratory, Earth Systems Science Division, Richland, WA, United States

Commercially available particulate amendments demonstrate high reactivity for effective treatment of water soluble organic and inorganic contaminants in laboratory studies; however, transport of these particles is constrained in the subsurface. In many field applications, particulate amendments are mixed with organic polymers to enhance mobility for direct push applications or stabilize suspensions for high mass loadings. As such, the interactions between particulate amendments, organic polymers and contaminant species need to be systematically investigated to properly understand mechanistic processes that facilitate predictive performance metrics for specific applications *in situ*. In this study, batch experiments were conducted to quantify the effects of organic polymers (xanthan gum, guar gum, and sodium alginate), polymer concentration (800 and 4,000 mg/L), and aging (up to 28 days) on chromate treatment rate and capacity by two classes of amendments: reductants [granular zero-valent iron (gZVI), micron-ZVI (mZVI), sulfur modified iron (SMI)], and an adsorbent (bismuth sub-nitrate). When particulate amendments were suspended in polymer solutions, reductants retained between 84–100% of the amendment treatment capacity. Conversely, the adsorbent maintained 63–97% relative treatment capacity of the no-polymer control. Polymer solutions had a more pronounced impact on the rate of chromate removal; first order rates of chemical reduction decreased by as much as 70% and adsorption by up to 81% relative to the no-polymer controls. Polymer–amendment aging experiments also showed decreased Cr(VI) treatment capacity; reductants decreased by as much as 24% and adsorption decreased by as much as 44% after 28 days of incubation. While polymer suspensions are needed to aid the injection of particulate amendments into the subsurface, the results from this study indicate potential losses of treatment capacity and a decrease in the rate of remedial performance due to the physical and chemical interactions between polymer suspensions and reactive particulate amendments. Simple batch systems provide baseline characterization of tripartite interactions for the removal of Cr(VI). Additional work is needed to quantify the full impact of polymers on remedial outcomes under site relevant conditions at field scale.

Keywords: particulate reactants, adsorption, reduction, chromate, polymers, remediation

OPEN ACCESS

Edited by:
Balaji Seshadri,
The University of Newcastle, Australia

Reviewed by:
Nicholas Kiprotich Cheruiyot,
National Kaohsiung University of Science and Technology, Taiwan
Yanju Liu,
The University of Newcastle, Australia

***Correspondence:**
Christopher E. Bagwell
Christopher.Bagwell@pnnl.gov

[†]These authors have contributed equally to this work and share first authorship

Specialty section:
This article was submitted to Toxicology, Pollution and the Environment, a section of the journal Frontiers in Environmental Science

Received: *30 April 2021*
Accepted: *10 November 2021*
Published: *30 November 2021*

Citation:
Muller KA, Zhong L and Bagwell CE (2021) Characterizing the Influence of Organic Polymers on the Specific Reactivity of Particulate Remedial Amendments. Front. Environ. Sci. 9:703851. doi: 10.3389/fenvs.2021.703851

1 INTRODUCTION

In situ remediation of sediment and groundwater often necessitates the introduction of reagents or reactive amendments to promote the degradation, mobilization, or stabilization of organic and inorganic contaminants within an acceptable timeframe (Muller et al., 2020). While the underlying mechanism(s) of a remediation technology may show promise at bench scale, flow behavior or other physical constraints can impede mass loading and the transport of remedial amendments through contaminant source zones (Kitanidis and McCarty, 2012). In practice, subsurface injection of remedial reagents can achieve reasonable coverage of high-permeability unsaturated sediment or aquifer strata; however, effective penetration into low-permeability zones remains a major challenge for *in situ* remediation (e.g., Orozco et al., 2015; Fan et al., 2017). Incomplete treatment of these less accessible regions is important because contamination will persist well after active remediation and will likely contribute to a rebound in contaminant concentrations in site groundwater (e.g., Switzer and Kosson, 2007; Thomson et al., 2008; Brusseau et al., 2011).

Numerous particulate amendments and suspensions are commercially available for the remediation of sediment and groundwater; however, the application of particulates is fundamentally limited by poor subsurface mobility (O'Carroll et al., 2013; Tosco et al., 2014a; Kocur et al., 2014). Grain size, permeability, heterogeneity of the geological formation, and groundwater velocity are the primary physical parameters that dictate particle transport, distribution, and retention in porous media. These parameters define the permissible particle size and injection pressures needed to successfully emplace amendments into the subsurface. Moreover, the electrostatic, chemical, and magnetic properties of the reactive particles and soil grain surfaces play an important role in the practical application of these remedial amendments in subsurface environments (Tufenkji and Elimelech, 2004). To overcome mobility challenges facing particulate amendment delivery in field implementation, particle size can be reduced, surface properties modified, or chemical additives used to enhance suspension stability, and extend particle penetration in heterogenous media (e.g., Fan et al., 2017; Lowry and Phenrat, 2019; Pavelková et al., 2020; Tiraferri et al., 2008; Tosco et al., 2014a; Truex et al., 2011; Velimirovic et al., 2012; Velimirovic et al., 2016). Such modifications introduce tradeoffs in remedial efficiency, treatment or reaction time, and potential cost. To help better understand these tradeoffs in advance, the complex and varied interactions between chemical additives, remedial amendments, contaminant species, and representative site conditions can be systematically investigated to gain a more predictive understanding of the mechanistic interactions that control subsurface reactions and influence remedial outcomes.

Natural and synthetic polymers have been used for borewell drilling in the petroleum industry for decades. More recently, similar techniques have been adopted by the remediation industry to improve applications for subsurface cleanup. For example, guar gum has been utilized extensively to transport hydraulic fracturing proppant, and xanthan gum has been used, though to a lesser extent, for direct push applications (Fink, 2015, Hasan and Abdel-Raouf, 2018; Smith et al., 2008; Tiraferri et al., 2008; Truex et al., 2011; Vecchia et al., 2009; Velimirovic et al., 2012; Velimirovic et al. 2014a; Velimirovic et al. 2014b; Velimirovic et al., 2016; Zhong et al., 2008; Zhong et al., 2013). Polymers assist subsurface injection of particulates in two ways-by increasing suspension stability and improving subsurface sweeping efficiencies (Hasan and Abdel-Raouf, 2018; Tosco et al., 2014b; Wu et al., 2017; Zhong et al., 2011; Zhong et al., 2013). Viscous polymer fluids reduce sedimentation and aggregation of particulate amendments, resulting in suspensions that are stable for hours and suitable for injection (Velimirovic et al., 2012). Furthermore, some bio-polymers exhibit non-Newtonian shear thinning properties which have been shown to extend penetration distances of particulate reactants through porous media in laboratory 1D columns (Zhong et al., 2008, Zhong et al., 2013), 2D wedges (Oostrom et al., 2007; Mondino et al., 2020), and modeling simulations (Tosco and Sethi, 2010; Bianco et al., 2016). These studies demonstrate that shear thinning polymers establish a more uniform injection front, decrease fingering in heterogenous media, and improve micron ZVI particle transport distances by as much as 40% from the point of injection. While the positive attributes of polymer additives are clear, systematic evaluation of the interactions between remedial components under site relevant conditions remains an important gap to ensure the efficacious treatment of contaminant species (e.g., Chuang et al., 2017; Velimirovic et al., 2012; Velimirovic et al., 2016).

The overarching objective of this work was to quantify the influence of polymer suspensions on the reaction kinetics and capacity of commercially available particulate remedial reactants. The selected polymer solutions represent industry accepted formulations and concentrations of guar gum, xanthan gum, and sodium alginate. Selected particulate amendments include two sizes of zero valent iron (ZVI) (granular [gZVI] and micron [mZVI]), sulfur modified iron (SMI), and bismuth sub-nitrate, wherein suspension combinations were evaluated for contaminant removal. Bismuth sub-nitrate was selected as a promising adsorbent material which consists of layered structures that effectively treat a variety of inorganic contaminant species and mixtures (Pearce et al., 2020). These studies incorporated chromate because it is a prevalent groundwater contaminant worldwide due to metals plating, textiles, wood preservation, and corrosion prevention (Testa et al., 2004; Gharbi et al., 2018). Hexavalent chromium, Cr(VI), is highly soluble in water and can be effectively removed from the aqueous phase by chemical reduction of Cr(VI) to the highly insoluble Cr(III), or adsorption. In this study, the interference of polymer additives was quantified against a selection of remedial amendments that vary in particle size, properties, and specific mode of action (i.e., reduction vs sorption); providing new insights into the tradeoffs between beneficial remedial delivery strategies and treatment efficiencies and outcomes.

TABLE 1 | Polymer characteristics.

	Xanthan gum	Guar gum	Alginate
Origin	*Xanthomonas campestris,* bacterial	*Cyamopsis tetragonoloba*, guar beans	*Phaeophyrene,* brown algae and seaweeds
Chemical Composition	Glucose-mannose-glucuronic acid (2:2:1)	Mannose backbone, galactose side chains	Mannuronate, guluronate copolymer
Features	Anionic, shear thinning, thickener	Neutral, hydrocolloid, shear thinning	Anionic, mild gelation hydrogel
ζ (mV) pH7/pH2	–58.2/–22.1[1]	–8.19/2.88[1]	–55.0/–8.5[2]
pH in AGW at 800/4,000 mg/L	8.02/6.78	8.06/7.80	8.11/6.99

Zeta potential measurements were reported by [1]Zhang et al. (2014), [2]Li et al. (2020).

2 MATERIALS AND METHODS

2.1 Remedial Amendments

Commercial grade particulate amendments, granular 325 mesh Zero-Valent Iron, gZVI, (Hepure), 20–80 mesh Sulfur-modified Iron, SMI (Hydrex™ 9670), and 1–5 μm micron-sized ZVI (mZVI) (Ashland) were used for the experiments described herein. Bismuth sub-nitrate, 100 mesh, was selected as the adsorbent material (Sigma-Aldrich). Experimental testing and reactivity measurements were conducted using hexavalent chromium as a model groundwater contaminant, capable of both being adsorbed and reduced. Various amounts of a 320 mg/L aqueous chromium stock solution (K_2CrO4, Sigma Aldrich) were used to achieve initial Cr to amendment ratios of 4.5–18.5 mg K_2CrO4/g solid amendment.

2.2 Chromium Assay

Aqueous samples were immediately processed for quantification of soluble Cr(VI). Samples were passed through a 0.2 μm syringe filter to remove particulate amendments prior to analysis and diluted in artificial groundwater. Aqueous concentration of chromium was measured spectrophotometrically following the optimized assay method described by Lace et al. (2019). Briefly, 0.5 ml of an aqueous sample was mixed with 0.25 ml of 0.2 M sulfuric acid, and 0.25 ml 0.5%(w/v) 1,5-diphenylcarbazide, and the absorbance was measured (λ = 540 nm). Potassium chromate standards were freshly prepared and analyzed with every set of experiments. Quantification standards were prepared by the dilution-method in artificial groundwater and had a linear range from 0.2–6.5 mg/L (slope = 11.4 ± 1.2, $R^2 > 0.994$).

2.3 Bio-Polymer Solution Properties

Xanthan gum, guar gum, and alginate are natural polymers that possess useful properties which are exploited for a variety of applications ranging from food additives, tissue bio-engineering, and geotechnical engineering. Relevant features to this study are summarized in **Table 1**. Typical polymer formations used to suspend particulate amendments range in concentration from 0.5–4 g/L (e.g., Tosco and Sethi, 2010; Truex et al., 2011; Tosco et al., 2014a; Velimirovic et al., 2016).

Particulate amendments were suspended in polymer solutions that were consistent with industry standard applications in both composition and concentration. Polymers included: 1) xanthan gum (MP Biomedicals); 2) guar gum (Sigma-Aldrich); and 3) sodium alginate (MP Biomedicals).

Two concentrations of xanthan gum, guar gum and sodium alginate solutions (800 mg/L and 4,000 mg/L) were tested in an artificial groundwater (AGW). The AGW has been modeled after typical groundwater compositions encountered at the Department of Energy's Hanford Site in Richland, Washington, United States (Truex et al., 2017). AGW composition is as follows: silicic acid ($H_2SiO_3.nH_2O$, 15.3 mg/L), potassium chloride (KCl, 8.2 mg/L), magnesium carbonate ($MgCO_3$, 13 mg/L), sodium chloride (NaCl, 15 mg/L), calcium sulfate ($CaSO_4$, 67 mg/L), and calcium carbonate ($CaCO_3$, 150 mg/L). The AGW medium was supersaturated with $CaCO_3$ (solubility is 14 mg/L) and stirred for one week to reach equilibrium (pH 7.8). The density of polymer solutions prepared in AGW was measured via a pycnometer. At 800 mg/L, polymer solution densities were near water at 0.9965 g/mL, 0.9967 g/mL, and 0.9968 g/mL, for xanthan gum, guar gum, and sodium alginate, respectively.

2.4 Batch Experiments With Particulate Amendment–Polymer Suspensions

Batch experiments were systematically conducted with pairwise combinations of remedial amendments (gZVI, mZVI, Bi, and SMI) suspended in polymer solutions (xanthan gum, guar gum, and sodium alginate) to measure the reaction kinetics and capacity for removal of K_2CrO_4 (aq) from solution. Batch experiments were composed in 20 ml borosilicate glass scintillation vials. Briefly, 0.1 g of particulate amendment was added directly to the prepared polymer solutions and well mixed to disperse amendments. Vials were spiked with a hexavalent chromium stock solution to produce a final Cr(VI) concentration of 23, 46, or 96 mg/L in a total aqueous volume of 20 ml. Vials were placed on a platform shaker (125 rpms, room temperature, in the dark) in between measurements to ensure reactants remained well mixed. Aqueous samples were collected at 2, 6, 24, and 48 h and processed immediately to measure the aqueous concentration of Cr(VI). Negative controls consisted of AGW and polymer solutions without particulate amendment to ensure no loss of K_2CrO_4 occurred. The no amendment control experiments (also sampled at 2, 6, 24 and 48 h) had average Cr recoveries of 104 ± 12, 100 ± 7, 102 ± 7, and 94 ± 6%, for no polymer, xanthan gum, guar gum, and sodium alginate solutions, respectively. Amendments without biopolymer solutions (no polymer controls) were also included to provide measurement of maximum reactivity and quantify interference from the

polymer solutions. The relative error for all experimental replicates ranged from 0–11%, with an average 5 ± 6%.

2.5 Remedial Amendment Aging Experiments

A pairwise matrix of particulate amendments and polymer solutions was evaluated to quantify the temporal interactions between specific polymer fluid–amendment combinations by measuring the preservation and longevity of treatment (reduction or adsorption) capacity. Particulate amendments were added directly to prepared polymer solutions in borosilicate glass scintillation vials. Batch experiments were placed on a platform shaker (125 rpms, room temperature, in the dark) for an aging duration of 1, 2, and 4 weeks. After the prescribed aging period, the K_2CrO_4 stock solution was added (4.5–18.5 mg K_2CrO4/g solid amendment) and the reaction kinetics and capacity were quantified by collecting aqueous samples after 24 and 48 h. Samples were processed immediately as described to measure the aqueous concentration of Cr(VI). Since the relative error among replicates for the treatment rate and capacity experiments described above was consistently low and never exceeded 11% (mean = 5 ± 6%), temporal aging measurements were collected as singlets.

2.6 Modeling Reactive Performance of Remedial Amendment Suspensions

Aqueous Cr(VI) concentrations for each temporal data series (t = 0, 2, 6, 24, and 48 h) were fit together to **Eq. 1** to quantify both the treatment capacity and kinetic rates. This model is derived from a first order rate expression that is modulated by a capacity term.

$$C(t) = C_{eq} + \left(C_0 - C_{eq}\right) * e^{-kt} \quad (1)$$

where: $C(t)$ = aqueous concentration at time t [mg/L]; C_{eq} is aqueous equilibrium concentration [mg/L]; C_0 is initial concentration [mg/L]; k is first order rate coefficient [hr^{-1}]; t is time [hr].

C_{eq} and k were fit to **Eq. 1** using experimental results for $C(t)$ and the known experimental starting condition for C_0. Reported errors are the standard error of parameter fit. Amendment capacity (C in mg Cr/g-amendment) was calculated from C_{eq} and the uncertainty was determined through error propagation. Both treatment capacity and first order rate coefficients were compared to the appropriate controls to quantify the influence of the polymer solution.

3 RESULTS AND DISCUSSION

Polymer composition, concentration, and background fluid characteristics (e.g., pH, net charge, and ionic strength) can have an important influence on remedial amendment properties in suspension. For example, that stability of milled ZVI (average size = 12 μm) suspensions were found to be inversely correlated with guar gum concentration (0, 0.5, 1 g/L), which was reflected by zeta potential which increased from −22 mV, to −15 mV, to −4 mV, respectively (Velimirovic et al., 2016). On the other hand, Velimirovic et al. (2016) found milled ZVI suspension stability was slightly improved with increased agar concentration (zeta potential decreased from −22 mV, −33 mV, and −30 mV respectively for 0, 0.5, and 1 g/L solutions), indicating the stability difference invoked by different types of polymers. Generally, zeta potential values < −30 mV or > +30 mV are considered stable while values falling between −30 mV and +30 mV are considered unstable. Based on reported literature values for polymer zeta potentials (Zhang et al., 2014; Li et al., 2020) and the measured pH values of our remedial solutions, xanthan gum and alginate suspensions are expected to be stable at pH > 4; while guar gum is unlikely to produce a stable suspension at any pH.

3.1 Amendment Reactivity

3.1.1 Reductants in Polymer Solutions

The overall treatment capacity (C) and first order rate of K_2CrO_4 reduction (k) were determined by fitting the experimental data to **Eq. 1** (**Figure 1**; **Table 2**).

Slight decreases in the treatment capacity of gZVI were measured in suspensions of 800 mg/L (final concentration) xanthan gum, guar gum, and sodium alginate; corresponding to 7.0 ± 0.1, 0.8 ± 0.1, and 12 ± 0.0%, respectively, less capacity than the gZVI no-polymer control (**Figure 1A**; **Table 2**). However, gZVI reduction rate coefficients were strongly influenced by the presence of the polymer, with Cr(VI) reduction rates decreasing 62 ± 9.3%, 41 ± 12, and 70 ± 4.0% in xanthan gum, guar gum, and sodium alginate solutions, respectively, relative to the gZVI no-polymer control.

The treatment capacity of SMI decreased 2.5 ± 0.2, 2.6 ± 0.2, and 16 ± 0.3%, in the presence of 800 mg/L xanthan gum, guar gum, and sodium alginate, respectively (**Figure 1B**; **Table 2**). Similar to the behavior of gZVI, polymer suspensions had a much more pronounced effect on the treatment rate coefficient for SMI where rates decreased 61 ± 29, 2 ± 28, and 58 ± 35% in the presence of xanthan gum, guar gum, and sodium alginate, respectively.

The effect of polymers on particle reactivity has not been fully characterized in the literature, though studies have described a temporal delay or loss of reactivity (Velimirovic et al., 2014a; Gastone et al., 2014). The significance of these implications remains to be determined, though the consensus is that the practical benefits, which range from delayed surface corrosion to enhanced transport behavior, potentially outweigh any negative interactions which may be inherently overcome by groundwater flow and biodegradation *in situ* (Velimirovic et al., 2012; Velimirovic et al., 2014a).

Micron sized ZVI was unresponsive for the reduction of Cr(VI) during these short duration experiments (**Figure 1C**; **Table 2**). Regardless of the polymer used, the aqueous concentration of Cr(VI) remained unchanged for up to 48 h of incubation in these batch experiments. This ZVI product is commercial grade, not lab grade purity, however the vendor specifications do not offer any clear explanation for the relatively slow reactivity.

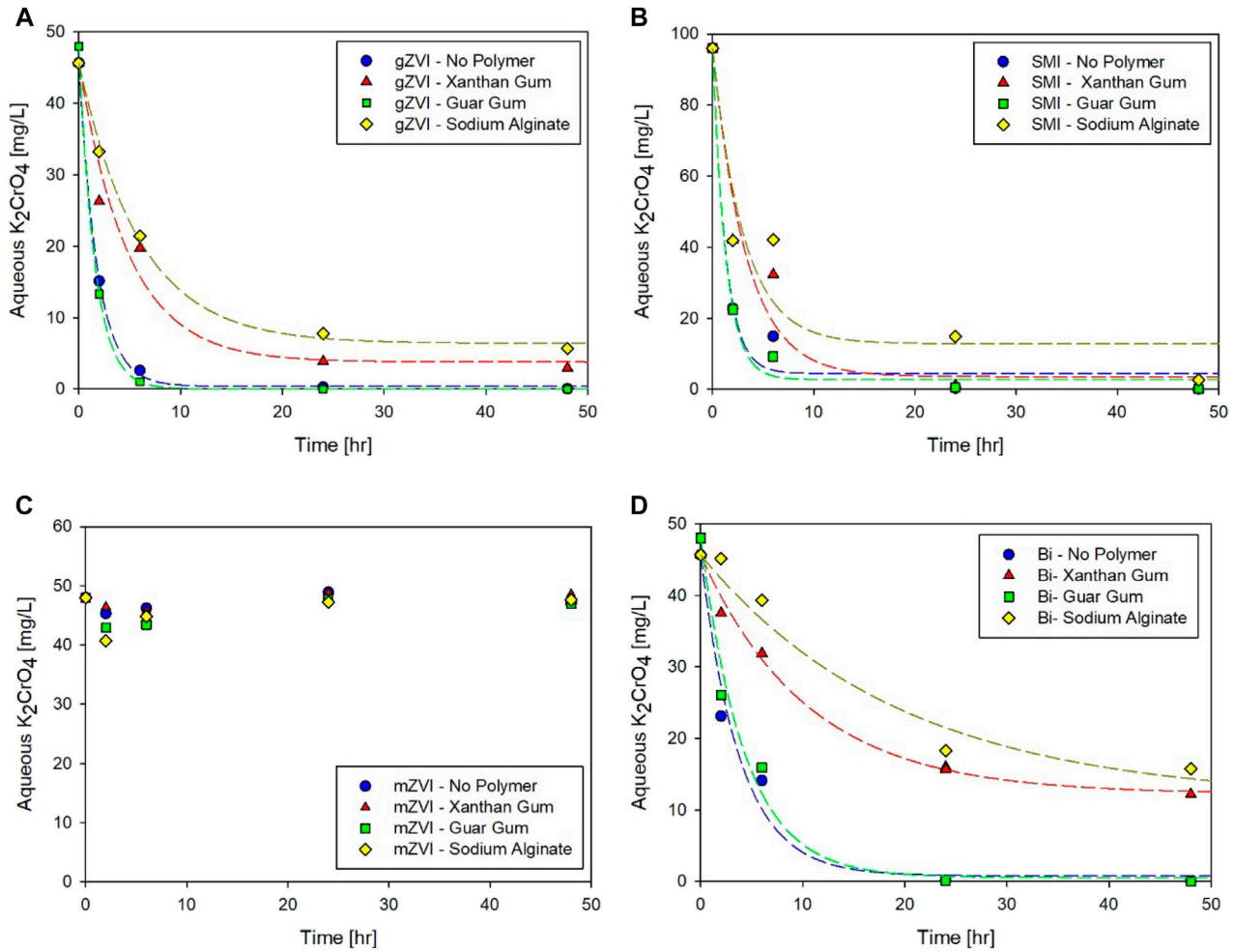

FIGURE 1 | Impact of polymer (800 mg/L) on K_2CrO_4 treatment via **(A)** gZVI, **(B)** SMI, **(C)** mZVI, and **(D)** Bismuth sub-nitrate. Symbols indicate experimental data points for each polymer type (circle = no polymer; triangle = xanthan gum, square = guar gum, diamond = sodium alginate). Dashed lines indicate corresponding kinetic model fits (**Eq. 1**). The relative error associated with experimental replicates ranged from 0–11% (average 5%).

3.1.2 Adsorbent in Polymer Solutions

In contrast to particulate reductants, the treatment capacity and rate of bismuth subnitrate to adsorb K_2CrO_4 from solution was generally more impaired by the polymer suspension (**Figure 1D**; **Table 2**). The adsorption capacity of bismuth decreased 37 ± 0.2, 2.9 ± 0.1, and 23 ± 0.1%, and adsorption rates decreased 30 ± 35, 81 ± 27, and 81 ± 27% in the presence of xanthan gum, guar gum, and sodium alginate, respectively. These results are consistent with studies showing that polymer suspensions can have substantial interference on the kinetics and capacity of remedial amendments. For example, the rate of trichloroethylene (TCE) reduction by milled ZVI decreased an order of magnitude, relative to controls, when suspended in agar (1 g/L) (Velimirovic et al., 2016). Similarly, reduction rates of TCE and other chlorinated aliphatics were 1–8 times slower when micron sized ZVI was suspended in guar gum (2, 4, or 6 g/L) (Velimirovic et al., 2012). In these studies, the loss of amendment reactivity was described as a reversible interaction between the polymer matrix and reaction sites on the ZVI particle surface, in which full reactivity could be restored by repeated rinsing or enzymatic treatment to eliminate the polymer from those sites (Velimirovic et al., 2012; Velimirovic et al., 2013). Polymers have also been used to form a hydrodynamic barrier on ZVI and SMI particle surfaces to slow oxidative reactions (Messali et al., 2017; Balachandramohan and Sivasankar, 2018; Palumbo et al., 2019). This explanation that polymers create a physical barrier to particle reaction sites is consistent with our results showing reduced performance metrics that indicate delayed reactivity with Cr(VI) over these short duration experiments. Longer temporal studies are needed, however, to determine whether treatment capacity (reduction or adsorption) is genuinely lost due to chemical reaction with the polymer or simply delayed due to the physical blocking of reaction sites.

The strength of electrostatic interactions between the polymer matrix, an amendment, and/or a contaminant ion, could compound the physical interferences between reactants. It is

TABLE 2 | K_2CrO_4 removal via solid phase amendments (kinetics and capacity).

Amendment	Polymer type	Polymer conc. [mg/L]	Fitted parameters			Relative to No polymer control	
			Capacity, *C*	Rate, *k*	Adj R^2	Capacity, *C*	Rate, *k*
			[mg cr/g]	[hr^{-1}]	[—]	[—]	[—]
gZVI	None	0	9.29 ± 0.00	0.55 ± 0.02	1.00	1.00 ± 0.00	1.00 ± 0.04
	Xanthan Gum	800	8.65 ± 0.01	0.21 ± 0.05	0.96	0.93 ± 0.00	0.38 ± 0.09
		4,000	9.29[a]			1.0[a]	
	Guar Gum	800	9.22 ± 0.01	0.32 ± 0.06	0.97	0.99 ± 0.00	0.59 ± 0.11
		4,000	9.22[a]			1.0[a]	
	Na-Alginate	800	8.19 ± 0.00	0.17 ± 0.01	1.00	0.88 ± 0.00	0.30 ± 0.02
SMI	None	0	18.20 ± 0.04	0.77 ± 0.19	0.97	1.00 ± 0.00	1.00 ± 0.35
	Xanthan Gum	800	17.74 ± 0.02	0.30 ± 0.09	0.92	0.97 ± 0.00	0.39 ± 0.15
		4,000	18.21 ± 0.00	0.28 ± 0.00	1.00	1.00 ± 0.00	0.36 ± 0.09
	Guar Gum	800	17.73 ± 0.02	0.76 ± 0.10	0.99	0.97 ± 0.00	0.98 ± 0.28
		4,000	18.61 ± 0.01	1.18 ± 0.04	1.00	1.02 ± 0.00	1.53 ± 0.38
	Na-Alginate	800	15.24 ± 0.03	0.33 ± 0.15	0.84	0.84 ± 0.00	0.42 ± 0.22
Bi	None	0	9.39 ± 0.01	0.26 ± 0.05	0.97	1.00 ± 0.00	1.00 ± 0.28
	Xanthan Gum	800	5.93 ± 0.02	0.18 ± 0.08	0.89	0.63 ± 0.00	0.70 ± 0.32
		4,000	5.93 ± 0.02	0.22 ± 0.09	0.88	0.63 ± 0.00	0.84 ± 0.37
	Guar Gum	800	9.12 ± 0.01	0.05 ± 0.03	0.94	0.97 ± 0.00	0.19 ± 0.10
		4,000	7.77 ± 0.01	0.14 ± 0.04	0.96	0.83 ± 0.00	0.54 ± 0.17
	Na-Alginate	800	7.19 ± 0.00	0.05 ± 0.02	0.96	0.77 ± 0.00	0.19 ± 0.09

Based on the total capacity of the individual amendment types, the K_2CrO_4 to amendment ratios were 18.5 mg/g for SMI, and 9.5 mg/g for gZVI, mZVI, and Bi.
The kinetics and capacity of the mZVI, results could not be interpreted with ***Eq. 1****.*
[a]*Reaction was too fast to successfully obtain kinetics and capacity using* ***Eq. 1****. Assumed capacity and relative capacity based on experimental results where little to no aqueous Cr was remaining.*
The relative error associated with experimental replicates ranged from 0–11% (average 5%).

worth noting that polymers may also alter the surface charge of a particle (Barany, 2015). In this case, if the net surface charge is negative then repulsion of negatively charged contaminant species could thereby reduce treatment capacity and retard reaction kinetics. This interpretation could partially explain why the highly negative charge of the alginate had the most Cr(VI) interference, as Cr predominately exists as CrO_4^{2-}, followed by the slightly negatively charged xanthan gum. By extension, the lack of interference experienced with guar gum could be attributed to it having a net neutral charge (at pH ~ 8). Zeta potential measurements were not included as part of this investigation but may be important for understanding specific mechanistic interactions between these remedial components.

3.2 Concentration Effects of Polymers on Amendment Reactivity

Many publications have evaluated the rheological properties of polymer solutions at relatively high concentrations; however, concentration dependent effects on amendment reactivity could be quite important depending on the remedial application. For example, highly viscous suspensions (4 to as high as 8 g/L) would be appropriate to emplace amendment mass in fractures and fissures, while shear thinning behavior at much lower polymer concentration is necessary for direct push injection of suspensions into the heterogenous subsurface. The effect of high polymer concentration (4,000 mg/L) on amendment treatment capacity (C) and first order rate of K_2CrO_4 reduction (k) were determined by fitting the experimental data to **Eq 1** (**Figure 2**; **Table 2**). Batch experiments were conducted as described above allowing for direct comparison between the two polymer concentrations (800 and 4,000 mg/L). Since alginate provided little rheological benefit (i.e., little increase in overall viscosity and no shear thinning behavior), limited improvement in suspension stability for the amendments considered here (data not shown), and high interference was exhibited with the various amendments, no further testing was performed.

3.2.1 Effect of Polymer Concentration on Reductants

Increasing the polymer concentration to 4,000 mg/L corresponded with a significant increase in gZVI treatment kinetics, which resulted in the reaction being too fast to successfully obtain fitted model values for capacity and kinetics (**Table 2**; **Figure 2A,B**). While parameters could not be fit for direct comparisons, due to the quick depletion of aqueous K_2CrO_4, results suggest that the higher polymer concentrations, for both xanthan and guar gum, created no capacity reduction and perhaps increased the reduction reaction rates compared to the no polymer control and experiments conducted at 800 mg/L polymer. Visual observations and suspension stability experiments for gZVI suggest that the high polymer concentrations created a more stable suspension (see supporting information). In this case, we surmise that the high polymer content reduced particle aggregation, thereby increasing effective surface area for rapid reduction of Cr(VI).

SMI treatment capacity was generally insensitive to increased polymer concentration; however, SMI reduction kinetics did show polymer specific trends (**Table 2**; **Figures 2C,D**).

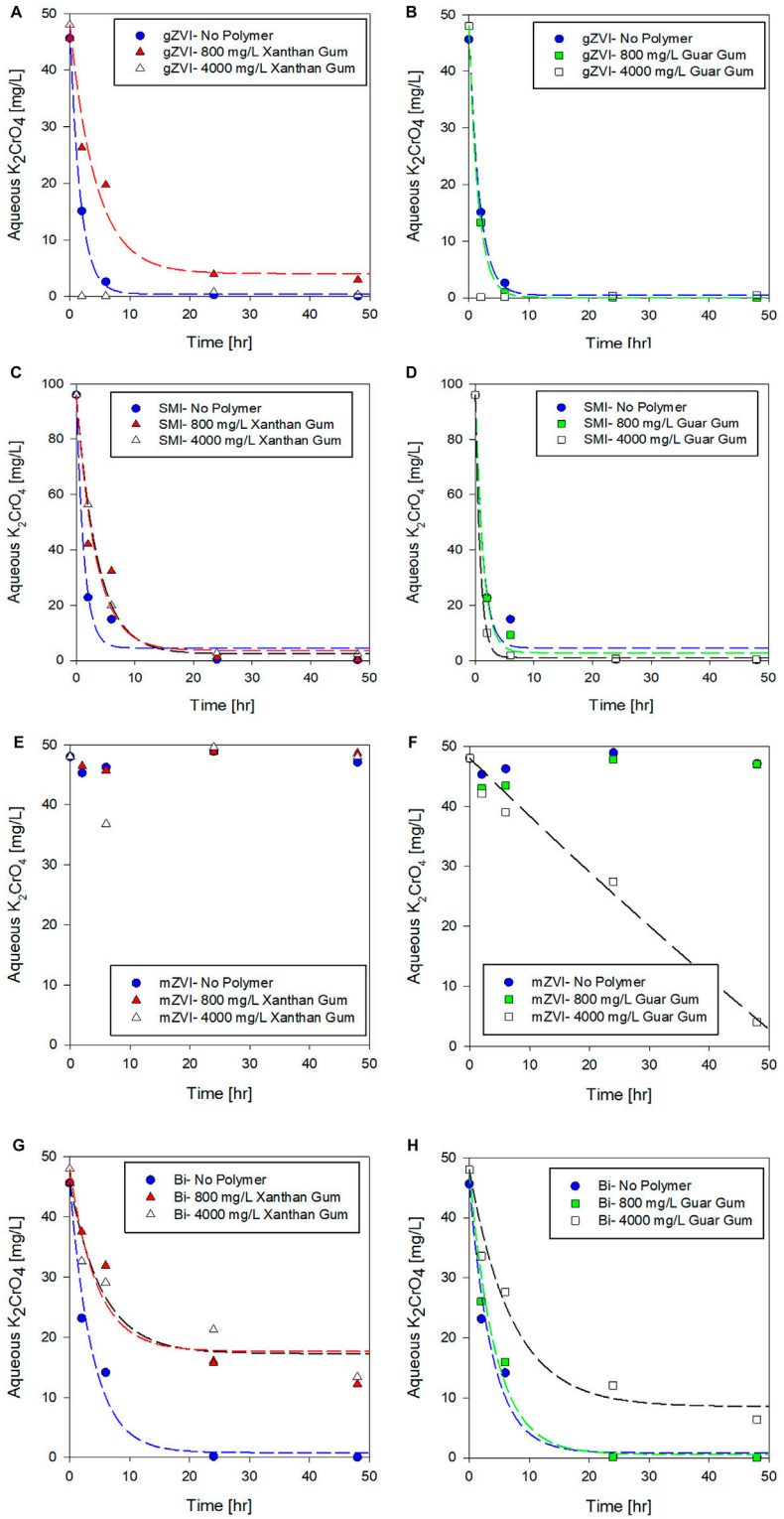

FIGURE 2 | Effect of Xanthan Gum and Guar Gum Concentration Effects on Reactivity of **(A,B)** gZVI, **(C,D)** SMI, **(E,F)** mZVI and **(G,H)** Bismuth, respectively. Symbols designate experimental data; lines indicate corresponding kinetic model fits (**Eq. 1**). The relative error associated with experimental replicates ranged from 0–11% (average 5%).

Xanthan gum, regardless of concentration (i.e., 800 or 4,000 mg/L), decreased treatment rates to 36–39% of the no polymer control kinetic rate. Guar gum showed the opposite trend, Cr(VI) removal kinetics increased by about 53% in a 4,000 mg/L guar gum suspension compared to the no polymer control and 56% compared to the lower concentration guar gum solution.

3.2.2 Effect of Polymer Concentration on Adsorbent

For bismuth subnitrate, increasing xanthan gum concentration from 800 mg/L to 4,000 mg/L did not create additional interference in terms of treatment capacity or treatment rate. The results summarized in **Figure 2G** suggest that maximum interference by xanthan gum on bismuth subnitrate was achieved at a concentration of 800 mg/L and thus, no further polymer concentration effects on Cr(VI) reduction were measured. This trend may suggest electrostatic interactions between the slightly positively charged bismuth and the strongly negatively charged xanthan gum are playing an important role. On the other hand, bismuth subnitrate adsorption capacity was reduced from 97 to 83% with increasing concentration of guar gum (**Figure 2H**), which may indicate that physical interactions predominate for net neutral guar gum, thus eliminating electrostatic forces from consideration. Clearly, the maximum interference displayed by guar gum was not exceeded at 800 mg/L, as was observed for xanthan gum, and concentration dependent effects were measured at 4,000 mg/L.

As with gZVI, a higher polymer concentration produced faster reaction kinetics for Cr(VI) removal. Bismuth treatment kinetics increased from 0.05 to 0.14 h^{-1} with increased guar gum concentration. Similarly, the fitted rate coefficient was higher for the 4,000 mg/L xanthan gum solution compared to the 800 mg/L solution, although the increase was within the estimated parameter error. As postulated for gZVI, polymer enhanced stability can improve reaction kinetics by minimizing particle aggregation and agglomeration; however, the obvious tradeoff for faster reaction kinetics is, presumably, time dependent impairment of treatment capacity. These types of experiments not only illustrate clear tradeoffs, but may also be used to quickly determine an optimal carrier concentration for an amendment-carrier pair, providing a balance between the ability of the carrier to increase suspension stability without creating significant interferences that reduce or delay treatment capacity.

We presume the primary interference for adsorbent materials, like Bi, is due to physical blocking of the surface reaction sites by a polymer. This is supported by published studies showing that particulate amendment reactivity can be restored if the polymer is removed (e.g., Velimirovic et al., 2012, Velimirovic et al., 2013), although it is unclear whether polymer interaction with reductants is strictly physical or possibly chemical as well. The implication of potentially reversible interference behavior is that particulate amendment reactivity could be fully restored through dilution, desorption, and/or degradation *in situ*. The former processes will be largely controlled by groundwater flow conditions and groundwater chemistry, and the latter by microbial densities and relative activity. Guar gum has been shown to be susceptible to degradation, while xanthan gum appears more refractory, though detailed degradation studies with quantitative data are lacking (e.g., Cadmus et al., 1982). Consequently, interferences and complex interactions between remedial reagents need to be systematically characterized to reliably understand *in situ* performance and temporal behavior, as well as to identify actionable interventions that ensure remedial goals are met.

3.3 Aging Effects on Amendment Reactivity

In application, emplaced amendments may naturally age *in situ* if exposure to contaminants is primarily controlled by slow groundwater transport. As such, this series of aging experiments provide insights into whether amendment reactivity is preserved over time in polymer suspensions, or if some amount of an amendment's remedial capacity is lost as it ages in a polymer suspension before contacting contaminant. To investigate the temporal effects of polymers on amendment reactivity, amendments were aged in polymer solutions for 7, 14, and 28 days prior to measuring Cr(VI) removal over a 24-h reaction period. Results from the aging experiments are summarized in **Figure 3** where the performance metrics and results described above (**Table 2**) were used as a baseline (t = 0 days) for comparison.

3.3.1 Aging of Reductants in Polymer Solutions

After 28 days of aging particulate amendments, approximately 86% of the gZVI treatment capacity was preserved in the no-polymer controls, whereas in xanthan gum, reduction capacity decreased from 91 to 66% by 28 days. Similarly, guar gum suspensions of gZVI maintained reduction capacity for up to 14 days of aging, reducing 98% of the aqueous Cr(VI); however, between 14 and 28 days of incubation, gZVI reduction capacity declined to only 27%.

The ability of SMI to effectively reduce Cr(VI) was not affected following 28 days of aging in any of the polymer suspensions. In all SMI aging tests at least 98% of the treatment capacity was retained, relative to no polymer baseline control, indicating the robust nature of SMI in the tested polymers. SMI is a potent chemical reductant, utilizing the dual action of zero-valent iron and reduced sulfur compounds, capable of rapidly neutralizing a variety of groundwater contaminants (Allred 2012). In particular, sulfidation of nZVI has been shown to minimize nonspecific, competitive reactions that deplete reducing potential, chiefly corrosive reactions that predominate during aging in water (Su et al., 2015), thereby improving overall treatment selectivity and reactivity for target compounds (Rajajayavel and Ghoshal, 2015; Fan et al., 2016).

Interestingly, mZVI was not only activated in response to aging, but the temporal activation period appeared shorted when suspended in a polymer compared to the no polymer control. In the mZVI–no polymer control, Cr(VI) concentration slowly declined after 7–14 days (8–9% Cr(VI) reduced) with a 28% decrease in Cr(VI) concentration after 28-days of aging. Lawter et al. (2018) demonstrated effective reduction of ^{99}Tc and ^{129}I with the same mZVI product over comparable time scales (days-weeks). For comparison, the mZVI–guar gum

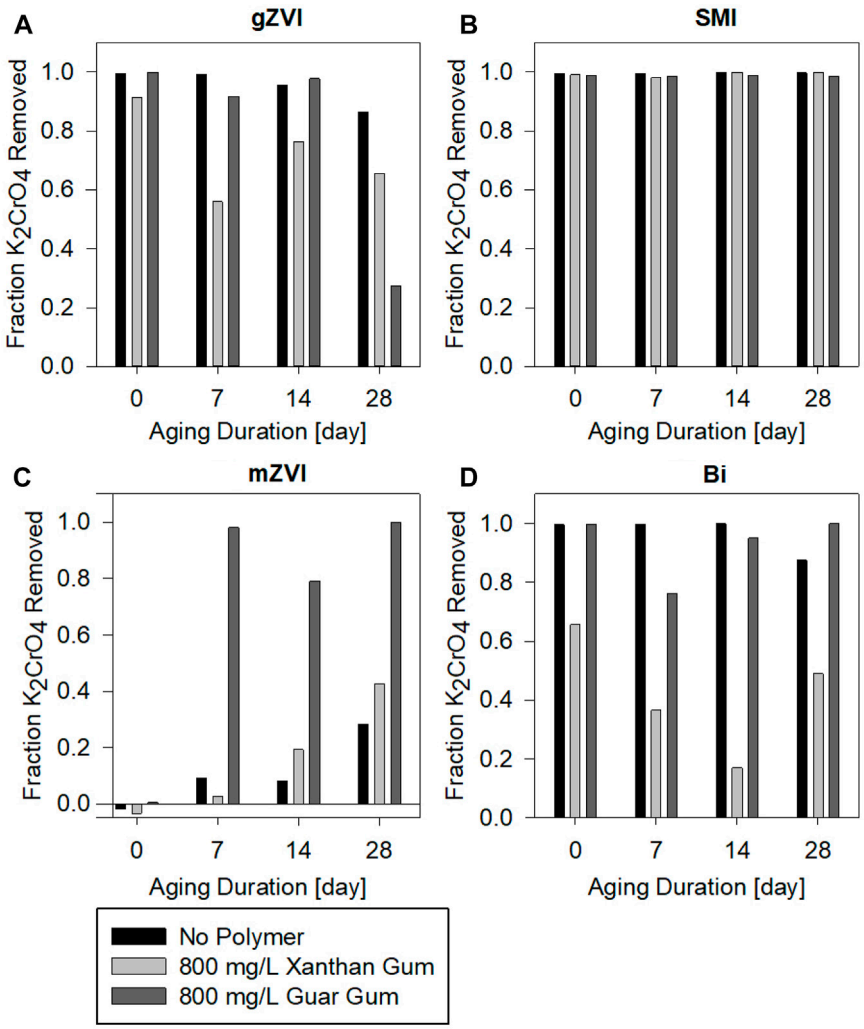

FIGURE 3 | Effect of polymer (800 mg/L)–amendment aging on K_2CrO_4 removal via **(A)** gZVI, **(B)** SMI, **(C)** mZVI, and **(D)** Bismuth sub-nitrate. Post aging, chromate was added to the polymer-amendment system and Cr(VI) concentration was measured after 24 h.

suspension removed over 98% Cr(VI) after 7 days of aging, and 100% after the full 28 days of aging. Similar trends, though lower in magnitude, were measured when mZVI was aged in xanthan gum; 43% Cr(VI) was removed after 28 days of aging in xanthan gum, compared to 28% in the no polymer control (**Figure 3**). We surmise that the measured delay in mZVI response could, in part, reflect competing reactions for available mZVI reaction sites (and reductant) between water, O_2, and Cr(VI). Additional work is needed to resolve the temporal delay in mZVI reduction activity, but this behavior contradicts conventional expectations relative to gZVI based on the established relationship between particle size and reactivity. It is most plausible that suspension stability plays a key role in mZVI reactive performance which clearly increased with high concentration of guar gum (**Figure 2**) and in response to aging which would increase particle disaggregation, creating more surface area for Cr(VI) reduction (**Figure 3**).

3.3.2 Aging of Adsorbent in Polymer Solutions

Consistent with the results summarized previously, adsorption capacity of bismuth subnitrate was more severely affected by aging compared to the chemical reductants investigated. When bismuth was suspended in xanthan gum, Cr(VI) removal capacity decreased from 65 to 37%–17% as suspensions were aged 0, 7, and 14 days, respectively. However, after 28 days, bismuth-xanthan gum capacity increased up to 49%, indicating a time-dependent behavior that seemingly restored some treatment capacity after 28 days of aging. Interestingly, bismuth suspended in guar gum did not exhibit this behavior. In fact, chromate removal capacity of bismuth suspended in guar gum remained 95 and 100%, after 14- and 28-days aging, respectively.

Overall, the batch experiment results illustrate how polymer specific attributes may differentially affect treatment capacity and reaction rate for reductants and adsorbents. Concentration

dependent behavior and likely a multitude of complex physical and chemical interactions between polymers and remedial amendments are highlighted for simple batch systems. We anticipate the complexity of the system will likely increase further as site specific geological media and biotic processes are also considered. Thus, remedial suspensions need to be systematically characterized in order to more completely understand these dynamic systems to enable a more predictive and translational knowledge of *in situ* treatment performance and longevity.

4 CONCLUSION

The results indicate that polymer composition, concentration, and temporal aging may all have important impacts on the treatment capacity and reaction kinetics of particulate amendments. Specific interactions between polymer and amendment varied, suggesting that both physical and chemical interactions impede reactivity. The main findings from this study are that polymer interferences: 1) were more pronounced for adsorption of Cr(VI) compared to chemical reduction, 2) were generally lower and less severe with guar gum compared to other polymers tested, 3) resulted in capacity lost for gZVI, but not SMI, during aging while Bi treatment capacity was temporally delayed but restored with time.

While this study does contribute incremental knowledge of specific interactions between combinations of remedial reagents, we expect that these interactions will become much more complex and dynamic under site relevant conditions (e.g., high sediment to water ratio with little mixing, heterogeneity). As such, the performance metrics reported here likely represent best case, baseline determinations for Cr(VI) removal whereby increasing system complexity will exacerbate interferences and disrupt desired remedial reactions. Additional studies are needed to systematically characterize the processes that most significantly affect remedial outcomes to help enable application design improvements and our ability to forecast *in situ* treatment outcomes with increased precision.

For any given amendment-polymer combination, there are clear trade-offs between beneficial rheological attributes and temporal impairment of remedial activity that must be considered in light of site-specific conditions and the remedial objectives. While fluid property requirements will differ by remedial application, the lowest polymer concentration that meets fluid characteristics for successful injection should be selected for use to limit carrier interference. While interferences are highly dependent on the mode of action of the remedial amendment, potential interferences should be considered and built into remedial design strategies. Upfront experimental screening, as conducted here, could help to identify preparation conditions for amendment suspensions that tune remedial amendment performance for specific site conditions and subsurface applications.

DATA AVAILABILITY STATEMENT

The raw data supporting the conclusion of this article will be made available by the authors, without undue reservation.

AUTHOR CONTRIBUTIONS

KM and CB contributed to conception and design of the study. KM, LZ, and CB conducted the experiments and analyzed the results. KM and CB wrote the manuscript. KM, LZ, and CB contributed to manuscript revision and approved the submitted version.

FUNDING

This work was funded by the United States Department of Energy (DOE) Richland Operations Office to the Deep Vadose Zone–Applied Field Research Initiative at Pacific Northwest National Laboratory (PNNL). PNNL is managed by Battelle Memorial Institute under Contract No. DE-AC05-76RL01830 with the United States Department of Energy.

ACKNOWLEDGMENTS

The coauthors would like to acknowledge Jim Szecsody and Carolyn Pearce for helpful discussion and meaningful contribution to the overall quality of this presentation.

SUPPLEMENTARY MATERIAL

The Supplementary Material for this article can be found online at: https://www.frontiersin.org/articles/10.3389/fenvs.2021.703851/full#supplementary-material

REFERENCES

Allred, B. J. (2012). Laboratory Evaluation of Zero Valent Iron and Sulfur-Modified Iron for Agricultural Drainage Water Treatment. *Groundwater Monit. Remediation* 32, 81–95. doi:10.1111/j.1745-6592.2011.01379.x

Balachandramohan, J., and Sivasankar, T. (2018). Ultrasound Assisted Synthesis of Guar Gum-Zero Valent Iron Nanocomposites as a Novel Catalyst for the Treatment of Pollutants. *Carbohydr. Polym.* 199, 41–50. doi:10.1016/j.carbpol.2018.06.097

Barany, S. (2015). Polymer Adsorption and Electrokinetic Potential of Dispersed Particles in Weak and strong Electric fields. *Adv. Colloid Interf. Sci.* 222, 58–69. doi:10.1016/j.cis.2014.09.009

Bianco, C., Tosco, T., and Sethi, R. (2016). A 3-dimensional Micro- and Nanoparticle Transport and Filtration Model (MNM3D) Applied to the Migration of Carbon-Based Nanomaterials in Porous media. *J. Contaminant Hydrol.* 193, 10–20. doi:10.1016/j.jconhyd.2016.08.006

Brusseau, M. L., Carroll, K. C., Allen, T., Baker, J., Diguiseppi, W., Hatton, J., et al. (2011). Impact of *In Situ* Chemical Oxidation on Contaminant Mass Discharge:

Linking Source-Zone and Plume-Scale Characterizations of Remediation Performance. *Environ. Sci. Technol.* 45 (12), 5352–5358. doi:10.1021/es200716s

Cadmus, M. C., Jackson, L. K., Burton, K. A., Plattner, R. D., and Slodki, M. E. (1982). Biodegradation of Xanthan Gum by Bacillus Sp. *Appl. Environ. Microbiol.* 44 (1), 5–11. doi:10.1128/aem.44.1.5-11.1982

Chuang, J. J., Huang, Y. Y., Lo, S. H., Hsu, T. F., Huang, W. Y., Huang, S. L., et al. (2017). Effects of pH on the Shape of Alginate Particles and its Release Behavior. *Int. J. Polym. Sci.* 2017, 3902704. doi:10.1155/2017/3902704

Fan, D., Gilbert, E. J., and Fox, T. (2017). Current State of *In Situ* Subsurface Remediation by Activated Carbon-Based Amendments. *J. Environ. Manage.* 204, 793–803. doi:10.1016/j.jenvman.2017.02.014

Fan, D., Johnson, G. O., Tratnyek, P. G., and Johnson, R. L. (2016). Sulfidation of Nano Zerovalent Iron (nZVI) for Improved Selectivity during In-Situ Chemical Reduction (ISCR). *Environ. Sci. Technol.* 50 (17), 9558–9565. doi:10.1021/acs.est.6b02170

Fink, J. K. (2015). *Petroleum Engineer's Guide to Oil Field Chemicals and Fluids*. Second Edition. Houston, Texas: Gulf Professional Publishing, 567–651. Chapter 17, Fracturing Fluids.

Flores Orozco, A., Velimirovic, M., Tosco, T., Kemna, A., Sapion, H., Klaas, N., et al. (2015). Monitoring the Injection of Microscale Zerovalent Iron Particles for Groundwater Remediation by Means of Complex Electrical Conductivity Imaging. *Environ. Sci. Technol.* 49, 5593–5600. doi:10.1021/acs.est.5b00208

Gastone, F., Tosco, T., and Sethi, R. (2014). Green Stabilization of Microscale Iron Particles Using Guar Gum: Bulk Rheology, Sedimentation Rate and Enzymatic Degradation. *J. Colloid Interf. Sci.* 421, 33–43. doi:10.1016/j.jcis.2014.01.021

Gharbi, O., Thomas, S., Smith, C., and Birbilis, N. (2018). Chromate Replacement: What Does the Future Hold? *Npj Mater. Degrad.* 2, 12. doi:10.1038/s41529-018-0034-5

Hasan, A. M. A., and Abdel-Raouf, M. E. (2018). Applications of Guar Gum and its Derivatives in Petroleum Industry: A Review. *Egypt. J. Pet.* 27, 1043–1050. doi:10.1016/j.ejpe.2018.03.005

Kocur, C. M., Chowdhury, A. I., Sakulchaicharoen, N., Boparai, H. K., Weber, K. P., Sharma, P., et al. (2014). Characterization of nZVI Mobility in a Field Scale Test. *Environ. Sci. Technol.* 48, 2862–2869. doi:10.1021/es4044209

Lace, A., Ryan, D., Bowkett, M., and Cleary, J. (2019). Chromium Monitoring in Water by Colorimetry Using Optimised 1,5-Diphenylcarbazide Method. *Ijerph* 16, 1803. doi:10.3390/ijerph.16101803

Lawter, A. R., Garcia, W. L., Kukkadapu, R. K., Qafoku, O., Bowden, M. E., Saslow, S. A., et al. (2018). Technetium and Iodine Aqueous Species Immobilization and Transformations in the Presence of Strong Reductants and Calcite-Forming Solutions: Remedial Action Implications. *Sci. Total Environ.* 636, 588–595.

Li, J., Jin, W., Xu, W., Liu, G., Huang, Q., Zhu, Z., et al. (2020). Effect of Charge Density of Polysaccharide on Self-Assembly Behaviors of Ovalbumin and Sodium Alginate. *Int. J. Biol. Macromolecules* 154, 1245–1254. doi:10.1016/j.ijbiomac.2019.10.279

Lowry, G. V., and Phenrat, T. (2019). "State of Knowledge and Future Needs for NZVI Applications in Subsurface Remediation," in *Nanoscale Zerovalent Iron Particles for Environmental Restoration*. Editors T. Phenrat and G. Lowry (New York, United States: Springer, Cham), 563–579. doi:10.1007/978-3-319-95340-3_16

Messali, M., Lgaz, H., Dassanayake, R., Salghi, R., Jodeh, S., Abidi, N., et al. (2017). Guar Gum as Efficient Non-toxic Inhibitor of Carbon Steel Corrosion in Phosphoric Acid Medium: Electrochemical, Surface, DFT and MD Simulations Studies. *J. Mol. Struct.* 1145, 43–54. doi:10.1016/j.molstruc.2017.05.081

Mondino, F., Piscitello, A., Bianco, C., Gallo, A., de Folly D'Auris, A., Tosco, T., et al. (2020). Injection of Zerovalent Iron Gels for Aquifer Nanoremediation: Lab Experiments and Modeling. *Water* 12 (3), 826. doi:10.3390/w12030826

Muller, K. A., Johnson, C. D., Bagwell, C. E., and Truex, M. J. (2020)). Methods for Delivery and Distribution of Amendments for Subsurface Remediation: A Critical Review. *Groundwater Monit. R.* 41, 46–75. doi:10.1111/gwmr.12418

O'Carroll, D., Sleep, B., Krol, M., Boparai, H., and Kocur, C. (2013). Nanoscale Zero Valent Iron and Bimetallic Particles for Contaminated Site Remediation. *Adv. Water Resour.* 51, 104–122. doi:10.1016/j.advwatres.2012.02.005

Oostrom, M., Wietsma, T. W., Covert, M. A., and Vermeul, V. R. (2007). Zero-Valent Iron Emplacement in Permeable Porous Media Using Polymer Additions. *Ground Water Monit. Remediation* 27, 122–130. doi:10.1111/j.1745-6592.2006.00130.x

Palumbo, G., Berent, K., Proniewicz, E., and Banaś, J. (2019). Guar Gum as an Eco-Friendly Corrosion Inhibitor for Pure Aluminium in 1-M HCl Solution. *Materials* 12, 2620. doi:10.3390/ma12162620

Paveklová, A., Stejskal, V., Vološčuková, O., and Nosek, J. (2020). Cost-effective Remediation Using Microscale ZVI: Comparison of Commercially Available Products. *Ecol. Chem. Engineer* 27, 211–224. doi:10.2478/eces-2020-0014

Pearce, C. I., Cordova, E. A., Garcia, W. L., Saslow, S. A., Cantrell, K. J., Morad, J. W., et al. (2020). Evaluation of Materials for Iodine and Technetium Immobilization through Sorption and Redox-Driven Processes. *Sci. Total Environ.* 716, 136167. doi:10.1016/j.scitotenv.2019.136167

P. K. Kitanidis and P. L. McCarty (Editors) (2012). *Delivery and Mixing in the Subsurface: Processes and Design Principles for* in Situ *Remediation* (Berlin, Germany: Springer Science & Business Media).

Rajajayavel, S. R. C., and Ghoshal, S. (2015). Enhanced Reductive Dechlorination of Trichloroethylene by Sulfidated Nanoscale Zerovalent Iron. *Water Res.* 78, 144–153. doi:10.1016/j.watres.2015.04.009

Smith, M. M., Silva, J. A. K., Munakata-Marr, J., and McCray, J. E. (2008). Compatibility of Polymers and Chemical Oxidants for Enhanced Groundwater Remediation. *Environ. Sci. Technol.* 42, 9296–9301. doi:10.1021/es800757g

Su, Y., Adeleye, A. S., Keller, A. A., Huang, Y., Dai, C., Zhou, X., et al. (2015). Magnetic Sulfide-Modified Nanoscale Zerovalent Iron (S-nZVI) for Dissolved Metal Ion Removal. *Water Res.* 74, 47–57. doi:10.1016/j.watres.2015.02.004

Switzer, C., and Kosson, D. S. (2007). Soil Vapor Extraction Performance in Layered Vadose Zone Materials. *Vadose zone j.* 6, 397–405. doi:10.2136/vzj2005.0131

Testa, S., Guertin, J., Jacobs, J., and Avakian, C. (2004). "Sources of Chromium Contamination in Soil and Groundwater," in *Chromium (VI) Handbook*. Editors J. Guertein, J. Jacobs, and C. Avakian (Boca Raton, FL: CRC Press), pp143–164. doi:10.1201/9780203487969.ch4

Thomson, N. R., Fraser, M. J., Lamarche, C., Barker, J. F., and Forsey, S. P. (2008). Rebound of a Coal Tar Creosote Plume Following Partial Source Zone Treatment with Permanganate. *J. Contaminant Hydrol.* 102, 154–171. doi:10.1016/j.jconhyd.2008.07.001

Tiraferri, A., Chen, K. L., Sethi, R., and Elimelech, M. (2008). Reduced Aggregation and Sedimentation of Zero-Valent Iron Nanoparticles in the Presence of Guar Gum. *J. Colloid Interf. Sci.* 324, 71–79. doi:10.1016/j.jcis.2008.04.064

Tosco, T., Gastone, F., and Sethi, R. (2014a). Guar Gum Solutions for Improved Delivery of Iron Particles in Porous media (Part 2): Iron Transport Tests and Modeling in Radial Geometry. *J. Contaminant Hydrol.* 166 (0), 34–51. doi:10.1016/j.jconhyd.2014.06.014

Tosco, T., Petrangeli Papini, M., Cruz Viggi, C., and Sethi, R. (2014b). Nanoscale Zerovalent Iron Particles for Groundwater Remediation: a Review. *J. Clean. Prod.* 77, 10–21. doi:10.1016/j.jclepro.2013.12.026

Tosco, T., and Sethi, R. (2010). Transport of Non-newtonian Suspensions of Highly Concentrated Micro- and Nanoscale Iron Particles in Porous media: A Modeling Approach. *Environ. Sci. Technol.* 44, 9062–9068. doi:10.1021/es100868n

Truex, M. J., Vermeul, V. R., Mendoza, D. P., Fritz, B. G., Mackley, R. D., Oostrom, M., et al. (2011). Injection of Zero Valent Iron into an Unconfined Aquifer Using Shear-Thinning Fluids. *Groundw. Monit. Rem.* 31, 50–58. doi:10.1111/j.1745-6592.2010.01319.x

Truex, M. J., Szecsody, J. E., Qafoku, N., Strickland, C. E., Moran, J. J., Lee, B. D., et al. (2017). Contaminant Attenuation and Transport Characterization of 200-DV-1 Operable Unit Sediment Samples. PNNL-26208; RPT-DVZ-AFRI-037 830403000. Richland WA: Pacific Northwest National Laboratory.

Tufenkji, N., and Elimelech, M. (2004). Deviation from the Classical Colloid Filtration Theory in the Presence of Repulsive DLVO Interactions. *Langmuir* 20 (25), 10818–10828. doi:10.1021/la0486638

Vecchia, E. D., Luna, M., and Sethi, R. (2009). Transport in Porous media of Highly Concentrated Iron Micro- and Nanoparticles in the Presence of Xanthan Gum. *Environ. Sci. Technol.* 43, 8942–8947. doi:10.1021/es901897d

Velimirovic, M., Larsson, P.-O., Simons, Q., and Bastiaens, L. (2013). Reactivity Screening of Microscale Zerovalent Irons and Iron Sulfides towards Different CAHs under Standardized Experimental Conditions. *J. Hazard. Mater.* 252-253, 252–253. doi:10.1016/j.jhazmat.2013.02.047

Velimirovic, M., Chen, H., Simons, Q., and Bastiaens, L. (2012). Reactivity Recovery of Guar Gum Coupled mZVI by Means of Enzymatic Breakdown and Rinsing. *J. Contaminant Hydrol.* 142-143, 1–10. doi:10.1016/j.jconhyd.2012.09.003

Velimirovic, M., Schmid, D., Wagner, S., Micić, V., von der Kammer, F., and Hofmann, T. (2016). Agar agar-stabilized Milled Zerovalent Iron Particles for *In Situ* Groundwater Remediation. *Sci. Total Environ.* 563-564, 713–723. doi:10.1016/j.scitotenv.2015.11.007

Velimirovic, M., Simons, Q., and Bastiaens, L. (2014a). Guar Gum Coupled Microscale ZVI for *In Situ* Treatment of CAHs: Continuous-Flow Column Study. *J. Hazard. Mater.* 265, 20–29. doi:10.1016/j.jhazmat.2013.11.020

Velimirovic, M., Tosco, T., Uyttebroek, M., Luna, M., Gastone, F., De Boer, C., et al. (2014b). Field Assessment of Guar Gum Stabilized Microscale Zerovalent Iron Particles for Iin-Ssitu Remediation of 1,1,1-trichloroethane. *J. Contaminant Hydrol.* 164, 88–99. doi:10.1016/j.jconhyd.2014.05.009

Wu, J., Wang, X.-B., and Zeng, R. J. (2017). Reactivity Enhancement of Iron Sulfide Nanoparticles Stabilized by Sodium Alginate: Taking Cr (VI) Removal as an Example. *J. Hazard. Mater.* 333, 275–284. doi:10.1016/j.jhazmat.2017.03.023

Zhang, S., Zhang, Z., and Vardhanabhuti, B. (2014). Effect of Charge Density of Polysaccharides on Self-Assembled Intragastric Gelation of Whey Protein/polysaccharide under Simulated Gastric Conditions. *Food Funct.* 5 (8), 1829–1838. doi:10.1039/c4fo00019f

Zhong, L., Oostrom, M., Truex, M. J., Vermeul, V. R., and Szecsody, J. E. (2013). Rheological Behavior of Xanthan Gum Solution Related to Shear Thinning Fluid Delivery for Subsurface Remediation. *J. Hazard. Mater.* 244-245, 160–170. doi:10.1016/j.jhazmat.2012.11.028

Zhong, L., Oostrom, M., Wietsma, T. W., and Covert, M. A. (2008). Enhanced Remedial Amendment Delivery through Fluid Viscosity Modifications: Experiments and Numerical Simulations. *J. Contaminant Hydrol.* 101, 29–41. doi:10.1016/j.jconhyd.2008.07.007

Zhong, L., Szecsody, J., Oostrom, M., Truex, M., Shen, X., and Li, X. (2011). Enhanced Remedial Amendment Delivery to Subsurface Using Shear Thinning Fluid and Aqueous Foam. *J. Hazard. Mater.* 191, 249–257. doi:10.1016/j.jhazmat.2011.04.074

Conflict of Interest: The authors declare that the research was conducted in the absence of any commercial or financial relationships that could be construed as a potential conflict of interest.

Publisher's Note: All claims expressed in this article are solely those of the authors and do not necessarily represent those of their affiliated organizations, or those of the publisher, the editors and the reviewers. Any product that may be evaluated in this article, orclaim that may be made by its manufacturer, is not guaranteed or endorsed by the publisher.

frontiers in Environmental Science

ORIGINAL RESEARCH
published: 17 December 2021
doi: 10.3389/fenvs.2021.784477

The Innovative Method of Purifying Polluted Air in the Region of an Inversion Layer

F. Jędrzejek, D. Gryboś, J. Zyśk, J. Leszczyński, K. Szarłowicz, M. Stobiński, B. Kubica and W. Suwała*

Faculty of Energy and Fuels, AGH University of Science and Technology, Kraków, Poland

Formation of the inversion layer causes a lack of vertical movement of the atmosphere and the occurrence of long-lasting high concentrations of pollution. The new invention makes use of shock waves, created by explosions of a mixture of flammable gases and air. These shock waves destroy the structure of the temperature inversion layer in the atmosphere and restore natural convection. Restoring vertical movements within the atmosphere causes a reduction in air pollution at the ground level. The system was tested at full technical scale in the environment. Preliminary effects indicate an average 24% reduction in PM10 concentration in the smog layer at ground level up to 20 m, with the device operating in 11-min series consisting of 66 explosions. It was also shown that the device is able to affect a larger area, at least 4 km^2.

Keywords: environmental pollution, air purification, particulate matter, air pollution, shock wave generator, urban space, temperature inversion

OPEN ACCESS

Edited by:
Ravi Naidu,
University of Newcastle, Australia

Reviewed by:
Atar Singh Pipal,
Ming Chi University of Technology, Taiwan
Allegrini Ivo,
Envint Srl, Italy

****Correspondence:***
F. Jędrzejek
jedrzejek@agh.edu.pl

Specialty section:
This article was submitted to Toxicology, Pollution and the Environment, a section of the journal Frontiers in Environmental Science

Received: *01 October 2021*
Accepted: *17 November 2021*
Published: *17 December 2021*

Citation:
Jędrzejek F, Gryboś D, Zyśk J, Leszczyński J, Szarłowicz K, Stobiński M, Kubica B and Suwała W (2021) The Innovative Method of Purifying Polluted Air in the Region of an Inversion Layer. Front. Environ. Sci. 9:784477. doi: 10.3389/fenvs.2021.784477

INTRODUCTION

According to data from the World Health Organization (WHO), 90% of the world's population is affected by polluted air. Exposure to air pollution causes about 4.2 million deaths annually (WHO Observatory, 2018). More than 60% of the global population is exposed to PM2.5 concentrations above 20 μg m^{-3} (van Donkelaar et al., 2016). Pollution negatively affects the human body, especially the respiratory, circulatory, reproductive, and nervous systems, causing many negative effects, including asthma, respiratory tract infections, and heart attacks (Sinha and Kumar, 2019). In the EU, Poland remains the most polluted by PM2.5. The world is facing a considerable challenge in improving air quality. The best known phenomenon associated with air pollution is smog. The term is applied to extensive contamination by atmospheric aerosol particles (London-type smog) or ozone (Los Angeles-type smog). London-type smog appears during winter, when a lot of particulate matter is emitted mainly from solid fuel furnaces used residentially. Because of these emissions released at a relatively low altitude (low-stack emission), together with the lack of pollutant dispersion under ground inversion, we can observe high concentrations of particulate matter and other pollutants. Los Angeles type of smog (called also photochemical or summer smog) appears due to the formation of ozone through the photochemical reaction of nitrogen oxides and volatile organic compounds emitted from vehicle engines (Seinfeld and Pandis, 1997).

Emission from the transportation, agriculture, and residential sectors is released at low altitudes (low-stack emissions), which makes it difficult to disperse pollutants (Ni et al., 2021). Unfavorable meteorological conditions (lack of wind and precipitation, temperature inversion) as well as terrain conditions (valleys) also hinder natural movements of air masses, causing local

pollution concentrations (Li et al., 2001; Paciorek et al., 2013; Bei et al., 2016; Iwanek et al., 2017; Giemsa et al., 2021). Such weather conditions favor the formation of an inversion layer. Temperature inversion (an increase in temperature with altitude in the troposphere) reduces the vertical air movement–convection and turbulence, which causes long-lasting high PM concentration (Janhäll et al., 2006; Feng et al., 2020). In this article, the term temperature inversion will be used to refer to ground-based inversion as the most common problem in inhabitant areas. This type of inversion occurs in the low troposphere as the result of various processes, including radiation inversion and advection inversion (Zhang et al., 2009). Predicting the possible application of the invention, we distinguish three regimes of smog under the inverse temperature layer: dynamic formation, smog stagnancy, and dynamic decomposition. Counteraction of dynamic formation may be the first solution. The temperature inversion layer can appear in a few situations. It appears mainly at night with no clouds and wind, when the radiative cooling of the ground leads to colder air near the surface level rather than above it. Temperature inversion can also be formed when hotter air masses from higher ground levels move to a valley, thus closing cooler air masses. When emitted pollutants are trapped in the stable air mass below the inverse temperature layer, the concentration of pollutants rapidly increases near the ground (Seinfeld and Pandis, 1997). In this phase, forecasting is crucial. The next solution is to shorten the periods of smog stagnancy. It should be understood as a lack of vertical and horizontal movements of the ambient air. Then the concentration of pollutants increases near the ground due to local emissions. The last stage is dynamic decomposition, when the air mass moves and the inversion layer breaks down within a few hours. Usually, due to Sun radiation, the ground and air start warming and the atmosphere becomes unstable. In this case, we also consider the possibility of speed-up.

Purification methods based on urban forest planting are well known (Hirabayashi, 2021). However, its sorption capacity is inefficient during periods of the highest concentration caused by meteorological conditions. A similar method based on surface sorption consists of using the synthetic SUNSPACE coating. The material can be applied to all city surfaces (for example, walls, roofs, etc.) (Zanoletti et al., 2018). Another type of coating material is airlite paint with purification capacity based on the photocatalytic oxidation effect of titanium dioxide. Its application is similar to that of SUNSPACE (AIRLITE, 2018). These methods are a type of passive measures, dedicated to the global reduction of PM concentrations. However, the efficiency is not very high and the big-scale effect is needed to obtain a noticeable reduction. Therefore, the application is costly, requiring regular replacement of sorption surfaces and regeneration of synthetic materials. Generally, passive methods have no impact on the conditions with the highest concentration.

In contrast, there are a few different systems based on active action, such as an immediate response to smog observation. For example, there are a few types of filtering towers: Airlabs tower, Purevento's filtrators, U-Earth's bioreactors (Zanni and Bonoli, 2014; Cyranoski, 2018; Laxmipriya et al., 2018; Burki, 2019; PURVENTO, 2019). The concept of these solutions is based on two different types of filtering methods: physical sorption on sieves (e.g., HEPA) with an ion generator, or chemical digestion. The only limitation is that towers can treat only small areas within a limited radius (Laxmipriya et al., 2018). There is no scientific evidence for their sufficient efficiency in open urban open spaces with relatively large areas. In reality, vacuum-like solutions could

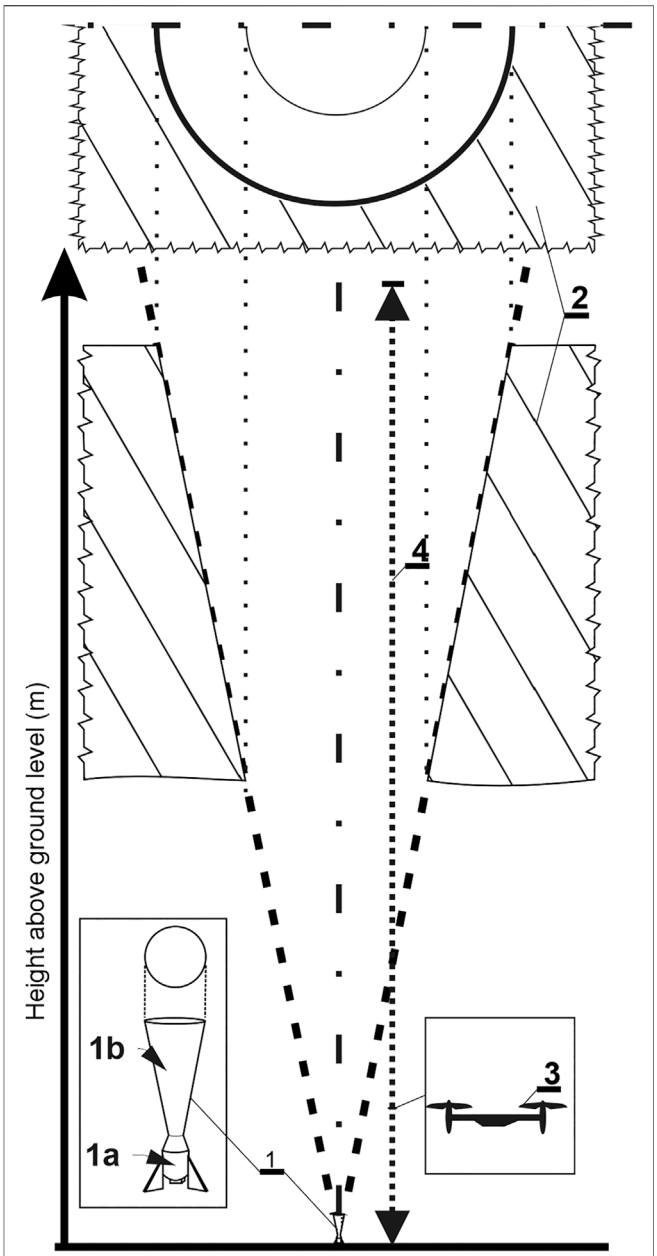

FIGURE 1 | Operational concept of the impact of the invention: 1—shock wave generator, **(A)**–detonation chamber, **(B)**–funnel-shaped barrel, 2–temperature inversion layer, 3–air quality monitoring system.

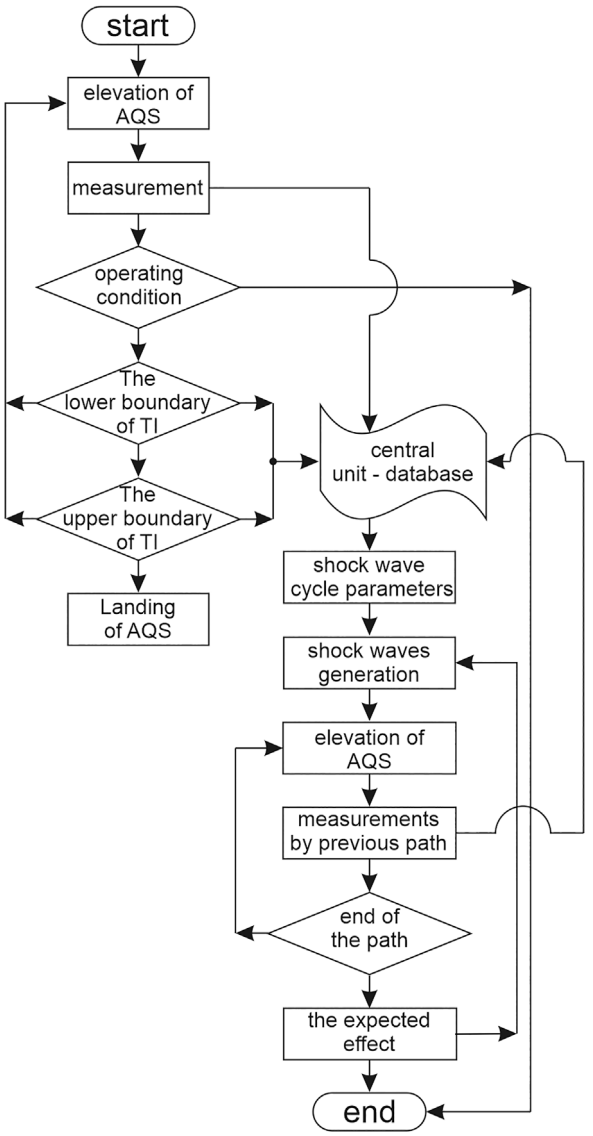

FIGURE 2 | Algorithm of the method of the invention: AQS–air quality monitoring system; TI–temperature inversion layer.

provide only indoor utility to create a smog-free closed zone (Guttikunda and Jawahar, 2020). However, these actions are highly necessary, because outdoor air pollution strongly affects indoor air conditions and exposure (Leung, 2015; Brągoszewska and Biedroń, 2021; Goldstein et al., 2021). Another type of active method involves inducing ventilation of an urban area by a group of ventilation towers placed in rows. It focuses on cooperation between ventilators to reduce the effects of air pollution and smog by generating a continuous airstream with sufficient velocity to aid natural ventilation (Flaga et al., 2019). The authors are considering the installation of ventilation towers of a height exceeding 70 m each. Although the model seems to be effective, its actual use is unrealistic due to the difficulty of its installation in a closed urban development. In addition, it constitutes a permanent interference in the landscape. In conclusion, all recent innovations available on the market are inefficient on a large scale. Solutions that would be applicable to urban areas are still in the conceptual phase and there is no complex technology.

Therefore, we would like to present a completely new approach with a slightly different functionality. The main difference is the expected impact on the inversion layer (a cause of smog) by the generation of a series of shock waves. The method was already tested in a full-scale field test, and this paper summarizes the obtained results. The basis of this technology is the generation of shock waves, which are created by explosions of a mixture of flammable gases and air. The main thesis is that shock waves can destroy the structure of the temperature inversion layer in the atmosphere. This restores vertical movements within the atmosphere that cause a reduction in air pollution at ground level. Hence, the operation of the device enables natural convection processes to disperse the particulate matter.

MATERIALS AND METHODS

The basic concept of operation is presented in **Figure 1**. The system consists of a mobile air quality monitoring system (3), equipped with devices for measuring air temperature, wind speed, and particulate matter concentration; and a shock wave generator 1) with a detonation chamber (1a) and a funnel-shaped barrel (1b). The operation was carried out according to the procedure provided by pending patent no. EU no. EP20217680.6–1001 (Leszczynski et al., 2020).

Figure 2 shows the system operation algorithm. First, air temperature, wind speed, and PM10, PM2.5 concentration are measured using the air quality monitoring system (AQS). Measurements of those measurables occur in the vertical profile by measuring from 0 to the altitude at which the temperature inversion layer is identified. Measurements are made at fixed points 1–20 m apart, preferably 1 m apart. If the average wind speed, calculated from previous measurements, is greater than 0.8 m s^{-1} and/or the temperature drop by every 10 m at altitude is greater than 1.0°C, there are conditions for natural dispersion of smog and the measurement is interrupted. On the other hand, in the case when the wind speed is lower than 0.8 m s^{-1} and/or the temperature drop by 10 m in altitude is lower than 1.0°C, the air quality monitoring system will continue the operation. If the air quality monitoring system records five consecutive measurements for which the concentration of PM10 and/or PM2.5 is greater than 50 μg m^{-3} and/or 25 μg m^{-3}, respectively and the temperature drop at the altitude of 10 m is less than 0.1°C, the studied area is considered as the temperature inversion layer (TI). The lower limit of this temperature inversion layer is the altitude at which the exceedances of the permissible particulate matter concentration values were measured. To determine the upper limit of the inversion layer, the measurements are continued until at least five consecutive measurements of PM10 and/or PM2.5 decrease below the permissible limits and a temperature drop at an altitude of 10 m is greater than 0.1°C. The upper limit of the

TABLE 1 | Specification of sensors.

Features	Specification
DJI MATRICE 200 V2	
Dimensions	883 × 886 × 398 mm
Maximum Take Off Mass	6.14 kg
Hovering accuracy	Vertical ± 0.1 m Horizontal ± 0.3 m
Monitoring System	
Particulate matter sensor (PM2.5; PM10)	Range: 0–4000 μg m^{-3} Resolution: 1 μg m^{-3} Accuracy: ±10%
Temperature	Range: 40–85°C Resolution: 0.1°C Accuracy: ± 0.5°C
Humidity	Range: 0–100 RH Resolution: 0.1% RH Accuracy: ± 2% RH
Pressure	Range: 300–1100 hPa Resolution: 1.6 Pa Accuracy: ± 1% hPa
Altimeter	Range: 0–4000 m Resolution: 0.5 m Accuracy: ± 1 m
Airly PM Sensor	
Particulate matter sensor (PM2.5; PM10)	Range: 0–1000 μg m^{-3} Accuracy ±10 μg m^{-3} (<100 μg m^{-3}) ±10% (>100 μg m^{-3})

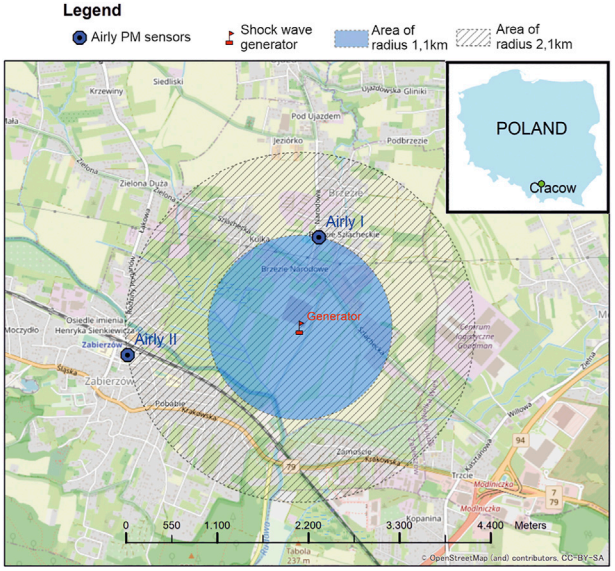

FIGURE 3 | The place of operations. The area of possible impact of the invention: blue label–certain; cross-hatch label–uncertain.

inversion layer is the last altitude at which the measurement showed exceeded the concentration values of PM2.5 and PM10. Based on these measurements, the height and thickness of the temperature inversion layer are determined, and the power, frequency, and duration of the shock wave cycle are calculated. Then, a series of shock waves are generated by inserting a fuel-air mixture into the detonation chamber in the shock wave generator. After the generated shock wave cycle, the concentration of particulate matter concentration is measured at a distance of 10–20 m from the shot axis using the air quality monitoring system. To check the effects of the generated shock wave cycle, the arithmetic mean is calculated from the concentration measurements taken from 0 m to the level of the upper inversion layer, before and after the shock wave generation cycle. If the average concentration of PM2.5 and PM10 decreased by 15%, the action is suspended for at least 1–4 h. If it was less than 15%, the shock wave generation cycle is repeated immediately.

The experiments were carried out in an open environment of Zabierzów municipality, located in the suburbs of Kraków–southern Poland. The test site was a partially built-up area. On one side there was a cultivated field and on the other there was a dense development of detached houses. The initial test 1 was conducted on November 25, 2019. The monitoring system consisted of a drone equipped with an altimeter, temperature, and pressure sensor, and a laser-type sensor to measure the concentration of particulate matter (PM10, PM2.5). The integrated system was made by Flytronic S.A, model: Nosacz 2 was mounted on a DJI MATRICE 200 drone. The full specification is presented in **Table 1**. The measurement with the monitoring system was performed in the vertical profile, where the recorded data was continuously transmitted by radio to the recorder. The results were averaged for every 5 m of altitude. The test started with the first vertical measurement. Then the drone was brought to the ground and then the generator system began to operate. The shock wave generator system was an acetylene-fed anti-hail gun with a detonation chamber with an approximate volume of 0.205 m^3. The detonation lasted 11 min in cycles of 10 s (there were 66 explosions in total). After the shock wave generation cycle, PM10 and PM2.5 were measured along an altitude of 0–100 m, at a distance of 10 m from the generator. During the second test, the detonation cycle lasted 29 min with about 174 explosions. Additional data was collected from two Airly PM stations, distanced from anit hail canon at 1.109 and 2.108 km, respectively, and installed near ground level. The Airly sensor specification is described in **Table 1**. The location of the test is presented in **Figure 3**.

RESULTS AND DISCUSSION

To identify the scale of the application, a data set from the Polish Environmental Protection Inspectorate was analysed. In Krakow, the average height of temperature inversion for most of the year is approximately 300 m, while in summer it is approximately 250 m (Godłowska, 2019). The analysis conducted in 1961 showed that the annual number of days when the inversion of temperature was reported to be in the range of 96–175 (Palarz, 2014). Due to the high emission of pollutants, unfavorable meteorological and terrain conditions, the air quality in Kraków and the surrounding towns is bad, especially in winter (Bokwa, 2011; Godłowska, 2019). The

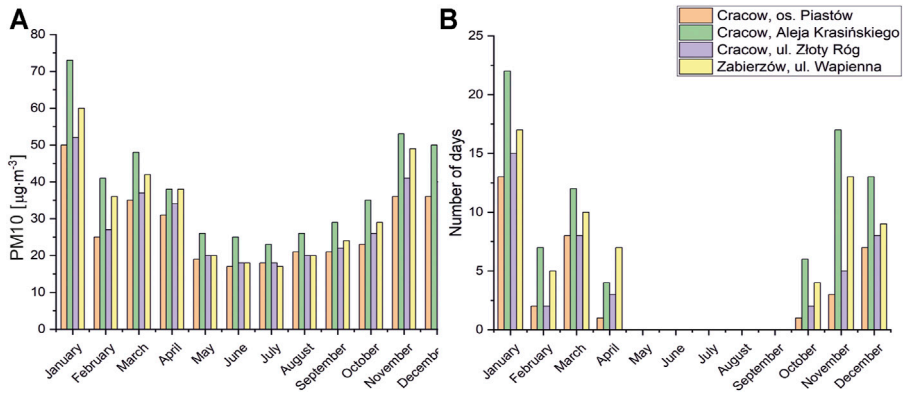

FIGURE 4 | Data set of selected stations in 2020: **(A)** Monthly average concentration of PM10 **(B)** Number of days when the PM10 concentration exceeded 50 µg m^{-3} (Inspectorate for Environmental Protection, 2020).

TABLE 2 | Atmospheric condition before operation.

Test (date)	PM10 µg m^{-3}	PM25 µg m^{-3}	Temp. (°C)	RH %	Avg. Wind m s^{-1}	Pressure hPa
TEST 1 (November 25, 2019)	81.6	41.1	1.7	97	0.4	986.4
TEST 2 (February 19, 2021)	84.8	59.8	2.2	98	0.5	992.6

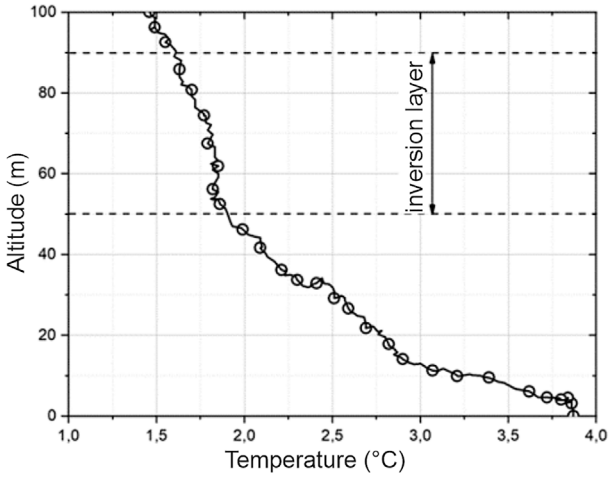

FIGURE 5 | Temperature distribution in the vertical profile, including the determined region of an inversion layer.

monthly average concentration of PM10 1) and the number of days when the concentration of PM10 was greater than 50 µg m^{-3} 2) in 2020 in selected stations located in Kraków and Zabierzów are presented in **Figure 4** (Inspectorate for Environmental Protection, 2020). According to the presented historical data, on average there were 56 days with a high concentration of PM in the studied area. The test location was settled in Zabierzów as the second most polluted region. The Aleje Krasińskiego was unfavorable due to the high-density housing.

The atmospheric conditions before the operation are described in **Table 2**, which shows the data at the ground level during both tests. According to **Table 2**, it can be seen that the PM concentrations were above the limits. In the EU, the annual average concentration of PM10 should not exceed 40 µg m^{-3} and should be no more than 35 days with a PM10 concentration greater than 50 µg m^{-3}. The average annual concentration of PM2.5 should not exceed 25 µg m^{-3}. In addition, the air had constant conditions (high humidity, low wind speed).

In Test 1, the temperature profile was also examined. **Figure 5** shows the temperature distribution in the vertical profile during the first measurement, before the shock generation was started. The aim of measuring the temperature was to show the presence of the inversion layer, an operational condition of the method. The inversion layer is connected with the inverted distribution of the temperature profile but also with the constant temperature in the profile. Both conditions lead to the disappearance of natural convection (Yasmeen, 2011). The presence of a temperature inversion is a fundamental condition for the operation of the invention, the main purpose of which is to restore natural convection in the atmosphere. The temperature inversion layer was observed during the test 1 operation from an altitude of 50–90 m, where the decrease was below the setup value (0.1°C/10 m). This is a typical ground inversion resulting from the ground cooling overnight.

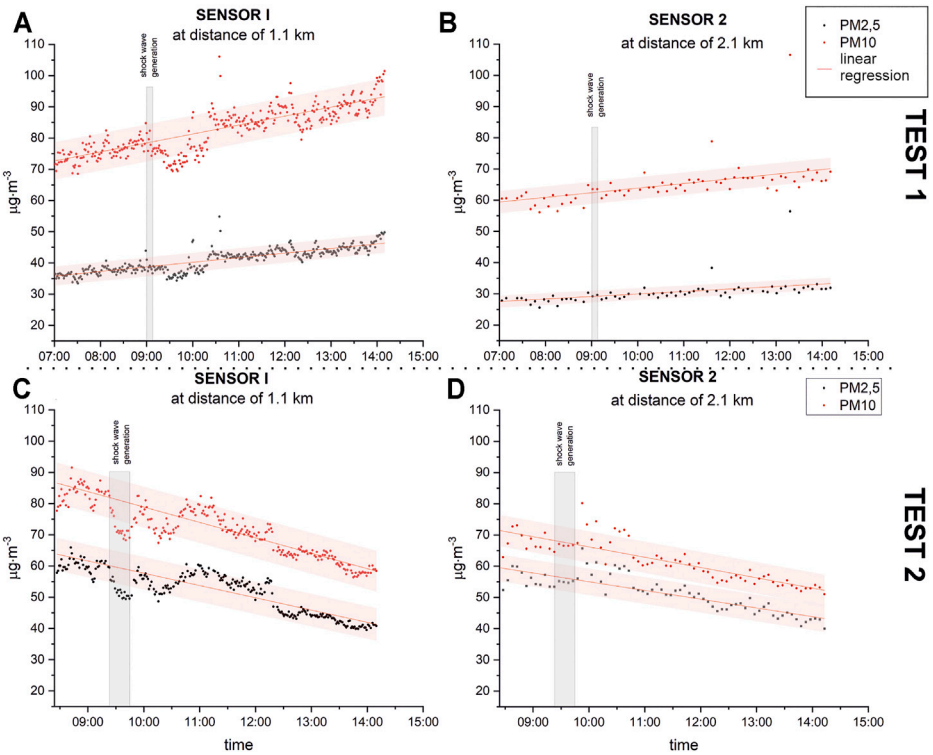

FIGURE 6 | Concentration of PM10 and PM2.5 in Airly sensors in adjacent areas during the initial test: **(A)** sensor 1 (test 1), distanced by 1.1 km; **(B)** sensor 2 (test 1) distanced by 2.1 km; **(C)** sensor 1 (test 2); **(D)** sensor 2 (test 2).

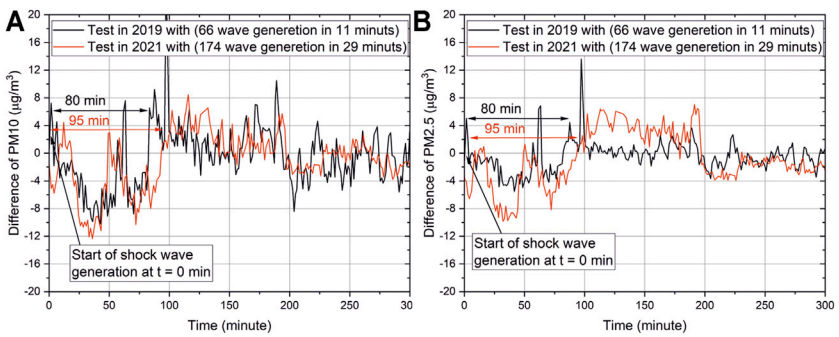

FIGURE 7 | The difference between the concentration and the linear approximation for: **(A)** PM_{10} and **(B)** $PM_{2.5}$.

To indicate a wider impact on air movement, the existing air monitoring system was used. **Figure 6** shows the variability of PM10 and PM2.5 concentrations during both tests performed. In the figure, the linear regression is marked, as well as an area of standard deviation, as a measure of variation. The results of test 1 (**Figures 6A,B**) and test 2 (**Figures 6C,D**) showed the following correlations. Sensor 2, located 2.1 km away, did not detect the impact of the shock wave in both tests. The readings did not exceed the area of standard deviation. Another correlation was detected with sensor 1, where the concentration values of all PM clearly exceeded the border of the standard deviation areas. The effect was observed to be greater for particles of larger diameter (PM10). It shows a region affected by the invention operations, which is larger than the area of 1.1 km in diameter and less than 2.1 km in diameter. It was assumed that the impact was the same in each direction from the generator. The area of possible impact is indicated in **Figure 3** by the blue region. These correlations were confirmed by performing test 2 under similar conditions.

To show the effectiveness of the interaction on a time scale, the variability of the concentration on the Airly PM sensors is

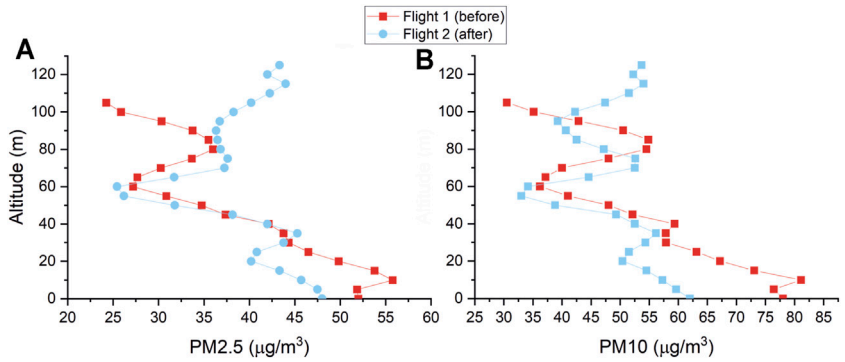

FIGURE 8 | Concentration graph (test 1) before and after shock wave generation: **(A)** PM10 and **(B)** PM2.5.

presented in **Figure 7**. The **Figures 7A,B** shows the difference between the measured concentration of PM10 and PM2.5 and a linear regression of them shown in **Figure 6**. In the linear regression of the concentration of PM10 and PM2.5, it was not include the period when the shock waves generator was operating. In Test 1, the generation of 66 shock waves for 10 min resulted in a maximum reduction in PM10 concentration by 10 μg/m^3 and in PM2.5 by approximately 5 μg/m^3. The lower concentration of PM10 and PM2.5 values persisted for 80 min, during which time we can consider the atmosphere to be less stable. After this time, the dynamics of changes in PM10 and PM2.5 concentration returned to the upward trend. In the case of the second test in 2021, the number of generated shock waves was almost tripled. This resulted in a greater reduction in PM10 and PM2.5 concentrations by 12 and 10 μg/m^3, respectively, and extended time of reduced PM10 and PM2.5 concentration to approximately 95 min after using the shock waves generator. After this time, the dynamics of the concentration changes returned to the previous trend. Therefore, with an increase in the duration of shock wave generation, the impact on PM10 and PM2.5 concentration was more noticeable in the longer term. Considering the atmosphere as a semi-equilibrum state, there is a visible tendency to return to the previous condition. However, it is possible to predict that a change in equilibrium will occur during the prolonged operation. The atmosphere is constantly changing to new equilibrium states by various factors. In case of a sufficiently long execution of the explosion, in relation to global changes, a new semi-equilibrium should be found under completely different conditions. This is a fundamental area that needs to be explored further.

The concentration of the PM10 and PM2.5 fractions is shown in **Figure 8**. It shows the distribution of both fractions during flight 1 and flight 2, which accordingly represents the condition before and 10 min after the shock wave generation. The analysis demonstrated the appearance of a lift force that impacts the particulate matter. At ground level, PM concentrations decreased; an increase in level was observed above 80 m. The average concentration of PM10 up to 20 m decreased by 24%, from 75.2 μg m^{-3}–56.8 μg m^{-3}. PM2.5 particles were less affected by air flow. The average concentration of PM2.5 up to 20 m decreased by 15%, from 52.6 μg m^{-3}–44.9 μg m^{-3}.

CONCLUSION

The air purification system has been shown to affect a larger area. The impact on PM concentration in air was observed at a distance of 1.1 km. This means that the effect could be perceived on an area of at least 4 km^2. We have obtained satisfactory results that demonstrate long-range impact in two independent seasons.

What is striking here is the significant impact during a short action. A reduction in PM10 and PM2.5 concentrations was observed in the short-range observation. The greatest impact was observed for PM10 particles; the average concentration near the ground was reduced by 24%. However, other particle concentrations of smaller diameter were also reduced.

The potential of the invention for destruction of the inversion layer was recognized along with the possibility of reducing the period of stagnation of the atmosphere. Therefore, the method can be used in highly urbanized areas with significant low stack emissions, where there are natural conditions for the presence of smog due to the formation of an inversion layer (basin, river valleys).

The method according to the invention does not require significant investment in infrastructure. The shock wave generator can be mounted on a vehicle and moved anywhere. It eliminates passive waiting for a change in atmospheric conditions, which will reduce the level of PM level in the area under the inversion layer. These results provide a significant first step towards the brand-new method of air purification.

For the purposes of the presented tests of the invention, the authors wished to demonstrate only effects on the basis of the initial and final parameters. This study provides the basis for a new method of air purification. Future research is needed to assess the potential of the scaling effect to achieve complete purification of a larger area.

DATA AVAILABILITY STATEMENT

The raw data supporting the conclusion of this article will be made available by the authors, without undue reservation.

AUTHOR CONTRIBUTIONS

All authors were engaged in obtaining data from both tests. FJ, DG, and JZ analyzed the data. FJ, DG, and JZ wrote the paper. JL, KS, MS, BK, and WS provided substantive comments, corrections and valuable suggestions for improving the manuscript.

FUNDING

This work was partially supported by the research subvention supported by the Polish Ministry of Education and Science grant number 16.16.210.476 and as part of the research project untitled "Development of an intervention system to reduce particulate matter concentration in the air" as part of the Innovation Incubation 4.0 project, application no. MNiSW/2020/316/DIR.

ACKNOWLEDGMENTS

The authors gratefully acknowledge use of the data from Airly Inc. Air monitoring system.

SUPPLEMENTARY MATERIAL

The Supplementary Material for this article can be found online at: https://www.frontiersin.org/articles/10.3389/fenvs.2021.784477/full#supplementary-material

REFERENCES

AIRLITE (2018). *AIRLITE*. United Kingdom: European Commision.

Bei, N., Xiao, B., Meng, N., and Feng, T. (2016). Critical Role of Meteorological Conditions in a Persistent Haze Episode in the Guanzhong Basin, China. *Sci. Total Environ.* 550, 273–284. doi:10.1016/j.scitotenv.2015.12.159

Bokwa, A. (2011). Influence of Air Temperature Inversions on the Air Pollution Dispersion Conditions in Krakow. *Prace Geograficzne* 126, 4219.

Brągoszewska, E., and Biedroń, I. (2021). Efficiency of Air Purifiers at Removing Air Pollutants in Educational Facilities: A Preliminary Study. *Front. Environ. Sci.* 9, 370. doi:10.3389/fenvs.2021.709718

Burki, T. K. (2019). The Innovations Cleaning Our Air. *Lancet Respir. Med.* 7 (2), 111–112. doi:10.1016/S2213-2600(19)30002-5

Cyranoski, D. (2018). China Tests Giant Air Cleaner to Combat Smog. *Nature* 555 (7695), 152–153. doi:10.1038/d41586-018-02704-9

[Dataset] Inspectorate for Environmental Protection (2020). Air Quality - Measurement Data Bank. Available at: https://powietrze.gios.gov.pl/pjp/archives (Accessed on: November 24, 2021).

Feng, X., Wei, S., and Wang, S. (2020). Temperature Inversions in the Atmospheric Boundary Layer and Lower Troposphere Over the Sichuan Basin, China: Climatology and Impacts on Air Pollution. *Sci. Total Environ.* 726, 138579. doi:10.1016/j.scitotenv.2020.138579

Flaga, Ł., Pistol, A., Pistol, A., Krajewski, P., and Flaga, A. (2019). Model Tests of Dynamic Action on the Atmospheric Boundary Layer - Linear Configuration of Ventilation Towers on a Rough Terrain. *Czasopismo Techniczne* 7, 63–79. doi:10.4467/2353737xct.19.072.10723

Giemsa, E., Soentgen, J., Kusch, T., Beck, C., Münkel, C., Cyrys, J., et al. (2021). Influence of Local Sources and Meteorological Parameters on the Spatial and Temporal Distribution of Ultrafine Particles in Augsburg, Germany. *Front. Environ. Sci.* 8, 280. doi:10.3389/fenvs.2020.609846

Godłowska, J. (2019). *Influence of Meteorological Conditions on Air Quality in Krakow. Comparative Research and an Attempt at a Model Approach*. Kraków, Poland: Institute of Meteorology and Water Management National Research Institute.

Goldstein, A. H., Nazaroff, W. W., Weschler, C. J., and Williams, J. (2021). How Do Indoor Environments Affect Air Pollution Exposure? *Environ. Sci. Technol.* 55 (1), 100–108. doi:10.1021/acs.est.0c05727

Guttikunda, S., and Jawahar, P. (2020). Can We Vacuum Our Air Pollution Problem Using Smog Towers? *Atmosphere* 11 (9), 922. doi:10.3390/atmos11090922

Hirabayashi, S. (2021). Technical Specifications of Urban Forests for Air Purification: A Case Study in Tokyo, Japan. *Trees, Forests and People* 4, 100078. doi:10.1016/j.tfp.2021.100078

Iwanek, J. S., Kamiński, J., Durka, P., Kobus, D., Kostrzewa, J., and Pecka, T. (2017). *Analysis of Selected Episodes of High Concentrations of PM10 from the Years 2013-2016*. Warsaw, Poland: Chief Inspectorate of Environmental Protection.

Janhäll, S., Olofson, K., Andersson, P., Pettersson, J., and Hallquist, M. (2006). Evolution of the Urban Aerosol during winter Temperature Inversion Episodes. *Atmos. Environ.* 40 (28), 5355–5366. doi:10.1016/j.atmosenv.2006.04.051

Laxmipriya, S., Kumar, A. A., Aravinthan, S., and Arunachalam, N. (2018). Reduction of Air Pollution Using Smog-Free-Tower a Review Paper. *IRJAET* 4, 3251–3255.

Leszczynski, J. K. B., Suwała, W., Stobiński, M., Szarłowicz, K., Zyśk, J., Jędrzejek, F., et al. (2020). *The Method of Reducing Dust Accumulation in the Smog Layer, Which Is the Inversion Layer*. Munich, Germany: European Patent Office, EP20217680.

Leung, D. Y. C. (2015). Outdoor-indoor Air Pollution in Urban Environment: Challenges and Opportunity. *Front. Environ. Sci.* 2, 69. doi:10.3389/fenvs.2014.00069

Li, W.-W., Orquiz, R., Garcia, J. H., Espino, T. T., Pingitore, N. E., Gardea-Torresdey, J., et al. (2001). Analysis of Temporal and Spatial Dichotomous PM Air Samples in the El Paso-Cd. Juarez Air Quality Basin. *J. Air Waste Manage. Assoc.* 51 (11), 1551–1560. doi:10.1080/10473289.2001.10464377

Ni, H., Huang, R.-J., Pieber, S. M., Corbin, J. C., Stefenelli, G., Pospisilova, V., et al. (2021). Brown Carbon in Primary and Aged Coal Combustion Emission. *Environ. Sci. Technol.* 55 (9), 5701–5710. doi:10.1021/acs.est.0c08084

[Online] PURVENTO (2019). Fresh Air for Kiel: City of Kiel and Purevento GmbH to Start Test Phase with City Air Purifier at Theodor-Heuss-Ring. Trittau, Germany: Kiel. February 6, 2019. Available at: https://www.purevento.com/wp-content/uploads/2019/02/Purevento_Kiel-tests-the-city-air-cleaner-pressinformation-EN.pdf (Accessed on: November 24, 2021).

Paciorek, M. K. E., Klejnowski, K., Ośródka, L., Hajto, M., Szeflińska, K., Wojtylak, M., et al. (2013). *Analysis of Selected Episodes of High PM10 Concentrations Based on Measurement and Meteorological Data and Trajectory Analysis*. Warsaw, Poland: Chief Inspectorate of Environmental Protection.

Palarz, A. (2014). Zmienność Inwersji Temperatury Powietrza Nad Krakowem W Świetle Warunków Cyrkulacyjnych. *Prace Geograficzne* 138, 29–43. doi:10.4467/20833113PG.14.016.2698

Seinfeld, J. H., and Pandis, S. N. (1997). *Atmospheric Chemistry and Physics : From Air Pollution to Climate Change*. New York: Wiley-Interscience.

Sinha, J., and Kumar, N. (2019). Mortality and Air Pollution Effects of Air Quality Interventions in Delhi and Beijing. *Front. Environ. Sci.* 7, 15. doi:10.3389/fenvs.2019.00015

van Donkelaar, A., Martin, R. V., Brauer, M., Hsu, N. C., Kahn, R. A., Levy, R. C., et al. (2016). Global Estimates of Fine Particulate Matter Using a Combined Geophysical-Statistical Method with Information from Satellites, Models, and Monitors. *Environ. Sci. Technol.* 50 (7), 3762–3772. doi:10.1021/acs.est.5b05833

WHO Observatory (2018). *Mortality from Household Air Pollution*. Luxembourg, Luxembourg: World Health Organization.

Yasmeen, Z. (2011). Inversion Layer and its Environmental Impact over Karachi. *Pakistan J. Meteorology* 7, 1–10.

Zanni, S., and Bonoli, A. (2014). Indoor Air Quality in Waste Treatment: Environmental Issue and Biotechnology Application for Air Pollution Containment, a Case Study. *WSEAS Trans. Environ. Develop.* 10, 529–541.

Zanoletti, A., Bilo, F., Borgese, L., Depero, L. E., Fahimi, A., Ponti, J., et al. (2018). SUNSPACE, A Porous Material to Reduce Air Particulate Matter (PM). *Front. Chem.* 6, 534. doi:10.3389/fchem.2018.00534

Zhang, Y. H., Zhang, S. D., and Yi, F. (2009). Intensive Radiosonde Observations of Lower Tropospheric Inversion Layers over Yichang, China. *J. Atmos. Solar-Terrestrial Phys.* 71 (1), 180–190. doi:10.1016/j.jastp.2008.10.008

Conflict of Interest: The authors declare that the research was conducted in the absence of any commercial or financial relationships that could be construed as a potential conflict of interest.

Publisher's Note: All claims expressed in this article are solely those of the authors and do not necessarily represent those of their affiliated organizations, or those of the publisher, the editors and the reviewers. Any product that may be evaluated in this article, or claim that may be made by its manufacturer, is not guaranteed or endorsed by the publisher.

frontiers in Environmental Science

REVIEW
published: 20 December 2021
doi: 10.3389/fenvs.2021.756404

The Key Factors for the Fate and Transport of Petroleum Hydrocarbons in Soil With Related *in/ex Situ* Measurement Methods: An Overview

Liang Wang[1,2]*, *Ying Cheng*[1,2], *Ravi Naidu*[1,2] and *Mark Bowman*[3]

[1]Global Centre for Environmental Remediation, College of Engineering, Science and Environment, University of Newcastle, Callaghan, NSW, Australia, [2]CRC for Contamination Assessment and Remediation of Environment, University of Newcastle, Callaghan, NSW, Australia, [3]The Department of Defence, Canberra, ATC, Australia

Once petroleum hydrocarbons (PHs) are released into the soil, the interaction between PHs and soil media is dependent not only upon the soil properties but also on the characteristics of PHs. In this study, the key factors influencing the interactions between PHs and soil media are discussed. The key factors include: 1) the characteristics of PHs, such as volatility and viscosity; and 2) soil properties, such as porosity, hydraulic properties and water status, and organic matter; and 3) atmospheric circumstances, such as humidity and temperature. These key factors can be measured either *ex-situ* using conventional laboratory methods, or *in situ* using portable or handheld instruments. This study overviews the current *ex/in situ* techniques for measuring the listed key factors for PH contaminated site assessments. It is a tendency to apply *in situ* methods for PH contaminated site characterisation. Furthermore, handheld/portable Fourier transform infrared spectroscopy (FTIR) instrument provides tremendous opportunities for in-field PH contaminated site assessment. This study also reviewed the non-destructive FTIR spectroscopy analysis coupling with handheld FTIR for in-field PH contaminated site characterisation, including determining the concentration of total PH, dominant PH fractions and soil key properties for PH transport modelling.

Keywords: petroleum hydrocarbons, contaminated site characterisation, soil properties, *in/ex-situ* measurements, handheld fourier transform infrared spectroscopy

OPEN ACCESS

Edited by:
Anabela Cachada,
University of Porto, Portugal

Reviewed by:
Veerasingam S.,
Qatar University, Qatar
Oliver Mullins,
Schlumberger, United States
Kaveh Sookhak Lari,
Commonwealth Scientific and Industrial Research Organisation (CSIRO), Australia

***Correspondence:**
Liang Wang
Liang.Wang@newcastle.edu.au

Specialty section:
This article was submitted to Toxicology, Pollution and the Environment, a section of the journal Frontiers in Environmental Science

Received: *10 August 2021*
Accepted: *23 November 2021*
Published: *20 December 2021*

Citation:
Wang L, Cheng Y, Naidu R and Bowman M (2021) The Key Factors for the Fate and Transport of Petroleum Hydrocarbons in Soil With Related in/ex Situ Measurement Methods: An Overview. Front. Environ. Sci. 9:756404. doi: 10.3389/fenvs.2021.756404

INTRODUCTION

Highly sophisticated and varied mixtures of hydrocarbons form the majority of the components in petroleum products (Irwin et al., 1998; Weisman, 1998). Soil is a porous material and a highly reactive adsorbent. When an oil spill or leak occurs on soil, physical, chemical, and biological processes alter the composition, toxicity, and distribution of petroleum hydrocarbons (PHs) within the soil ecosystem, known as weathering processes (Brassington et al., 2007; Ayoubi et al., 2020; Ayoubi et al., 2021). The sequestration and distribution mechanisms of PHs within soil include adsorption, volatilization, transportation and transformation (Yong et al., 1992). Adsorbed PHs, including volatiles and oil or light non-aqueous phase liquid (LNAPL), undergo natural attenuation processes, including biodegradation by the intrinsic soil microbial community. Mullins and the team developed multicomponent diffusion models based on field data and column studies to simulate both oil and gas charges and degradation in soil, which are simple and provide excellent guidance to

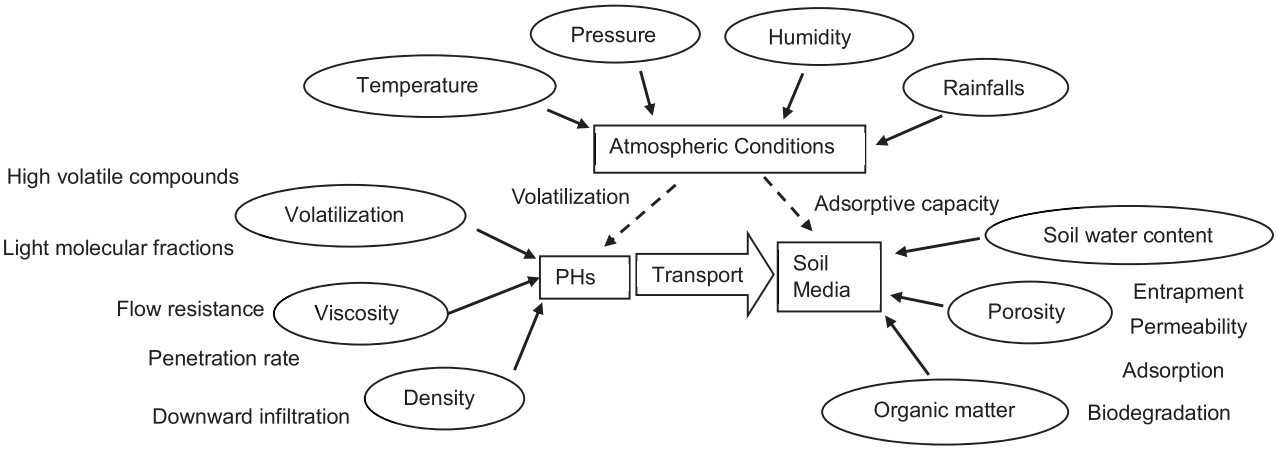

FIGURE 1 | The key factors influencing the interaction between PHs and soil media.

diffusion over geologic time (Zuo et al., 2015; Pan et al., 2016). Many studies have focused on the impacts on the soil ecosystem when oil pollution occurs (Uzoije and Agunwamba, 2011; Nudelman et al., 2002; Everett, 1978; Mercer and Cohen, 1990; Williams et al., 2002-2003; Barakat et al., 2001). PH pollution impacts both the chemical and physical properties of soil. Physical impacts include clumping soil particles into plaques, decreasing porosity, enhancing resistance to penetration, and increasing hydrophobicity (Uzoije and Agunwamba, 2011). Chemical impacts include boosting soil organic matter by creating anaerobic conditions that eliminate most aerobic microorganisms and reducing cation exchange capacity (Pan et al., 2016). (Everett, 1978; Nudelman et al., 2002).

The hydraulic and physical characteristics of the soil, as well as its water condition, influence multiphase sequestration and PH distribution in porous soil medium. The capacity of soils to filter, retain or release PHs is fundamental to understanding environmental contamination and remediation. In the 1990s, Mercer and Cohen reviewed the properties, models, characterisation and remediation of LNAPLs in subsurface soils (Mercer and Cohen, 1990). Yong et al. described the principles of the fate and transport of LNAPLs in soil media (Yong et al., 1992). Fine et al. evaluated and highlighted the key implications of soil components on the fate of petroleum products in soils, such as hydrocarbon retention, volatilization, and transport, as influenced by soil physical and chemical characteristics (Fine et al., 1997). More recently, Williams et al. (Williams et al., 2002-2003), investigated the fate and transport of PHs in soil and groundwater at contaminated sites in the U.S. According to Williams et al., once PHs are released into the soil, the interaction between PHs and soil media is dependent not only upon the soil properties but also on the characteristics of PHs (Williams et al., 2002-2003). Barakat et al. (2001), investigated compositional changes of naturally weathered oil residues in an arid terrestrial environment. Several aromatic PH compounds with varied ratios were found to be stable in oil residues throughout a wide range of weathering and hydrocarbon concentrations, according to their findings (Barakat et al., 2001).

Brassington et al. (2007), reviewed the key factors influencing the interactions between PHs and soil media for site characterisation, risk assessment and bioremediation of weathered hydrocarbons.

These key factors, summarized in **Figure 1**, include: 1) the characteristics of PHs, such as volatility and viscosity; and 2) soil properties, such as porosity, hydraulic properties and water status, and organic matter; and 3) atmospheric circumstances, such as humidity and temperature. These key factors can be measured either *ex-situ* using conventional laboratory methods, or *in situ* using portable or handheld instruments. The *ex-situ* methods are often traditional laboratory-based. Albeit with a large volume of soil samples, labour intensive and time-consuming, the conventional laboratory methods can provide higher accuracies and lower detection limits. On the opposite, in the field, portable instrument methods offer rapid results and better coverage, which could satisfy the requirements of locating hotspots (Rostron et al., 2014). It is a tendency to apply *in situ* methods for PH contaminated site characterisation. This study reviews the current *ex/in situ* techniques for measuring the listed key factors for PH contaminated site assessments.

Fourier transform infrared spectroscopy (FTIR) has been widely applied for quantifying the total amount of PH in contaminated soil, and soil property analysis (Czarnecki and Ozaki, 1996a; Kebbekus and Mitra, 1998; Bradley, 2007; Griffiths and De Haseth, 2007) (Soriano-Disla et al., 2014). Thanks to the recent development of handheld FTIR, it is possible to determine PH and soil properties rapidly in the field. In previous studies, handheld FTIR was applied to quantify total PH (TPH) and classify dominated PH fractions for contaminated site assessment (Wang et al., 2019). Furthermore, soil properties were also studied using handheld FTIR to provide inputs for soil contamination transport models for site assessment (Wang et al., 2020). This study also critically reviewed the non-destructive FTIR spectroscopy analysis for in-field PH contaminated site characterisation.

PH CHARACTERISATION

Volatilization and Solubility

Volatilization is dominant in the loss of low molecular weight aliphatics and is the most substantial change in petroleum. Evaporation of PHs will result in the enrichment of high molecular weight, low volatile components in the residual hydrocarbon mixture (Fine et al., 1997). Volatilization is the process by which a compound evaporates in the vapour phase to the atmosphere (Yong et al., 1992). It is an important mechanism responsible for the loss of PHs from the soil to the air. Raoult's and Henry's laws can be applied to estimate the rate of Volatilization of a hydrocarbon compound from soil to air. More volatile compounds penetrate more rapidly from porous media than less volatile molecules. Volatilization losses are also dependent on many factors, such as soil properties, chemical properties and environmental conditions (Fine et al., 1997). The primary properties of a chemical controlling it's volatilization are its vapour pressure and solubility in water. For example, the penetration of PHs increases with vapour pressure (Fine et al., 1997; Irwin et al., 1998). There is less than 5% of PHs will dissolve in water (Fine et al., 1997). Aromatic hydrocarbons, particularly BTEX (benzene, toluene, ethylbenzene, and xylenes), are the most water-soluble fraction of crude oil and other petroleum compounds, and because of their high toxicity and mobility in comparison to other petroleum hydrocarbons, they are frequently the main groundwater contaminant of concern at petroleum release sites (Williams et al., 2002-2003). The interaction of crude oil and reservoir aquifers has been mapped through the BTEX and other alkyl-aromatic compounds (Forsythe et al., 2017; Forsythe et al., 2019). In particular, the loss of alkylbenzenes, alkyl-naphthalenes and alkyl-phenanthrenes have been measured in crude oils as a metric of water washing. A series of related reservoirs have been shown to be water-washed sequentially, mild, moderate and severe based on the extent of water washing. Moreover, the loss of compounds from the crude oils was shown to tightly correlate to their water solubility (Forsythe et al., 2017; Forsythe et al., 2019). It is worth noting that soil adsorption reduces the activity of PHs by affecting vapour density and the subsequent volatilization rate. Further, the vapour density is also inversely related to the soil texture, moisture and organic matter contents in soil (Guenzi and Bear, 1974).

Viscosity and Density

The dispersal of PHs from surface spills is controlled by its density and viscosity. Viscosity can be described as a fluid's resistance to flow. The higher a fluid's thickness, the more resistive it is to flow. Increases in the viscosity of LNAPLs are accompanied by an increase in heavy fractions, which reduces the preferential volatilization of light fractions. The hydrocarbon vapour penetrates around two to three times faster than LNAPLs (Fine et al., 1997). Hence, during LNAPL infiltration into fine soils, the intrinsic infiltration rate is decreased with increases in viscosity. The erosion of polluted soils is often accompanied by the transfer of very viscous PHs. The viscosity ratio (oil to water) increases when the temp decreases, changing the fractional flow of water and oil and also the intrinsic soil permeability (Torabzadeh and Handy, 1984). Temperature and thus density are essentially constant in most underground habitats, and some researchers claim that

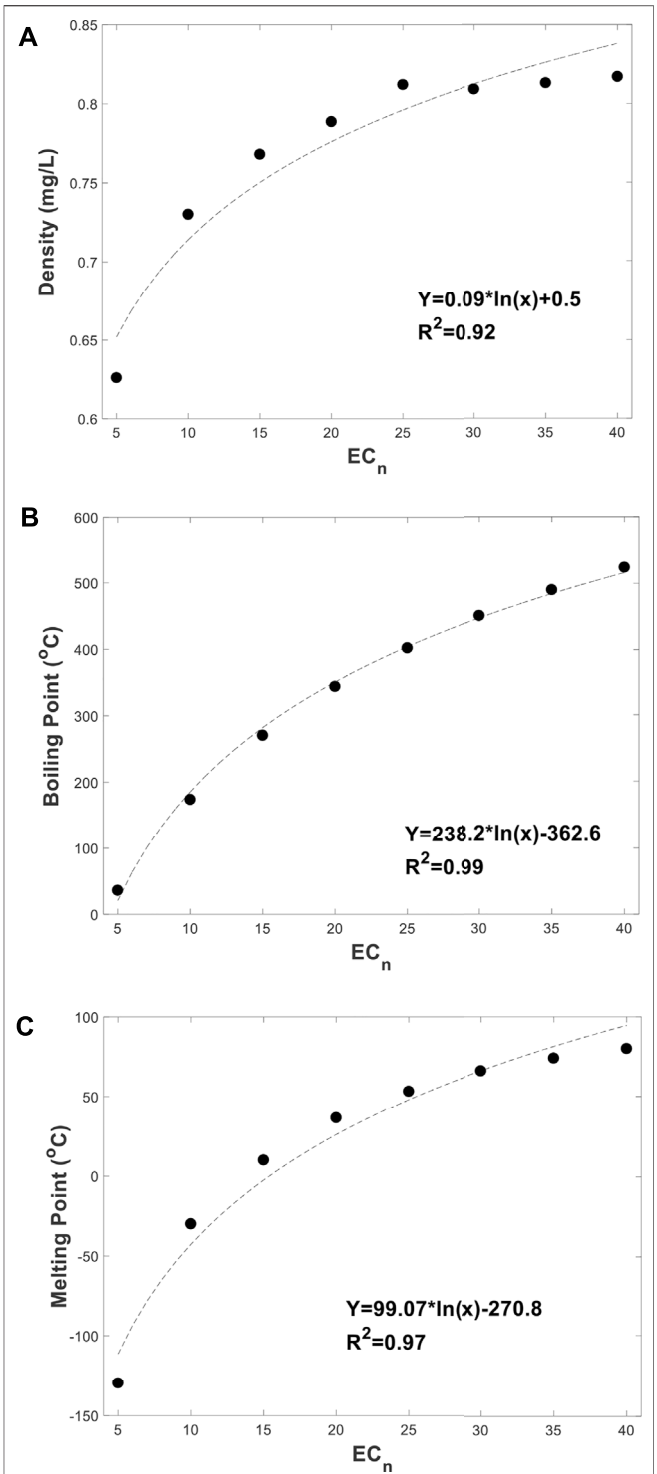

FIGURE 2 | (A) The relationships between the C_n and their density. **(B)** The relationships between the C_n and their boiling point. **(C)** The relationships between the Cn and their melting point.

viscosity does not affect relative permeability (Sandberg et al., 1958; Odeh, 1959). It is worth mentioning the heaviest components in PH, asphaltenes, are normally nanocolloidally suspended in crude oil and impart the viscosity. The molecular structure and other properties have been studied and reported (Schuler et al., 2015; Schuler et al., 2017).

The density of a substance is defined as its mass per unit volume, and it is an important component determining the vertical infiltration of fluids in soil by gravity (Torabzadeh and Handy, 1984). The density of LNAPLs is also vital for controlling the mobility, or the rate at which LNAPLs are transported in soil (Keller and Simmons, 2005). Density is affected by several factors, the most important of which is temperature. Knowing the density of petroleum spilt at a place is critical since it is used to estimate the volume of petroleum leaked. The density of LNAPLs can be presented as American Petroleum Institute (API) gravity, which is an inverse measure of the density relative to water, using a hydrometer, which is a sealed hollow glass tube with a larger bottom that is used to measure liquid densities using buoyancy.

Equivalent Carbon Numbers (C_n)

To represent PH fractions, equivalent carbon numbers (Cn) are used, with Cn values based on a variety of physical-chemical properties and simple partitioning models (otal Petroleum Hyd, 1005). In general, small linear PHs is in the gas phase while medium-sized linear PHs is LNAPL. The chains under C_7, known as naphthas, are relatively light and quickly vaporised, and are commonly used as dry-cleaning solvents. For petrol, which is more volatile than water, the chains from C_7 to C_{11} are commonly mixed and employed. Kerosene is next, from C_{12} to C_{15}, followed by diesel and other heavier fuel oils, from C_{12} to C_{30}. Branched PHs of intermediate size tend to be waxed with low melting points (Bray et al., 2020). Carbon chains in lubricating oils, such as engine and motor oils, ranging from C_{25} to C_{40}. Long PHs ($>C_{50}$) tend to be a solid phase, such as tars. Chemical structure, carbon number, and structure-activity connections are used to determine PH fractions (Interim Final Petroleum R, 1994). Heavier fractions of PHs are those with a greater Cn, or carbon chains that are longer. Higher viscosity, density, boiling temperatures, and longer residence durations in soil characterise the heavier PH fractions (Interim Final Petroleum R, 1994). Linear compounds up to C_{30}, for example, may dissipate within a month. By contrast, those with up to C_{37} need at least 200 days. Indeed, the entire fraction can persist for 4 years or longer (Gudin, 1978). The properties of the alkanes with different C_n, can be found at the open chemistry database, PubChem (Sadler et al., 2003). The relationships between the C_n and their densities, boiling points and melting points, are collected from the database and summarized in **Figure 2**. At the range of 5–45 of C_n, all the values of these properties were increased logarithmically following the increase of the C_n. However, based on **Figure 2A**, the values of density were slightly increased when the carbon chain length was longer than 25 of C_n. While the boiling points are increased linearly after the alkane contains more than twenty carbons in the chain (**Figure 2B**). According to Uzoije et al. (Uzoije and Agunwamba, 2011), crude oil samples with heavier molecular weights or high carbon numbers provide higher impacts on the soil bulk density, percentage of organic matter and porosity. C_n can be determined by their boiling points using gas chromatography. Because crude oil and petroleum products have complicated chemical compositions with a lot of variation between them, it's impossible to isolate unique chemical "fingerprints" for each oil to determine where the weathered oil pollution originated (Wang and Fingas, 1995).

PH Measurement

Ex Situ Measurement

It's critical to understand the viscosity and density of petroleum at a spill site, as this information is often needed to estimate the amount of petroleum spilt. The oil's kinematic viscosity can be measured using capillary tube viscometers. The oil sample is placed in a capillary glass tube and allowed to flow through the tube under gravity in this method. More viscous grades of oil take a longer flowing time. However, The viscosity of an oil is nonsensical unless the temperature at which it was measured is specified. The viscosity is usually measured at one of two temperatures: 40 or 100°C. The viscosity of most industrial oils is commonly measured at 40°C. Similarly, most engine oils are routinely measured at 100°C. The density of LNAPLs can be present as API gravity, which is an inverse measure of the density relative to water. A hydrometer can be used to measure API gravity.

To measure PH components in contaminated soil, they need to be extracted from soils before standardized soil extraction procedures. Methanol extraction is recommended for volatile substances including BTEX and gasoline, according to EPA method 5035, alternatively, direct headspace analysis can be used. Soxhlet, sonication, and supercritical fluid extractions are routinely used for semi-volatile substances (Weisman, 1998). To reach low detection limits, sample concentration methods, such as Snyder trapping column or nitrogen evaporation are adopted. There are several approaches for PH determinations including total PH (TPH), PH group type and individual PH component measurements (Weisman, 1998). Gas chromatography (GC) and infrared spectrometry (IR) are the two common analytical techniques employed for TPH determinations. High-performance liquid chromatography and GC are commonly used for PH group type analysis. GC with mass spectrometry (GC/MS) is commonly used for individual PH component measurements. It's worth mentioning that non-petroleum substances detected by GC-based technologies may cause TPH concentrations to be overestimated. For example, chlorinated compounds in gasoline samples may be detected by GC-based methods and reported as TPH.

In Situ Measurement

Today, on-site real-time assessment of industrial chemicals with relatively rapid qualitative analysis using portable GC/MS, has been demonstrated in a number of literature (Meuzelaar et al., 2000; Leary et al., 2016; Visotin and Lennard, 2016). For example, the US military used a "HAPSITE Smart GC-MS system" to detect toxic gases (Leary et al., 2016). However, on-site measurement with a field-friendly method providing near laboratory quality data for rapid quantitative, conclusive and

defensible sampling of airborne chemicals has remained challenging. A field-portable Torion-T9 GC-MS, which provides analytical information that is definitive for many types of samples containing the organic analyte(s) using solid-phase microextraction (SPME) and Needle Trap as the default sampling method. As demonstrated in our previous study (Wang et al., 2021a; Wang et al., 2021b), Torion-T9 portable GC-MS can provide results within minutes and is suitable for on-site analysis.

The handheld IR technique can be applied for analysing PHs sequestrated in soil, where the PHs can be identified based on the information of spectral peaks (Wang et al., 2020). The IR methodology takes significantly less time and costs to analyse than GC and HPLC-based technologies. However, it is difficult to interpret the raw IR spectral data as obtained and classify these petroleum products based on carbon chain lengths by mere observation. The interferences are represented by a sequence of more or less overlapping bands in the spectrum line form (band). These bands represent absorbed or scattered individual molecules (Czarnecki and Ozaki, 1996b; Kebbekus and Mitra, 1998; Bradley, 2007; Griffiths and De Haseth, 2007). When analysing a material with an unknown mixture of PHs, extracting information and identifying components from overlapping IR spectra is a critical problem. Separating heavily overlapping bands, according to Czarnecki and Ozaki, takes both an experienced researcher and some knowledge of the system under study (Czarnecki and Ozaki, 1996b). Therefore, IR analyses are commonly used for such chemical structure studies. Limited researches have been done on using these spectrum approaches to determine the PH fractions.

According to our previous study of using an handheld FTIR with diffuse reflectance infrared spectroscopy (DRIFTS) mode to classify dominant PH fractions, the similarity of the MIR peaks in the functional/group frequency region from 3,000–2,800 cm^{-1}, indicates the major compounds in the petroleum products have identical molecular structures, which is the carbon-hydrogen bonding for long-chain alkanes due to–C-H stretching vibrations (Wang et al., 2019). Two bands coherent to the doublet were discovered at locations 2,954 and 2,872 cm^{-1}, which can be used to determine the proportion of carbon chains (Wang et al., 2019). Another two doublets were found between 1,480 and 1,450 cm^{-1}, as well as between 750 and 730 cm^{-1}. Following the increase in Cn (Griffiths and De Haseth, 2007), the intensity of one coherent band was detected to increase in each of these regions. The cohesive bands intensity ratio can be used to determine the Cn (Wang et al., 2019).

It is worth noticing that there are two types of sampling modes for using the FTIR, DRIFTS and attenuated total reflections (ATR). According to recent studies (Koçak et al., 2021; Volkov et al., 2021), both techniques can be applied in soil analysis, but DRIFTS is more sensitive in soil applications. DRIFTS entails minimal sample preparation, i.e., drying and grinding, which is suitable for soil sample direct measurement. On the other hand, ATR can be applied as a complement to DRIFTS for soil minerals, organic matters with dark colour and in the presence of water.

Non-invasive geophysical subsurface imaging techniques including electromagnetic (EM) induction, ground-penetrating radar (GPR), nuclear Magnetic Resonance (NMR), Electrical Resistivity Tomography (ERT) and Induced Polarisation (IP) have been applied for PH, especially LNAPLs contaminated site characterisation, to detect and delineate PH contaminants in soil subsurface.

The principle of EM induction for subsurface PH detection is used to measure the electrical conductivity/resistivities in the subsurface (Johansen et al., 2005; Behroozmand et al., 2015; Ayoubi et al., 2020; Ayoubi et al., 2021). A sending coil generates a primary magnetic field in the space surrounding it—even underground—by passing through it a primary alternating electric current of known frequency and magnitude. The eddy currents generated in the ground cause a secondary current to flow via underground conductors, resulting in an alternating secondary magnetic field that is detected by the receiving coil. A phase lag distinguishes the second field from the primary field. The ratio of the magnitudes of the primary and secondary currents is proportional to the terrain conductivity. The depth of penetration is determined by coil separation and orientation. Unlike conventional resistivity techniques, no ground contact is required. This eliminates direct electrical coupling problems and allows much more rapid data acquisition.

NMR has already been validated by more than 50 years of development and innovation by the petroleum exploration industry. This technique has widely used in lithology to see fluids (such as LNAPLs) and gas distribution in porous media (Behroozmand et al., 2015). The very recent development of small-diameter, economical, and portable NMR tools (Spurlin et al., 2019) now permits the non-invasive use of this technology within existing polyvinyl chloride (PVC)-cased well infrastructure or open holes, which provides repeatability for long-term monitoring with low costs, as well as a direct-push approach that enables reconnaissance PH contaminated site characterisation. The physical principle of NMR logging is the same principle underlying magnetic resonance imaging technology used in medicine and NMR spectroscopy in chemistry, by emitting a series of radio-frequency pulses and recording the returning signal, referred to as "spin echoes" and the NMR tool measures the NMR response in the sensitive zone. The characteristics of the measured NMR signal reflect the quantity of hydrogen protons, where the total amplitude of the signal is directly proportional to the total amount of groundwater or PHs. NMR has been effectively applied to geology applications for soil water content and permeability characterisation (Spurlin et al., 2019). There is little difference in the detection of petroleum hydrocarbon fluids and water. However, the environmental application of NMR is still in its early stage.

GPR detects reflected signals from subsurface structures by using electromagnetic radiation at UHF/VHF frequencies in the radio spectrum (Jol, 2009) (Knight, 2001). When the electromagnetic energy emitted from GPR, encounters a buried object with different permittivity, it may be reflected or refracted or scattered back to the surface. A receiving antenna can then record the variations in the return signal (Jol, 2009). The disparity in dielectric characteristics between the contaminated region and the pristine region is the basis for employing GPR to image a contaminant (Knight, 2001). GPR has become a valuable method utilised by a variety of scientists, engineers and

consultants from many disciplines. For PH contaminated site applications, GPR can be applied for locating and predicting the fate and transport of contaminants in the subsurface soil and shallow groundwater, for contamination site assessment (Daniels et al., 1995; Babcock and Bradford, 2014). The presence of a layer of LNAPL on top of the water table reduces the capillary fringe and results in steady reflected radar signal amplitudes (Singer, 2007). The water in the pore space is replaced by LNAPL, which lowers the conductivity and dielectric characteristic of porous soil, increasing the radar propagation velocity (Jol, 2009). Nevertheless, for mixed contamination, the presence of inorganic contaminants in the subsurface typically increases electrical conductivity through their dissolution into the groundwater. A further drawback, using GPR to characterise contaminated sites will depend on the specific nature. For example, GPR is highly suited to most applications in dry sands, where penetration depth can exceed 50 m with low-frequency antennas. However, in wet clays, penetration depths are typically less than 1 m.

For delineation of a PH contaminated site, subsurface imaging method ERT and IP are also applied (Aranda et al., 2012). ERT and IP are well-established methods in the area of hydro-geophysics. Both of the techniques apply to explore electrical properties (resistivity and capacity) of the subsurface using the same four-electrode measurement approach. The devices introduce a known current flow to two electrodes and record the potential and capacity values from another set of electrodes at a set distance away, hence the electrical resistivity and IP can be calculated accordingly using inversion algorithms, such as Res2Dinv. The difference is ERT uses the injected current values and the receiving voltages to calculate the Earth resistivity, while the time-domain IP methods measure considers the resulting voltage following a change in the injected current. Soil and contaminant properties and state variables are linked to electrical resistivity and capacity, which makes the techniques valuable to study contaminant spatial distribution. ERT can be used to relate soil hydrocarbon contaminant characteristics (Aranda et al., 2012). When only surface electrodes are used, ERT&IP suffer from a decrease of sensitivity and resolution with increasing depth. A way to overcome the resolution problem is to include borehole electrodes to measure either between two (or more) boreholes and surface (Ochs and Klitzsch, 2020). However, the combination of surface and borehole ERT and IP techniques have little been studied in locating contaminants in environmental applications.

SOIL PROPERTIES

Soil solids can retain PHs by trapping in soil capillaries and pores or adsorption on particle surfaces (Fine et al., 1997). Mineral particles account for around 50% of the volume of soil, followed by 25% water, 20% air, and 5% organic matter (Wild, 1993). The processes occurring within soil that are instrumental in controlling PHs distribution include entrapment, adsorption, volatilization and transport. **Figure 3** shows a schematic of the weathering processes of PHs in soil. Less volatile components will permeate through soil pores in the form of LNAPL, being trapped in pores or adsorbed on mineral and organic matter surfaces. While the highly volatile fraction will rapidly volatilize into the gas phase in soil pores. Entrapment by soil and sorption decrease LNAPL volatilization, water dissolution and degradation rates (Greene-Kelly, 1954a; Greene-Kelly, 1954b; German and Harding, 1969; Olejnik et al., 1974; Nathwani and Philips, 1997). The degree of hydrocarbon entrapment and sorption is controlled by physical and chemical features of the soil solid phases, such as water content, texture, and organic matter concentration.

Soil Textural Information

Particles of variable size, shape, and chemical content represent the mineral elements of soils. A typical soil has about 50% porosity, however, the pores are normally filled with air or water depending on the moisture level. The entrapment of LNAPLs is strongly influenced by soil texture (Singer, 2007). The smaller soil particles have small porosity and permeability, with higher hydrocarbon adsorption and holding capacity. According to (Nye et al., 1994), clayey soils have very small pore spaces and have the highest hydrocarbon adsorption and holding capacity. It was found that the total sorption capacity of clayey soil for PHs was markedly greater than the of sandy soil. Silty soils have higher hydrocarbon adsorption and holding capacity than sandy soils but are highly erosive. Moreover, the porosity is also affected by polydispersity of soil practical size and shape (Schulze et al., 2015). Soil tortuosity and hysteresis phenomena result from pore shape irregularity, size and distribution, known as pore throat-size distribution (Rezanezhad et al., 2009; Ghanbarian et al., 2017). Soil hysteresis has been demonstrated to impact natural LNAPL depletion or mass migration within the LNAPL body by recent studies (Sookhak Lari et al., 2016).

In/Ex-Situ Measurement

Sufficient textural information should be obtained to permit the classification of soils. Particle Size Analysis is a reliable, reproducible technique widely applied in the laboratory (Bowman and Hutka, 2002). There are two major soil particle size analysis methods, hydrometer and pipette methods (Bowman and Hutka, 2002). The hydrometer method consists in using a hydrometer to measure the density of water suspension of soil at time intervals based on Stoke's law. The pipette method consists in using a pipette to take a known volume of a water suspension of a soil sample from the desired depth after a specific stirring time. This is accomplished by allowing different-sized soil particles to settle out of the solution at different periods (small clay particles take the longest). The portion of sand, silt and clay are determined based on the sample weight after drying. For both of the methods, soil pre-treatment can be required to remove organic materials and salts to increase soil dispersion. Based on the relative proportions of sand, silt and clay as a percentage, the soil texture triangle is used to convert particle size distribution into a recognised texture class (Bowman and Hutka, 2002). For field measurement, the clay percentage of soil can be approximated using a sieve and hands. According to

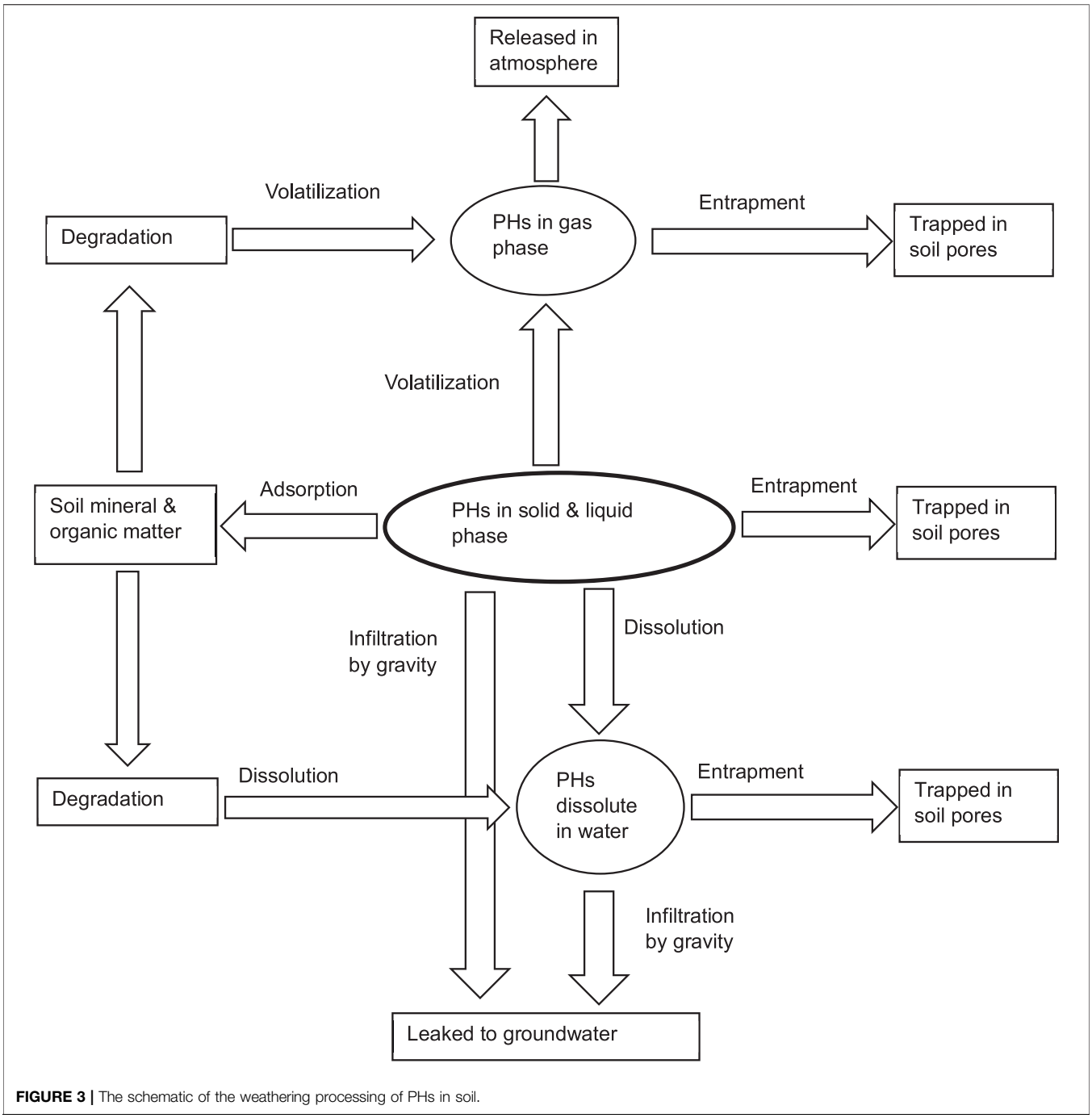

FIGURE 3 | The schematic of the weathering processing of PHs in soil.

(McDonald et al., 1998), Firstly, a sample of soil can be sieved by a 2 mm diameter sieve. Wet the soil with some water, knead it into a bolus, and then extrude a 2 mm thick, 1 cm wide ribbon. The length of the formed ribbon can provide estimated information on soil texture.

Porosity is defined as the proportion of pore volume to total volume (bulk volume) (Saidian et al., 2014). Saidian et al., comprehensively studied the measurement methods for soil porosity, including gas porosimetry, saturation methods and NMR (Saidian et al., 2014). Gas porosimetry relies on the expansion of gas, i.e., helium, and measure the effective porosity of the media. This method is still controversial. The arguments include gas can penetrate pores that are much smaller than the viscous fluid can; on the other hand, surface tension with gas-liquids is much higher than liquids-liquids to gas entry through water-filled pore throats can be less than oil entry (Danesh). Saturation methods measure the effective porosity of the media depending on the saturation with a certain fluid. With

suitable calibrations, portable NMR determines the concentration of hydrogen nuclei of soil in the field, which directly translates to pore volume and, as a result, porosity (Saidian et al., 2014).

Pore diameters are dispersed over a wide range of values in the vast majority of porous media. There is also a probability density function that describes the pore volume distribution for given pore size. The interstitial surface area of the spaces and pores per unit mass or unit bulk volume of the porous material is defined as the specific surface of the porous material. In several porous media applications, the specific surface area plays a significant role. Pore size distribution can be measured using the subcritical nitrogen adsorption technique (Saidian et al., 2014). Isotherms are used to measure pressure and temperature while nitrogen gas is being injected into the sample.

Infrared Spectroscopy

Instead of applying the conventional lab-based soil column measurement methods, handheld infrared spectroscopy can be employed to provide such information rapid in the field (Wang et al., 2020). For soil chemical properties, The most prevalent component of sand is quartz, which can be used to assess sand concentration in soils. Kaolinite is a prominent natural clay substance found in abundance in Australian soils, particularly in warm and humid climates. Smectite and illite are the other two common natural materials. Quantitative prediction of quartz and kaolinite (or other clay materials) can approximate sand and clay, and can thus act as a proxy for soil texture.

Our previous study provides more details about soil texture determination using the handheld FTIR with DRIFTS mode (Wang et al., 2020). Quartz could be calibrated at 1,080 cm^{-1}, which relates to the Si-O stretching vibration (Soriano-Disla et al., 2014). As suggested by (Ayoubi et al., 2020), Si-O bending vibration at 796 cm^{-1} can also be considered as a quantitative peak. The Si-O stretching peak is observed at 1,080 cm^{-1}, from quartz overlapped with other unknown peaks. Band composition was be applied to separate these two bands for quantification purposes. For clay, kaolinite, previous research suggested the calibration can utilize the strong O-H stretching vibration presenting as the doublets at 3,690–3,620 cm^{-1}. Smectite and illite can be determined at 3,400–3,300 cm^{-1} (Soriano-Disla et al., 2014).

Soil Permeability

Permeability is an important measure for soil drainage, which can influence fluids infiltration, storage, surface run-off and groundwater recharge (Azadmard et al., 2020). It is also known as hydraulic conductivity, which measures the rate of transmission of fluids and gas in soil (Odeh, 1959) (Gardner, 1956). Permeability is a complex feature of soils, varying with the location, soil porosity, depth, soil water content (SWC) and direction of flow. Horizontal permeability is often higher than vertical permeability because of soil layers (horizons). Soils with low permeability, such as heavy clay-rich soil, have up to two times the retention capacity of soils with high permeability, such as light sandy soils (Fine et al., 1997). SWC and permeability have an inverse relationship in unsaturated soils, as permeability fluctuates with soil moisture content (Odeh, 1959).

Soil permeability can be calculated using Darcy's law, as a simple proportional relationship between the instantaneous discharge rate through a porous medium, the viscosity of the fluid and the pressure drop over a given distance at a constant elevation. Effective porosity may be reduced by the presence of hydrocarbon films on soil surfaces, especially with the swelling of clay materials (Fine et al., 1997). The calculation can only provide approximate results because the velocity of fluid flow through a pore is proportional to the fourth power of its diameter (Poiseuille's law), even a slight change in the effective diameter of the pores can have a big impact on permeability. For *ex-situ* measurement, single/double infiltration ring methods can be applied for measuring the permeability based on the soil texture. For *in situ* measurements, soil permeability can be measured using a permeameter, which is a tube-like instrument is inserted into soil to measure the rate at water flows into the underlying soil.

Soil Water Content (SWC)

The transport in soil describes and predicts the directional movement and the flow rate of the reservoir fluids. When oil is spilt on soil its transport includes infiltration and imbibition. Infiltration represents the consequence of the vertical movements influent by gravity and evaporation, and imbibition represents the influence of soil capillary suction or fluid absorption by adhesive force, which can occur horizontally without the influence of gravity (Keller and Simmons, 2005). Changes in the SWC can inversely change the soil adsorptive capacity for PHs – Water retained in small soil capillaries reduces the effective soil porosity and hinders LNAPL transport through the soil in imbibition (Fine et al., 1997). This is because the water in both the vapour and liquid phase competes for sorption sites with PHs in surface soil capillaries. According to Fine et al., at soil moisture equivalent to 70% of field capacity, the adsorption of hydrocarbons can be negligible (Fine et al., 1997). Another study demonstrated that clay's sorption capacity can be doubled by using oven-dry rather than air-dry (Nye et al., 1994). Many studies have shown that increasing SWC reduces soil adsorptive capacity and enhances the PH into infiltrating (Acher et al., 1989; Yaron, 1989; Jarsjö et al., 1994) (van Darn, 1967).

Ex Situ Measurement

SWC can be measured gravimetrically as a fraction of the total soil weight. However, this method is destructive and time-consuming and is impractical for measuring SWC in the field. In moist soils, the evaporation of light carbon fractions of PHs from soil is maintained by the soil water (Yong et al., 1992). In the absence of other force fields, the soil diffusivity is presented by the ratio of the hydraulic conductivity and the differential water capacity or the flux of water per unit gradient of moisture content (Hayes et al., 2007). The pressure plate outflow method, which is based on volumetric outflow measurements of water over time from a soil sample subjected to variations in matric suction, is the most widely used laboratory method for assessing soil water diffusivity in unsaturated soils (Gardner, 1956).

In geotechnical engineering, Atterberg limits are frequently used to identify, describe, and classify soils, as well as to make

early assessments of the critical water contents (Nazir, 2011; Zolfaghari et al., 2015a; Zolfaghari et al., 2015b) (Das, 2006). For example, soil Atterberg limits were applied to indicate soil properties and land use in Western Iran (Zolfaghari et al., 2015a; Zolfaghari et al., 2015b). Atterberg limits or consistency limits are characterised by shrinkage, plastic and liquid limits (Nazir, 2011). The liquid limit represents the minimum water content at which soil particles flow under their weight. The plastic limit is the minimum water content at which soil is moulded without breaking. The water content at which further moisture loss will not result in any further volume reduction is known as the shrinkage limit. These limits control the consistency of the soils as wetting conditions change. These tests are most commonly employed on clayey or silty soils, which expand and shrink as a result of moisture content. Clays and silts change size and shear strength as a result of their reactions with water (Das, 2006).

In Situ Measurement

In the field, SWC can be determined by measuring a related variable that is affected by the amount of soil water through calibration curves (Bittelli, 2011). Dielectric sensors, for example, take advantage of changes in soil dielectric characteristics as a function of SWC. Heat dissipation and flux sensors measure soil's thermal properties and heat capacity variations (Hanks and Ashcroft, 1980). The neutron scattering approach relies on high-energy neutrons colliding with other atoms, particularly hydrogen in the water molecule, to lose energy (Bittelli, 2011). Alternatively, the hydraulic soil status can be estimated by using a GPR, and the working theory has been mentioned (Hubbard et al., 1997).

Using infrared spectroscopy, SWC can be measured using the oxygen-hydrogen stretching bonding, a broad peak centred at around 3,400 cm^{-1}. By increasing the water content, the intensity of the characteristic water peak was enhanced while the peaks from the sand were impaired. The loss in spectral quality in the sand is due to significant surface reflection from water film (Soriano-Disla et al., 2014). Since kaolinite can be determined using the IR region similar to water, water content needs to be minimized especially for measuring clay soils. When FTIR with DRIFT mode, the presence of water in the field can have a negative impact on the IR spectra. Hence, ATR mode should be applied to the FTIR for measuring a soil sample with significant SWC. To calculate the water content, the water characteristic peak is broad and robust. The absorbance area or intensity of the peak can be applied directly for calibration.

Soil Organic Matter (SOM)

The SOM consists of plant and animal wastes in various stages of decomposition, soil microbes and chemicals synthesised by them (Falahatkar et al., 2014; Havaee et al., 2014). The most abundant components of SOM are humic substances, which include humic acids, fulvic acids and humins. Other components primarily consist of polysaccharides, polypeptides, and altered lignin (Hayes et al., 2007). A study conducted by Benka-Cooker and Ekundayo indicates that SOM dominates LNAPL absorption when it is present at greater than 1% (Benka-Cooker and Ekundayo, 1995). Soils with a higher organic matter content adsorbed more PHs (Benka-Cooker and Ekundayo, 1995; Uzoije and Agunwamba, 2011). At low SOM, the adsorptive capacity of clays and other mineral matter may become vital, especially when they are dry (Benka-Cooker and Ekundayo, 1995). In contrast to LNAPL, in the case of vapour absorption, free mineral surfaces rather than organic matter seize control (Karickhoff, 1981). On the other hand, the presence of dissolved organic matter can also reduce the soil adsorption capacity due to competitive adsorption on mineral surfaces (Yong et al., 1992).

It is useful to express the partitioning of organic substances in soil by the soil organic carbon-water partitioning coefficient (K_{oc}). K_{oc} is the ratio of the mass of a chemical that is absorbed in the soil per unit mass of organic carbon over the equilibrium chemical concentration in solution. The mobility of organic soil pollutants can be predicted using K_{oc} values. Large K_{oc} values represent slowly mobile organic chemicals and low K_{oc} values represent high mobile organic chemicals. For example, BTEX compounds have a lower K_{oc} than most of the common aromatic hydrocarbons. Benzene (K_{oc} of 59) is considered to be highly mobile in soil, toluene (K_{oc} of 182) is considered to be moderate to highly mobile in soil, and xylenes (K_{oc} of 363–407) are considered to be moderately mobile in soil (National primary drinking, 1995). Because of their low volatility, the majority of PAHs are categorised as semi-volatile organic compounds. PAHs are difficult to dissolve in water in general. Because of their low solubilities and high K_{oc}, they are more likely to partition into sediments and soils than groundwater. As a result, the transport of PAHs from soils tends to be associated primarily with the transportation of the solid phase by the erosion of contaminated soils and sediments. As adsorption is an exothermic process, the K_{oc} values usually decrease inversely with temperature (Yong et al., 1992). A 10% decrease in K_{oc} would be expected for temperature rises from 20 to 30°C, and an18% increase would be expected for a temperature drop from 20 to 5°C (Yong et al., 1992).

Laboratory Measurement

SOM is mostly made up of soil organic carbon (SOC), which accounts for roughly 58 percent of the total mass, with the rest made up of water and other elements, such as potassium, calcium, magnesium, nitrogen, phosphorous and sulphur contained in organic residues (Combs and Nathan, 1998). Because SOM is often difficult to measure directly in laboratories, scientists prefer to measure SOC instead, and then multiply SOC by 1.72 to get SOM (Hoyle, 2013). SOC is most commonly analysed using either the Walkley-Black digestion method or the weight loss on ignition (LOI) method (Hayes et al., 2007). The Walkley-Black method uses chromic acid to measure the oxidisable organic carbon in soil samples. Oxidisable organic carbon is oxidised by 1 N $K_2Cr_2O_7$ solution. The reaction is assisted by the heat generated when two volumes of H_2SO_4 are mixed with one volume of the dichromate. Ferrous sulphate is used to titrate the residual dichromate. The amount of organic carbon in the soil sample has an inverse relationship with the titre. The weight LOI

method is based upon measuring the weight loss at different temperatures from 300 to 550°C for 2 h, then correlated to oxidisable organic carbon to determine SOM (Abella, 2007; Yerokun et al., 2007). According to the study of the comparison of determining SOM using the Walkley-Black method and the LOI procedure at 300, 360, 400, 500 and 550°C, a temperature of around 360°C was found to be optimal because it burned the most organic carbon, damaged the least inorganic carbon, caused the least clay structural water loss, and utilised the least amount of electrical energy (Salehi et al., 2011). An instrument known as a LECO carbon analyser or LECO method can be applied to measure SOC by combusting the organic carbon and measuring the resulting carbon dioxide produced (Gazulla et al., 2012). Before analysis, soil samples need to be acid-treated to remove inorganic carbon, i.e. carbonates from rocks. The amount of organic carbon is directly proportional to the amount of carbon dioxide produced. The Walkley-Black method has higher accuracy for measuring low SOM soils (<2%), while the weight-loss method is more suitable for measuring soil with greater than 6% SOM (Hayes et al., 2007).

Infrared Spectroscopy

According to (Soriano-Disla et al., 2014; Asgari et al., 2020), for organic matter, alkyl groups are monitored using mid-IR at 2,930–2,850 cm^{-1}, protein amide at 1,670–1,530 cm^{-1}, 1720 cm^{-1} for carboxylic acid, and 1,600–1,570 cm^{-1} for aromatic groups. Humic acid is a dark colour chemical, and the IR spectra at high levels of humic acid produced a low signal to noise ratio. When using FTIR with DRIFTS mode, the dark colour of humic acid substances may absorb more IR energy and cause less signal reflected in the IR signal receiver. Hence, ATR mode should be applied to the FTIR for SOM measurement. Since humic acid is not a single compound, all the peaks which indicated different functional groups should be used for calibration. According to (Irwin et al., 1998), numerous quartz peaks below 2000 cm^{-1} almost overlap entirely with the soil organic matter, which is composed mainly of humic acid. According to our previous study (Wang et al., 2020), it is noted that there are minor peaks resembling noise at roughly 3,500 cm^{-1} and 1720–1,630 cm^{-1}, which can be considered as humic acid compounds. When humic acid content was greater than 10%, small peaks at about 2,930 cm^{-1} were found, which can be used for humic acid calibration in pristine soil. However, this area can only represent one humic acid functional group. Moreover, soil Vis/Near IR spectroscopy at the region between 350 and 1,150 nm wavelength can also provide significant characterising signals for SOM determination (Asgari et al., 2020).

Soil Microbiological Characterisation

Indigenous soil microbes represent approximately 5% of the total organic matter but play important roles in degrading PHs (Head et al., 2003). The natural bacteria or fungi transform, decrease or eliminate PHs by degrading or transforming more complex petroleum components into relatively simple components that pose less risk in the environment. This is referred to as biodegradation (Head et al., 2003). Biodegradation is an important natural attenuation process in soil and a primary weathering process for petroleum. Most soils and sediments contain bacteria and other organisms capable to degrade PHs (Potter and Simmons, 1998). In unpolluted environments, hydrocarbon-degrading bacteria can be found in small numbers, however, once they adapt to energy-rich PHs, they can attain great densities (Head et al., 2003). Biodegradation rates fluctuate depending on microbial densities and hydrocarbons, as well as the geochemical and hydrological conditions present in the subsurface soil (Potter and Simmons, 1998). Zones with different biodegradation rates can be identified using geochemical and microbiological data. In optimal environmental conditions, biodegradation rates of low to intermediate molecular weight aliphatic, alicyclic, and aromatic hydrocarbons can be accelerated. As the molecular weight of the hydrocarbon grows, so does its resistance to biodegradation (Wiedemeier et al., 1995). Peters and Moldowan developed a pH biodegradation classification scheme, known as PM scale, to rank the level of biodegradation of PHs from one to ten (Peters and Moldowan, 1993). The PM scale has been widely applied for light and conventional oils. There are other scales developed for a more comprehensive list of compounds and heavy oils (Wenger et al., 2002; Larter et al., 2012). According to Head (Head et al., 2003), more than 70% of PAH and 80% of benzo [a]pyrene in petroleum were partitioned to the residual LNAPL. Weathered PHs have low bioavailability, are resistant to environmental degradation and exist in the soil for a long time (Guerin, 2000).

Optimising the environmental conditions by bio-stimulation and bio-augmentation, including temperature, PH, moisture, permeability and oxygen level are vital for the degradation of weathered PHs. There are ample microbial processes and growth models have been developed to simulate the biodegration for optimisation. Sookhak Lari et al. have reviewed the models expecially for natural source zone depletion (NSZD) of LNAPL (Sookhak Lari et al., 2019). Garg et al. overviewed the control factors of processing LNAPL in NSZD (Garg et al., 2017). In the common pratice, Mesophilic temperatures, between 20 and 45°C, soil pH range of 5.0–9.0 and SWC between 50–80% by weight of the water-holding capacity are used for bioremediation (Brassington et al., 2007; Frysinger et al., 2003; E (2000). Contamina, 2000). In addition, the saturated permeability (K_{sat}) for soil should be greater than 10^{-3} cm/s, to maintain the aerobic metabolism condition with essential oxygen in soil water (Head et al., 2003). However, the soil can become anaerobic if oxygen is consumed faster than it can be replenished from the atmosphere. Biodegradation can also be conducted in anaerobic conditions albeit with a reduction of degradation rate and synthesis of unpleasant odorous compounds, such as hydrogen sulphide and methane (Head et al., 2003). Soil nutrients, such as phosphorus and nitrogen, are also critical for microorganism and bacteria. Therefore, optimising the environmental conditions is an essential factor for the stimulation and augmentation of biodegradation. Computer simulations are commonly used for understanding the basic processes and the rate-determining factors for biodegradation in different environmental conditions. For example, Gogoi et al., conducted laboratory

and field pilot bioremediation studies on PH contaminated sites in India based on computer simulation methods (Gogoi et al., 2003).

Ex Situ Measurement

There are two commonly used microbiological characterisation methods, enumeration studies and soil respirometry. Microbial enumeration is a qualitative measurement that employs plate counts to determine relative numbers of total microbial hydrocarbon degraders (Head et al., 2003). Soil respirometry measures oxygen depletion and carbon dioxide production in soil and provide an indirect measurement of biological activities (Head et al., 2003). The existence of catabolic genes and enzymes play essential biochemical roles to enable the soil endemic microbes to consume the PHs for carbon and energy by decomposition (Srinivasulu and Rangaswamy, 2006). Hence, soil enzymatic activities and microbial biomass carbon (C_{mic}) are two crucial biological activities that regulate PH attenuation (Alrumman et al., 2015). Well-known enzymes include amylase, arylsulphatases, b-glucosidase, cellulose, chitinase, dehydrogenase, phosphatase, protease, and urease (Das and Varma, 2011). To measure soil enzyme activities, different methodological approaches have been critically and thoroughly examined to distinguish among the various categories of soil enzymes (Nannipieri et al., 2002).

One of the popular techniques is to measure microbial growth and enzyme activity against C_{mic} throughout incubation with carbon and nitrogen treated soil samples (Srinivasulu and Rangaswamy, 2006). Another popular method is to measure both intracellular and extracellular enzyme activities due to the lysis of microbial cells after $CHCl_3$ fumigation or ultrasonic treatment (Srinivasulu and Rangaswamy, 2006). The most common procedure to determine C_{mic}, is the chloroform fumigation-extraction approach. According to (Setia et al., 2012), in this method, soils are exposed to chloroform vapour for more than 24 h to lyse the microbial cells. With extraction using 0.5 M K_2SO_4, the difference between fumigated and non-fumigated carbon is related to C_{mic} with calibration curves.

In situ Measurement

Gas Flux Measurement

Emerging research has recently improved the gaseous expression of PH degradation (Amos et al., 2005; Davis et al., 2005; Johnson et al., 2006; Sihota et al., 2011; McCoy et al., 2014). Soil microbes, methanogenesis comsume PHs and produce methane (CH_4) in an anaerobic condition, then the methane is oxidised by soil oxygen to CO_2 (CARE, 2018). LNAPL degradation rates in soil subsurface can be determined indirectly using gas flux measurement devices in the field (CARE, 2018). There should be are three soil gas flux methods: gradient method with monitoring sensors (O_2, CO_2, CH_4 and VOC); passive flux trap (PFT) method with caustic CO_2 sorbents in a static chamber; and dynamic closed chamber (DCC) with a field gas analyser connected to a ground-mounted chamber. According to CRC CARE technical report 2018 (CARE, 2018), gradient method is suitable for short and long term measurement for NSZD. While the pre-concentrated methods, PFT and DCC are more sensitive and can be applied at sites where CO_2 is migrating via diffusion and advection.

Infrared Spectroscopy

Recent research found clay/bacteria interactions can be observed at the range of 1,400–1800 cm^{-1} wavelength, where Ca-MMT/P. *syringae* biomass activities can be observed (Fung-Khee, 2020). IR spectroscopy can only provide indications for functioning groups and is not able to distinguish the living and dead organic matter in soil. To determine soil biological activities, instead of locating the characterise IR peaks, an alternative method is to build a calibration model with chemometric regression methods using the IR spectral data. Nath et al. applied spectroscopy data with partial least square regression to predict soil biological activities such as soil microbial biomass, soil enzymes, and Q10 (Nath et al., 2021). The same approach was employed by Janu et al. to determine biochar and biomass (Janu et al., 2021). In their application, multiple linear regressions, such as principal component analysis (PCA) were applied to determine the most important IR peak regions that contributed to soil bio-properties.

ATMOSPHERIC CIRCUMSTANCES

Temperature and Pressure

Increasing the atmospheric temperature and pressure can increase the molecular kinetic movements and cause a decrease in the surface soil adsorption capacity. The soil adsorption capacity can be decreased by nearly 20% by raising the atmospheric temperature from 5 to 20°C (Yong et al., 1992). Theoretically, an increase in temperature and pressure usually increase the loss of PHs in surface soils by increasing the volatilization rate. However, there is no substantial evidence to support this theory in a practical condition (Spencer, 1970). Adversely, the loss of light PHs might not be affected by the temperature and pressure due to the balance of the soil adsorption process (Spencer, 1970). Volatilization might continue in frozen temperature soils due to the diffusion (Spencer, 1970). Furthermore, Barometric pressure changes or wind may drive the advection of PH vapours. When the atmospheric pressure is lower than the pressure in the subsurface, PH vapours are drawn out to the atmosphere. When the atmospheric pressure is greater than the pressure in the subsurface, PH vapours may be forced into the subsurface (Spencer, 1970).

Humidity and Rainfalls

As previously stated, modifying the SWC affects the soil adsorptive capacity and the PH's volatilization process. Changes in air humidity and temperature are the sole factors that affect surface SWC (Ravi et al., 2004). Changes in air humidity can have a major impact on surface SWC in arid environments as changes in the SWC can inversely change the soil adsorptive capacity for PHs (Ravi et al., 2004). When the water evaporates, the PHs may hold firmly onto dry soils. The volatilization rate and the vapour density of PHs become

reduced by adsorption especially on the dry soil (Yong et al., 1992). As mentioned before, the loss of compounds from the crude oils was shown to tightly correlate to their water solubility (Forsythe et al., 2017; Forsythe et al., 2019). The PHs adsorbed on the surface soil particles can be moved by wind erosion which is widespread in arid and semi-arid regions, where soils are drier and with sparse vegetation cover (Ravi et al., 2004). Intense rainfalls can significantly increase the SWC, until the saturated condition, where the adsorption of hydrocarbons can be reduced to negligible. Rainfall will cause saturation and the PHs in LNAPLs initially adsorbed on the surface soils will be carried to on top of the runoff water with the overland flow as erosion.

CONCLUSION

Sorption, volatilization, transport and biological transformations occur within soil, and are instrumental in controlling PHs distribution. The degree of hydrocarbon entrapment and sorption is controlled by the physical and chemical properties of the solid phase of soils, such as texture, water, and organic matter content. The smaller soil particles have low porosity and permeability, resulting in significant hydrocarbon adsorption and holding capacity. Changes in the SWC will inversely change the soil adsorptive ability for PHs. For the atmospheric circumstances, both soil adsorption capacity and the volatilization rate of PHs can be affected by the atmospheric temperature and pressure. However, there is no reliable evidence related to these two factors and the loss of PHs in surface soil. It was found that hydrocarbon adsorption occurs predominantly by partitioning into organic matter in the soil. Bacteria and other species capable of decomposing petroleum hydrocarbons can be found in nearly all soils and sediments. Different microbial populations, hydrocarbons, and geochemical and hydrological conditions in the subsoil affect biodegradation rates.

There are pros and cons for both *ex-situ* and *in-situ* measurement methods. It is often true that the *ex-situ* methods can provide higher accuracies and lower detection limits while *in situ* methods provide rapid results and better coverage. Nevertheless, it is a tendency to use a portable and handheld instrument for fast in-field contaminated land characterisation.

AUTHOR CONTRIBUTIONS

LW: Public responsibility for the content, including participation in the concept, design, analysis, writing, or revision of the manuscript. YC: Public responsibility for the content, including participation in the concept, design, analysis, writing, or revision of the manuscript. RN: Public responsibility for the content, including participation in the concept, design, analysis, writing, or revision of the manuscript. MB: Public responsibility for the content, including participation in the concept, design, writing and revision of the manuscript.

FUNDING

This research was funded by CRC CARE Pt Ltd. The research was conducted in the laboratories of the Global Centre for Environmental Remediation (GCER) at the University of Newcastle.

REFERENCES

Abella, S. R. (2007). Estimating Organic Carbon from Loss-On-Ignition in Northern Arizona forest Soils. *Soil Sci. Soc. America J.* 71, 545–550. doi:10.2136/sssaj2006.0136

Acher, A. J., Boderie, P., and Yaron, B. (1989). Soil Pollution by Petroleum Products, I. Multiphase Migration of Kerosene Components in Soil Columns. *J. Contaminant Hydrol.* 4, 333–345. doi:10.1016/0169-7722(89)90032-6

Developments in Petroleum Science in *8-Interfacial Tension*. Editor A. Danesh (Amsterdam, Netherlands: Elsevier), Vol. 47.

Alrumman, S. A., Standing, D. B., and Paton, G. I. (2015). Effects of Hydrocarbon Contamination on Soil Microbial Community and Enzyme Activity. *J. King Saud Univ. - Sci.* 27, 31–41. doi:10.1016/j.jksus.2014.10.001

Amos, R. T., Mayer, K. U., Bekins, B. A., Delin, G. N., and Williams, R. L. (2005). Use of Dissolved and Vapor-phase Gases to Investigate Methanogenic Degradation of Petroleum Hydrocarbon Contamination in the Subsurface. *Water Resour. Res.* 41 (2), W02001. doi:10.1029/2004wr003433

Aranda, R., Pagan, P, M., and Cano, A, F. (2012). Methodology for the Detection of Contamination by Hydrocarbons and Further Soil Sampling for Volatile and Semi-volatile Organic Enrichment in Former Petrol Stations, SE Spain. *Eurasian J. Soil Sci.* 1 (1), 10–15.

Asgari, N., Ayoubi, S., Dematte, J. A. M., and Dotto, A. C. (2020). Carbonates and Organic Matter in Soils Characterized by Reflected Energy from 350–25000 Nm Wavelength. *J. Mountain Sci.* 17 (7), 1636–1651. doi:10.1007/s11629-019-5789-9

Ayoubi, S., Khademi, H., Shirvani, M., and Gyasi-Agyei, Y. (2020). Using Magnetic Susceptibility for Predicting Hydrocarbon Pollution Levels in a Petroleum Refinery Compound in Isfahan Province, Iran. *J. Appl. Geophys.* 172, 8. doi:10.1016/j.jappgeo.2019.103906

Ayoubi, S., Samadi, M. J., and Shirvani, M. (2021). Changes in Iron Mineralogy and Magnetic Susceptibility during Crude Oil Incubation in Four Textural Soils in Central Iran. *J. Appl. Geophys.*, 190, 104338. doi:10.1016/j.jappgeo.2021.104338

Azadmard, B., Mosaddeghi, M. R., AyoubiChavoshi, S. E., Chavoshi, E., and Raoof, M. (2020). Estimation of Near-Saturated Soil Hydraulic Properties Using Hybrid Genetic Algorithm-Artificial Neural Network. *Ecohydrology & Hydrobiology* 20, 437–449. doi:10.1016/j.ecohyd.2019.09.001

Babcock, E., and Bradford, J. H. (2014). Reflection Waveform Inversion of Ground-Penetrating Radar Data for Characterizing Thin and Ultrathin Layers of Nonaqueous Phase Liquid Contaminants in Stratified media. *Geophysics* 80 (2)H1-H11. doi:10.1190/geo2014-0037.1

Barakat, A. O., Qian, Y., Kim, M., and Kennicutt, M. C. (2001). Chemical Characterization of Naturally Weathered Oil Residues in Arid Terrestrial Environment in Al-Alamein, Egypt. *Environ. Int.* 27, 291–310. doi:10.1016/s0160-4120(01)00060-5

Behroozmand, A. A., Keating, K., and Auken, E. (2015). A Review of the Principles and Applications of the NMR Technique for Near-Surface Characterization. *Surv. Geophys.* 36, 27–85. doi:10.1007/s10712-014-9304-0

Benka-Cooker, M. O., and Ekundayo, J. A. (1995). Effects of Oil Spill on Soil Physio-Chemial Properties of a Spill Site in the Niger delta Area of Nigeria. *Environ. Monit. Assess.* 36, 93–109.

BIOWISE (2000). *Contaminated Land Remediation - A Review of Biological Technology*. Oxon, UK: BIOWISE.

Bittelli, M. (2011). Measuring Soil Water Content: a Review. *hortte* 21, 293–300. doi:10.21273/horttech.21.3.293

Bowman, G. M., and Hutka, J., Particle Size Analysis, in *In Soil Physical Measurement and Interpretation for Land Evaluation*. 2002, CSIRO Publishing: Victoria. p. 224–239.

Bradley, M. (2007). *Curve Fitting in Raman and IR Spectroscopy: Basic Theory of Line Shapes and Applications*. U. S.: Thermo Fisher Scientific.

Brassington, K. J., Hough, R. L., Paton, G. I., Semple, K. T., Risdon, G. C., Crossley, J., et al. (2007). Weathered Hydrocarbon Wastes: A Risk Management Primer. *Crit. Rev. Environ. Sci. Technology* 37, 199–232. doi:10.1080/10643380600819625

Bray, D. J., Anderson, R. L., Warren, P. B., and Lewtas, K. (2020). Wax Formation in Linear and Branched Alkanes with Dissipative Particle Dynamics. *J. Chem. Theor. Comput.* 16, 7109–7122. doi:10.1021/acs.jctc.0c00605

Care, C. "Technical Measurement Guidance for LNAPL Natural Source Zone Depletion," in CRC CARE Technical Report No. 44. *2018* (Newcastle, Australia: CRC for Contamination Assessment and Remediation of the Environment).

Combs, S. M., and Nathan, M. V. (1998). "Soil Organic Matter," in *Recommended Chemical Soil Test Procedures for the North Central Region* (Columbia, MO: Missouri Agricultural Experiment Station), 53–58.

Czarnecki, M. A., and Ozaki, Y. (1996). Determination of Integrated Intensities of Overlapped IR Bands by Curve-Fitting, Fourier Self-Deconvolution and a Combination of Both Methods. *Spectrochimica Acta A* (52), 1593–1601. doi:10.1016/0584-8539(96)01710-2

Czarnecki, M. A., and Ozaki, Y. (1996). Determination of Integrated Intensities of Overlapped IR Bands by Curve-Fitting, Fourier Self-Deconvolution and a Combination of Both Methods. *Spectrochimica Acta A: Mol. Biomol. Spectrosc.* 52, 1593–1601. doi:10.1016/0584-8539(96)01710-2

Daniels, J. J., Roberts, R., and Vendl, M. (1995). Ground Penetrating Radar for the Detection of Liquid Contaminants. *J. Appl. Geophys.* 33, 195–207. doi:10.1016/0926-9851(95)90041-1

Das, B. M. (2006). *Principles of Geotechnical Engineering*. U. S.: CENGAGE Learning.

Das, S. K., and Varma, A. (2011). Role Of Enzymes in Maintaining Soil Health *in* Soil Enzymology. Berlin/Heidelberg, Germany: Springer.

Davis, G. B., Rayner, J. L., Trefry, M. G., Fisher, S. J., and Patterson, B. M. (2005). Measurement and Modeling of Temporal Variations in Hydrocarbon Vapor Behavior in a Layered Soil Profile. *Vadose Zone J.* 4, 225–239. doi:10.2136/vzj2004.0029

Everett, K. R. (1978). Some Effects of Oil on the Physical and Chemical Characteristics of Wet Tundra Soils. *ARCTIC* 31, 260–276. doi:10.14430/arctic2657

Falahatkar, S., Hosseini, S. M., Salman Mahiny, A., Ayoubi, S., and Wang, S.-q. (2014). Soil Organic Carbon Stock as Affected by Land Use/cover Changes in the Humid Region of Northern Iran. *J. Mt. Sci.* 11 (2), 507–518. doi:10.1007/s11629-013-2645-1

Fine, P., Graber, E. R., and Yaron, B. (1997). Soil Interactions with Petroleum Hydrocarbons: Abiotic Processes. *Soil Technology* 10, 133–153. doi:10.1016/s0933-3630(96)00088-8

Forsythe, J. C., Martin, R., De Santo, I., Tyndall, R., Arman, K., Pye, J., et al. (2017). Integrating Comprehensive Two-Dimensional Gas Chromatography and Downhole Fluid Analysis to Validate a Spill-Fill Sequence of Reservoirs with Variations of Biodegradation, Water Washing and Thermal Maturity. *Fuel* 191, 538–554. doi:10.1016/j.fuel.2016.11.081

Forsythe, J. C., O'Donnell, M., Betancourt, S. S., Masurek, N., Gisolf, A., Bennett, B., et al. (2019). Biodegradation and Water Washing in a Spill-Fill Sequence of Oilfields. *Fuel* 237, 707–719. doi:10.1016/j.fuel.2018.09.144

Frysinger, G. S., Gaines, R. B., Xu, L., and Reddy, C. M. (2003). Resolving the Unresolved Complex Mixture in Petroleum-Contaminated Sediments. *Environ. Sci. Technol.* 37, 1653–1662. doi:10.1021/es020742n

Fung-Khee, F. (2020). "FTIR Analysis of Bacteria Biomass-Mineral Interactions in Soils," in *CUNY Academic Works*. Available at: https://academicworks.cuny.edu/cc_etds_theses/841.

Gardner, W. R. (1956). Calculation of Capillary Conductivity from Pressure Plate Outflow Data. *Soil Sci. Soc. America J.* 20, 317–320. doi:10.2136/sssaj1956.03615995002000030006x

Garg, S., Newell, C. J., Kulkarni, P. R., King, D. C., Adamson, D. T., Renno, M. I., et al. (2017). Overview of Natural Source Zone Depletion: Processes, Controlling Factors, and Composition Change. *Groundwater Monit. R.* 37 (3), 62–81. doi:10.1111/gwmr.12219

Gazulla, M., F., Rodrigo, M., Orduña, M., and Gómez, C. M. (2012). Determination of Carbon, Hydrogen, Nitrogen and Sulfur in Geological Materials Using Elemental Analysers. *Geostandards geoanalytical Res.* 36 (2), 201–217. doi:10.1111/j.1751-908x.2011.00140.x

German, W. L., and Harding, D. A. (1969). The Adsorption of Aliphatic Alcohols by Montmorillonite and Kaolinite. *Clay miner.* 8, 213–227. doi:10.1180/claymin.1969.008.2.09

Ghanbarian, B., Ioannidis, M. A., and Hunt, A. G. (2017). Theoretical Insight into the Empirical Tortuosity-Connectivity Factor in the Burdine-Brooks-Corey Water Relative Permeability Model. *Water Resour. Res.* 53 (12), 10395–10410. doi:10.1002/2017wr021753

Gogoi, B. K., Dutta, N. N., Goswami, P., and Krishna Mohan, T. R. (2003). A Case Study of Bioremediation of Petroleum-Hydrocarbon Contaminated Soil at a Crude Oil Spill Site. *Adv. Environ. Res.* 7, 767–782. doi:10.1016/s1093-0191(02)00029-1

Greene-Kelly, R. (1954). Sorption of Aromatic Organic Compounds by Montrnorillonite. Part II. Packing Studies with Pyridine. *Trans. Faraday Soc.* 51, 425–430. doi:10.1039/TF9555100425

Greene-Kelly, R. (1954). Sorption of Aromatic Organic Compounds by Montrnorillonite. Part I. Orientation Studies. *Trans. Faraday Soc.* 51, 412–424. doi:10.1039/TF9555100412

Griffiths, P. R., and De Haseth, J. A. (2007). *Fourier Transform Infrared Spectrometry*. U. S.: John Wiley & Sons.

Gudin, C. (1978). Interaction between Oil-Vegetation and Soil. *International Symposium on Ground Water Pollution by Oil Hydrocarbons*. Prague: International press Praha, 411–417.

Guenzi, W. D., and Bear, W. E. (1974). *Volatilization of Pesticides*. Chapter 6, Pesticides in Soil and Water. U S: Soil Science Society of America.

Guerin, T. F. (2000). Long-term Performance of a Land Treatment Facility for the Bioremediation of Non-volatile Oily Wastes. *Resour. Conservation Recycling* 28, 105–120. doi:10.1016/s0921-3449(99)00036-1

Hanks, R. J., and Ashcroft, G. L. (1980). *Applied Soil Physics: Soil Water and Temperature Application*. Berlin/Heidelberg, Germany: Springer-Verlag.

Havaee, S., Ayoubi, S., Mosaddeghi, M. R., and Keller, T. (2014). Impacts of Land Use on Soil Organic Matter and Degree of Compactness in Calcareous Soils of central Iran. *Soil Use Manage* 30 (1), 2–9. doi:10.1111/sum.12092

Hayes, M. H. B., Tseng, T. Y., and Wang, M. K. (2007). Chemistry of Soil Organic Matter. *Taiwan J. Sci.* 22, 215–226.

Head, I. M., Singleton, I., and Milner, M. G. (2003). *Bioremediation: A Critical Review*. England: Horizon Scientific Press.

Hoyle, F., C. (2013). in *Managing Soil Organic Matter: A Practical Guide*. Editor J. Paterson (Barton, ACT: Grains Research and Development Corporation).

Hubbard, S. S., Rubin, Y., and Majer, E. (1997). Ground-penetrating-radar-assisted Saturation and Permeability Estimation in Bimodal Systems. *Water Resour. Res.* 33, 971–990. doi:10.1029/96wr03979

Interim Final Petroleum Report: Development of Health-Based Alternative to the Total Petroleum Hydrocarbon (TPH) Parameter. 1994, Boston, MA, U. S.: Massachusetts Department of Environmental Protection, Executive Office of Environmental Affairs

Irwin, R. J., Stevens, L., Seese, M. D., and Basham, W. (1998). *Environmental Contaminants Encyclopaedia*. Washington, DC: National government publication.

Janu, R., Mrlik, V., Ribitsch, D., Hofman, J., Sedláček, P., Bielská, L., et al. (2021). Biochar Surface Functional Groups as Affected by Biomass Feedstock, Biochar Composition and Pyrolysis Temperature. *Carbon Resour. Convers.* 4, 36–46. doi:10.1016/j.crcon.2021.01.003

Jarsjö, J., Destouni, G., and Yaron, B. (1994). Retention and Volatilization of Kerosene: Laboratory Experiments on Glacial and post-glacial Soils. *J. Contaminant Hydrol.* 17, 167–185. doi:10.1016/0169-7722(94)90020-5

Johansen, S. E., Amundsen, H. E. F., Røsten, T., Ellingsrud, S., Eidesmo, T., and Bhuiyan, A. H. (2005). Subsurface Hydrocarbons Detected by Electromagnetic Sounding. *First Break* 23 (3). doi:10.3997/1365-2397.2005005

Johnson, P., Lundegard, P., and Liu, Z. (2006). Source Zone Natural Attenuation at Petroleum Hydrocarbon Spill Sites-I: Site-specific Assessment Approach. *Groundwater Monit. Remediation* 26 (4), 82–92. doi:10.1111/j.1745-6592.2006.00114.x

Jol, H. M. (2009). *Ground Penetrating Radar : Theory and Applications*. Amsterdam, Netherlands: Elsevier.

Karickhoff, S. W. (1981). Semi-empirical Estimation of Sorption of Hydrophobic Pollutants on Natural Sediments and Soils. *Chemosphere* 10, 833–846. doi:10.1016/0045-6535(81)90083-7

Kebbekus, B. B., and Mitra, S. (1998). *Environmental Chemical Analysis*. U. K.: Thomson Science.

Keller, J. M., and Simmons, C. S. (2005). *The Influence of Selected Liquid and Soil Properties on the Propagation of Spills over Flat Permeable Surfaces*. Washington: Pacific Northwest National Laboratory.

Knight, R. (2001). Ground Penetrating Radar for Environmental Applications. *Annu. Rev. Earth Planet. Sci.* 29, 229–255. doi:10.1146/annurev.earth.29.1.229

Koçak, A., Wyatt, W., and Comanescu, M. A. (2021). Comparative Study of ATR and DRIFT Infrared Spectroscopy Techniques in the Analysis of Soil Samples. *Forensic Sci. Int.*, 328. doi:10.1016/j.forsciint.2021.111002

Larter, S., Huang, H., Adams, J., Bennett, B., and Snowdon, L. R. (2012). A Practical Biodegradation Scale for Use in Reservoir Geochemical Studies of Biodegraded Oils. *Org. Geochem.* 45, 66–76. doi:10.1016/j.orggeochem.2012.01.007

Leary, P. E., Dobson, G. S., and Reffner, J. A. (2016). Development and Applications of Portable Gas Chromatography-Mass Spectrometry for Emergency Responders, the Military, and Law-Enforcement Organizations. *Appl. Spectrosc.* 70, 888–896. doi:10.1177/0003702816638294

McCoy, K., Zimbron, J., Sale, T., and Lyverse, M. (2014). Measurement of Natural Losses of LNAPL Using CO2Traps. *Groundwater* 53 (4), 658–667. doi:10.1111/gwat.12240

McDonald, R. C., Isbell, R. F., Speight, J. G., Walker, J., and Hopkins, M. S. (1998). *Australian Soil and Land Survey Field Handbook* (Canberra, Austrlia: ustralian Collaborative Land Evaluation Program).

Mercer, J. W., and Cohen, R. M. (1990). A Review of Immiscible Fluids in the Subsurface. *J. Contam. Hydrol.* 6, 7–163. doi:10.1016/0169-7722(90)90043-g

Meuzelaar, H. L. C., Dworzanski, J. P., Arnold, N. S., McClennen, W. H., and Wager, D. J. (2000). Advances in Field-Portable mobile GC/MS Instrumentation. *Field Analyt. Chem. Technol.* 4, 3–13. doi:10.1002/(sici)1520-6521(2000)4:1<3:aid-fact2>3.0.co;2-m

Nannipieri, P., Kandeler, E., and Ruggiero, P. (2002). "Enzyme Activities and Microbiological and Biochemical Processes in Soil," in *Enzymes in the Environment: Activity, Ecology and Applications*. Editor R. P. D. R. G. Burns (New Yorker: CRC Press), 1–33.

Nath, D., Laik, R., Meena, V. S., Pramanick, B., and Singh, S. K. (2021). Can Mid-infrared (Mid-IR) Spectroscopy Evaluate Soil Conditions by Predicting Soil Biological Properties? *Soil security* 4, 100008. doi:10.1016/j.soisec.2021.100008

Nathwani, J. S., and Philips, C. R. (1997). Adsorption-desorption of Selected Hydrocarbons in Crude Oil and Soils. *Chemosphere* 4, 157–162.

National primary drinking (1995). *National Primary Drinking Water Regulations, Contaminant Specific Fact Sheets, Volatile Organic Chemicals—Technical Version.* U.S. Environmental Protection Agency

Nazir, A. K. (2011). Effect of Motor Oil Contamination on Geotechnical Properties of over Consolidated clay. *Alexandria Eng. J.* 50, 331–335. doi:10.1016/j.aej.2011.05.002

Nudelman, N. S., Rios, I. S., and Katusich, O. (2002). Fate of the Oil Residuals in Patagonian Soils Effects of the Environmental Exposure Time. *J. Environ. Assess. Remediation* 3, 1–8.

Nye, P. H., Yaron, B., Galin, T., and Gerstl, Z. (1994). Volatilization of a Multicomponent Liquid through Dry Soils: Testing a Model. *Soil Sci. Soc. America J.* 58, 269–277. doi:10.2136/sssaj1994.03615995005800020002x

Ochs, J., and Klitzsch, N. (2020). Considerations Regarding Small-Scale Surface and Borehole-To-Surface Electrical Resistivity Tomography. *J. Appl. Geophys.* 172, 103862. doi:10.1016/j.jappgeo.2019.103862

Odeh, A. S. (1959). Effect of Viscosity Ratio on Relative Permeability (Includes Associated Paper 1496-G). *Pet. Trans. AIME* 216, 346–353. doi:10.2118/1189-g

Olejnik, S., Posner, A. M., and Quirk, J. P. (1974). Swelling of Montmorillonite in Polar Organic Liquids. *Clays and Clay Minerals* 22, 361–365. doi:10.1346/ccmn.1974.0220407

Pan, S., Zuo, J. Y., Chen, Y., and Mullins, O. C. (2016). A Multicomponent Diffusion Model for Gas Charges into Oil Reservoirs. *Fuel* 180, 384–395. doi:10.1016/j.fuel.2016.04.055

Peters, K. E., and Moldowan, J. M. (1993). *The Biomarker Guide: Interpreting Molecular Fossils in Petroleum and Ancient Sediments*. United States.

Potter, T. L., and Simmons, K. E. (1998). "Composition of Petroleum Mixtures," in *Total Petroleum Hydrocarbon Criteria Working Group Series* (Amherst: Amherst Scientific Publishers), 2, 102.

Ravi, S., D'Odorico, P., Over, T., and Zobeck, T. (2004). On the Effect of Air Humidity on Soil Susceptibility to Wind Erosion: The Case of Air-Dry Soils. *Geophys. Res. Lett.*, 31. doi:10.1029/2004gl019485

Rezanezhad, F., Quinton, W. L., Price, J. S., Elrick, D., Elliot, T. R., and Heck, R. J. (2009). Examining the Effect of Pore Size Distribution and Shape on Flow through Unsaturated Peat Using 3-D Computed Tomography. *Hydrol. Earth Syst. Sci. Discuss.* 6, 3835–3862.

Rostron, P. D., Heathcote, J. A., and Ramsey, M. H. (2014). Comparison Betweenin Situandex Situgamma Measurements on Land Areas within a Decommissioning Nuclear Site: a Case Study at Dounreay. *J. Radiol. Prot.* 34, 495–508. doi:10.1088/0952-4746/34/3/495

Sadler, R., and Connell, D. (2003). "Analytical Methods for the Determination of Total Petroleum Hydrocarbons in Soil," in *The Fifth National Workshop on the Assessment of Site Contamination*. Editors A. Langley and M. B. GilbeyKennedy (Canberra ACT: The National Environment Protection Council), 133–150.

Saidian, M., Kuila, U., Godinez, L. J., Rivera, S., and Prasad, M. (2014). "A Comparative Study of Porosity Measurement in MudRocks," in *SEG Denver 2014 Annual Meeting*. Denver, Colorado, 2433. doi:10.1190/segam2014-0426.1

Salehi, M. H., Hashemibeni, O., Beigiharchegani, H., Esfandiarpour Borujeni, I., and Motaghian, H. R. (2011). Refining Soil Organic Matter Determination by Loss-On-Ignition. *Pedosphere* 21, 473–482. doi:10.1016/s1002-0160(11)60149-5

Sandberg, C. R., Gournay, L. S., and Sippel, R. F. (1958). The Effect of Fluid-Flow Rate and Viscosity on Laboratory Determinations of Oil-Water Relative Permeabilities. *Pet. Trans. AIME* 213, 36–43. doi:10.2118/709-g

Schuler, B., Fatayer, S., Meyer, G., Rogel, E., Moir, M., Zhang, Y., et al. (2017). Heavy Oil Based Mixtures of Different Origins and Treatments Studied by Atomic Force Microscopy. *Energy Fuels* 31 (7), 6856–6861. doi:10.1021/acs.energyfuels.7b00805

Schuler, B., Meyer, G., Peña, D., Mullins, O. C., and Gross, L. (2015). Unraveling the Molecular Structures of Asphaltenes by Atomic Force Microscopy. *J. Am. Chem. Soc.* 137 (31), 9870–9876. doi:10.1021/jacs.5b04056

Schulze, S., Nikrityuk, P. A., and Meyer, B. (2015). Porosity Distribution in Monodisperse and Polydisperse Fixed Beds and its Impact on the Fluid Flow. *Particularte Sci. Technology* 33. doi:10.1080/02726351.2014.923960

Setia, R., Verma, S. L., and Marschner, P. (2012). Measuring Microbial Biomass Carbon by Direct Extraction - Comparison with Chloroform Fumigation-Extraction. *Eur. J. Soil Biol.* 53, 103–106. doi:10.1016/j.ejsobi.2012.09.005

Sihota, N. J., Singurindy, O., and Mayer, K. U. (2011). CO2-Efflux Measurements for Evaluating Source Zone Natural Attenuation Rates in a Petroleum Hydrocarbon Contaminated Aquifer. *Environ. Sci. Technol.* 45, 482–488. doi:10.1021/es1032585

Singer, D. V. E. M. (2007). *Well Logging for Earth Scientists*. Dordrecht: Springer.

Sookhak Lari, K., Davis, G. B., and Johnston, C. D. (2016). Incorporating Hysteresis in a Multi-phase Multi-Component NAPL Modelling Framework; a Multi-Component LNAPL Gasoline Example. *Adv. Water Resour.* 96, 190–201. doi:10.1016/j.advwatres.2016.07.012

Sookhak Lari, K., Davis, G. B., Rayner, J. L., Bastow, T. P., and Puzon, G. J. (2019). Natural Source Zone Depletion of LNAPL: A Critical Review Supporting Modelling Approaches. *Water Res.* 157, 630–646. doi:10.1016/j.watres.2019.04.001

Soriano-Disla, J. M., Janik, L. J., Viscarra Rossel, R. A., MacDonald, L. M., and McLaughlin, M. J. (2014). The Performance of Visible, Near-, and Mid-infrared Reflectance Spectroscopy for Prediction of Soil Physical, Chemical and Biological Properties. *Appl. Spectrosc. Rev.* 49, 139–186. doi:10.1080/05704928.2013.811081

Spencer, W. F. (1970). "Distribution of Pesticides between Soil, Water and Air," in *Pesticides in the Soils: Ecology, Degradation and Movement* (Michigan, U. S.: Michigan State University), 120–128.

Spurlin, M. S., Barker, B. W., Cross, B. D., and Divine, C. E. (2019). Nuclear Magnetic Resonance Logging: Example Applications of an Emerging Tool for Environmental Investigations. *Remediation* 29, 63–73. doi:10.1002/rem.21590

Srinivasulu, M., and Rangaswamy, V. (2006). Activities of Invertase and Cellulase as Influenced by the Application of Tridemorph and Captan to Groundnut (*Arachis hypogaea*) Soil. *Afr. J. Biotechnol.* 5, 175–180.

TNRCC Total Petroleum Hydrocarbons, TNRCC Method 1005, Revision 03. *2001*. Texas, U.S.: TNRCC.

Torabzadeh, S. J., and Handy, L. L. (1984). *The Effect of Temperature and Interfacial Tension on Water/Oil Relative Permeabilities of Consolidated Sands*. Tulsa, Oklahoma: SPE-AIME.

Uzoije, A. P., and Agunwamba, J. C. (2011). Physiochemical Properties of Soil in Relation to Varying Rates of Crude Oil Pollution. *J. Environ. Sci. Technology* 4, 313–323. doi:10.3923/jest.2011.313.323

van Darn, J. (1967). *The Migration of Hydrocarbons in a Water-Bearing Stratum, Joint Problems of the Oil and Water Industries*. London: The institution of Petroleum.

Visotin, A., and Lennard, C. (2016). Preliminary Evaluation of a Next-Generation Portable Gas Chromatograph Mass Spectrometer (GC-MS) for the On-Site Analysis of Ignitable Liquid Residues. *Aust. J. Forensic Sci.* 48, 203–221. doi:10.1080/00450618.2015.1045554

Volkov, D. S., Rogova, O, B., and Proskurnin, M. A. (2021). Organic Matter and Mineral Composition of Silicate Soils: FTIR Comparison Study by Photoacoustic, Diffuse Reflectance, and Attenuated Total Reflection Modalities. *agronomy* 11 (1879), 30. doi:10.3390/agronomy11091879

Wang, L., Cheng, Y., Lamb, D., Dharmarajan, R., Chadalavada, S., and Naidu, R. (2019). Application of Infrared Spectrum for Rapid Classification of Dominant Petroleum Hydrocarbon Fractions for Contaminated Site Assessment. *Spectrochimica Acta Part A: Mol. Biomol. Spectrosc.* 207, 183–188. doi:10.1016/j.saa.2018.09.024

Wang, L., Cheng, Y., Lamb, D., and Naidu, R. (2020). The Application of Rapid Handheld FTIR Petroleum Hydrocarbon-Contaminant Measurement with Transport Models for Site Assessment: a Case Study. *Geoderma* (114017), 361. doi:10.1016/j.geoderma.2019.114017

Wang, L., Cheng, Y., Naidu, R., Chadalavada, S., Bekele, D., Gell, P., et al. (2021a). Application of Portable Gas Chromatography-Mass Spectrometer for Rapid Field Based Determination of TCE in Soil Vapour and Groundwater. *Environ. Technol. Innov.* 1001274, 21. doi:10.1016/j.eti.2020.101274

Wang, L., Cheng, Y., Naidu, R., Gell, P., and Bowman, M. (2021b). Rapid In-Field Approaches for Delineating VOC in Both Soil Vapour and Groundwater for Vapour Intrusion Assessment. *Front. Environ. Sci.* 9. doi:10.3389/fenvs.2021.746195

Wang, Z., and Fingas, M. (1995). Differentiation of the Source of Spilled Oil and Monitoring of the Oil Weathering Process Using Gas Chromatography-Mass Spectrometry. *J. Chromatogr. A* 712, 321–343. doi:10.1016/0021-9673(95)00546-y

Weisman, W. (1998). Analysis of Petroleum Hydrocarbons in Environmental media. *Total Pet. Hydrocarbon Criteria Working Group Ser.* 1, 98.

Wenger, L. M., Davis, C. L., and Isaksen, G. H. (2002). Multiple Controls on Petroleum Biodegradation and Impact on Oil Quality. *SPE Reservoir Eval. Eng.* 5, 375–383. doi:10.2118/80168-pa

Wiedemeier, T. H., Wilson, J. T., Kampbell, D. H., Miller, R. N., and Hansen, J. E. (1995). "Technical Protocol for Implementing Intrinsic Remediation with Long-Term Monitoring for Natural Attenuation of Fuel Contamination Dissolved in Groundwater," in *T.T.D. Ir Force Center for Environmental Excellence* (Texas, United States: Brooks Air Force Base), 295.

Wild, A. (1993). *Soils and the Environment: An Introduction*, 156. Cambridge,U K: Cambridge University Press, 429.

Williams, S. D., Ladd, D. E., and Farmer, J. J. (2002). "Fate and Transport of Petroleum Hydrocarbons in Soil and Ground Water at Big South Fork National River and Recreation Area," in Geological Survey Scientific Investigations Report 2005-2014. *2003* (U.S.: Tennessee and Kentucky), 29.

Yaron, B. (1989). On the Behavior of Petroleum Hydrocarbons in the Unsaturated Zone: Abiotic Aspects. *Ecol. Study* 73, 211–230. doi:10.1007/978-3-642-74468-6_10

Yerokun, O. A., Chikuta, S., and Mambwe, D. (2007). An Evaluation of Spectroscopic and Loss on Ignition Methods for Estimating Soil Organic Carbon in Zambian Soils. *Int. J. Agric. Res.* 2 (11), 965–970. doi:10.3923/ijar.2007.965.970

Yong, R. N., Mohamed, A. M. O., and Warkentin, B. P. (1992). *Principles of Contaminant Transport in Soils*. Amsterdam: Elsevier.

Zolfaghari, Z., Mosaddeghi, M. R., and Ayoubi, S. (2015). ANN-based Pedotransfer and Soil Spatial Prediction Functions for Predicting Atterberg Consistency Limits and Indices from Easily Available Properties at the Watershed Scale in Western Iran. *Soil Use Manage* 31 (1), 142–154. doi:10.1111/sum.12167

Zolfaghari, Z., Mosaddeghi, M. R., Ayoubi, S., and Kelishadi, H. (2015). Soil Atterberg Limits and Consistency Indices as Influenced by Land Use and Slope Position in Western Iran. *J. Mt. Sci.* 12 (6), 1471–1483. doi:10.1007/s11629-014-3339-z

Zuo, J. Y., Jackson, A., Herold, B., Kumar, S., Santo, I. D., Dumont, H., et al. (2015). Diffusion Model Coupled with the Flory-Huggins-Zuo Equation of State and Yen-Mullins Model Accounts for Large Viscosity and Asphaltene Variations in a Reservoir Undergoing Active Biodegradation. *Energy Fuels* 29, 1447–1460. doi:10.1021/ef502586q

Conflict of Interest: The authors declare that the research was conducted in the absence of any commercial or financial relationships that could be construed as a potential conflict of interest.

Publisher's Note: All claims expressed in this article are solely those of the authors and do not necessarily represent those of their affiliated organizations, or those of the publisher, the editors, and the reviewers. Any product that may be evaluated in this article, or claim that may be made by its manufacturer, is not guaranteed or endorsed by the publisher.

frontiers | Frontiers in Environmental Science

SYSTEMATIC REVIEW
published: 04 May 2022
doi: 10.3389/fenvs.2022.732734

Evolution and Trend Analysis of Research Hotspots in the Field of Pollution-Intensive Industry Transfer—Based on Literature Quantitative Empirical Study of China as World Factory

Langang Feng[1,2], *Shu Shang*[2], *Xin Feng*[3]*, *Ying Kong*[4] *and Jiahe Bai*[2]

[1]Guizhou Key Laboratory of Big Data Statistical Analysis, Guizhou University of Finance and Economics, Guiyang, China, [2]School of Big Data Applications and Economics, Guizhou University of Finance and Economics, Guiyang, China, [3]School of Economics and Management, Yanshan University, Qinhuangdao, China, [4]School of Foreign Languages and Culture, Hebei Geo University, Shijiazhuang, China

OPEN ACCESS

Edited by:
Balaji Seshadri,
The University of Newcastle, Australia

Reviewed by:
Elena Sezenna,
Politecnico di Milano, Italy
Yanju Liu,
The University of Newcastle, Australia

***Correspondence:**
Xin Feng
149987543@qq.com

Specialty section:
This article was submitted to Toxicology, Pollution and the Environment, a section of the journal Frontiers in Environmental Science

Received: 29 June 2021
Accepted: 29 March 2022
Published: 04 May 2022

Citation:
Feng L, Shang S, Feng X, Kong Y and Bai J (2022) Evolution and Trend Analysis of Research Hotspots in the Field of Pollution-Intensive Industry Transfer—Based on Literature Quantitative Empirical Study of China as World Factory. Front. Environ. Sci. 10:732734. doi: 10.3389/fenvs.2022.732734

Background: The transfer of pollution-intensive industries in China accounts for an increasing proportion of industrial transfer, and related studies emerge endlessly. Fully exploring its research and development breadth and depth will help clarify the development trend in this field and point out the direction for future research.

Method/Process: From the perspective of bibliometric analysis, with keywords as the core and cluster analysis of research hotspots as the basis, the keywords of pollution-intensive industry transfer in CNKI database are analyzed by CiteSpace software and divided into five categories. Established the text corpus model, and the network analysis transformed into a visual form. Due to the diverse research hotspots in pollution-intensive industry transfer, this article analyzes the evolution of research hotspots in this field to predict its future development trend.

Conclusion/Significance: China, as the world's factory, is affected by relevant policies, and industrial transfers have generally occurred. Industrial transfer, especially the transfer of pollution-intensive industries, has gradually attracted the attention of academic circles and has become a hot topic. When dealing with the transfer of pollution-intensive industries, industrial transfer only transfers pollution across regions. If we want to reduce pollution from the origin, innovation is an essential means. In retrospect, there were rare articles concerning the emerging polluting industries, however, recently since the emerging polluting industries have already constituted as the main source of pollution, more academic attentions are definitely needed. Although the mainstream measurement methods, the related share index method, and the input-output table have their weaknesses, respectively, the deviation share method can overcome the shortcomings of both. Therefore, it can be used as a reference for scholars to measure the transfer of pollution-intensive industries in the future.

Keywords: pollution-intensive industry, industry transfer, bibliometric analysis, environmental pollution, China

INTRODUCTION

The pollution-intensive industries refer to those industries that produce a large number of pollutants indirectly or directly in the process of production. If humans do not treat them, they will be harmful to human, animal, and plant health, affect the quality of the ecological environment, and lead to environmental deterioration (Fang-dao et al., 2013). The pollution-intensive industries usually shift from high-income areas to low-income areas and move from developed areas to underdeveloped regions.

Environmental degradation and environmental quality degradation have become hot topics, and the academic circle is paying more and more attention to environmental issues. Pollutants from pollution intensive industries are the main source of environmental pollution. Zhang et al. (2019) and Wang and Li (2020) proposed that the industrial sector is closely related to the environment, especially the pollution-intensive industries, which are the leading cause of environmental degradation and top priority energy conservation and emission reduction. Keting and Jianjian (2011) proposed that carbon emissions mainly come from industries, and the energy-intensive industries account for about 80% of the total industrial emissions. Tao (2013) and Haixia et al. (2020) believed that although industrial enterprises have gained some economic gains, they have also paid a massive price to damage the environment. Marland and Rotty (1984) studied that carbon dioxide (CO_2) emission generated from urban industrial fossil fuels is gradually recognized as a significant contributor to global climate change. Deng et al. (2012) believed that China is the world's largest energy consumer and dominates global energy consumption, global crude oil imports, global coal consumption, global electricity consumption, and global CO_2 emissions. Arce et al. (2016) studied that China has become the world's largest carbon dioxide emitter. In recent decades, China has become the "world factory" (World Trade Organization, 2019), so most existing research is on how to reduce pollution emissions in China to improve the current climate. Simultaneously, due to the environmental regulations and innovation capabilities in different regions of China, the transfer of pollution-intensive industries[1] has become increasingly common, leading to a broader national ecological pollution problem. Caiyun and Yanqing (2015) exclaimed that the environment in developed countries and regions had been continuously improving. In contrast, the environment in developing countries and underdeveloped areas has deteriorated rapidly due to pollution transfer. Therefore, the study of this article on the transfer of pollution-intensive industries in the world's factories in China has important practical significance.

Due to the authority and subjectivity of China's pollution-intensive industry transfer policy, there is a lot of literature in this field. The previous study mostly adopted the traditional literature review method and only summarized the research contents of the transfer of pollution-intensive industries. For example, Qiwen et al. (2020) systematically summarized the concepts and categories of polluting enterprises/industries, and summarized the transfer characteristics, patterns, and dynamic mechanisms of polluting enterprises/industries. However, as far as we know, few studies have used bibliometrics to conduct literature reviews. Therefore, it is essential to systematically sort out, measure, and analyze the literature on the transfer of pollution-intensive industries. This article uses literature analysis, word frequency statistics, and cluster analysis to study the existing literature on the transfer of pollution-intensive industries with data extracted from CNKI (database of over 2000 Chinese journals) to analyze keyword frequency, hotspot clustering, changes, and trends. Besides, it uses CiteSpace to visualize the filtered data to clarify the evolution and development trend of hot spots in this field and to provide a quantitative basis for policy-making.

DATA ACQUISITION AND RESEARCH METHODS

Data Acquisition

This article takes CNKI database as the literature retrieval system to comprehensively analyze the evolution and trend changes of research hotspots in the field of pollution-intensive industrial transfer. The selected keywords, based on Jiang et al. (2017) are "pollution industry transfer" or "pollution-intensive industry transfer" or "energy industry transfer" or "heavy pollution industry transfer" or "steel industry transfer" or "chemical industry transfer,"[2] and source category selection "all journals." The time span is set from 1990 to 2020.[3] The selected data include the following information: "Title," "Summary," and "Keywords." In order to reflect the typicality and relevance of the selected literature, the repetitive literature is manually removed, finally 593 authoritative and comprehensive academic journal articles are have been finally obtained. Then the papers are downloaded in the text file "txt" format, and the contents of "Title," "Summary," and "Keywords" in these 593 papers are used as data samples for this analysis.

Research Method

Bibliometrics is a kind of measurement method which statistically analyses the research status and research products of a particular

[1]Changes in the geographical spatial distribution of pollution-intensive industries or industrial group, i.e., from one country or region to another.

[2]Pollution industry, energy industry, heavy pollution industry, steel industry, and chemical industry will produce more pollutants in the production process (Jiang Shurui et al., 2017). This article selects the above industries to represent pollution intensive industries.

[3]1990 was selected as the starting point as the earliest research literature data appeared in that year.

field. Compared with traditional ways of literature review, the use of professional bibliometric methods is characterized by large capacity, long time span, and multi-dimensional analysis and visual presentation. This article uses the bibliometric method to analyze and summarize the research on the transfer of pollution-intensive industries. It primarily uses the literature analysis, the word frequency statistical, and the cluster analysis as follows:

1) Literature analysis method refers to a technique that makes quantitative statistics on bibliographies, abstracts, or indexes of a particular research topic and draws statistical results or analytic conclusions. It can help investigators form a general impression of the research objects, help them grasp the historical dynamics of the research objects, and also study the research objects that are impossible to approach, such as those who have already died. This article uses the CNKI database to collect data from the literature on the evolution of characteristics in pollution-intensive industry transfer and count the number of existing research in this field.
2) Word frequency statistical method is mainly a statistical analysis of the number of keywords that can reveal the core content of literature in a certain field. It is an important means of text mining and a traditional and representative content analysis method in bibliometrics. The basic principle is to determine the hot spots and their changing trends through the change of word frequency (Heting, 2019). The higher the frequency of keyword occurrence, the higher the attention on this topic. This method can determine hotspots of the research and development status in a specific area. This article analyzes the frequency of keywords on the transfer of pollution-intensive industries in three parts, i.e., title, summary, and keywords, aiming to determine the hot spots and their changing trends in this field.
3) Cluster analysis is a statistical method that divides the research objects in a particular field into several groups. The research objects in each group have similar characteristics, and each group is mutually exclusive (Xin et al., 2020). Cluster analysis from the selection of keywords analysis to the generation of clusters is carried out in the form of mathematical statistics, which can reduce human intervention and make the results of co-word clustering objectively and truly reflect the current situation of literature group content (Wenjin et al., 2008). This method can form an intuitive network graph of several research objects in a specific field. This article uses the Log-Likelihood Ratio (LLR) algorithm in Citespace software to cluster the keywords in the three parts of title, abstract, and keywords in the field of pollution-intensive industrial transfer research, and then forms an intuitive keyword clustering view.

Research Tool

This article uses CiteSpace software to analyze, draws a visual map of the research on the transfer of pollution-intensive industries, analyzes the high-frequency keywords and co-occurrence network, and predicts the development trend of the pollution-intense industry transfer field through keyword time zone diagram. It is beneficial to understand the area of pollution-intensive industry transfer better by clarifying the internal dynamic mechanism of the study and exploring the subject development of the pollution-intensive industry transfer.

ANALYSIS OF RESEARCH RESULTS

High-Frequency Keywords and Keyword Co-Occurrence Network

In order to grasp the research hotspots in the field of pollution-intensive industry transfer, this article makes a statistical analysis of the keywords in the "title," "summary," and "keywords" parts of 593 papers on pollution-intensive industry transfer, and obtains the frequency of keywords and the information of their first occurrence years. The content of this research field is mainly from five categories: basic theory, measure method, influence factors, hot area, and economy and environment. The basic theory mainly discusses the relevant hypothesis and theory in the field of pollution-intensive industry transfer; the measure method shows the relevant methods to measure the transfer of pollution-intensive industries; and the influence factors affecting the transfer of pollution-intensive industries are introduced. For example, environmental regulations with different intensities in various regions will make the transfer of pollution-intensive industries from regions with higher environmental regulations to regions with lower environmental regulations occur. The mechanism of environmental policies such as environmental protection policies and carbon emission regulations is similar to that of environmental regulations. In addition, different levels in regional innovation and foreign direct investment also can lead to pollution-intensive industries transfer; the hot area indicates that Chinese regions which once were key research areas for pollution-intensive industrial have now transferred in the analyzed literature; the economy and environment, economy refers to the economic change caused by the transfer of pollution-intensive industries, or the transfer of pollution-intensive industries caused by different economic factors. Environment refers to the change of environmental situation in the field of pollution-intensive industry transfer and the environmental protection measures taken.

These five categories are discussed from three perspectives: research foundation, research process, and research results; the basic theory and measure method belong to the research basis, the influencing factors belong to the research process, and the hot spots and the economic consequences belong to the study results. These three perspectives cover the vast majority of research contents in the field of pollution-intensive industry transfer. Therefore, in the literature's data set, the literature's keywords are statistically arranged in frequency from more to less. The keywords with higher frequency are divided into five categories according to the research aspects to comprehensively analyze the hot spot evolution and trend of the research in pollution-intensive industry transfer. The reasons and mechanisms of the transfer of pollution-intensive industries are analyzed to explore the high-frequency keywords in this field. This article

TABLE 1 | The ranking of the frequency of keywords in the field of pollution-intensive industry transfer.

Classification	Keyword	Frequency	Year
Basic theory	Environmental Kuznets curve	10	2006
	The hypothesis of pollution haven	10	2006
	Green barrier	4	2002
	Environmental welfare effect	2	2006
	Total	26	—
Measure method	Deviation share analysis	12	2013
	Industrial competitiveness model	1	2017
	Industrial gradient coefficient	1	2012
	Total	14	—
Influence factor	Environmental regulation	65	1995
	Foreign direct investment	35	2006
	Environmental protection policy	8	2004
	International trade	3	2005
	Innovation	2	2007
	International direct investment	2	2005
	Development strategy	2	2009
	Carbon emission regulation	1	2015
	Total	118	—
Hot area	Central and western region	11	2007
	Beijing-Tianjin-Hebei integration	9	2015
	Guangdong province	5	2007
	One Belt and One Road	3	2016
	Yangtze River economic belt	3	2016
	Tianjin	2	2013
	Beibu Gulf economic zone	2	2008
	Total	35	—
Economy and environment	Environmental protection	15	2003
	Economic growth	9	2013
	Industrial structure	8	2001
	International industrial transfer	7	2004
	Economic development	5	2003
	Air pollution	5	2004
	Carbon emission	3	2014
	Gross domestic product	2	2014
	Environmental investment	2	1998
	Ecological environment protection	2	2005
	Carbon transfer	2	2017
	Eco-environmental effect	2	2009
	CO_2 emission	2	2010
	Globalization	2	2006
	Low carbon economy	2	2015
	Regional economy	2	2015
	Total	70	—

summarizes the occurrence frequency of the top keywords and the information on the first occurrence year (**Table 1**). Among them, the keywords shown in **Table 1** are only some of the top keywords, while the keywords with low occurrence frequency do not show too much.

By dividing the keywords into five categories for research, we can see the high-frequency keywords and their evolution trend in each type of the pollution-intensive industry transfer research field and make a comprehensive analysis of this field. However, it is not easy to thoroughly analyze the five categories' effects in this field and their relationship only through the frequency of keywords and the year of their first appearance. Therefore, this article also adds a mechanism analysis chart to consider the influencing factors and economic consequences in the transfer of pollution-intensive industries and show the relationship between the two categories and the field.

1) Basic theory

From the research in China, the keyword frequency of the primary theory category is 26 times, including environmental Kuznets curve, the hypothesis of pollution haven, green barrier, and environmental welfare effect. They first appeared between 2002 and 2006. With the deepening of the research, the theoretical basis of the transfer of pollution-intensive industries in China is becoming more affluent. Scholars have also realized that the

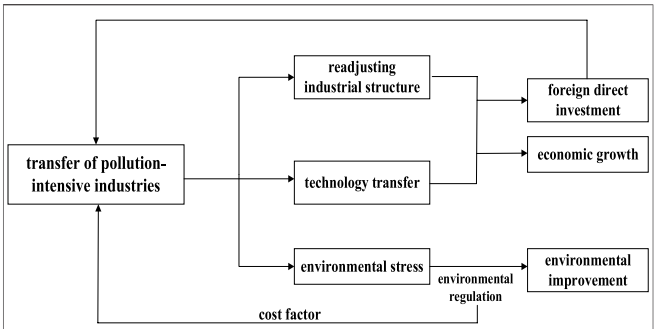

FIGURE 1 | Analysis of the transfer mechanism of pollution-intensive industries.

research on the transfer of pollution-intensive industries is developing dynamically. It is necessary to add the game analysis between the transferor and the receiver into the research framework of the transfer of pollution-intensive industries.

2) Measure method

The keyword frequency of measure method class is 14 times in total, including deviation share analysis, industrial competitiveness, and industrial gradient coefficient. The industrial gradient coefficient was first introduced into the study of pollution-intensive industry transfer in 2012, and "deviation share analysis" was firstly applied to the transfer measure of pollution-intensive industries in 2013. It was only in 2017 that the industrial competitiveness model was combined with the transfer of pollution-intensive industries.

3) Influence factor

The keyword frequency of influencing factors appeared 118 times in total. The keyword of environmental regulation appeared in 1995 and was the earliest keyword with a frequency of 65 times, indicating that environmental regulation is the most crucial factor affecting the transfer of pollution-intensive industries. Besides the ecological regulations, various policies and measures also impact the transfer of pollution-intensive industries, such as environmental protection policy, development strategy, and carbon emission regulation. Among them, regions with strict environmental regulations have high pollution costs. The pollution-intensive industries shift from areas with increased environmental regulations to low environmental regulations to save costs. International trade also plays a decisive role in influencing the transfer of pollution-intensive industries. Foreign direct investment appeared 35 times in 2006; international trade appeared three times in 2005; and international direct investment appeared two times in 2005. Innovation first appeared in 2007 and appeared twice. Innovation ability is a relatively new influencing factor and the primary means to solve the root causes of global environmental pollution caused by the transfer of pollution-intensive industries. We firmly believe that research on innovation ability is worthy of scholars' attention.

To clarify the relationship between this field and other categories of mechanical principles with influencing factors, **Figure 1** is drawn to analyze the mechanism in this field. From this, we can see that the transfer of pollution-intensive industries leads to industrial restructuring, technology transfer, environmental pressure, and other economic consequences. Industrial restructuring and technology transfer promote foreign direct investment and enable economic growth; because of the high environmental stress, the environmental regulations formulated by the government tend to be stricter, which in turn improves the environment. Besides, stringent environmental regulations raise costs for enterprises, which definitely lead to the relocation of pollution-intensive industries. Therefore, conclusion is drawn that the economic consequences generated by the transfer of pollution-intensive industries further promote the influencing factors, which in turn stimulate the transfer of pollution-intensive industries, forming a mutual promotion mechanism.

4) Hot area

The keyword frequency of hot area was 35 times in total, including central and western regions, Beijing-Tianjin-Hebei integration, Guangdong province, One Belt and One Road Region, and Yangtze River Economic Belt, which firstly appeared in 2007, 2015, 2007, 2016, and 2016, respectively. Overall, research in the central and western regions appeared earlier. But in recent years, as regional development strategy demonstration belts Beijing-Tianjin-Hebei, One Belt and One Road Region, and Yangtze River Economic Belt have gradually attracted academic attentions. The Beijing-Tianjin-Hebei region is called the "Capital Economic Circle" in China. The Yangtze River Economic Belt and One Belt and One Road Region are the primary development strategies of China at present. Simultaneously, Beijing-Tianjin-Hebei, Yangtze River Delta, and other regions are economically developed regions and heavily polluted regions as well, which have already become research hotspots in recent years.

5) Economic consequences

The keyword frequency of economic consequences was 35 times in total, including environmental protection, economic growth, industrial structure, international industrial transfer, economic development, air pollution, and carbon emission, which first appeared in 2003, 2013, 2001, 2004, 2003, 2004, and 2014, respectively. The keywords of economic consequences run through the fundamental research, which is a hot spot in the transfer of pollution-intensive industries and a bridge linking pollution-intensive industries with the influencing factors.

By analyzing high-frequency keywords, we find that, as the world's factory, China is affected by environmental policies and other factors. Industrial transfer generally occurs especially in the transfer of pollution-intensive industries, which has gradually attracted academic attention. While environmental regulation is the most crucial factor affecting the transfer of pollution-intensive industries, innovation ability is a relatively new

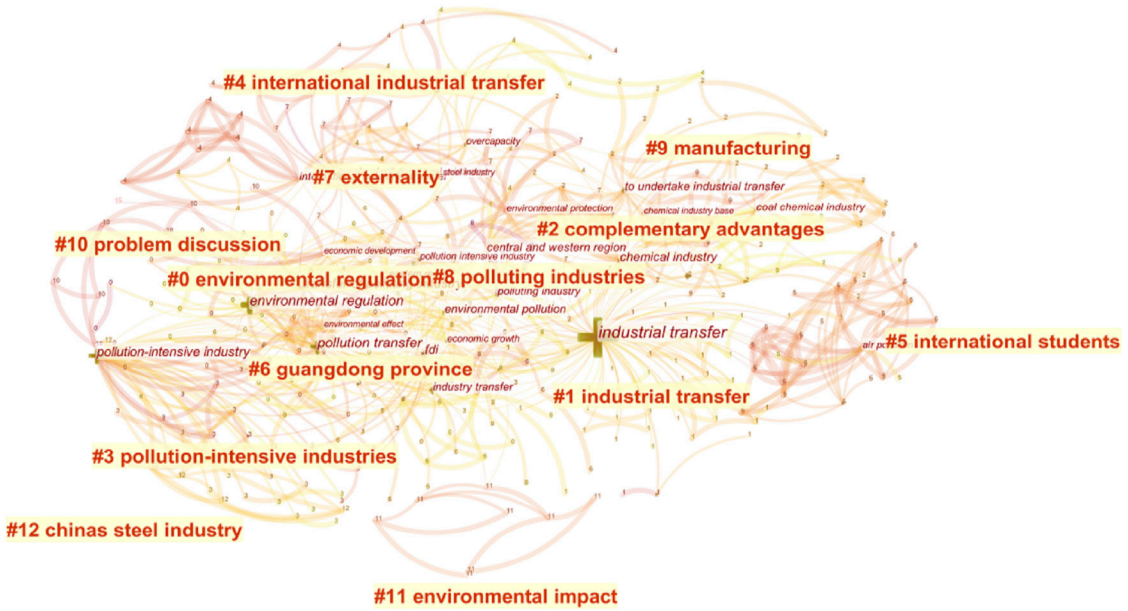

FIGURE 2 | Clustering view of keywords for the transfer of the pollution-intensive industries.

influencing factor. As the theoretical basis for the transfer of pollution-intensive industries in China is becoming more and more abundant, the measurement methods are also changing rapidly. Deviation share analysis was first combined with the transfer of pollution-intensive industries in 2013. It is the most frequently used measurement method so far, and the one we believe has the best research prospect.

Research Hotspot Cluster Analysis

To quickly and accurately sort out the Frontier hotspots in this study field, find out which keywords are vital in the literature network, this study uses the Log-Likelihood Ratio (LLR) algorithm to conduct cluster analysis on the study hotspots through CiteSpace software. Through the cluster view, we can find the Frontier hotspots and keywords in the field of pollution-intensive industry transfer research. This article selects the top 50 keywords from each article for statistical analysis and clustering and obtains a total of 527 keywords[4] (**Figure 2**).

Through cluster analysis, the keywords of the research literature in the field of pollution-intensive industry may be grouped into 12 categories, including environmental regulation, industrial transfer, complementary advantages, pollution-intensive industries, international industrial transfer, international students, Guangdong province, externality, polluting industries, manufacturing, problem discussion, and China's steel industry (**Figure 2**). Cluster analysis can quickly understand the clustering situation of the research field to grasp the hot study topics in this field. Besides, this article further divides the 12 clusters into five categories according to the above categories for specific analysis: theoretical basis, measurement method, influencing factors, research area, and economic consequences to clarify the research context of the transfer of pollution-intensive industries and capture the Frontier hotspots in this field.

1) Basic theory

The theoretical basis category, pollution haven, environmental Kuznets curve, and green barrier are the fundamental theories in pollution-intensive industry transfer. Scholars such as Chichilnisky (1994), Copeland (1994), Baumol and Oates (1988), Copeland and Taylor (2004), and Dean et al. (2008) theoretically explained the existence of pollution refuges. Qiying and Haitao (2019) based on the two opposing theories of "pollution haven" and "pollution halo," tested the pollution refuge effect of foreign investment. Hui and Jin-xi (2020) used the environmental Kuznets curve to measure the pollution transfer in Beijing and Hebei Province.

2) Measure method

The measure methods include the deviation share method, the industrial competitiveness model, and the industrial gradient coefficient, which shows that scholars mainly use these models in the pollution-intensive industrial transfer. The industrial competitiveness model and the industrial gradient coefficient belong to the relative share index method. Based on the basic idea of the deviation share method, Ai-hua and Fan (2018) constructed an improved model of regional industrial transfer and pollution transfer and carried out quantitative measurement

[4]The top 50 keywords in each article have the same rate, so the number of keywords obtained is less than the total number of articles.

of restricted industrial transfer and pollution transfer in China. Mei (2006) used the industrial competitiveness coefficient to prove the regional correlation of the effects of carbon emission influencing factors. Through literature review, we found three main categories of measurement methods for the transfer of pollution-intensive industries. In addition to the two mentioned above, many scholars also use input-output tables to measure the transfer of pollution-intensive industries. For example, Hong-guang et al. (2011) established a quantitative method to calculate the regional industrial transfer using the regional input-output model. They also combined the China regional input-output table, and estimated the regional industrial transfer in China from 1997 to 2007.

3) Influence factor

The influencing factors mainly include environmental regulation and foreign direct investment. Besides, innovation capacity also has a specific impact on the transfer of pollution-intensive industries. For example, Bing-tao and Li-ming (2019) studied that with the relative environmental regulation intensity from low to high, the environmental pollution caused by the transfer of highly polluting industries became severe. Bing-tao and Li-ming (2019) studied the relationship between the foreign direct investment of American enterprises and the cost of pollution reduction. They found that industries with high price of emission reduction were more inclined to make foreign investment. The impact of international trade on the transfer of pollution-intensive industries is noticeable. Wang and Huang (2015) explored that in the long run, effectiveness means to solve the problem of environmental pollution mainly depending on technological progress, especially green technology-oriented innovation (Zhiqing et al., 2014).

4) Hot area

The study regions mainly include Guangdong, Western China, Beijing-Tianjin-Hebei, One Belt and One Road Region, and Yangtze River Economic Belt. Among them, the central and western regions are the essential places for industrial transfer, and the eastern areas are the main places for industrial transfer. Longbin (2013) confirmed that the west part is the transfer area of most polluting industries through the statistics of the transfer and outflow of representative products of polluting industries in different regions of China; Qi (2014) found that the east part is the leading area of industrial transfer, while the central and western are the main receiving areas for industrial transfer; Hui and Jinxi (2020) found that along with the regional industrial transfer between Beijing and Hebei province, there is also a noticeable transfer of regional environmental pollution sources in them; Tang et al. (2017) considered that the Beijing-Tianjin-Hebei Integration Strategy was driving industrial transfer from Beijing to Hebei; Chen et al. (2017) by applying LMDI method to the industrial transfer theory, evaluated driving forces of carbon emission changes from manufacturing industries in the Pearl River Delta (PRD) of China; Youjin et al. (2020) considered the technological symbiosis, industrial symbiosis and market symbiosis are critical transmission paths to promote China's industrial transfer to "One Belt and One Road" countries to achieve mutual benefits; Chen et al. (2019) considered that there is a trend of gradient transfer of "One Belt and One Road" industries, especially polluting industries.

5) Economic consequences

Economic consequences mainly summarize a series of effects of the transfer of pollution-intensive industries, such as complementary, international industrial transfer, problem discussion, environmental pollution, industrial upgrading, economic growth, and industrial structure adjustment. Wen-bin and Fang-yi (2018) believed the pollution-intensive industries were important primary industries, and there were many related industries upstream and downstream which provided essential raw materials and energy for China's economic construction and played a vital role in supporting the development of the national economy. Bo et al. (2020) suggested that manufacturing was directly or indirectly linked to nearly three-quarters of China's energy-related greenhouse gas emissions in 2012. Ke-ting and Jian-jian (2011) studied that pollution-intensive industries consumed a lot of energy and were characterized as high emissions and pollution sources, putting tremendous pressure on ecological and environmental protection and national energy security. Mulatu, (2014) discussed that environmental pollution from the pig industry is an urgent problem to be studied and solved, especially on large-scale pig farms.

Throughout the academic circles, we found that the current research in this field focuses on environmental pollution, environmental protection, economic growth, industrial structure adjustment, and other impacts of the transfer of pollution-intensive industries, while ignoring the research of the transfer location. Thus, the study on the intensive industry transfer field is designed to be conducted from two aspects. The first one is the positive effect of industrial transfer on transfer, including improving industrial status, promoting advanced industrial structure, and improving environmental pollution; the second is the negative effect of industrial transfer on transfer, including reducing the competitiveness and employment of transferred industries.

Keywords Vicissitude and Trend Forecast

The transfer of pollution-intensive industries will not only promote economic development but also bring some environmental problems. This article combines the time zone diagram of research keywords in pollution-intensive industry transfer (**Figure 3**), in the environmental regulation research field from 1990 to 2020. Among them, the abscissa represents each year, and the ordinate represents keyword clustering.

The time zone diagram of key words in the study of pollution-intensive industry transfer can intuitively show the change process of research direction over time. From the time trend of the time zone diagram, hot keywords appeared less frequently in 1990–1993, and keywords increased significantly since 1994. However, in order to clarify the research stage of the transfer of pollution-intensive industries, it is not enough to rely far on time zone diagrams. Therefore, based on the analysis of the time zone diagram of pollution-intensive industry transfer, combined with

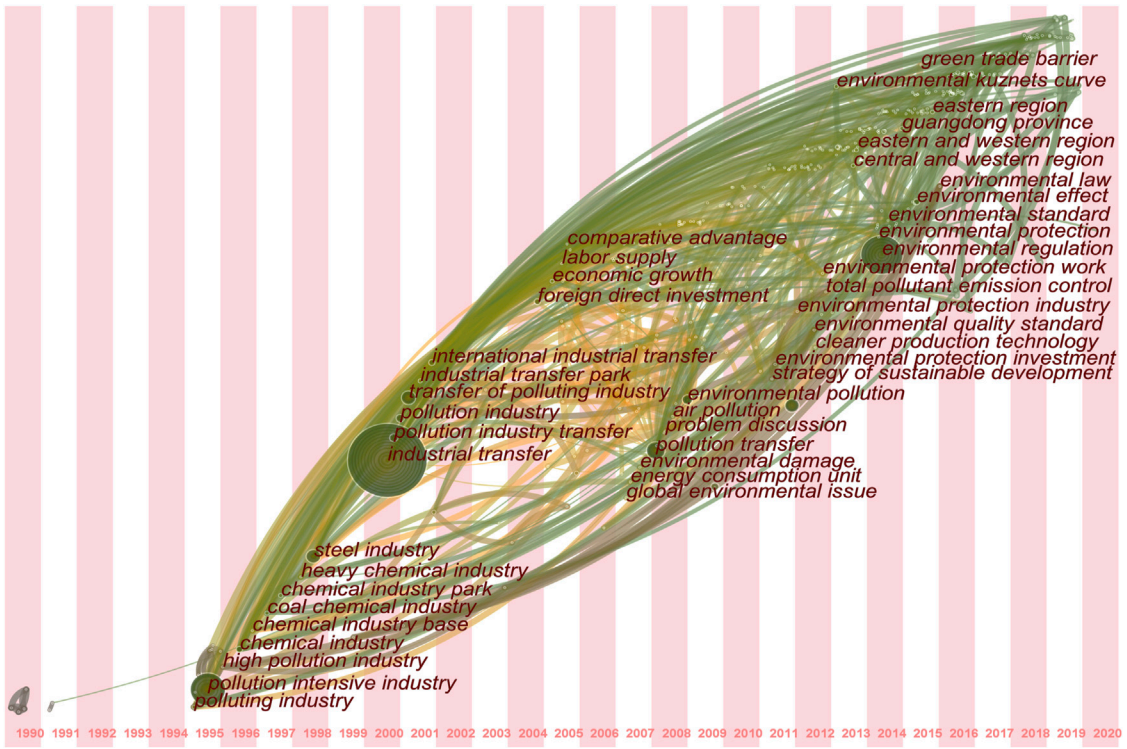

FIGURE 3 | The transfer time zone of pollution-intensive industries.

the specific situation of the fourth and fifth industrial transfer in the world,[5] this article discusses the hot spots of each research stage in the field of pollution-intensive industry transfer. Also, this research can be roughly divided into two research stages: the embryonic stage from 1990 to 2008 and the development stage from 2009 to 2020.

In the embryonic stage from 1990 to 2008, it was the fourth industrial transfer in the world. The importing country was the developing country, which was the biggest beneficiary. At this stage, the study direction of the transfer of pollution-intensive industries in China focuses on the positive benefits of foreign direct investment, economic benefits of pollution industry development, and other developing industries such as manufacturing. In the development stage of 2009–2020, after the outbreak of the international financial crisis in 2008, the fifth world industrial transfer has been ushered in. At this stage, the research direction of scholars is more focused on environmental regulation, environmental pollution, air pollution, environmental control, environmental standard, central region, etc. Based on the embryonic stage, scholars can objectively study the economic effects of the transfer of pollution-intensive industries from both positive and negative sides. At the same time, they enrich their theoretical basis through the Environmental Kuznets curve theory and also begin to conduct in-depth study and reflection on the transfer of pollution-intensive industries in different regions. For example, Jianhua et al. (2016) evaluated some basic problems faced by inter-regional transfer of polluting industries in China, including how to fully define polluting industries, what are the advantages of transfer status, and whether there are some rules to control this situation. Bingtao and Liming (2018) calculated the dynamic agglomeration index of high-pollution industries, the agglomeration index of environmental pollution, and the intensity index of relative environmental regulation, and found that the transfer of high-pollution industries mainly brought about the deepening of the agglomeration degree of industrial wastewater pollution and industrial waste gas pollution.

The study on the transfer of pollution-intensive industries in the two different periods has a different focus, mainly due to the other characteristics of the global industrial transfer in these different periods, thus indicating that the transfer of pollution-intensive industries has a vital "timeliness." In short, the research enthusiasm for fundamental theories and methods in the transfer of pollution-intensive industries has a relatively long duration. In contrast, some special hot spot issues have a relatively short period and are easily affected by the macroeconomic environment at that time. After the 2008 financial crisis, research on whether pollution-intensive industry transfer can solve the financial crisis and improve the economic level has

[5]The time period of the fourth industrial transfer in the world is from the 1980s to the 1990s, and the time of the fifth industrial transfer in the world is after the 2008 financial crisis. The motivation of the world industrial transfer is mainly the change of the world economic situation. Therefore, this article takes these two periods as the basis for dividing the stages of pollution-intensive industrial transfer.

increased rapidly. With the economic recovery, people began to pursue a higher quality of living environment (Hang et al., 2012). So the research on the economic benefits brought by the transfer of pollution-intensive industries has become a hot topic. In the development stage of the transfer of pollution-intensive industries after 2008, the focus of academic research in this field has shifted to the environment (Lihui and Chuanqing, 2021). The government and society have also paid more and more attention to the environmental effect of the transfer of pollution-intensive industries (Zhang et al., 2020), which will force the transfer of pollution-intensive industries to develop toward improving the ecological civilization system, establishing the environmental responsibility of enterprises, and paying attention to the regional differences in the environment, and finally realize the harmonious coexistence of man and nature to jointly build a beautiful world.

CONCLUSION AND OUTLOOK

This article reveals the basic overview of the research field of pollution-intensive industrial transfer in the past 3 decades. Through bibliometric analysis of the literature on pollution-intensive industrial transfer, the following three conclusions are drawn: First, when dealing with pollution-intensive industrial transfer, we found that the transfer of pollution-intensive industries refers to the transfer of pollution-intensive industries across regions, that is, the transfer of pollution-intensive industries from one region to another. This kind of behavior makes the pollutant discharge place of polluting industry change from the place where the polluting industry was transferred from to the current place where the polluting industry is transferred to, which does not reduce the discharge of pollutants from the origin. In order to reduce pollution from the source, corresponding innovations in pollution-intensive industries are the means that must be followed (Wang and Huang, 2015). Secondly, most of the previous articles discussed traditional polluting industries, and the research on traditional polluting industries has been abundant. There are many research countermeasures for the environmental pollution problems caused by traditional polluting industries. However, there are few existing literatures about emerging polluting industries, and there are few solutions for pollution control of emerging polluting industries. The environmental pollution caused by emerging polluting industries, such as pig raising and home appliance industry, has become a major problem, which deserves the attention of scholars. Finally, the mainstream method related to the share index method and the input-output table has certain shortcomings, where the deviation share method can just make up for them both. Among them, the relevant share index method cannot directly show the specific industrial transfer volume; the input-output table is only compiled every 5 years and cannot reflect the latest industrial transfer characteristics. Therefore, the deviation share method is a method that has become popular in recent years. Since this method can overcome the shortcomings mentioned above, it can be used as a reference for future scholars to further study the transfer of pollution-intensive industries.

At present, the research on the transfer of pollution-intensive industries focuses on traditional polluting industries and the areas where pollution-intensive industries are transferred. However, with the continuous emergence of new environmental factors, those problems are becoming more and more serious. In the future, the research on the transfer of pollution-intensive industries should focus on the followings:

1) It is imminent to solve the global pollution caused by the transfer of pollution-intensive industries from the origin.

We found that due to the influence of relevant policies, industrial transfer has occurred generally. With the increase of industrial transfer, industrial transfer, especially the transfer of pollution-intensive industries, has gradually attracted the attention of the academic community becoming a hot topic. The transfer of polluting industries refers to the transfer of polluting industries between regions. This behavior of polluting industries can only change the pollutant discharge places from the place of once out-transfer to the place of in-transfer nowadays. It cannot reduce the environment pollution from the origin. Therefore, in order to reduce the environmental pollution caused by pollution-intensive industries, innovation is the only means that must be followed, i.e., only technological innovation and progress can truly reduce pollution from the very beginning (Peng and Li-wen, 2014). Innovation is not only a key factor affecting the transfer of pollution-intensive industries, but also an important means to solve pollution from the origin, which is worthy of further research by scholars.

2) The out-transfer of industries and the whole transfer of emerging polluting industries will attract academic attentions.

Throughout the academic world, most of the current research focuses on the place where pollution-intensive industries are inherited, while ignoring the places where pollution-intensive industries are transferred. Scholars in the future can conduct in-depth research on the changes in the status, industrial structure, environmental conditions, and employment of the outgoing real estate industry from the perspective of industrial transfer. Here, we refer to non-traditional polluting industries as emerging polluting industries, such as the pig industry mentioned by Mulatu (2014). In the past, farmers were both farming and raising pigs. Pigs to fertile fields and planting constructed a beneficial cycles with each other, so the pressure on environmental protection was relatively low. However, with the specialization and expansion of aquaculture, the main bodies of cultivation and cultivation are separated, therefore, causing serious pollution to the environment. Jianjun et al. (2018) pointed out that since the beginning of the 21st century, the regional transfer of the pig industry has become more and more obvious. Through literature review, we found that most of the previous articles focused on the economic consequences of traditional polluting industries and their industrial transfer, while the economic consequences of emerging polluting

industries were rarely involved. With the advancement of technology, the pollution generated by traditional pollution-intensive industries is easier to solve, while the pollution generated by emerging heavy polluting industries has become a major problem, such as water pollution caused by the pig industry (Jianjun et al., 2018) and household appliances secondary pollution caused by improper disposal of waste household appliances (Ai et al., 2012), unfortunately, there are few related studies related to the field. Therefore, the emerging polluting industries and their transfer deserve the attention of scholars.

3) The deviation share method has become an inevitable choice for measuring the transfer of pollution-intensive industries.

In the measurement method, the relevant share index method is a method with high frequency, but it cannot directly show the specific industrial transfer volume. We found that the inter-regional input-output table and the inter-regional input-output model are more popular research methods. Unfortunately, the input-output table is only compiled every 5 years, so it cannot reflect the latest characteristics of industrial transfer. At present, in the quantitative measurement research of industrial transfer, more and more scholars use the deviation share method to study the problem of industrial transfer. In the research of pollution-intensive industrial transfer, this method has become more popular in recent years and can make up for some deficiencies as for the relevant share index method and the investment-output table. Therefore, it can be used as a reference for future scholars to study the transfer of pollution-intensive industries.

In today's vision of a beautiful world, the transfer of pollution-intensive industries has become a hot topic. This article believes that technological innovation for promoting energy-saving and consumption-reducing equipment renewal as well as production process innovation are the fundamental countermeasure to solve the impact of pollution-intensive industries on the environment. It is suggested that all industrial transfers should aim at "building beautiful and ecological world," fully consider the needs of the ecological well-being of the people, and reduce the impact of industries on the environment from the source. To sum up, we cannot simply pursue the speed of economic development, but fundamentally achieve "good and fast" economic development.

DATA AVAILABILITY STATEMENT

The original contributions presented in the study are included in the article/**Supplementary Material**, further inquiries can be directed to the corresponding author.

AUTHOR CONTRIBUTIONS

LF: conceptualization, methodology, writing-original, funding. SS: writing-original, writing-review-editing, data curation. XF: visualization, formal analysis. YK: translate, supervision. JB: supervision.

FUNDING

The article is supported by the National Natural Science Foundation of China (No: 11905042), Natural Science Foundation of Hebei Province (No: G2021203011), Humanities and Social Science Research Project of Hebei Education Department (No: BJ2017089), and Guizhou Key Laboratory of Big Data Statistical Analysis (No: BDSA20200109).

SUPPLEMENTARY MATERIAL

The Supplementary Material for this article can be found online at: https://www.frontiersin.org/articles/10.3389/fenvs.2022.732734/full#supplementary-material

REFERENCES

Ai, X., Xiangpei, H., and Gao, S. (2012). A Three-Player Game Analysis Among Governments, Enterprises and Consumers in the Green Supply Chain of the Home Appliance Industry. *Sci. Techn. Manage. Res.* 32 (23), 236–240. doi:10.3969/j.issn.1000-7695.2012.23.051

Ai-hua, C., and Fan, Z. (2018). Quantitative Measure on Inter-regional Industry Transfer and Pollution Transfer Based on the Idea of Shift Share Analysis. *China Popul. Resour. Environ.* 28, 49–57. doi:10.12062/cpre.20171209

Arce, G., López, L. A., and Guan, D. (2016). Carbon Emissions Embodied in International Trade: The post-China Era. *Appl. Energ.* 184, 1063–1072. doi:10.1016/j.apenergy.2016.05.084

Baumol, W. J., and Oates, W. E. (1988). The Theory of Environmental Policy. *Public Choice* 27, 127–128. doi:10.1017/cbo9781139173513

Bing-tao, Q., and Li-ming, G. (2019). Whether the Transfer of Highly Polluting Industries in China Aggravates Environmental Pollution—Empirical Analysis Based on the Threshold Model of Relative Environmental Regulation Strength. *China Environ. Sci.* 39, 3572–3584. doi:10.19674/j.cnki.issn1000-6923.20190604.001

Bingtao, Q., and Liming, Ge. (2018). Relative Environmental Regulations,pollution-Intensive Industry Transfer and Pollution Agglomeration in China. *China Popul. Resour. Environ.* 28 (12), 52–62.

Caiyun, Z., and Yanqing, G. (2015). Can Pollution-Intensive Industry Transfer Achieve Win-Win Development in Economy and Environment? from the Perspective of Environmental Regulation. *J. Finance Econ.* 41, 96–108. doi:10.16538/j.cnki.jfe.2015.10.001

Chen, J.-X., Zhang, Y., and Zheng, S. (2019). Ecoefficiency, Environmental Regulation Opportunity Costs, and Interregional Industrial Transfers: Evidence from the Yangtze River Economic Belt in China. *J. Clean. Prod.* 233, 611–625. doi:10.1016/j.jclepro.2019.06.117

Chen, L., Xu, L., and Yang, Z. (2017). Accounting Carbon Emission Changes under Regional Industrial Transfer in an Urban Agglomeration in China's Pearl River Delta. *J. Clean. Prod.* 167, 110–119. doi:10.1016/j.jclepro.2017.08.041

Chichilnisky, G. (1994). North-south Trade and the Global Environment. *Am. Econ. Rev.* 84, 851–874.

Copeland, B. R. (1994). International Trade and the Environment: Policy Reform in a Polluted Small Open Economy. *J. Environ. Econ. Manage.* 26 (1), 44–65. doi:10.1006/jeem.1994.1004

Copeland, B. R., and Taylor, M. S. (2004). Trade, Growth, and the Environment. *J. Econ. Lit.* 42, 7–71. doi:10.1257/002205104773558047 10.1257/.42.1.7

Dean, J. M., Lovely, M. E., and Wang, H. (2009). Are Foreign Investors Attracted to Weak Environmental Regulations? Evaluating the Evidence from China. *J. Develop. Econ.* 90, 1–13. doi:10.1016/j.jdeveco.2008.11.007

Deng, X., Han, J., and Yin, F. (2012). Net Energy, CO2 Emission and Land-Based Cost-Benefit Analyses of Jatropha Biodiesel: A Case Study of the Panzhihua Region of Sichuan Province in China. *Energies* 5, 2150–2164. doi:10.3390/en5072150

Fang-dao, Q., Tao, J., Chun-min, Z., and Yong-bing, S. (2013). Spatial Relocation and Mechanism of Pollution-Intensive Industries in Jiangsu Province. *Scientia Geographica Sinica* 33. doi:10.13249/j.cnki.sgs.2013.07.003

Haixia, Z., Liu, Y., Lindley, S., Meng, F., and Niu, M. (2020). Change, Mechanism, and Response of Pollutant Discharge Pattern Resulting from Manufacturing Industrial Transfer: A Case Study of the Pan-Yangtze River Delta, China. *J. Clean. Prod.* 244, 118587. doi:10.1016/j.jclepro.2019.118587

Hang, L., Jingfeng, Z., and Hang, Wu. (2012). The Heterogeneity of the Decoupling of Chinese Industries Discharging Densely Different Pollutants and the Industrial Transformation. *China Population,Resources Environ.* 22 (04), 150–155. doi:10.3969/j.issn.1002-2104.2012.04.025

Heting, C. (2019). Major Research Methods in LIS: Understanding. *Selection and Use* 63 (01), 146–152. doi:10.13266/j.issn.0252-3116.2019.01.021

Hong-guang, L., Wei-dong, L., and Zhi-gao, L. (2011). The Quantitative Study on Inter-regional Industry Transfer. *China Ind. Econ.* 6, 79–88. doi:10.19581/j.cnki.ciejournal.2011.06.008

Hui, Z., and Jinxi, W. (2020). Measurement of Environmental Pollution Transfer in Beijing-Hebei Region Based on the Environmental Kuznets Curve. *China Popul. Resour. Environ.* 30, 90–97. doi:10.12062/cpre.20191202

Jiang, S., Wang, Y., Wang, M., Shi, L., Ma, Z., and Lu, G. (2017). Industrial Sectors and Pollution in China Based on the Regional Perspective. *China Environ. Sci.* 37 (11), 4380–4387. doi:10.3969/j.issn.1000-6923.2017.11.044

Jianhua, Y., Zheng, M., and Li, X. (2016). Interregional Transfer of Polluting Industries: a Consumption Responsibility Perspective. *J. Clean. Prod.* 112, 4318–4328. doi:10.1016/j.jclepro.2015.07.103

Jianjun, Z., Weitao, L., and Ying, T. (2018). Analysis on the Influence of Environmental Regulation on Poultry Production Layout and Industrial Transfer—Empirical Research Based on Space Measurement. *Heilongjiang Anim. Sci. Vet. Med.* 16, 24–31. doi:10.13881/j.cnki.hljxmsy.2018.01.0413

Keting, S., and Jianjian, G. (2011). Environmental Pollution, Technical Progress, and Productivity Growth of Energy-Intensive Industries in China—Empirical Study Based on ETFP. *China Ind. Econ.* 25-34. doi:10.19581/j.cnki.ciejournal.2011.12.003

Lihui, Y., and Chuanqing, W. (2021). Environmental Regulation and the Ecological Efficiency of Pollution-Intensive Industries in the Yangtze River Economic Belt. *China Soft Sci.* 08, 181–192. doi:10.3969/j.issn.1002-9753.2021.08.018

Longbin, H. (2013). The Inter-region Transfer Path and Extension of Domestic Pollution-Intensive Industries--Panel Data of the Output of Related Industrial Products over the 2000-2011 Period. *Economics* 06, 8–86. doi:10.16158/j.cnki.51-1312/f.2013.06.009

Marland, G., and Rotty, R. M. (1984). Carbon Dioxide Emissions from Fossil Fuels: a Procedure for Estimation and Results for 1950-1982. *Tellus Ser. B-chemical Phys. Meteorology* 36B, 232–261. doi:10.1111/j.1600-0889.1984.tb00245.x

Mei, Z. (2006). On the FDI and Environment Protection in China. *Ecol. Economy.* 3, 66–70. doi:10.3969/j.issn.1671-4407.2006.03.017

Mulatu, A., and Wossink, A. (2014). Environmental Regulation and Location of Industrialized Agricultural Production in Europe. *Land Econ.* 90, 509–537. doi:10.3368/le.90.3.509

Peng, W., and Li-wen, X. (2014). Pollution Control InvestmentEnterprise Technical Innovation and Pollution Control Efficiency. *China Population, Resources Environ.* 24, 51–58. doi:10.3969/j.issn.1002-2104.2014.09.008

Qi, Y. (2014). The Transfer Trend and Undertaking Competitive Situation of China's Regional Industry. *Econ. Geogr.* 34, 91–97. doi:10.15957/j.cnki.jjdl.2014.03.017

Qiwen, D., Jingyun, Y., Xiaoqi, Z., and Senlin, H. (2020). Transfer Characteristics, Patterns and Mechanisms of Polluting Enterprises and Industries. *Geographical Res.* 39 (07), 1511–1533. doi:10.11821/dlyj020190637

Qiying, R., and Haitao, W. (2019). Will the Pollution Shelter Effect of Foreign Direct Investment Always Exist?——An Empirical Analysis Based on the Dynamic Threshold Panel Model. *Ecol. Economy* 35 (04), 152–159.

Tao, H. (2013). Study on Influence Factors of Pollution Intensive Industry Transfer to China. *J. Shanxi Univ. Finance Econ.* 35, 55–65. doi:10.13781/j.cnki.1007-9556.2013.08.004

Wang, C., and Li, J. (2020). The Evaluation and Promotion Path of Green Innovation Performance in Chinese Pollution-Intensive Industry. *Sustainability* 12 (10), 4198. doi:10.3390/su12104198

Wang, M., and Huang, Y. (2015). China's Environmental Pollution and Economic Growth. *China Econ. Q.* 14, 557–578. doi:10.13821/j.cnki.ceq.2015.02.007

Weijin, D., Jia, L., and Xingju, Y. (2008). The Research of Co-word Analysis(3)-The Principle and Characteristics of the Co-Word Cluster Analysis [J]. *J. Inf.* 7, 118–120. doi:10.3969/j.issn.1002-1965.2008.07.038

Wen-bin, S., and Fang-yi, L. (2018). Driving Forces Analysis of Growth of Energy-intensive Industries in China under the Background of Overcapacity. *Soft Sci.* 32, 41–46. doi:10.13956/j.ss.1001-8409.2018.01.09

World Trade Organization (2019). World Trade Report.

Xin, F., Xue, L., Yue, Y., Jiapei, L., Mengyao, L., and Ye, W. (2020). Study on Construction of Emergent Public Health Event Data Platform Based on Knowledge Entity. *Knowledge Manage. Forum* 5, 175–190. doi:10.13266/j.issn.2095-5472.2020.016

Youjin, L., Yanzhao, Y., and Xiaoming, Z. (2020). Mutualism Effect of China's Industrial Transfer to the Belt and Road Countries:Based on the Perspective of Bilateral Value Chain Upgrade. *Econ. Geogr.* 40, 136–146. doi:10.15957/j.cnki.jjdl.2020.10.016

Zhang, B., Zhang, Y., Wu, X., Guan, C., and Qiao, H. (2020). How the manufacturing economy impacts China's energy-related GHG emissions: Insights from structural path analysis. *Sci. Total Environ.* 743, 140769. doi:10.1016/j.scitotenv.2020.140769

Zhang, G., Deng, N., Mou, H., Zhang, Z. G., and Chen, X. (2019). The impact of the policy and behavior of public participation on environmental governance performance: Empirical analysis based on provincial panel data in China. *Energy Policy* 129, 1347–1354. doi:10.1016/j.enpol.2019.03.030

Zhang, G., Liu, W., and Duan, H. (2020). Environmental regulation policies, local government enforcement and pollution-intensive industry transfer in China. *Comput. Ind. Eng.* 148, 106748. doi:10.1016/j.cie.2020.106748

Zhao, D., Tang, Y., Liu, J., and Tillotson, M. R. (2017). Water footprint of Jing-Jin-Ji urban agglomeration in China. *J. Clean. Prod.* 167, 919–928. doi:10.1016/j.jclepro.2017.07.012

Zhiqing, D., Xiao, C., and Linhui, W. (2014). The Direction of Technical Change, Urban Land Size Environment Quality. *Econ. Res. J.* 49, 111–124.

Conflict of Interest: The authors declare that the research was conducted in the absence of any commercial or financial relationships that could be construed as a potential conflict of interest.

Publisher's Note: All claims expressed in this article are solely those of the authors and do not necessarily represent those of their affiliated organizations, or those of the publisher, the editors and the reviewers. Any product that may be evaluated in this article, or claim that may be made by its manufacturer, is not guaranteed or endorsed by the publisher.

frontiers | Frontiers in Environmental Science

ORIGINAL RESEARCH
published: 20 May 2022
doi: 10.3389/fenvs.2022.830087

First Report of the Hyperaccumulating Potential of Cadmium and Lead by *Cleome rutidosperma* DC. With a Brief Insight Into the Chemical Vocabulary of its Roots

Ekta Bhattacharya and Suparna Mandal Biswas**

Agricultural and Ecological Research Unit, Indian Statistical Institute, Kolkata, India

OPEN ACCESS

Edited by:
Ravi Naidu,
University of Newcastle, Australia

Reviewed by:
Safdar Bashir,
Ghazi University, Pakistan, Pakistan
Anjan Hazra,
University of Calcutta, India
Nirjhar Dasgupta,
Guru Nanak Institute of Pharmaceutical Science and Technology, India

***Correspondence:**
Ekta Bhattacharya
ektabhattacharya1990@gmail.com
Suparna Mandal Biswas
mondalsupa@gmail.com

Specialty section:
This article was submitted to Toxicology, Pollution and the Environment, a section of the journal Frontiers in Environmental Science

Received: *06 December 2021*
Accepted: *12 April 2022*
Published: *20 May 2022*

Citation:
Bhattacharya E and Mandal Biswas S (2022) First Report of the Hyperaccumulating Potential of Cadmium and Lead by Cleome rutidosperma DC. With a Brief Insight Into the Chemical Vocabulary of its Roots. Front. Environ. Sci. 10:830087. doi: 10.3389/fenvs.2022.830087

Phytoremediation is gaining interest in recent years as it is a simple and effective strategy for heavy metal decontamination. The most straightforward strategy for successful heavy metal clean-up is searching for efficient hyperaccumulator species that grow naturally in contaminated sites. The present study, therefore, is the first detailed account of hyperaccumulator potentialities of a neglected and underutilized (NUS) species, *Cleome rutidosperma* DC. Hydroponic screening experiment against cadmium and lead revealed that even at 10 mg/kg concentration, it could accumulate 42.49 mg/kg of Cd and 27.79 mg/kg of Pb in shoots, while it could accumulate 134.71 mg/kg Cd and 491.35 mg/kg of Pb in its roots, and these values were significantly higher than those of the control plants. This plant could efficiently accumulate as high as 639.07 mg/kg of Cd, 8,726.03 mg/kg of Pb in its roots, while it could accumulate 752.83 mg/kg Cd and 3,732.64 mg/kg Pb in its shoots as evident from the pot experiments. In the case of Cd, there was no significant effect of toxicity on the phytophysiological parameters. But increasing concentrations of Pb did have toxic effects on the total chlorophyll content. This plant showed to have a BCF >1 in most of the tested concentrations. At the highest treatment concentration, however, both the BCF and TF were found to be greater than 1. This indicated that *C. rutidosperma* can accumulate and translocate the heavy metals to its aerial parts when the metal concentration is extremely high, proving itself to be an efficient hyperaccumulator. In order to decode the chemical signals, this plant may emit through the roots to cope with stress; root exudates were collected, purified, and analyzed through GCMS. This revealed the presence of five major compounds, namely, palmitic acid, linoleic acid, oleic acid, campesterol, and stigmasterol, which mainly are metabolic markers for detoxification mechanisms triggered by various stresses. Therefore, based on this study, *C. rutidosperma* can be termed a potent hyperaccumulator and can further be exploited for remediation of other classes of environmental pollutants.

Keywords: phytoremediation, phytoextraction, chemical signaling, heavy metal, campesterol

1 INTRODUCTION

Pollution and heavy metal contamination of the environment is one of the most severe problems in the world (Liu et al., 2009; Mishra et al., 2019). Such contamination is posing serious threats to the health of all the living beings on this planet by degrading the quality of the main resources which allow life to thrive, that is, water, air, and soil. The main reasons behind such deterioration are anthropogenic activities like imprudent industrialization, exhaustive agricultural activities, and uncontrolled mining practices. These have led to a drastic increase in inorganic contaminants like cadmium (Cd), chromium (Cr), zinc (Zn), arsenic (As), and lead (Pb) in the soil (Zhang et al., 2010; Alengebawy et al., 2021). Cd and Pb are two of the major environmental pollutants, and are known to contaminate the food chain. Cd can enter the human body through food crops (Rigby and Smith 2020). Even if present at low concentrations in soil, it may cause toxic effects (Sharma et al., 2010). Cd has been listed seventh on the priority list of hazardous substances (Agency for Toxic Substances and Disease Registry, 2019).

Lead (Pb) is released into the environment from the burning of coal, vehicular exhausts, electric batteries, paints, explosives, sewage sludge, petroleum, and metallurgical activities (Sharma and Dubey 2005; Masindi, and Muedi 2018; Weldeslassie et al., 2018). Pb has been ranked second on the priority list of hazardous substances (Agency for Toxic Substances and Disease Registry, 2019). In plants, Cd and Pb have no physiological relevance, and are readily taken up by the plants to toxic concentrations, posing a serious threat to the consumers (Ramesar et al., 2014). The toxic effects include retardation of various metabolic processes like photosynthesis, respiration, water transport, nitrogen metabolism and nutrient uptake (Amari et al., 2017).

Recently, many conventional and non-conventional techniques have been suggested for the decontamination of polluted soils. The major goals of such strategies are as follows: 1) to decrease the heavy metal content of the contaminated soils and 2) to re-establish the chemical and biological qualities of the soil to maintain its fertility. The conventional clean-up techniques like soil excavation, solidification, vitrification, stabilization, incineration, soil flushing, electro-kinetic systems, and landfill have several drawbacks including cost, procedural complexity, regulatory burden, and lack of complete degradation (Agnello et al., 2016; Ghosal et al., 2016; Yan et al., 2020).

The use of plants to reduce contaminants and restore our natural resources like soil, water, and the air is gaining much attention from environmental perspectives (Yan et al., 2020). Phytoremediation has emerged as a promising, *in situ*, cost-effective, green, and cleaner technology that employs hyperaccumulator plant species for the treatment of contaminants (Datta and Sarkar 2005; de Souza Miranda et al., 2022). Hyperaccumulator plants have higher fitness to tolerate and grow on metal-rich soils (Cappa and Pilon-Smits 2014). Phytoextraction and phytostabilization are the two main strategies implemented by the plants, to decrease the metal content and/or immobilize those in the polluted soils (Anjum et al., 2014). A remediation system can be successful depending on the efficiency of the plant of interest to endure and grow luxuriantly under heavy metal stress during phytoextraction and phytostabilization (Ali et al., 2013). The most forthright strategy for heavy metal clean-up is searching for efficient hyperaccumulator species. A feasible approach for the same is the observation of naturally proliferating species at the contaminated sites, which can help in identifying potential plant species. It has been widely reported that plants that are native to contaminated sites like sewage disposal sites and household dumpyards have shown promise for phytoextraction (Merkl et al., 2005). Therefore, identification and exploration of novel species inhabiting such areas that yield high biomass and grow naturally were our foremost criteria for the successful phytoremediation of Cd- and Pb-contaminated soils. According to the earlier studies, most of the plants that were reported to be highly efficient in phytoextraction mostly belonged to family Brassicaceae. While screening the literature, we came across family Cleomaceae which is the sister family of Brassicaceae (Chase and Reveal 2009). This family has three species, namely, *Cleome rutidosperma*, *C. viscosa*, and *C. gynandra* that are ubiquitously present in India. Studies carried out by Abidemi et al., 2014 showed heavy metal accumulation abilities in *Cleome viscosa*. In our field studies, however, we observed that *Cleome rutidosperma* was growing profusely in local waste dumpyards throughout the year. Therefore, we were interested to study the capabilities of this species to tolerate and proliferate in such contaminated soil.

Cleome rutidosperma DC. is an annual herb that grows up to the height of 1 m. This plant was selected for our study due to its distinctive growth habitat. This species characteristically grows and proliferates naturally in disturbed, waste dump areas (Burkill 1995). The plant habit is erect, and has alternate trifoliate leaves and an extensive root system. Flowers are small, and pink or violet in color. The fruits are capsules with an average length of 5–7 cm producing seeds as small as 2 mm in diameter (Hooker 1872; Saxena and Saxena 2001). *C. rutidosperma* is a native species of West Africa but has naturalized in vast areas of tropical America as well as Southeast Asia (Burkill 1995). According to traditional use, the different parts like leaves, roots, and seeds of the plants of the *Cleome* genus are used as stimulants, antiscorbutic, diuretic, anthelmintic, rubefacient, vesicant, and carminative (Ghosh et al., 2019).

Our present work is the first report of *Cleome rutidosperma* as a potent phytoremediator plant. Therefore, we have encompassed a meticulous study of the phytoremediation potential of *Cleome rutidosperma* against two of the most notorious heavy metals cadmium and lead through hydroponic as well as pot culture experiments. It accounts for the uptake and immobilization of both the tested heavy metals by the plant body and takes into consideration the toxic effects of the high concentrations of metals mainly depicted as the biomass content and total chlorophyll content. The plants interact with the environment through signaling compounds that code for their unique language. The plants mainly communicate through the root with the help of chemical signals. Therefore, we were also interested in analyzing the bioactive compounds present in the root exudates of this plant with the help of GCMS in order to

decrypt the distinctive vocabulary this species uses that enables it to survive in the highly contaminated areas.

2 MATERIALS AND METHODS

2.1 Plant Material and Soil Collection

Mature plants with flowers and fruits were collected from the local waste disposal areas around Kolkata (22.6494° N, 88.3805° E), West Bengal, India, in August 2019, and identified with the type specimen at the Botanical Survey of India, Shibpur, Howrah, West Bengal, India. A voucher specimen (Cr02a) is preserved in our departmental herbarium for future reference. Seeds of the identified plants were collected after proper ripening of fruits. Those were surface-sterilized with 0.01% of $HgCl_2$ and washed properly with distilled water repeatedly (Sidhu et al., 2017). Then the seeds were placed on moist filter papers and were allowed to germinate for 10 days. The healthy seedlings of 3–4 cm were selected for further experiments.

The soil required for the pot experiments was collected from the institute garden. The garden was mainly a region of natural vegetation and was free from any external disturbance. The topsoil (up to 20 cm depth) was taken manually. The soil was then air-dried inside the laboratory storehouse for a week. The air-dried soil was then crushed manually and sieved through a sieve of <4 mm mesh size to remove small stones or gravels or any unwanted debris. The dimension of the pots were 12 cm × 8 cm (dia x height). The pots filled with soil were kept for 7 days for maturing, and the planting was done afterward (Sidhu et al., 2018).

2.2 Hydroponic Screening Experiment

Plants were grown in a hydroponic environment to study their ability to accumulate and tolerate heavy metal stress of Cd and Pb (Niu et al., 2007). Seedlings were placed through perforations in a plastic platform in a 1000-ml glass jar containing 500 ml of Hoagland's solution (Hoagland and Arnon, 1938) so that the roots were immersed in a liquid medium and the shoots remained above the platform. The heavy metal salts (reagent grade) used in this study included $CdCl_2{\cdot}2.5H_2O$ and $Pb(NO_3)_2{\cdot}H_2O$. The salts were separately dissolved in deionized water and added into hydroponic plant culture, respectively. Treatments were prepared at 10 mg/kg concentrations for both metals. A control that contained a nutrient medium devoid of the metal salts was maintained. All solutions were adjusted to pH 7.0–7.2. The experimental setup was maintained for 60 days. After the incubation in greenhouse conditions, the plants were harvested and phytophysiological parameters were recorded.

2.3 Pot Experiments

Pot experiments were performed following a completely randomized design under greenhouse conditions (Sidhu et al., 2018). The natural soil was spiked with heavy metals salts, namely, $CdCl_2{\cdot}2.5H_2O$ and $Pb(NO_3)_2{\cdot}H_2O$. Three replicates were setup for each of the 10 different concentration levels of the metal treatments including control. Altogether, 30 individual pots were maintained in this study. There were nine different Pb and Cd concentrations, equivalent to 10, 20, 30, 40, 50, 75, 100, 150, and 200 mg/kg soil, respectively. The spiked soils (1 kg each) were filled in polythene bags and placed in plastic pots to avoid metal leaching from soils. After spiking prior to the seedling plantation, the soils were equilibrated for 7 days. The plants were maintained for 60 days under the same conditions before harvesting. Triplicates of the control plants were maintained in soil devoid of metal salts. The moisture content was maintained at 60% throughout the experimental period using distilled water.

2.4 Analysis of Heavy Metals

The heavy metal concentration in the plant tissue as well as in the soil was analyzed using the AAS. Plants were harvested after 60 days and separated into root and shoot. The plant parts were washed repeatedly with distilled water and 0.01% EDTA solution to get rid of any heavy metal residue in them. The plant tissues were then oven-dried at 80°C for 72 h. The dried plant parts were then weighed, grounded, and digested using the tri-acid mixture (Hseu 2004).

2.5 Soil Properties

Physicochemical analyses of the soil that is used in the experiment including pH, organic carbon, and available NPK (Jackson 1958) were carried out along with Cd and Pb contents for the same. The physicochemical characteristics revealed pH of 7.45 ± 0.05, organic carbon of 0.83 ± 0.17 (%), phosphorous of 11.3 ± 0.54 mg/kg, potassium of 93.2 ± 1.21 mg/kg, available nitrogen of 112 ± 1.93 mg/kg, Cd content of 3.875 ± 0.125 mg/kg, and Pb content of 3.75 ± 0.5 mg/kg. The residual Cd and Pb contents in the soil (in the control and different treatments) and removal percentages for both the metals, after 60 days of growth period, are given in **Supplementary Table S1**.

2.6 Determination of Phytophysiological Effects of Toxicity

The phytophysiological effects of the heavy metal stress were determined using two parameters, namely, change in dry biomass and total chlorophyll content. The total chlorophyll content was measured using the following equation (Arnon 1949).

$$\text{Chlorophyll (a + b) (mg/g tissue)} = \frac{[\mathbf{20.21}\ (\boldsymbol{A_{645}}) + \mathbf{8.02}\,(\boldsymbol{A_{663}})]*\boldsymbol{V}}{\mathbf{1000}*\boldsymbol{W}},$$

where A = absorbance of specific wavelength, V = final volume of chlorophyll extract in 80% acetone, and W = fresh weight of the tissue extract.

2.7 Determination of Bioconcentration Factor and Translocation Factor

In order to determine the type of remediation a plant performs, that is, whether it has phytoextraction abilities or it immobilizes the heavy metals by phytostabilization, two main indices, namely, bioconcentration factor (BCF) and translocation factor (TF), are

FIGURE 1 | Collection of root exudates from *Cleome rutidosperma* DC. **(A)** Total experimental setup, **(B)** root exudates trapping system, and **(C)** roots extend downward into the conical flasks containing distilled water.

calculated based on the heavy metal contents of the plant parts. Plants can be considered good phytoextractors if the BCF >1 and TF > 1 which indicate that those plants can translocate the heavy metals into their shoots. On the other hand, if a plant exhibits the BCF >1 but TF < 1, then those species can be categorized as phytostabilizer which have the ability to immobilize the heavy metal in its rhizosphere (Ali et al., 2013).

BCF signifies the ability of the plant to accumulate and immobilize the heavy metals in its tissues. It is expressed as the ratio of metal accumulated in the below-ground tissues (roots) of the plant to that present in the soil (Zhuang, et al., 2007; Bonanno and Vymazal 2017).

$$\textbf{Bioconcentration factor (BCF)} = C_{root}/C_{soil}.$$

TF is the efficiency of plants to translocate the metal accumulated to its above-ground tissues (stem and leaves). It is expressed as the ratio of the metal content in the shoots to that of the roots of a plant (Zhuang et al., 2007; Bonanno and Vymazal 2017).

$$\textbf{Translocation factor (TF)} = C_{shoot}/C_{root}.$$

2.8 Collection and Purification of Root Exudates of *C. rutidosperma*

Cleome rutidosperma plants were grown in special root exudate trapping systems (**Figure 1**) which consist of a Buchner funnel (dia = 110 mm) and conical flasks of 500 ml capacity (Jana and Biswas 2011). The sieve inside the Buchner funnel was removed. The funnel was filled with soil after placing a piece of cotton cloth at the mouth of the funnel to hold the soil. The conical flasks were painted black to avoid the growth of fungus or algae. The germinated seeds (6–10) of *C. rutidosperma* were sown in each funnel. An average of 5–6 plants depending on the growth, size, and number of leaves were allowed to grow in each set till maturity. Plant roots penetrated the soil in the funnel and extended into the flasks after 20–25 days. The flasks contained distilled water. The plants release compounds into the water, which is further referred to as the root exudates. Root exudates were collected every 7 days, and the flasks were filled with fresh distilled water. This procedure was performed for a period of 4 months. The collected exudates were dried in a vacuum evaporator, extracted, and purified using the solvent extraction method followed by TLC and column chromatography. The purified root exudates were then sent for identification using GCMS analysis.

2.9 GC-MS Analysis of Purified Root Exudates of *C. rutidosperma*

Purified root exudates of *C. rutidosperma* were subjected to GC-MS analysis (Model No. Agilent Technologies, GC-6860N Network GC System with 5973 inert Mass Selective Detector) for detecting bioactive compounds. The GC-MS analysis was done at the National Test House, Salt Lake, Sector V, Kolkata, WB, India. HP-1MS column (25 m × 0.33 mm, i. d. 0.25 µm) was used; 0.1 µL of root exudates of *C. rutidosperma* (dissolved in chloroform) was injected into GC set in the split mode for analysis at an injector temperature of 280°C. Helium gas was used as the carrier gas with a flow rate of 1 ml/min. The oven temperature was programmed as follows: 45°C (1 min hold), 45–220°C at 7°C/min, and 220–300°C at 6°C/min, 200°C (2 min). The electron ionization mode with ionization energy of 70 eV was employed by the MS. A full scan mode was used with an ion source temperature of 280°C and an acquisition rate of 0.2 s. The mass range was adjusted to 50–350 Da.

The compound identification was performed by comparing the mass spectra with the spectral data of the NBS75K library provided by the GC/MS control and data processing software.

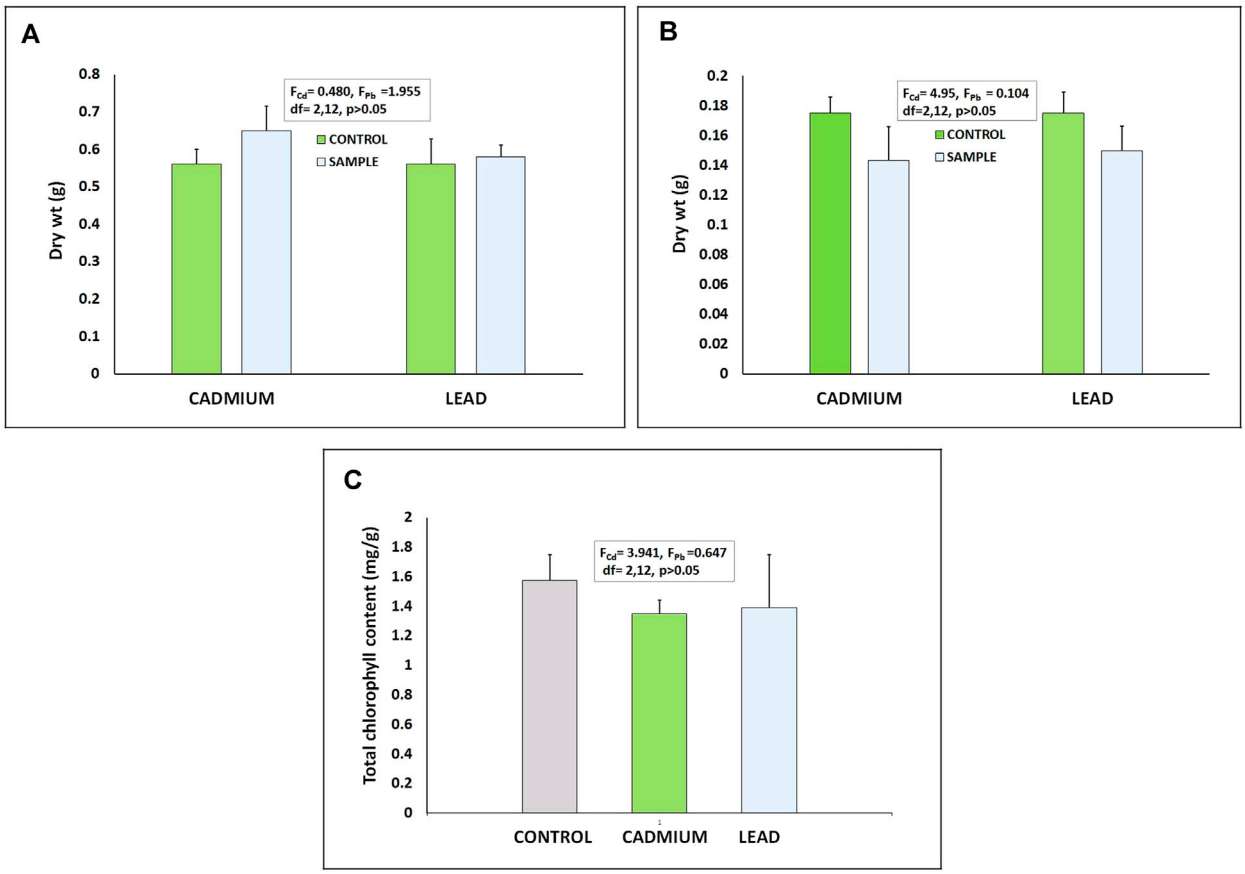

FIGURE 2 | Phytophysiological effects of heavy metal stress on *Cleome rutidosperma* based on hydroponic experiments: **(A)** and **(B)** biomass of shoot and root, respectively, and **(C)** total chlorophyll content. The results did not differ significantly w.r.t control (F values and "degrees of freedom (df)" are given in the respective graphs).

2.10 Statistical Analysis

The data were tested for normality using the Kruskal–Wallis test. T-test and one-way ANOVA were performed to analyze the differences in the parameters of the treated plants with respect to the experimental control. The correlation between the parameters and the tested concentrations was also studied. The statistical analysis was performed using SPSS 21 (IBM Corp. Released, 2012) software.

3 RESULTS AND DISCUSSION

3.1 Hydroponic Screening Experiment

The hydroponic screening experiment revealed that the biomass of root for the control was 0.56 ± 0.04 g, while the biomass for the Cd and Pb treated plants were 0.65 ± 0.06 g and 0.58 ± 0.03 g, respectively (**Figure 2**). The total chlorophyll content was recorded to be 1.576 ± 0.17 mg/g in the control, while it was 1.39 ± 0.35 mg/g and 1.35 ± 0.09 mg/g in Cd- and Pb-treated plants, respectively. Statistically, no significant differences were observed in the total biomass and total chlorophyll content compared to the control, which indicate that the plant can tolerate heavy metal stress without showing any significant signs of toxicity. Our results were in accordance with hydroponic studies done on *Brassica juncea*, which showed no significant difference along the Cd treatments ranging from 1 to 50 μM Cd (Ying et al., 2021). But the AAS analysis revealed that even at the low concentration of 10 mg/kg, *C. rutidosperma* could accumulate 42.49 mg/kg of Cd in shoots and 134.71 mg/kg of Cd in roots. In the case of Pb, the plant could store 27.79 mg/kg in shoots and 491.35 mg/kg in its roots. These values were significantly higher than those of control plants (**Figure 3**).

3.2 Pot Experiments

C. rutidosperma could efficiently accumulate as high as 639.07 mg/kg of Cd, 8,726.03 mg/kg of Pb in its roots, while could accumulate 752.83 mg/kg of Cd and 3,732.64 mg/kg of Pb in its shoots at the highest treatment concentrations of 200 mg/kg of Cd and 150 mg/kg of Pb, respectively (**Figure 4**). The Cd content significantly increased from 256.5 mg/kg to 639.07 mg/kg in roots and from 90.93 mg/kg to 752.83 mg/kg in shoots. There was a linear increase in the uptake of both the metals in their shoots and roots with increasing heavy metal exposure

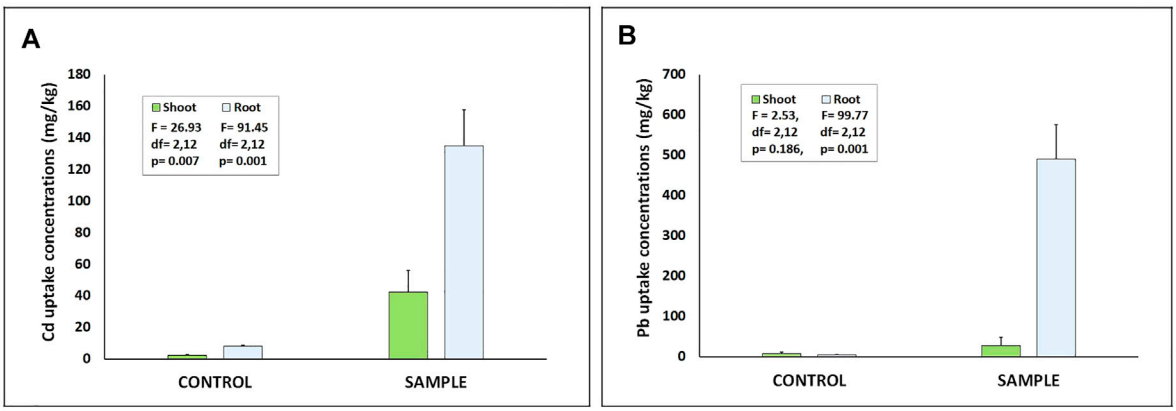

FIGURE 3 | Heavy metal uptake by roots and shoots of *Cleome rutidosperma* recorded in hydroponic experiments at 10 mg/kg tested concentration of **(A)** cadmium and **(B)** lead. There was a significant difference in the metal concentrations in the sample w.r.t control as well as the roots w.r.t to the shoots (F values and "df" are given in the respective graphs).

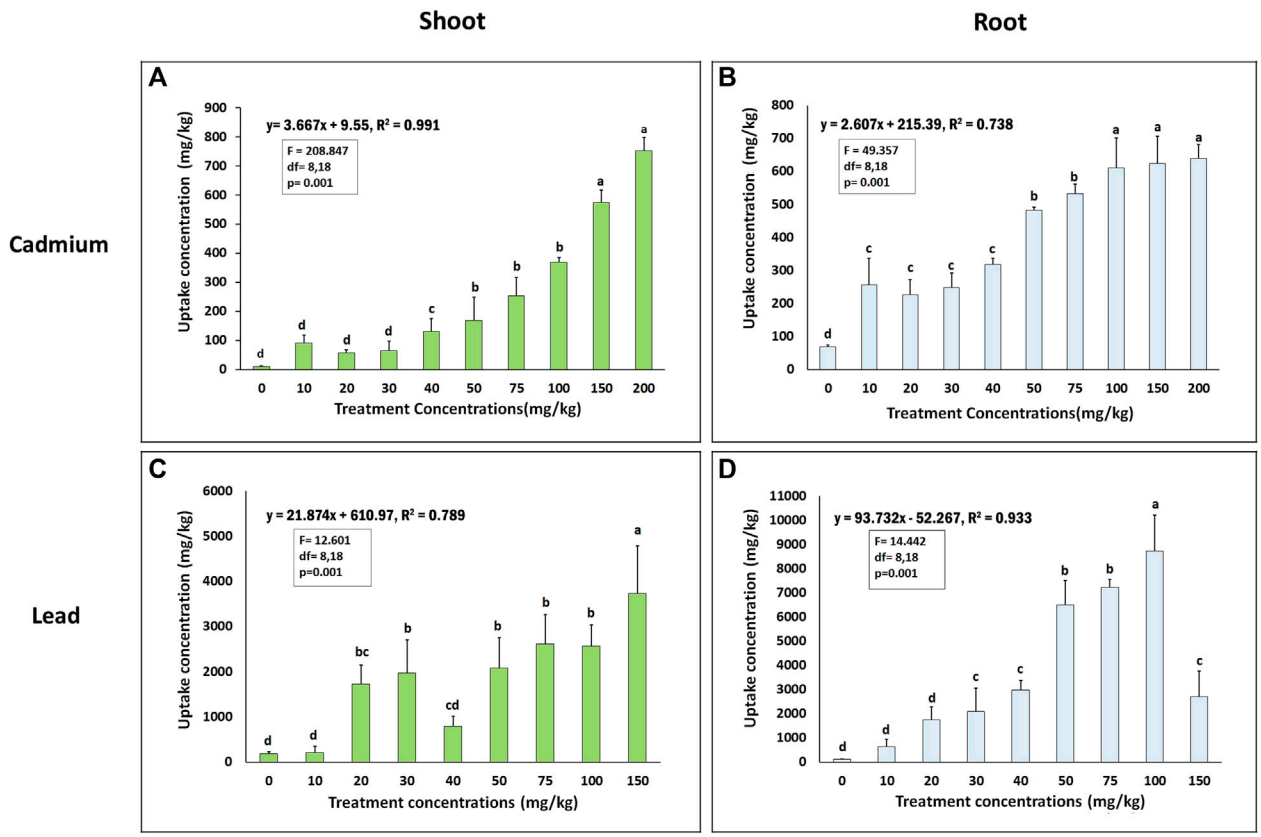

FIGURE 4 | Heavy metal uptake by roots and shoots of *Cleome rutidosperma* recorded in pot experiments under different treatment concentrations of **(A)** and **(B)** cadmium, **(C)** and **(D)** lead in shoots and roots, respectively. The bars marked with different alphabets **(a,b,c,d)** are significantly different from each other (F values and "df" are given in the respective graphs). R^2 represents the correlation between the content of metal in root–shoot tissues *versus* the soil at $p \leq 0.05$.

(10–200 mg/kg). The R^2 values for Cd uptake in shoots and roots were 0.991 and 0.738, respectively.

In the case of Pb, *C. rutidosperma* could efficiently accumulate about 80 times more Pb in its roots as compared to the amount of Pb in the soil. In several studies, Pb has been reported to be preferentially stored in roots (Wang et al., 2014). The plant could accumulate a maximal amount of Pb, that is, 8,726.03 mg/kg, in its roots at the 100 mg/kg concentration, while the plant accumulated

3,732 mg/kg of Pb in its shoots at 150 mg/kg treatment. There was a linear correlation in the Pb uptake for both the shoot and roots with an R^2 value of 0.789 and 0.933, respectively.

In agreement with other findings, we observed that the roots of the plants that were primarily exposed to heavy metal stress retained a significant amount of Cd as well as Pb (Gavrilescu 2022). As reported in Cd hyperaccumulator species, namely, *Arabis paniculata*, *Brassica napus*, and *Calendula officinalis*, the main organic compounds are metallothioneins and phytochelatins that help to sequester and accumulate Cd within the root cells (Liu et al., 2008; Zeng et al., 2009; Ehsan et al., 2014; Awa and Hadibarata 2020). *Celosia cristata pyramidalis*, an ornamental plant, has been reported to accumulate up to three times more Pb in its roots than shoots (Cui et al., 2013). As explained by the earlier studies, such accumulation of metals in roots could be attributed to the subcellular compartmentalization of metals in vacuoles by the plant that helps it to cope with the possible toxicity imposed by increased heavy metal uptake (Riyazuddin et al., 2021). Another reason could be the formation of insoluble metal phosphates, carbonates, and bicarbonates that precipitate in the intercellular root spaces (Brennan and Shelley 1999), which in turn reduces the translocation of the same from roots to the shoots (Cunningham and Berti 2000).

C. rutidosperma may employ such strategies to restrict the excess translocation of Cd and Pb, therefore, protecting itself from metal-induced toxicity. However, *C. rutidosperma* also showed the tendency to translocate significant amounts of Cd and Pb in its aerial parts, which is a key criterion for a plant to have phytoextraction efficiency. This plant showed significant translocation at the higher treatment concentrations, which was also the trend observed in species of *Brassica* (Mourato et al., 2015). The plant accumulated 752.8 mg/kg of Cd and 3,732.63 mg/kg of Pb in its shoots at 200 mg/kg and 150 mg/kg treatment concentration, respectively. Such translocation of metals may have occurred due to the increase in the internal transport of aqueous free Cd and Pb ions, a process mediated by xylem loading while being regulated by xylem flux and endodermis (Uraguchi et al., 2009). The uptake of these metals may take place along with the essential metal nutrients like Zn, Cu, and Fe *via* the membrane transporters (Zheng et al., 2011) and also by the production of phytochelatins followed by formation of Pb–phytochelatin complexes within the vascular tissues (Andra et al., 2009).

In summary, the heavy metal content in roots and shoots of *C. rutidosperma* plants at all the treatments was well above the threshold level for Cd hyperaccumulators (˜100 mg/kg) and for Pd hyperaccumulators (>1,000 mg/kg) (Pollard et al., 2002; Sidhu et al., 2017). Moreover, unpalatability, high biomass yield, and shorter life span provide added advantages to make *C. rutidosperma*, a novel plant species to be exploited for Cd and Pb extraction from the polluted soils. These findings strongly support the potential of *C. rutidosperma* for both phytostabilization and phytoextraction of Cd and Pb from the polluted soils.

3.3 Phytophysiological Effects of Heavy Metal Toxicity on *C. rutidosperma*

Plant biomass and growth were significantly impacted by increasing heavy metal stress (**Figure 5**). In the case of Cd, the dry wt of both root and shoot increased significantly at Cd treatment concentrations of 20–40 mg/kg, respectively. The exact reason for such promotion in growth cannot be explained. However, such a response may be attributed to the phenomenon called hormesis in which a stimulatory effect in growth is noticed under the physiological toxic doses of heavy metal ions (Tang et al., 2009; Poschenrieder et al., 2013).

The cadmium stress, however, did not show any significant effect on the total chlorophyll content of *C. rutidosperma*. The difference was not significant with respect to the control sets. On the contrary, the total chlorophyll content of *C. rutidosperma* exposed to lead stress did decrease significantly compared to the control in a dose-dependent manner ($y = -0.005x + 1.2256$; $R^2 = 0.957$). The plants treated with 200 mg/kg Pb, in our studies, failed to survive. Therefore, we have the data of plants treated with 10–150 mg/kg of Pb. Similar observations were also reported in *Coronopus didymus* (Sidhu et al., 2017), *Brassica napus* (Shakoor et al., 2014), and *Eichornia crassipes* (Malar et al., 2014) under Pb stress where a decrease in the total chlorophyll content was detected.

3.4 Analysis of Bioconcentration Factor and Translocation Factor for *C. rutidosperma*

BCF was observed as greater than 1 for all the treatment concentrations in both the targeted heavy metals, that is, Cd and Pb. In the hydroponic experiments, with a treatment concentration of 10 mg/kg, the plant showed the highest BCF of 16.12 for Cd and 57.82 for Pb (**Table 1**). However, the TF values were lesser than 1 for both the metals tested. Pot culture experiments showed a similar trend. BCF values were all greater than 1 for both the metals at all the tested concentrations. The highest BCF recorded for Cd was 27, while that for Pb was 847.23 (**Table 1**). Here, an interesting fact observed was that the TF > 1 at the highest treatment concentration. The TF was 1.18 at 200 mg/kg concentration of Cd and 1.38 at 150 mg/kg concentration of Pb. An explanation to this may be that the higher heavy metal content in the rhizospheric soil had catalyzed the rapid uptake of heavy metal in the roots and from roots to its aerial parts (Islam et al., 2020). If we look closely, the metal uptake of Pb reached maximum at the preceding concentration of 100 mg/kg in the roots. Interestingly, however, the uptake drastically decreased at 150 mg/kg concentration. This may be due to the toxic effects of heavy metals induced at this threshold concentration (Ying et al., 2021). Additionally, the TF > 1 at that concentration, which indicates that the plant was translocating the Pb taken up by the roots efficiently (Wang et al., 2014). According to the studies done on heavy metal sequestration and detoxification, it was reported that plants tend to cope with the heavy metal stress by translocating and sequestering them in the aerial tissues (Singh et al., 2016). But when exposed to even higher stress levels, that is, 200 mg/kg, the plant failed to survive (Dubey et al., 2018).

3.5 Chemical Profiling of the Purified Root Exudates Using GCMS

GCMS spectra of purified root exudates of *C. rutidosperma* revealed the presence of five major peaks along some minor

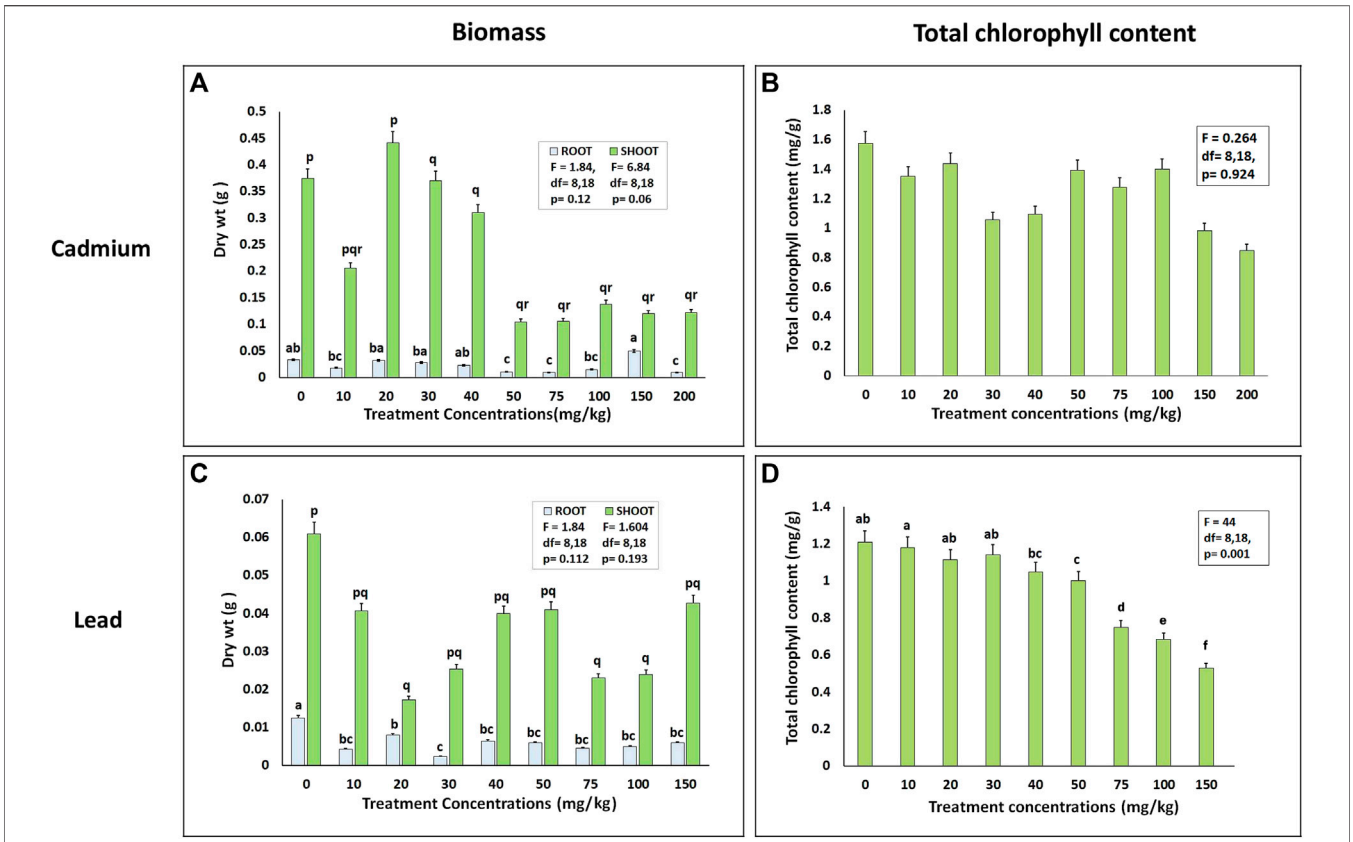

FIGURE 5 | Phytophysiological effects of heavy metal stress on *Cleome rutidosperma* at different tested concentrations of **(A)** and **(B)** cadmium, **(C),** and **(D)** lead in terms of biomass and total chlorophyll content, respectively. The bars marked with different alphabets (a,b,c,d and p,q,r,s) are significantly different from each other (F values and "df" are given in the respective graphs).

TABLE 1 | Bioconcentration factor (BCF) and translocation factor (TF) of *Cleome rutidosperma* for both the hydroponic and pot experiments against Cd and Pb. The values marked with (*) are greater than 1, showing positive translocation of heavy metal to the aerial parts of the plant.

Experiment type	Treatment (mg/kg)	BCF		TF	
		Cd	Pb	Cd	Pb
Hydroponic experiment	10	13.47	49.13	0.31	0.05
	0	17.63	17.69	0.16	0.16
Pot experiment	10	28.77	120.54	0.35	0.33
	20	17.08	225.81	0.25	0.99
	30	14.84	370.59	0.26	0.93
	40	14.68	410.48	0.41	0.265
	50	20.98	847.23	0.35	0.32
	75	18.05	608.85	0.47	0.36
	100	15.29	601.79	0.6	0.29
	150	14.55	129.52	0.92	1.38*
	200	10.65	-	1.18*	-

peaks based on the percentage area of the peak (**Figure 6**). The major compounds detected were palmitic acid (retention time = 22.847), linoleic acid (retention time = 25.801), oleic acid (retention time = 25.89), campesterol (retention time = 39.099), and stigmasterol (retention time = 39.427). The minor compounds include stearic acid, ethyl lineolate, ethyl oleate, behenic acid, tricosanoic acid, and lignoceric acid.

Heavy metal stress induces the plant cells to generate highly reactive oxygen species (ROS) which can oxidize and degenerate cellular macromolecules such as DNA, pigments, proteins, lipids, and other essential molecules irreversibly (Berni et al., 2019; Castro

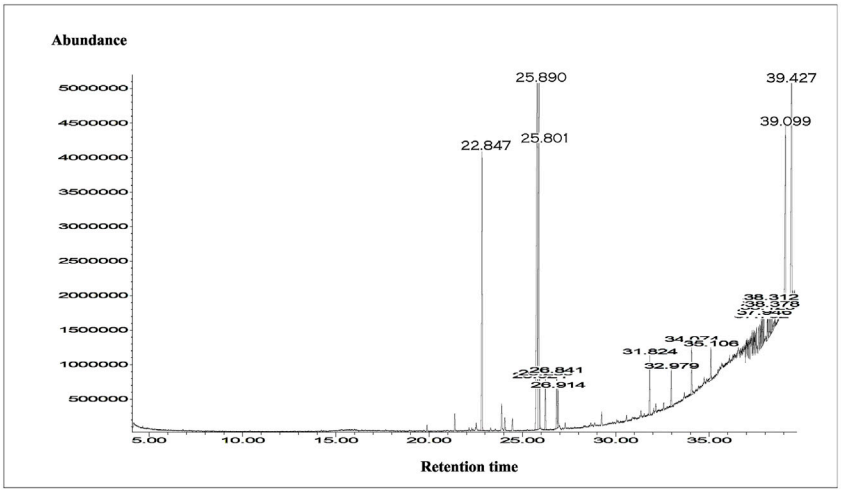

Compounds	Area%	Retention time
Palmitic acid *	11.13	22.847
Linoleic acid *	25.57	25.801
Oleic acid *	17.89	25.890
Stearic acid	2.11	26.237
Ethyl Linoleate	2.02	26.839
Ethyl Oleate	1.44	26.912
Behenic acid	1.44	31.825
Tricosanoic acid	1.36	32.977
Lignoceric acid	1.36	34.072
Campesterol *	9.77	39.099
Stigmasterol *	15.32	39.427

FIGURE 6 | GCMS spectra of the purified root exudates of *Cleome rutidosperma*. The list of main compounds with the respective retention times is given in the table provided. The area % provides information about the abundance of the respective compounds. The compounds marked with (*) are the main compounds based on the abundance and sharp peaks.

et al., 2021). In order to prevent that, plants enable their defense strategies mainly by producing some alternate bioactive molecules which act as reaction centers for the generated ROS (Singh et al., 2016). Unsaturated fatty acids and esters like linoleic acid, ethyl linoleate, oleic acid, and ethyl oleate are compounds acting as molecular targets that scavenge ROS. The presence of these compounds in the root exudates clearly indicates their increased production to cope with the heavy metal stress (De Bigault Du Granrut and Cacas 2016). Peroxidation of reactive target molecules like linoleic acid and its methyl ester derivatives through radicals generated by the heavy metal stress protects the cells from extensive injury to cellular DNA (Guerzoni et al., 2001; Berni et al., 2019). Plants communicate with the environment using these chemical signals. In a study done by Yi and Crowley (2007), it has been reported that fatty acids act as a metabolic marker which stimulates poly-aromatic-hydrocarbon (PAH) degradation through roots. Therefore, this plant may also have a tendency to remediate such PAHs, which provides a future scope that requires thorough investigation. Apart from fatty acids, the precursor of steroidal compounds mainly brassinosteroids, that is, campesterol and stigmasterol, were also identified in the root exudates. There have been reports about the roles of these compounds in detoxification mechanisms in heavy metal stress conditions (Kapoor et al., 2022). The studies done on Cd-treated plants of *Arabidopsis thaliana* support these statements as concentrations of these compounds were observed to be considerably increased in the stress exposed plants as compared to the untreated control (Sun et al., 2010).

4 CONCLUSION

Our observations, therefore, provide enough information about a novel candidate plant species that can further be used for phytoremediation implications. It was also observed that there is a threshold value of Cd and Pb concentrations after which *C. rutidosperma* translocates the heavy metal to its aerial parts. Thus, it can be hypothesized that *Cleome rutidosperma* DC. may act as a phytostabilizer in low metal-contaminated areas, but may also act as an efficient hyperaccumulator in highly contaminated areas. The plant also possessed the characteristics of being able to remediate poly-aromatic-hydrocarbons either with help of its root exudates or by using microbes as mediators. Hence, to conclude, we proposed this plant as a potential candidate to be incorporated into successful phytoremediation strategies based on the results of our study supported by its natural habit and habitat.

DATA AVAILABILITY STATEMENT

The original contributions presented in the study are included in the article/**Supplementary Material**, further inquiries can be directed to the corresponding authors.

AUTHOR CONTRIBUTIONS

EB performed the experiments, analyzed the data, and prepared the manuscript. SMB has designed the experiments, provided the resources, and edited the manuscript.

SUPPLEMENTARY MATERIAL

The Supplementary Material for this article can be found online at: https://www.frontiersin.org/articles/10.3389/fenvs.2022.830087/full#supplementary-material

REFERENCES

Abidemi, I. O., Bosede, O. M., and Oladele, O. (2014). Lead and Cadmium Phytoremediation Potentials of Plants from Four lead Smelting Slags Contaminated Sites. *Nat. Environ.* 2 (3), 33–38. doi:10.12966/ne.11.01.2014

Agency for Toxic Substances and Disease Registry (ATSDR) (2019). CERCLA Priority List of Hazardous Substances. Available at: https://www.atsdr.cdc.gov/spl/index.html. Accessed on 20th Oct 2021.

Agnello, A. C., Bagard, M., van Hullebusch, E. D., Esposito, G., and Huguenot, D. (2016). Comparative Bioremediation of Heavy Metals and Petroleum Hydrocarbons Co-contaminated Soil by Natural Attenuation, Phytoremediation, Bioaugmentation and Bioaugmentation-Assisted Phytoremediation. *Sci. Total Environ.* 563-564, 693–703. doi:10.1016/j.scitotenv.2015.10.061

Alengebawy, A., Abdelkhalek, S. T., Qureshi, S. R., and Wang, M.-Q. (2021). Heavy Metals and Pesticides Toxicity in Agricultural Soil and Plants: Ecological Risks and Human Health Implications. *Toxics* 9 (3), 42. doi:10.3390/toxics9030042

Ali, H., Khan, E., and Sajad, M. A. (2013). Phytoremediation of Heavy Metals-Concepts and Applications. *Chemosphere* 91, 869–881. doi:10.1016/j.chemosphere.2013.01.075

Amari, T., Ghnaya, T., and Abdelly, C. (2017). Nickel, Cadmium and lead Phytotoxicity and Potential of Halophytic Plants in Heavy Metal Extraction. *South Afr. J. Bot.* 111, 99–110. doi:10.1016/j.sajb.2017.03.011

Andra, S. S., Datta, R., Sarkar, D., Makris, K. C., Mullens, C. P., and Sahi, S. V. (2009). Induction of lead-binding Phytochelatins in Vetiver Grass [*Vetiveria Zizanioides* (L.)]. *J. Environ. Qual.* 38, 868–877. doi:10.2134/jeq2008.0316

Anjum, N. A., Umar, S., and Iqbal, M. (2014). Assessment of Cadmium Accumulation, Toxicity, and Tolerance in Brassicaceae and Fabaceae Plants—Implications for Phytoremediation. *Environ. Sci. Pollut. Res.* 21, 10286–10293. doi:10.1007/s11356-014-2889-5

Arnon, D. I. (1949). Copper Enzymes in Isolated Chloroplasts. Polyphenoloxidase in *Beta Vulgaris*. *Plant Physiol.* 24, 1–15. doi:10.1104/pp.24.1.1

Awa, S. H., and Hadibarata, T. (2020). Removal of Heavy Metals in Contaminated Soil by Phytoremediation Mechanism: a Review. *Wat. Air Soil Poll.* 231 (2), 1–15. doi:10.1007/s11270-020-4426-0

Berni, R., Luyckx, M., Xu, X., Legay, S., Sergeant, K., Hausman, J. F., et al. (2019). Reactive Oxygen Species and Heavy Metal Stress in Plants: Impact on the Cell wall and Secondary Metabolism. *Environ. Exp. Bot.* 161, 98–106. doi:10.1016/j.envexpbot.2018.10.017

Bonanno, G., and Vymazal, J. (2017). Compartmentalization of Potentially Hazardous Elements in Macrophytes: Insights into Capacity and Efficiency of Accumulation. *J. Geochem. Explor.* 181, 22–30. doi:10.1016/j.gexplo.2017.06.018

Brennan, M. A., and Shelley, M. L. (1999). A Model of the Uptake, Translocation, and Accumulation of lead (Pb) by maize for the Purpose of Phytoextraction. *Ecol. Eng.* 12, 271–297. doi:10.1016/S0925-8574(98)00073-1

Burkill, H. M. (1995). *The Useful Plants of West Tropical Africa*. 2. ed., 1-3. Richmond, UK: Royal Botanic Gardens, Kew, 976.

Cappa, J. J., and Pilon-Smits, E. A. (2014). Evolutionary Aspects of Elemental Hyperaccumulation. *Planta* 239, 267–275. doi:10.1007/s00425-013-1983-0

Castro, B., Citterico, M., Kimura, S., Stevens, D. M., Wrzaczek, M., and Coaker, G. (2021). Stress-induced Reactive Oxygen Species Compartmentalization, Perception and Signalling. *Nat. Plants* 7 (4), 403–412. doi:10.1038/s41477-021-00887-0

Chase, M. W., and Reveal, J. L. (2009). A Phylogenetic Classification of the Land Plants to Accompany APG III. *Bot. J. Linn. Soc.* 161 (2), 122–127. doi:10.1111/j.1095-8339.2009.01002.x

Cui, S., Zhang, T., Zhao, S., Li, P., Zhou, Q., Zhang, Q., et al. (2013). Evaluation of Three Ornamental Plants for Phytoremediation of Pb-Contamined Soil. *Int. J. Phytorem* 15, 299–306. doi:10.1080/15226514.2012.694502

Cunningham, S. D., and Berti, W. R. (2000). "Phytoextraction and Phytostabilization: Technical, Economic and Regulatory Considerations of the Soil-lead Issue," in *Phytoremediation of Contaminated Soil and Water*. Editors N. Terry and G. S. Banuelos (Boca Raton, FL: CRC Press), 359–376.

Datta, R., and Sarkar, D. (2005). Phytoextraction of Zinc and Cadmium from Soils Using Hyperaccumulator Plants. *Water Encyclopedia* 5, 369–374. doi:10.1002/047147844X.gw856

De Bigault Du Granrut, A., and Cacas, J. L. (2016). How Very-Long-Chain Fatty Acids Could Signal Stressful Conditions in Plants? *Front. Plant Sci.* 7, 1490. doi:10.3389/fpls.2016.01490

de Souza Miranda, R., Boechat, C. L., Bomfim, M. R., Santos, J. A. G., Coelho, D. G., Assunção, S. J. R., et al. (2022). "Phytoremediation: A Sustainable green Approach for Environmental Cleanup," in *Phytoremediation Technology for the Removal of Heavy Metals and Other Contaminants from Soil and Water* (Netherlands: Elsevier), 49–75. doi:10.1016/B978-0-323-85763-5.00017-9

Dubey, S., Shri, M., Gupta, A., Rani, V., and Chakrabarty, D. (2018). Toxicity and Detoxification of Heavy Metals during Plant Growth and Metabolism. *Environ. Chem. Lett.* 16 (4), 1169–1192. doi:10.1007/s10311-018-0741-8

Ehsan, S., Ali, S., Noureen, S., Mahmood, K., Farid, M., Ishaque, W., et al. (2014). Citric Acid Assisted Phytoremediation of Cadmium by *Brassica Napu*s L. *Ecotox. Environ. Safe* 106, 164–172. doi:10.1016/j.ecoenv.2014.03.007

Gavrilescu, M. (2022). Enhancing Phytoremediation of Soils Polluted with Heavy Metals. *Curr. Opin. Biotechnol.* 74, 21–31. doi:10.1016/j.copbio.2021.10.024

Ghosal, D., Ghosh, S., Dutta, T. K., and Ahn, Y. (2016). Current State of Knowledge in Microbial Degradation of Polycyclic Aromatic Hydrocarbons (PAHs): a Review. *Front. Microbiol.* 7, 1369. doi:10.3389/fmicb.2016.01369

Ghosh, P., Chatterjee, S., Das, P., Karmakar, S., and Mahapatra, S. (2019). Natural Habitat, Phytochemistry and Pharmacological Properties of a Medicinal weed-*Cleome Rutidosperma* DC. (Cleomaceae): A Comprehensive Review. *Int. J. Pharm. Sci. Res.* 10 (4), 1605–1612. doi:10.13040/IJPSR.0975-8232.10(4).1605-12

Guerzoni, M. E., Lanciotti, R., and Cocconcelli, P. S. (2001). Alteration in Cellular Fatty Acid Composition as a Response to Salt, Acid, Oxidative and thermal Stresses in *Lactobacillus Helveticus*. *Microbiology* 147 (8), 2255–2264. doi:10.1099/00221287-147-8-2255

Hoagland, D. R., and Arnon, D. I. (1938). The Water-Culture Method for Growing Plants without Soil[J]. *Calif. Agric. Exp. Stn. Bull.* 347, 36–39.

Hooker, J. D. (1872). *Flora of British India*, Dehra Dun: Reprint by Bishen Singh Mahendra Pal Singh, Publishers, 1. 169.

Hseu, Z. Y. (2004). Evaluating Heavy Metal Contents in Nine Composts Using Four Digestion Methods. *Bioresour. Technol.* 95 (1), 53–59. doi:10.1016/j.biortech.2004.02.008

IBM Corp. Released (2012). *IBM SPSS Statistics for Windows, Version 21.0*. Armonk, NY: IBM Corp.

Islam, M. D., Hasan, M. M., Rahaman, A., Haque, P., and Rahman, M. M. (2020). Translocation and Bioaccumulation of Trace Metals from Industrial Effluent to Locally Grown Vegetables and Assessment of Human Health Risk in Bangladesh. *SN Appli. Sci.* 2 (8), 1–11. doi:10.1007/s42452-020-3123-3

Jackson, M. L. (1958). *Soil Chemical Analysis*. New Delhi: Prentice Hall of India, 38–134. doi:10.2307/477540

Jana, A., and Biswas, S. M. (2011). Lactam Nonanic Acid, a New Substance from Cleome viscosa with Allelopathic and Antimicrobial Properties. *J. Biosci.* 36 (1), 27–35. doi:10.1007/s12038-011-9001-9

Kapoor, D., Bhardwaj, S., Gautam, S., Rattan, A., Bhardwaj, R., and Sharma, A. (2022). "Brassinosteroids in Plant Nutrition and Heavy Metal Tolerance," in *Brassinosteroids in Plant Developmental Biology and Stress Tolerance* (London: Academic Press), 217–235. doi:10.1016/B978-0-12-813227-2.00008-4

Liu, J. N., Zhou, Q. X., Sun, T., Ma, L. Q., and Wang, S. (2008). Growth Responses of Three Ornamental Plants to Cd and Cd–Pb Stress and Their Metal Accumulation Characteristics. *J. Hazard. Mater.* 151, 261–267. doi:10.1016/j.jhazmat.2007.08.016

Liu, Z., He, X., Chen, W., Yuan, F., Yan, K., and Tao, D. (2009). Accumulation and Tolerance Characteristics of Cadmium in a Potential Hyperaccumulator—*Lonicera japonica* Thunb. *J. Hazard. Mater.* 169, 170–175. doi:10.1016/j.jhazmat.2009.03.090

Malar, S., Vikram, S. S., Favas, P. J., and Perumal, V. (2014). Lead Heavy Metal Toxicity Induced Changes on Growth and Antioxidative Enzymes Level in Water Hyacinths [*Eichhornia crassipes* (Mart.)]. *Bot. Stud.* 55, 1–11. doi:10.1186/s40529-014-0054-6

Masindi, V., and Muedi, K. L. (2018). "Environmental Contamination by Heavy Metals," in *Heavy Metals*. London: IntechOpen, 10, 115–132. doi:10.5772/intechopen.76082

Merkl, N., Schultze-Kraft, R., and Infante, C. (2005). Assessment of Tropical Grasses and Legumes for Phytoremediation of Petroleum-Contaminated Soils. *Water Air Soil Pollut.* 165 (1), 195–209. doi:10.1007/s11270-005-4979-y

Mishra, S., Bharagava, R. N., More, N., Yadav, A., Zainith, S., Mani, S., et al. (2019). "Heavy Metal Contamination: an Alarming Threat to Environment and Human Health," in *Environmental Biotechnology: For Sustainable Future* (Singapore: Springer), 103–125. doi:10.1007/978-981-10-7284-0_5

Mourato, M. P., Moreira, I. N., Leitão, I., Pinto, F. R., Sales, J. R., and Martins, L. L. (2015). Effect of Heavy Metals in Plants of the Genus Brassica. *Int. J. Mol. Sci.* 16 (8), 17975–17998. doi:10.3390/ijms160817975

Niu, Z. X., Sun, L. N., Sun, T. H., Li, Y. S., and Hong, W. A. N. G. (2007). Evaluation of Phytoextracting Cadmium and lead by sunflower, Ricinus, Alfalfa and Mustard in Hydroponic Culture. *J. Environ. Sci.* 19 (8), 961–967. doi:10.1016/S1001-0742(07)60158-2

Pollard, A. J., Powell, K. D., Harper, F. A., and Smith, J. A. C. (2002). The Genetic Basis of Metal Hyperaccumulation in Plants. *Crit. Rev. Plant Sci.* 21, 539–566. doi:10.1080/0735-260291044359

Poschenrieder, C., Cabot, C., Martos, S., Gallego, B., and Barceló, J. (2013). Do toxic Ions Induce Hormesis in Plants? *Plant Sci.* 212, 15–25. doi:10.1016/j.plantsci.2013.07.012

Ramesar, N. S., Tavarez, M., Ebbs, S. D., and Sankaran, R. P. (2014). Transport and Partitioning of Lead in Indian Mustard (*Brassica Juncea*) and Wheat (*Triticum aestivum*). *Biorem. J.* 18, 345–355. doi:10.1080/10889868.2014.933170

Riyazuddin, R., Nisha, N., Ejaz, B., Khan, M. I. R., Kumar, M., Ramteke, P. W., et al. (2021). A Comprehensive Review on the Heavy Metal Toxicity and Sequestration in Plants. *Biomolecules* 12 (1), 43. doi:10.3390/biom12010043

Saxena, N. B., and Saxena, S. (2001). *Plant Taxonomy*. Meerut, Uttar Pradesh: Reprint by Pragati Prakashan, 224–228.

Shakoor, M. B., Ali, S., Hameed, A., Farid, M., Hussain, S., Yasmeen, T., et al. (2014). Citric Acid Improves lead (Pb) Phytoextraction in *Brassica Napus* L. By Mitigating Pb-Induced Morphological and Biochemical Damages. *Ecotox. Environ. Safe.* 109, 38–47. doi:10.1016/j.ecoenv.2014.07.033

Sharma, P., and Dubey, R. S. (2005). Lead Toxicity in Plants. *Braz. J. Plant Physiol.* 17, 35–52. doi:10.1590/S1677-04202005000100004

Sharma, R. K., Agrawal, M., and Agrawal, S. B. (2010). Physiological and Biochemical Responses Resulting from Cadmium and Zinc Accumulation in Carrot Plants. *J. Plant Nutr.* 33, 1066–1079. doi:10.1080/01904161003729774

Sidhu, G. P. S., Bali, A. S., Singh, H. P., Batish, D. R., and Kohli, R. K. (2018). Phytoremediation of lead by a Wild, Non-edible Pb Accumulator *Coronopus Didymus* (L.) Brassicaceae. *Int. J. Phytoremediation* 20 (5), 483–489. doi:10.1080/15226514.2017.1374331

Sidhu, G. P. S., Singh, H. P., Batish, D. R., and Kohli, R. K. (2017). Alterations in Photosynthetic Pigments, Protein, and Carbohydrate Metabolism in a Wild Plant *Coronopus Didymus* L. (Brassicaceae) under lead Stress. *Acta Physiol. Plant* 39, 176. doi:10.1007/s11738-017-2476-8

Singh, S., Parihar, P., Singh, R., Singh, V. P., and Prasad, S. M. (2016). Heavy Metal Tolerance in Plants: Role of Transcriptomics, Proteomics, Metabolomics, and Ionomics. *Front. Plant Sci.* 6, 1143. doi:10.3389/fpls.2015.01143

Sun, X., Zhang, J., Zhang, H., Ni, Y., Zhang, Q., and Chen, J. (2010). The Responses of *Arabidopsis thaliana* to Cadmium Exposure Explored via Metabolite Profiling. *Chemosphere* 78 (7), 840–845. doi:10.1016/j.chemosphere.2009.11.045

Tang, Y. T., Qiu, R. L., Zeng, X. W., Ying, R. R., Yu, F. M., and Zhou, X. Y. (2009). Lead, Zinc, Cadmium Hyperaccumulation and Growth Stimulation in *Arabis Paniculata* Franch. *Environ. Exp. Bot.* 66 (1), 126–134. doi:10.1016/j.envexpbot.2008.12.016

Rigby, H., and Smith, S. R. (2020). The Significance of Cadmium Entering the Human Food Chain via Livestock Ingestion from the Agricultural use of Biosolids, with Special Reference to the UK. *Environ. Int.* 143, 105844. doi:10.1016/j.envint.2020.105844

Uraguchi, S., Mori, S., Kuramata, M., Kawasaki, A., Arao, T., and Ishikawa, S. (2009). Root-to-shoot Cd Translocation via the Xylem Is the Major Process Determining Shoot and Grain Cadmium Accumulation in rice. *J. Exp. Bot.* 60, 2677–2688. doi:10.1093/jxb/erp119

Wang, S., Shi, X., Sun, H., Chen, Y., Pan, H., Yang, X., et al. (2014). Variations in Metal Tolerance and Accumulation in Three Hydroponically Cultivated Varieties of *Salix Integra* Treated with lead. *PloS one* 9 (9), e108568. doi:10.1371/journal.pone.0108568

Weldeslassie, T., Naz, H., Singh, B., and Oves, M. (2018). "Chemical Contaminants for Soil, Air and Aquatic Ecosystem," in *Modern Age Environmental Problems and Their Remediation* (Cham: Springer), 1–22. doi:10.1007/978-3-319-64501-8_1

Yan, A., Wang, Y., Tan, S. N., Mohd Yusof, M. L., Ghosh, S., and Chen, Z. (2020). Phytoremediation: a Promising Approach for Revegetation of Heavy Metal-Polluted Land. *Front. Plan. Sci.* 11, 359. doi:10.3389/fpls.2020.00359

Yi, H., and Crowley, D. E. (2007). Biostimulation of PAH Degradation with Plants Containing High Concentrations of Linoleic Acid. *Environ. Sci. Technol.* 41 (12), 4382–4388. doi:10.1021/es062397y

Ying, R., Xia, B., Zeng, X., Qiu, R., Tang, Y., and Hu, Z. (2021). Adsorption of Cadmium by *Brassica Juncea* (L.) Czern. And *Brassica Pekinensis* (Lour.) Rupr in Pot Experiment. *Sustainability* 14 (1), 429. doi:10.3390/su14010429

Zeng, X., Ma, L. Q., Qiu, R., and Tang, Y. (2009). Responses of Non-protein Thiols to Cd Exposure in Cd Hyperaccumulator *Arabis Paniculata* Franch. *Environ. Exp. Bot.* 66, 242–248. doi:10.1016/j.envexpbot.2009.03.003

Zhang, S., Chen, M., Li, T., Xu, X., and Deng, L. (2010). A Newly Found Cadmium Accumulator—*Malva Sinensis* Cavan. *J. Hazard. Mater.* 173, 705–709. doi:10.1016/j.jhazmat.2009.08.142

Zheng, R., Li, H., Jiang, R., Römheld, V., Zhang, F., and Zhao, F. (2011). The Role of Root Hairs in Cadmium Acquisition by Barley. *Environ. Pollut.* 159, 408–415. doi:10.1016/j.envpol.2010.10.034

Zhuang, P., Yang, Q. W., Wang, H. B., and Shu, W. S. (2007). Phytoextraction of Heavy Metals by Eight Plant Species in the Field. *Water Air Soil Pollut.* 184 (1), 235–242. doi:10.1007/s11270-007-9412-2

Conflict of Interest: The authors declare that the research was conducted in the absence of any commercial or financial relationships that could be construed as a potential conflict of interest.

Publisher's Note: All claims expressed in this article are solely those of the authors and do not necessarily represent those of their affiliated organizations, or those of the publisher, the editors, and the reviewers. Any product that may be evaluated in this article, or claim that may be made by its manufacturer, is not guaranteed or endorsed by the publisher.

frontiers | Frontiers in Environmental Science

TYPE Original Research
PUBLISHED 19 September 2022
DOI 10.3389/fenvs.2022.978850

OPEN ACCESS

EDITED BY
Ravi Naidu,
University of Newcastle, Australia

REVIEWED BY
Shobit Thapa,
National Bureau of Agriculturally Important Microorganisms (ICAR), India
Murugan Kumar,
National Bureau of Agriculturally Important Microorganisms (ICAR), India

*CORRESPONDENCE
Marjetka Suhadolc,
marjetka.suhadolc@bf.uni-lj.si

SPECIALTY SECTION
This article was submitted to Toxicology, Pollution and the Environment,
a section of the journal
Frontiers in Environmental Science

RECEIVED 11 July 2022
ACCEPTED 31 August 2022
PUBLISHED 19 September 2022

CITATION
Maček I, Pintarič S, Šibanc N, Rajniš T, Kastelec D, Leštan D and Suhadolc M (2022), Plants play a crucial role in the development of soil fungal communities in the remediated substrate after EDTA washing of metal-contaminated soils.
Front. Environ. Sci. 10:978850.
doi: 10.3389/fenvs.2022.978850

Plants play a crucial role in the development of soil fungal communities in the remediated substrate after EDTA washing of metal-contaminated soils

Irena Maček[1], Sara Pintarič[2], Nataša Šibanc[3], Tatjana Rajniš[3], Damijana Kastelec[2], Domen Leštan[2] and Marjetka Suhadolc[2]*

[1]Department of Biology, Biotechnical Faculty, University of Ljubljana, Ljubljana, Slovenia, [2]Department of Agronomy, Biotechnical Faculty, University of Ljubljana, Ljubljana, Slovenia, [3]Department of Forest Physiology and Genetics, Slovenian Forestry Institute, Ljubljana, Slovenia

In this study, we investigated the importance of plant cover for secondary succession and soil fungal community development in remediated substrates after EDTA washing of metal-contaminated soils. The abundance of the total fungal community, determined by ITS fungal marker genes (Internal Transcribed Spacer region), and root colonisation by arbuscular mycorrhizal (AM) fungi were monitored in two types of soil material (*calcareous and acidic*) sown with perennial ryegrass (*Lolium perenne* L.) and without plant cover (*bulk soil*). Four months after the start of the experiment, the abundance of ITS genes in the soil clearly showed that the presence of plants was the main factor affecting the total fungal community, which increased in the rhizosphere soil in most treatments, while it remained at a low level in the bulk soil (without plants). Interestingly, the addition of environmental inoculum, i.e., rhizosphere soil from a semi-natural meadow, did not have a positive effect on the abundance of the total fungal community. While fungal ITS genes were detected in soils at the end of the first growing season, arbuscular mycorrhizal (AM) structures were scarce in *Lolium* roots in all treatments throughout the first season. However, in the second season, more than a year after the start of the experiment, AM fungal colonisation was detected in *Lolium roots* in virtually all treatments, with the frequency of colonised root length ranging from 30% to >75% in some treatments, the latter also in remediated soil. This study demonstrates the importance of plants and rhizosphere in the development and secondary succession of fungal communities in soil, which has important implications for the revitalisation of remediated soils and regenerative agriculture.

KEYWORDS

heavy metals, arbuscular mycorrhiza, remediation, revitalisation, secondary succession, biodiversity, qPCR, toxic metals pollution

Introduction

Fertile soil is a valuable and finite resource. The formation of soil is a slow process, taking millennia to form a few cm of soil. Soils contaminated with potentially toxic metals (also called *heavy* metals) are of particular concern because toxic metals are not degradable and remain in the environment for long periods (Amundson et al., 2015). In most cases, such soils are lost to their intended uses, or their continued use poses a serious threat to humans and other living organisms in the contaminated area as toxic metals enter food webs and ecological networks (Hartley and Lepp, 2008). Soil contamination with toxic metals is common even in heavily populated urban and rural areas (Li and Huang, 2007). Despite contamination, people often have vegetable gardens and grow their food on contaminated soil, even in polluted areas. Children are particularly vulnerable to metal contamination, which can trigger serious health problems (Jez and Lestan, 2015). Slovenia and many other countries have areas of arable and urban land (garden soils) contaminated with heavy metals due to industrial activities in the 20th century (EEA 2020, The EU Environment, State and Outlook). In this study, we used Pb- and Zn-contaminated soils from two sites, calcareous soils with neutral pH from Mežica, Slovenia (SI) and acidic soils from Arnoldstein, Austria (AT), to investigate the effects of remediation procedures specifically designed for different soil types on soil microbiota, especially on soil fungi.

Soil biodiversity is essential for soil health and regulation of soil functions (Griffiths and Philippot, 2013; Delgado-Baquerizo et al., 2016). Microbes represent the most diverse group of soil organisms, and understanding the mechanisms of soil microbial community development is urgently needed to predict the ecological impacts of environmental change (Maček et al., 2019). In particular, soil fungi are susceptible to mechanical and chemical disturbances, as many are filamentous organisms. Their hyphae are easily damaged during mechanical tillage of the soil, which can also affect their communities. For example, some fungi disappear from intensively managed agricultural soils with high levels of mechanical soil disturbance (Helgason et al., 1998; Oehl et al., 2010). Among soil fungi, the ancient and ubiquitous group of arbuscular mycorrhizal (AM) fungi (Glomeromycotina/Glomeromycota) (Spatafora et al., 2016; Tedersoo et al., 2018) is of particular interest because they are known to colonise plant roots and live in mutualistic symbiosis with more than 2/3rd of all terrestrial plants (Fitter and Moyersoen, 1996), including crops, vegetables, and fruit trees. Highlighting the importance of AM fungi in agroecosystems goes hand in hand with the Sustainable Development Goals. Awareness of the importance of sustainable food production and self-sufficiency is increasing as many people tend to grow their own food and try to do so in a sustainable and ecological way, with minimal disturbance to the soil and reduced use of mineral fertilisers and pesticides. Rising prices in the food market and producing healthy, homegrown food will become even more critical in the future. This way of growing vegetables at home also promotes the regeneration of soil biodiversity, including indigenous AM fungal communities in the soil, and can be an important factor in regenerative agriculture.

The method of soil washing with the chelating agent EDTA (ethylenediamine tetraacetic acid) and extraction of the contaminants have been shown to be highly efficient in the removal of metals (Pb, Zn, Cd) (e.g., Finžgar and Leštan, 2007; Pociecha and Lestan, 2012; Voglar and Lestan, 2013). The method has been modified for large-scale remediation of heavy metal contaminated soils and tested in demonstrational vegetable garden experiments (e.g., Gluhar et al., 2021a; Gluhar et al., 2021b; Kaurin et al., 2021). While the removal of various forms of toxic metals reduces hazards to humans and the environment, the process also has significant effect on microbial activity in the soil (Jelusic and Lestan, 2014; Maček et al., 2016; Kaurin et al., 2021). Particularly strong effects have been reported on fungal communities in the soil, reflected as lower mycorrhizal potential in the soil (Maček et al., 2016; Kaurin et al., 2021). In a demonstrational garden experiment with vegetable beds, the function of EDTA-washed soil was evaluated using enzyme and microbial indicators, including root colonisation by AM fungi (Kaurin et al., 2021). Conventional gardening largely restored the biological functions of the remediated soil; however, the most significant and long-lasting negative impact was confirmed on symbiotic AM fungi. Their colonisation recovered to some degree after several years of outdoor gardening, as indicated by root fungal colonisation recovery. However, there are currently no data on the composition and diversity of AM fungal communities in remediated systems. Based on the abundance of the total fungal community (qPCR targeting ITS genes) and root colonisation with AM fungi, this study is the first step in demonstrating the potential of recovery of fungal communities in remediated soils in outdoor settings and showing the importance of plants in this process.

In this study, we investigated the extent to which plants (*Lolium perenne* L.) that create a uniform plant cover and rhizosphere can contribute to faster and more intense establishment of fungal communities in remediated soils after EDTA washing treatment. We tested the following hypotheses: 1) EDTA washing procedure reduces fungal potential in soil and reduces the abundance of the total fungal community shown as ITS gene copy number 2). The potential for plant root colonisation by root endophytes, including arbuscular mycorrhizal fungi, is significantly reduced after EDTA treatment but rebuilds over time. 3) Plant cover and rhizosphere are the most important factors for the development and secondary succession of fungal communities in remediated soils.

Methods

Experiment set-up and soil remediation

Soils used for the mesocosm experiment were collected from the top 30 cm layer from a vegetable garden in Mežica, Slovenia

(SI) and farmland in Arnoldstein, Austria (AT). The initial content of Pb, Cd and Zn before remediation was higher in SI soil with 1,029.7 mg Pb kg^{-1}, 699 mg Cd kg^{-1} and 7.3 mg Zn kg^{-1} soil, while AT soil had 799.8 mg Pb kg^{-1}, 437 mg Cd kg^{-1} and 5.4 mg Zn kg^{-1} soil. As pH is the most influential parameter for metal availability in soil, pH-neutral SI soil and acidic AT were selected (pH 6.9 vs. pH 5.0, respectively). Non-contaminated soil from grassland site in Ljubljana—Savlje, Slovenia, pedogenetically similar to Mežica soil, e.g. calcareous with pH 7.4, was used as control (CONT) with low levels of metals: 29.9 mg Pb kg^{-1}, 64 mg Cd kg^{-1} and 0.4 mg Zn kg^{-1} soil, and pH 7.4.

Half of the soils from all three sites were remediated by washing using EDTA based (the ReSoil®) technology as described by Lestan (2017), Gluhar et al. (2019), and Gluhar et al. (2021a) using 60 mM Ca-EDTA kg^{-1} for the AT soil and 100 mM Ca-EDTA kg^{-1} for SI and CONT soils (remediated soil), and the other half was left untreated (original soil). The original and remediated soils from all three sites were placed in 35-L mesocosms (80 mesocosms; 24 cm diameter, 42 cm height) on 23 June 2016, filled with a 5-cm layer of quartz sand (1–3 mm) at the bottom, and covered with a plastic mesh (0.2 mm).

The contaminated SI and AT soils were examined in the experiment according to three factors: the first factor was remediation with two levels: no remediation (ORIG) and remediation (REM). The second factor was the presence of plants in the mesocosm with two levels: no plant (BULK) and plant (RHIZO). The third factor was inoculum (uncontaminated semi-natural grassland rhizosphere soil with plant roots): absence (no inoculum) or presence of inoculum in the soil (inoculum). In the case of the CONT soil, treatments were determined by only two factors: remediation (ORIG, REM) and plant (BULK, RHIZO). No inoculum was added at CONT. Thus, treatments with all combinations of the four factors ($2 \times 2 \times 2 \times 2 + 2*2 = 20$ treatments) were applied in the experiment. Each treatment was replicated in four mesocosms ($n = 4$).

Half of the treatments were planted (40 mesocosms, RHIZO) with 70 ml of sterilised (2 min in 10% bleach) plant seeds (*Lolium perenne* L.) on 11 July 2016, and half of the treatments were left unplanted (bare soil) (40 mesocosms, BULK). We added inoculum (rhizosphere soil and roots) to the mesocosms as treatments (32 mesocosms) to determine its effect on soil microbial communities (100 ml inoculum in each mesocosms of the treatment). The rhizosphere inoculum was taken from uncontaminated semi-natural grassland in Ljubljana and mixed only into the top 5 cm of the soil layer in the mesocosms.

Soil and root sampling

Soil samples were collected twice, at the beginning of the mesocosm experiment, just before the soils were placed into the mesocosms (summer 2016), and 4 months after plants seeds and inoculum were added to mesocosms (2 November 2016). These soil samples were dried at 40°C for 24 h and sieved through a 2 mm mesh sieve to remove roots and stones, and used for soil chemo-physical analyses and heavy metals content measurements. For the second soil sampling (2 November 2016), soil samples were collected from mesocosms at a depth of 0–5 cm, homogenised, the roots and stones were removed, and each soil sample was divided into three parts. One part of the sample was oven dried at 40°C for 24 h and used for chemical analysis. The second part was placed on dry ice and stored at -20°C for molecular analysis. Plant roots were sampled for AM fungal colonisation on 3 August 2016, 2 November 2016, and 17 November 2017. Roots were collected in a 3 × 15 cm soil core from each mesocosm, washed with tap water, and stored in 70% ethanol until root colonisation was measured.

Soil analyses

Analyses of soil material were performed separately for each of the three locations, two contaminated (AT, SI) and one non-contaminated (CONT) soil. For the soil analyses, samples were air-dried and sieved to 2 mm (ISO11464, 2006). Total metal contents (Pb, Cd and Zn) were measured using inductively coupled plasma mass spectrometry (ICP-ES/MS) after digestion in aqua regia (Bureau Veritas Mineral laboratories, Canada). Soil organic carbon (SOC) and total nitrogen (TN) were determined by dry combustion (ISO 10694 1996; ISO 13878 1987) using an elemental analyser (Elementar vario MAX instrument, Germany). Carbonates were determined manometrically after a soil reaction with HCl (ISO 10693, 1995) and soil texture by the pipette method (ISO 11277, 2009). Soil pH was measured in a 1/2.5 (w/v) ratio of soil and 0.01 M $CaCl_2$ suspension (ISO 10390 2005).

Quantification of fungal marker genes (qPCR)

DNA was extracted from 0.5 g of fresh soil using the PowerSoil DNA Isolation Kit (MoBIO Laboratories, Carlsbad, CA, United States) following the recommended manufacturers protocol and stored at -20°C until further use. The quality and concentration of DNA extracts were determined spectrophotometrically (NanoDrop 2000 UV–vis Spectrometer; Thermo Fisher Scientific, Waltham, Massachusetts, United States).

Quantification of target ITS genes was done with a standard curve using SYBR green chemistry on the 7,500 Fast Real-Time PCR System (Applied Biosystems, Carlsbad, CA, United States). Reactions were performed in a 15 µl reaction volume containing 2 µl of DNA template (1 ng $µl^{-1}$), 7.5 µl ABsolute Blue QPCR

SYBR Green Rox mix (Thermo Fischer Scientific, Waltham, Massachusetts, United States), and 1.5 µl of 10 µM of ITS primers (ITS 3F, ITS 4R) (White et al., 1990). Two independent quantitative PCR assays were performed. The qPCR conditions were 95°C for 15min, followed by 35 cycles of 15 s at 95°C, 30 s at 55°C, 30 s at 72°C and a final step of 30 s at 80°C at which fluorescence was acquired. Standard curves were obtained using serial dilutions of the plasmid standard of the ITS gene ranging from 10^7 to 10^2 copies per reaction.

We used plasmid standards obtained from transformed *Escherichia coli* cells (strain JM109) with inserted plasmid PGEM-T (Promega, Madison, WI, United States). We greatly acknowledge Dr Laurent Philippot (INRAE, Dijon, France) for providing the ITS standard. No PCR inhibition was detected as tested by spiking samples with a known amount of external pGEM-T plasmid (Promega, Madison, Wisconsin, United States) and comparing its Cq values with positive control containing only plasmid. Melting curves were analysed for all runs to ensure PCR specificity. We calculated the copy numbers of gene per gram of dry soil to determine absolute gene abundance.

Root colonisation with AM fungi

The roots were cleaned with hot 10% KOH (90°C) and acidified with 1 N HCl. The fungal tissue inside the roots was stained with 0.05% trypan blue in lactoglycerol. Several parameters of AM fungal colonisation of roots (F - frequency of mycorrhiza in the root system, M—intensity of the mycorrhizal colonisation in the root system, m—intensity of the mycorrhizal colonisation in the root fragments, A—abundance of arbuscules in the root system, a—arbuscular density in colonised root fragments, and S/V—spore/vesicle abundance in the root system) were determined by detailed estimation of AM fungal structures in roots according to Trouvelot et al. (1986) using an Olympus Provis AX70 microscope (n = 30 mixed root segments of 1 cm length for each pooled root sample—separate pot).

Statistical analysis

The results of the four-factor experiment for the frequency of the fungal ITS genes were evaluated using a linear model. In Table ANOVA for the four-factor experiment, the four-factor interaction was statistically significant, indicating that the influence of remediation, plant, or inoculum is not the same for all soil types. Contrast analysis was performed to evaluate the differences between the means of ITS gene abundance between treatments. Data were log transformed to meet the assumption of homogeneity of variance between treatments. In the case of AM fungal colonisation data (F, M, and m), only three factors were examined because all measurements were made only in the pots with plants. All three variables were transformed using the asin [sqrt()] transformation. A generalised linear model was used for the variable m to account for the different variance modelling in the different treatments. To evaluate the colonisation of plant roots by arbuscular mycorrhizal fungi, we divided the contrasts into three groups. First, we examined the difference in colonisation between heavy metal contaminated (AT and SI) and control sites; second, we focused on the effect of the remediation procedure on colonisation; and third, the effect of inoculum addition on colonisation. All statistical analyses were performed in an R environment (R Core Team, 2021).

Results

Soil properties

Soil remediation efficiently removed Pb, Zn, and Cd in both contaminated soils. In the SI soil, Pb was reduced from 1,029.7 mg kg^{-1} to 451.9 mg kg^{-1}, Cd from 699 mg kg^{-1} to 493 mg kg^{-1} and Zn from 7.3 mg kg^{-1} to 3.7 mg kg^{-1}. An efficient reduction of toxic metals after remediation was also observed in AT soils, with a reduction of Pb from 799.8 mg kg^{-1} to 216.8 mg kg^{-1}, Cd from 437.0 mg kg^{-1} to 243.0 mg kg^{-1}, and Zn from 5.4 mg kg^{-1} to 1.3 mg kg^{-1}. It is important to note that after remediation, the Pb, Cd and Zn contents in both soils, SI and AT, are below the critical values according to Slovenian legislation (Ur, 1996). In addition to efficient metal removal, EDTA remediation increased soil pH in both soils, e.g., by 0.4 pH units in SI soil and 1.2 pH units in AT soil, to a pH of 7.3 and 6.2 in SI and AT soil, respectively. In addition, soil organic carbon content (SOC) was decreased in both soils: from 6.6% to 4.1% in SI and from 3.0% to 2.8% in AT. Changes in soil texture were also observed after remediation, with heavier soils after remediation. Clay content increased from 5.8% to 7.3% and from 11.4% to 14.9% for soils SI and AT, respectively. Silt content increased from 36.7% to 52.6% and from 44.9% to 50.6% for soil SI and AT, respectively. No significant changes in soil chemical properties after remediation, including Pb, Zn and Cd contents, were observed in CONT soil, while remediation changed soil texture, similarly to soils SI and AT soils. In CONT soil, clay content increased from 9.2% to 11.9%, and silt increased from 44.7% to 50%.

Abundance of the total fungal community

The abundance of fungal ITS genes was significantly affected by the interaction between all factors (remediation, plant, inoculum and location) ($p < 0.027$). Among the three soils, fungal abundance was significantly lower in CONT soil, compared to AT and SI soils, but this effect varied depending on remediation, plant and inoculum (Table 1; Figure 1). A

TABLE 1 Estimated ratios of means of fungal ITS abundance [location (AT, SI, CONT), remediation (ORIG, REM), plant (RHIZO, BULK), inoculum (I, NoI)] in contrast analysis with 95% confidence intervals. Only statistically significant contrasts are shown.

Contrast	Exp(estimate)	Lower CL	Upper CL	*p* value
ORIG.BULK.I:AT-SI	0.23	0.06	0.96	*
REM.BULK.NoI:SI-CONT	5.31	1.28	22.00	**
REM.RHIZO.NoI:SI-CONT	4.93	1.19	20.42	*
ORIG.BULK.NoI:AT-CONT	5.02	1.21	20.79	*
REM.BULK.NoI:AT-CONT	4.19	1.01	17.36	*
AT.ORIG.I: BULK-RHIZO	0.10	0.02	0.42	***
CONT.ORIG: BULK-RHIZO	0.10	0.02	0.40	***
SI.ORIG.NoI: BULK-RHIZO	0.23	0.05	1.08	.
SI.REM.NoI: BULK-RHIZO	0.16	0.04	0.67	**
SI.REM.I: BULK-RHIZO	0.18	0.04	0.73	**
AT.ORIG.BULK:NoI-I	9.12	2.20	37.80	***
AT.REM.RHIZO:NoI-I	6.05	1.46	25.07	**
SI.REM.BULK:NoI-I	3.75	0.91	15.56	.
SI.REM.RHIZO:NoI-I	4.09	0.99	16.96	.

*** = $p < 0.001$, ** = $p < 0.01$, * = $p < 0.05$, < 0.1.

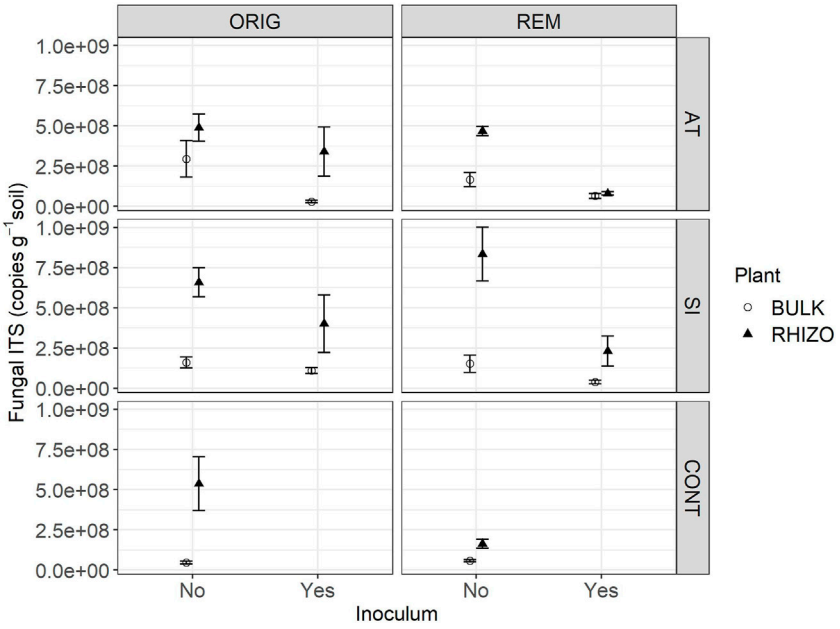

FIGURE 1
Fungal ITS abundance in Austrian (AT), Slovenian (SI) and control (CONT) soil, before (ORIG) and after remediation (REM). Soil from mesocosms was sampled 4 months after the addition of plants seeds and indigenous inoculum (rhizosphere soil and roots from a grassland) (2 November 2016). Mean ± SE of four replicates is shown.

significant difference in fungal abundance between AT and SI soils was evident only in ORIG BULK soils with inoculum (Table 1), where the fungal abundance was significantly higher in SI soil than in AT soil. On an average, the fungal ITS gene abundance in AT ORIG BULK soil with inoculum was 23% (6 %–96%) of that in SI ORIG BULK soil with inoculum.

It also showed that the influence of plant and inoculum on fungal abundance was different in different soils (AT, SI, CONT),

TABLE 2 Linear model estimates of mean ± SE AM fungal root colonisation (sampled on 17 November 2017) calculated as frequency of mycorrhization (F), intensity of root cortex colonisation (M) and intensity of colonisation within individual mycorrhizal roots (m).

Soil	Remediation	Inoculum	F (%)	M (%)	m (%)
AT	Original	No inoculum	57.3 ± 13.6	15.3 ± 5.3	23.7 ± 14.5
		With inoculum	25.8 ± 12.0	6.5 ± 3.6	27.0 ± 8.6
	Remediated	No inoculum	83.9 ± 10.1	43.2 ± 7.3	55.2 ± 1.7
		With inoculum	28.7 ± 12.4	8.0 ± 4.0	17.1 ± 11.0
SI	Original	No inoculum	58.0 ± 13.5	15.1 ± 5.3	28.2 ± 5.7
		With inoculum	38.2 ± 13.3	18.2 ± 5.7	47.3 ± 3.4
	Remediated	No inoculum	32.4 ± 12.8	3.9 ± 2.8	13.7 ± 6.9
		With inoculum	32.6 ± 12.9	7.4 ± 3.9	21.4 ± 4.9
Control	Original	No inoculum	41.5 ± 13.5	13.9 ± 5.1	32.4 ± 10.8
	Remediated	No inoculum	52.4 ± 13.7	23.6 ± 6.2	46.6 ± 4.8

while remediation had no effect. The variability of values within treatments differed among treatments and was greater at higher values, especially in treatments with plant presence (Figure 1). When plants were present, fungal abundance was higher on average than in treatments without plants. The highest fungal abundance was found in SI REM and ORIG RHIZO soil (8.33×10^8 and 1.60×10^8 copies/g soil, respectively), compared to that without plants. On average, fungal abundance in SI REM BULK and SI ORIG BULK soil was 16% (4%–67%) and 23% (5%–108%) of that in SI REM and ORIG RHIZO soil, respectively. In addition, fungal abundance was significantly higher in AT ORIG soil with inoculum, SI REM soil with inoculum and CONT ORIG soil due to plant presence (Table 1; Figure 1). The opposite pattern was observed in the treatments with inoculum compared to the treatments without. Due to inoculum addition, we observed lower fungal abundance in SI REM BULK and RHIZO, AT ORIG BULK and AT REM RHIZO soils (Table 1; Figure 1).

Plant root colonisation with arbuscular mycorrhizal fungi

AM fungal colonisation of *Lolium perenne* roots was detected only in two mesocosms during the first growing season, 1 month after the start of the experiment, both from original AT soil (sampled on 3 August 2016, 1 month after *L. perenne* seeding). The addition of inoculum to the original AT soil increased the frequency of mycorrhiza (F), the intensity of root cortex colonisation (M), and the intensity of colonisation within individual mycorrhizal roots (m) (13.3%, 2.1% and 15.5%, respectively) compared to the mesocosms with the original AT soil without the addition of inoculum (3.3%, 0.03% and 1.0%, respectively). In addition, the frequency of vesicles and spores in the mesocosms with the original AT soil with added inoculum was 13.3% (F), 2.1% (M), 15.5% (m), 29.0% (a) and 0.6% (A), respectively. In all other mesocosms, AM colonisation was not yet established.

One year and 5 months after the start of the experiment (sampled on 17 November 2017), AM fungal colonisation (Table 2) was established in all sampled mesocosms. No significant difference in AM fungal colonisation (F—Figure 2, M—Figure 3 and m—Figure 4) was observed between the contaminated ORIG (AT and SI) and CONT soils ($p > 0.99$). The remediation process had a significant effect on frequency of plant roots colonised with arbuscular mycorrhizal fungi (F) in SI soils ($p = 0.0103$), where we have observed significantly higher F in ORIG SI soil (58.0 ± 13.5%) compared to REM SI soils (32.4 ± 12.8%).

The significant effect of inoculum addition on F was observed only in REM AT soils ($p = 0.0451$). REM AT soil without added inoculum (83.9 ± 10.1%) had significantly higher F compared to REM AT soil with added inoculum (28.7 ± 12.4%).

The intensity of mycorrhizal colonisation in the root system (M) was significantly different in both ORIG soils (SI and AT) before and after remediation, showing a clear effect of the remediation process on AM colonisation. In AT soils, the remediation process significantly ($p = 0.047$) increased M from 15.3 ± 5.3% in ORIG soil to 43.2 ± 7.3% in REM soil, whereas in SI soil, M was significantly ($p = 0.077$) decreased from 15.1 ± 5.3 in ORIG to 3.9 ± 2.8% in REM soil. Addition of inoculum had a significant effect on M only in REM AT soils ($p = 0.0028$) and showed a decrease in M when inoculum was added to the soil (43.2 ± 7.3 to 8.0 ± 4.0%).

The remediation process significantly affected the intensity of mycorrhizal colonisation in root fragments (m) in SI soils ($p =$

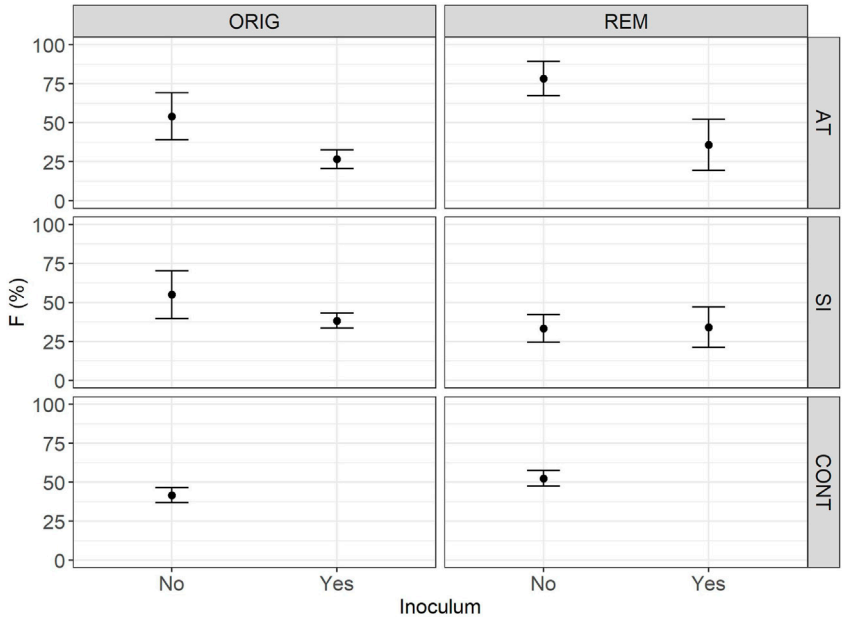

FIGURE 2
Mean relative frequency (F) of plant roots colonised with arbuscular mycorrhizal fungi (F) in *Lolium perenne* L. in Austrian (AT), Slovenian (SI) and control soil (CONT), before (ORIG) and after remediation (REM). Root sampling on 17 November 2017. The addition of indigenous inoculum (rhizosphere soil and roots from a grassland) is indicated with yes/no. Presented are means ± SE of measured values.

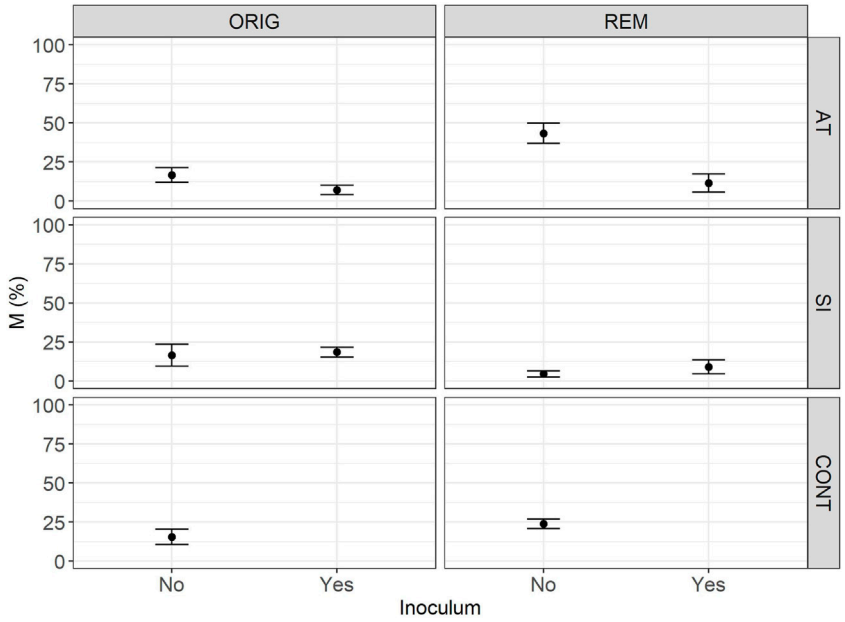

FIGURE 3
Mean intensity (M) of mycorrhizal colonisation in the root system (M) in *Lolium perenne* L. in Austrian (AT), Slovenian (SI) and control soil (CONT), before (ORIG) and after remediation (REM). Root sampling on 17 November 2017. The addition of indigenous inoculum (rhizosphere soil and roots from a grassland) is marked yes/no. Shown are the measured values of mean and SE.

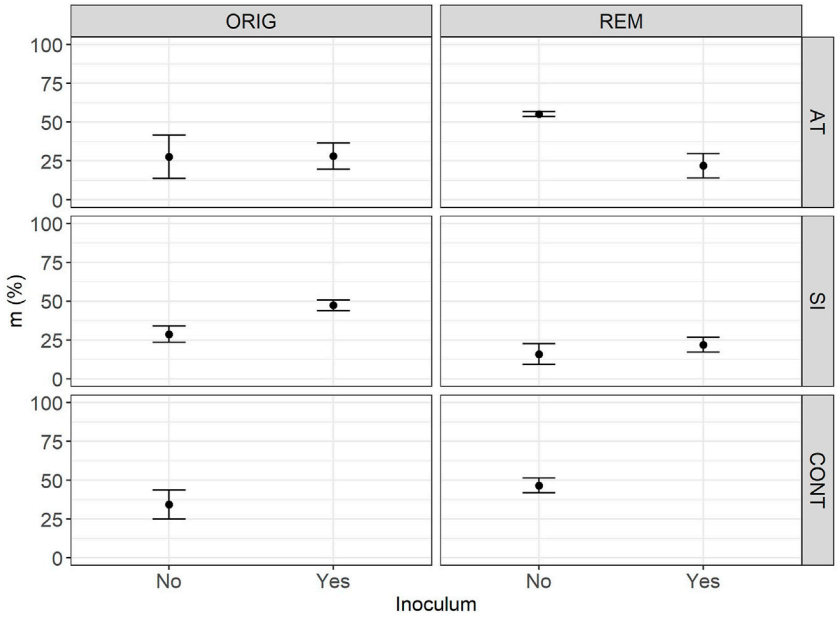

FIGURE 4
Mean intensity of mycorrhizal colonisation in root fragments (m) in *Lolium perenne* L. in Austrian (AT), Slovenian (SI) and control (CONT) soil, before (ORIG) and after remediation (REM). Root sampling on 17 November 2017. The addition of indigenous inoculum (rhizosphere soil and roots from a grassland) is marked yes/no. Shown are the measured values of mean and SE.

TABLE 3 Spores and vesicles abundance in the root system (S + V), sampled on 17 November 2017. Presented is measured value of one replicate per treatment.

Soil	Remediation	Inoculum	S + V (%)
AT	Original	No inoculum	21.67
		With inoculum	2.45
	Remediated	No inoculum	40.38
		With inoculum	
SI	Original	No inoculum	
		With inoculum	
	Remediated	No inoculum	
		With inoculum	
Control	Original	No inoculum	0.03
	Remediated	No inoculum	8.20

0.0111), reducing m from 28.2 ± 5.7% in ORIG SI soil to 13.7 ± 6.9% in REM SI soil. There was no significant effect of the addition of inoculum on m ($p > 0.23$).

Arbuscular abundance in the mycorrhizal parts of the root fragments (a) was still very low 1 year and 5 months after the start of the field experiment. A large proportion of the roots did not have arbuscules, so only the measured average values with standard error are reported. The highest percentage of arbuscules in the mycorrhizal parts of the root fragments (12.2 ± 11.6%) was found in ORIG SI soil, followed by REM CONT soil (9.6 ± 4.6%). The percentage was very low In ORIG AT soil and REM soil with and without added inoculum (< 1%).

The highest abundance of arbuscules in the root system (A) was observed in CONT REM soils (2.0 ± 0.9%), followed by ORIG SI soil (1.0 ± 0.9%), while in AT soils, the average abundance in root system was below 0.3%.

Another parameter indicating the presence of AM fungi in the roots was vesicles and spores, which were very variable in the different treatments. The highest abundance (40.4%) of spores and vesicles in the root system (S/V%) was found in *Lolium* grown in remediated AT soil (Table 3).

Discussion

This study reveals the time-scale of the revitalisation of remediated soil by fungi and highlights the importance of plant cover for secondary succession of soil fungal communities in remediated soils. While root colonisation by symbiotic AM fungi showed a slower response, soil fungal ITS molecular markers indicate that fungal communities begin to develop relatively fast after remediation and within a few months after the initiation of the outdoor experiment with remediated soil. Furthermore,

neither the fungal ITS markers nor AM fungal root colonisation showed a positive response to the addition of environmental inoculum regardless of soil characteristics (SI or AT soil). Because microbes, including fungi, play essential functional roles in soils (Griffiths and Philippot, 2013; Delgado-Baquerizo et al., 2016), higher abundance of the total fungal community may reflect ecologically relevant functional traits (e.g., mycelium growth, phosphate, nitrogen and carbon metabolism, and other functional traits) associated to fungal taxa identity (e.g., Maček et al., 2019; Põlme et al., 2020).

EDTA remediation has been shown to successfully remove toxic metals from the soil, and the remediated soil has been tested and confirmed to be well suited as a plant substrate for vegetable production (e.g., Gluhar et al., 2021b; Kaurin et al., 2021). Maintaining plant cover has been shown to be an important factor in soil health and is also part of the practice of sustainable and regenerative agriculture (Sherwood and Uphoff, 2000; Cappelli et al., 2022). When plants, including their roots, are removed from the soil, an important source of carbon is lost as plants are known to support the rhizosphere by transferring approximately 30% of photosynthetically sequestered carbon to their roots (Bago et al., 2000). Therefore, the post-remediation soil revitalisation procedure must consider the importance of continuous plant presence and a plant rhizosphere for the development of a functional fungal community the soils. This contributes to the restoration of soil biodiversity after intensive remediation treatment with EDTA washing and mechanical disturbance in addition to other already tested practices (e.g., Kaurin et al., 2021).

The internal transcribed spacer regions (ITS) are used as molecular markers for fungi (Schoch et al., 2012) and are not specific to arbuscular mycorrhizal fungi. Therefore, markers of other fungal groups, including non-symbiotrophs are also amplified using ITS primers. In our study, the abundance of ITS genes was consistently higher in treatments with *Lolium perenne* plants that formed a functional rhizosphere, regardless of the remediation treatments (Figure 1). The presence of plants and their rhizosphere supports several microbial (fungal) groups in the soil, which is also indicated in our results (Figure 1), but it is crucial and obligatory in the case of arbuscular mycorrhiza, as AM fungi are mutualistic biotrophs and receive all their carbon from partner plants, in our case *Lolium*.

Amendments in the form of compost and other substrates (Gluhar et al., 2021b; Kaurin et al., 2021) to the remediated substrate can work well as a source of local soil microbiota, but care should be taken to ensure that these substrates do not contain additional toxic substances, especially if they were also produced in the contaminated area. Interestingly, original (contaminated) soil that is left untreated and usually deposited in a loose state in a given location until a remediation treatment is applied often loses a significant amount of its vitality, which translates into reduced mycorrhizal potential in terms of the potential of the fungal inocula present in the soil to initiate mycorrhiza with newly seeded plants, as indicated in our study (Figures 2–4; Table 2). This has been observed in several studies where soils from the ORIG treatment also had relatively low mycorrhizal potential at the beginning of the experiment, even though the soil was not treated with chemicals and mechanical treatments as part of the remediation process (e.g., Maček et al., 2016; Kaurin et al., 2021).

In our experiment, mycorrhizal structures were detected in roots in some of the treatments already in the first growing season, one and 4 months after the start of our experiment, but in a very small proportion of roots. In the second growing season of 2017, F reached >30% of root parts colonised with mycorrhizal fungi in all experimental soil treatments (Figure 2). This result implies that soil processing during the remediation procedure, in addition to mechanical disturbance (mixing and sieving of soil), negatively affects the potential of AM fungi to form a functional symbiosis even in the non-remediated soil treatment, but mycorrhiza establishes with time in an outdoor setting (Figures 2–4; Table 2).

Other important mycorrhizal parameters (a—arbuscule abundance in the mycorrhizal parts of the root fragments and calculated A—abundance of arbuscules in the root system) and the presence of spores and vesicles indicate the mycorrhizal potential of AM fungi and compatibility with the plant partner, showed that mycorrhizal symbiosis was well established in the second season. In particular, a relatively high number of vesicles and spores in the roots of *Lolium*, which serve as reproductive and reserve organs for AM fungi to store lipids, indicated that a significant amount of carbon photosynthetically fixed by *Lolium* was transferred to the rhizosphere and stored in fungal tissues. In particular, the arbuscules are indicative of a functional symbiosis and nutrient exchange between plants and AM fungi. However, their low density in our experiment could be a consequence of the relatively late sampling time in November 2017. The timing of root sampling, which was conducted relatively late in the season in November, was chosen to minimize disruption to the experimental system, as root sampling is always invasive and can interfere with rhizosphere and root processes.

In a vegetable garden study using the same type of remediated soil (SI carbonate soil) and a range of vegetable plant species, the full extent of mycorrhizal colonisation was established, with abundance densities approaching 50% in all soil treatments, but vary depending on the identity of the plant host (Kaurin et al., 2021). The trend of arbuscule formation has been shown to follow a similar pattern to the frequency of the roots mycorrhiza (F), but with some time lag (Kaurin et al., 2021).

Data on colonisation of roots by AM fungi do not provide information on the diversity of fungi in the root system. Therefore, to gain better insight into the ecology and diversity of the AM fungal community in the experiment, additional molecular sequencing of marker genes for fungal community analysis should be performed as a next step. Previous studies on revitalisation of remediated soils with AM fungi (Maček et al., 2016) showed that the most abundant taxa in the newly established AM fungal communities belonged to fungi known for their ruderal (opportunistic) strategy and tolerating anthropogenic disturbances. Among them, *Funneliformis mosseae*, which is also described as a disturbance-resistant fungus in many studies, and other fungal taxa from the *Funneliformis* and *Rhizophagus* clades were also common in a small-scale pot experiment with SI remediated soil (Maček et al., 2016). These AM fungal taxa may also be responsible for the majority of plant root colonisation in this study, but this could only be verified using molecular methods and sequencing. The identity of AM fungal taxa is important because they are functionally distinct and different taxa provide different benefits to host plants, so changes in symbiotic AM fungal populations have the potential to resonate throughout their associated plant communities (Maček et al., 2019). This can lead to changes in above-ground competition dynamics and ecosystem productivity also in systems that develop on remediated soils. Therefore, soil microbes, including soil fungi, and their changes in population density in response to remediation procedures can have significant impact on terrestrial plant communities that develop on these soils and also on their productivity, which is particularly important in agroecosystems.

Conclusion

The results of our experiments clearly show that fungal communities and functional arbuscular mycorrhiza can be established in remediated soils with or without the addition of inoculum when the soils are outdoors and surrounded by semi-natural grassland that allows spontaneous inoculation with fungal spores by wind, water, and animals. Care should be taken to ensure that the remediated substrate is always covered by plants to encourage the development of symbiotic root endophytic fungi that are completely dependent on their host plant as a carbon source.

Data availability statement

The raw data supporting the conclusions of this article will be made available by the authors, without undue reservation.

Author contributions

IM and MS contributed to the conception and design of the study. DL was responsible for the EDTA remediation of soils. SP, NS, and TR carried out pot experiment and laboratory analyses. DK performed the statistical analysis. IM wrote the first draft of the manuscript. SP, NS, DK and MS wrote sections of the manuscript. All authors contributed to manuscript revision, read, and approved the submitted version.

Funding

The authors acknowledge the financial support from the Slovenian Research Agency (projects J4-7052 and J4-3098 and Research Core Funding No. P4-0085 and P4-0107).

Acknowledgments

We also thank Simon Gluhar for technical assistance and Natalija Dovč and Rok Damjanić for the help with data analysis.

Conflict of interest

The authors declare that the research was conducted in the absence of any commercial or financial relationships that could be construed as a potential conflict of interest.

Publisher's note

References

Amundson, R., Berhe, A. A., Hopmans, J. W., Olson, C., Sztein, A. E., and Sparks, D. L. (2015). Soil science. Soil and human security in the 21st century. *Science* 80, 1261071. doi:10.1126/science.1261071

Bago, B., Pfeffer, P., and Shachar-hill, Y. (2000). Carbon metabolism and transport in arbuscular mycorrhizas. *Plant Physiol.* 124, 949–958. doi:10.1104/pp.124.3.949

Cappelli, S. L., Domeignoz-Horta, L. A., Loaiza, V., and Laine, A. L. (2022). Plant biodiversity promotes sustainable agriculture directly and via belowground effects. *Trends Plant Sci.* 27, 674–687. doi:10.1016/j.tplants.2022.02.003

Delgado-Baquerizo, M., Maestre, F. T., Reich, P. B., Jeffries, T. C., Gaitan, J. J., Encinar, D., et al. (2016). Microbial diversity drives multifunctionality in terrestrial ecosystems. *Nat. Commun.* 7, 10541–10548. doi:10.1038/ncomms10541

EEA (2020). The EU environment, state & outlook. Available at https://www.eea.europa.eu/publications/soer-2020.

Finžgar, N., and Leštan, D. (2007). Multi-step leaching of Pb and Zn contaminated soils with EDTA. *Chemosphere* 66, 824–832. doi:10.1016/j.chemosphere.2006.06.029

Fitter, A. A. H., and Moyersoen, B. (1996). Evolutionary trends in root-microbe symbioses evolutionary trends in root-microbe symbioses. *Philosophical Trans. R. Soc. B Biol. Sci.* 351, 1367–1375.

Gluhar, S., Jez, E., and Lestan, D. (2019). The use of zero-valent Fe for curbing toxic emissions after EDTA-based washing of Pb, Zn and Cd contaminated calcareous and acidic soil. *Chemosphere* 215, 482–489. doi:10.1016/j.chemosphere.2018.10.074

Gluhar, S., Kaurin, A., Finžgar, N., Gerl, M., Kastelec, D., and Lestan, D. (2021a). Demonstrational gardens with EDTA-washed soil. Part I: Remediation efficiency, effect on soil properties and toxicity hazards. *Sci. Total Environ.* 792, 149060. doi:10.1016/j.scitotenv.2021.149060

Gluhar, S., Kaurin, A., Vodnik, D., Kastelec, D., Zupanc, V., and Lestan, D. (2021b). Demonstration gardens with EDTA-washed soil. Part III: Plant growth, soil physical properties and production of safe vegetables. *Sci. Total Environ.* 792, 148521. doi:10.1016/j.scitotenv.2021.148521

Griffiths, B. S., and Philippot, L. (2013). Insights into the resistance and resilience of the soil microbial community. *FEMS Microbiol. Rev.* 37, 112–129. doi:10.1111/j.1574-6976.2012.00343.x

Hartley, W., and Lepp, N. W. (2008). Remediation of arsenic contaminated soils by iron-oxide application, evaluated in terms of plant productivity, arsenic and phytotoxic metal uptake. *Sci. Total Environ.* 390, 35–44. doi:10.1016/j.scitotenv.2007.09.021

Helgason, T., Daniell, T., Husband, R., Fitter, A., and Young, J. (1998). Ploughing up the wood-wide web? *Nature* 394, 431. doi:10.1038/28764

Jelusic, M., and Lestan, D. (2014). Effect of EDTA washing of metal polluted garden soils. Part I: Toxicity hazards and impact on soil properties. *Sci. Total Environ.* 475, 132–141. doi:10.1016/j.scitotenv.2013.11.049

Jez, E., and Lestan, D. (2015). Prediction of blood lead levels in children before and after remediation of soil samples in the upper Meza Valley, Slovenia. *J. Hazard. Mat.* 296, 138–146. doi:10.1016/j.jhazmat.2015.04.049

Kaurin, A., Gluhar, S., Maček, I., Kastelec, D., and Lestan, D. (2021). Demonstrational gardens with EDTA-washed soil. Part II: Soil quality assessment using biological indicators. *Sci. Total Environ.* 792, 148522–148529. doi:10.1016/j.scitotenv.2021.148522

Lestan, D. (2017). Novel chelant-based washing method for soil contaminated with Pb and other metals: A pilot-scale study. *Land Degrad. Dev.* 28, 2585–2595. doi:10.1002/ldr.2818

Li, X., and Huang, C. (2007). Environment impact of heavy metals on urban soil in the vicinity of industrial area of Baoji city, P.R. China. *Environ. Geol.* 52, 1631–1637. doi:10.1007/s00254-006-0608-3

Maček, I., Clark, D. R., Šibanc, N., Moser, G., Vodnik, D., Müller, C., et al. (2019). Impacts of long-term elevated atmospheric CO2 concentrations on communities of arbuscular mycorrhizal fungi. *Mol. Ecol.* 28, 3445–3458. doi:10.1111/mec.15160

Maček, I., Šibanc, N., Kavšček, M., and Lestan, D. (2016). Diversity of arbuscular mycorrhizal fungi in metal polluted and EDTA washed garden soils before and after soil revitalization with commercial and indigenous fungal inoculum. *Ecol. Eng.* 95, 330–339. doi:10.1016/j.ecoleng.2016.06.026

Oehl, F., Laczko, E., Bogenrieder, A., Stahr, K., Bösch, R., van der Heijden, M., et al. (2010). Soil type and land use intensity determine the composition of arbuscular mycorrhizal fungal communities. *Soil Biol. Biochem.* 42, 724–738. doi:10.1016/j.soilbio.2010.01.006

Pociecha, M., and Lestan, D. (2012). Washing of metal contaminated soil with EDTA and process water recycling. *J. Hazard. Mat.* 235–236, 384–387. doi:10.1016/j.jhazmat.2012.08.001

Põlme, S., Abarenkov, K., Henrik Nilsson, R., Lindahl, B. D., Clemmensen, K. E., Kauserud, H., et al. (2020). FungalTraits: A user-friendly traits database of fungi and fungus-like stramenopiles. *Fungal Divers.* 105, 1–16. doi:10.1007/s13225-020-00466-2

R Core Team (2021). *R: A language and environment for statistical computing*. Vienna, Austria: R Foundation for Statistical Computing. Available at: https://www.R-project.org/.

Schoch, C. L., Seifert, K. A., Huhndorf, S., Robert, V., Spouge, J. L., Levesque, C. A., et al. (2012). Nuclear ribosomal internal transcribed spacer (ITS) region as a universal DNA barcode marker for Fungi. *Proc. Natl. Acad. Sci. U. S. A.* 109, 6241–6246. doi:10.1073/pnas.1117018109

Sherwood, S., and Uphoff, N. (2000). Soil health: Research, practice and policy for a more regenerative agriculture. *Appl. Soil Ecol.* 15, 85–97. doi:10.1016/S0929-1393(00)00074-3

Spatafora, J. W., Chang, Y., Benny, G. L., Lazarus, K., Smith, M. E., Berbee, M. L., et al. (2016). A phylum level phylogenetic classification of zygomycete fungi based on genome scale data. *Mycologia* 108, 1028–1046. doi:10.3852/16-042

Tedersoo, L., Sánchez-Ramírez, S., Kõljalg, U., Bahram, M., Döring, M., Schigel, D., et al. (2018). High-level classification of the Fungi and a tool for evolutionary ecological analyses. *Fungal Divers.* 90, 135–159. doi:10.1007/s13225-018-0401-0

Trouvelot, A., Kough, J. L., and Gianinazzi-Pearson, V. (1986). "»Mesure du taux de mycorhization VA d'un systeme radiculaire. Recherche de methods d'estimation ayant une signification fonctionnelle," in *« in physiological and genetical aspects of mycorrhizae*. Editors V. Gianinazzi-Pearson and S. Gianinazzi (Paris): INRA), 217–221.

Ur (1996). *Uredba o mejnih, opozorilnih in kritičnih imisijskih vrednostih nevarnih snovi v tleh*,

Voglar, D., and Lestan, D. (2013). Pilot-scale washing of Pb, Zn and Cd contaminated soil using EDTA and process water recycling. *Chemosphere* 91, 76–82. doi:10.1016/j.chemosphere.2012.12.016

White, T. J., Burns, T., Lee, S., and Taylor, J. (1990). "Amplification and direct sequencing of fungal ribosomal RNA genes for phylogenetics," in *PCR Protocols: A Guide to Methods and Applications*. Editors M. A. Innis, D. H. Gelfand, J. J. Snisky, and T. J. White (San Diego: Academic Press), 315–322. doi:10.1016/b978-0-12-372180-8.50042-1

Frontiers in Environmental Science

Explores the anthropogenic impact on our natural world

An innovative journal that advances knowledge of the natural world and its intersections with human society. It supports the formulation of policies that lead to a more inhabitable and sustainable world.

Discover the latest Research Topics

See more →

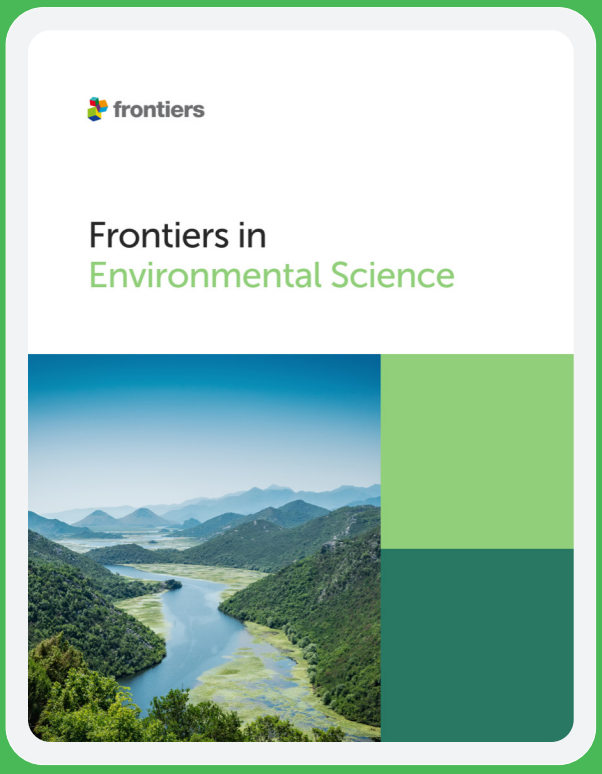

Frontiers

Avenue du Tribunal-Fédéral 34
1005 Lausanne, Switzerland
frontiersin.org

Contact us

+41 (0)21 510 17 00
frontiersin.org/about/contact